

ISSN 2413-452X

doi.org/10.62965/tnu.sns.2024.2

ПАЁМИ
ДОНИШГОҶИ МИЛЛИИ ТОҶИКИСТОН
Баҳши илмҳои табиӣ
2024. №2.

ВЕСТНИК
ТАДЖИКСКОГО НАЦИОНАЛЬНОГО УНИВЕРСИТЕТА
Серия естественных наук
2024. № 2.

BULLETIN
OF THE TAJIK NATIONAL UNIVERSITY
Series of natural sciences
2024. No.2.



МАРКАЗИ
ТАБЪУ НАШР, БАҶГАРДОН ВА ТАРҶУМА
ДУШАНБЕ – 2024

BULLETIN OF THE TAJIK NATIONAL UNIVERSITY

Series of natural sciences

Founder of the journal:

TAJIK NATIONAL UNIVERSITY

The journal was established in 2012. Issued 4 times a year.

CHIEF EDITOR:

**Solihov
Davlat Kuvatovich**

Doctor of Physical and Mathematical Sciences, Professor

DEPUTY CHIEF EDITOR:

**Safarmamadov Safarmamad
Muborakshoevich**

Doctor of Chemical Sciences, Professor

DEPUTY CHIEF EDITOR:

**Ismonov Karomatullo
Badridinovich**

Candidate of philology sciences, associate professor, director of the Publishing Center of the Tajik National University

MEMBERS OF THE EDITORIAL BOARD:

01.01.00 - Mathematics

Abdulkarimov Mahmadsalim

Doctor of Physical and Mathematical Sciences, Professor (Tajikistan)

Faizulloevich

Doctor of Physical and Mathematical Sciences, Professor (Tajikistan)

Komiliyen

Faizali Sadulla

Doctor of Physical and Mathematical Sciences, Professor, Academician (Tajikistan)

Rajabov

Nusrat

Rajabova

Doctor of Physical and Mathematical Sciences, Professor (Tajikistan)

Lutfiy Rajabovna

Soldatov Alexander

Doctor of Physical and Mathematical Sciences, Professor (Russia)

Pavlovich

Shabozov Mirgand

Doctor of Physical and Mathematical Sciences, Professor, Academician (Tajikistan)

Shabozovich

01.04.00 - Physics

Dvinin Sergei

Doctor of Physical and Mathematical Sciences, Associate Professor (Russia)

Aleksandrovich

Komilov Kosim

Doctor of Physical and Mathematical Sciences, Professor (Tajikistan)

Makhsudov

Barot Isломovich

Doctor of Physical and Mathematical Sciences, Professor (Tajikistan)

Normatov Inom

Sherovich

Doctor of Chemical Sciences, Professor, Academician (Tajikistan)

Chong-Geng Ma

Doctor of Physical and Mathematical Sciences, Professor (China)

02.00.00 - Chemical sciences

John Nobleman

Doctor of Chemical Sciences, Professor (America)

Zolotsky Semyon

Solomonovich

Doctor of Chemical Sciences, Professor (Russia)

Konketa Giankola

Doctor of Chemical Sciences, Professor (Italy)

Samihov Shonavruz

Rajabov Sirojiddin

Doctor of Chemical Sciences, Professor

Usacheva Tatyana

Rudolfovna

Doctor of Chemical Sciences, Professor (Russia)

Juraev Tukhtasun Juraevich

Doctor of Chemical Sciences, Professor

he journal is included in the List of peer-reviewed scientific journals of the Higher Attestation Commission of the Ministry of Education and Science of the Russian Federation from 03.06.2016, No. 1922.

*The journal accepts scientific articles on the following scientific specialties: **01.01.00 - Mathematics; 01.04.00 - Physics; 02.00.00 - Chemical sciences.***

The journal is included in the database of the Russian Scientific Citation Index (RSCI).

The journal is printed in Tajik, Russian and English languages.

Full-text versions of published materials are posted on the official website of the journal (www.vestnik-tnu.com).

**Bulletin of the Tajik National University.
Series of natural sciences**

– 2024. – №2.

ISSN 2413-452X

The journal is registered in the Ministry of Culture of the Republic of Tajikistan, No.183\МҚ-97, 19.02.2021.

The journal is being prepared for publication in the Publishing Center of TNU.

Address of the Publishing Center:
17, Rudaki Avenue, Dushanbe, 734025,
Republic of Tajikistan,

Web site of the journal: www.vestnik-tnu.com

E-mail: vestnik-tnu@mail.ru

Phone: (+992 37) 227-74-41

© TNU, 2024

**USING LINEAR PROGRAMMING METHODS TO SOLVE PROBLEMS OF
OPTIMIZING THE BANK'S ADVERTISING BUDGET**

Oдинаев R.N., Afzalshohi S.

In a competitive banking environment, the effective use of advertising resources plays a key role in achieving financial performance. Optimization of the advertising budget is one of the methods of increasing the effectiveness of investments in advertising. In this paper, the optimization of the bank's advertising budget is considered. With the help of a mathematical model and optimization methods, the selection of the most effective options for the distribution of the advertising budget will be carried out. The results of the study can be useful for the banking sector in general and for individual banks in particular, as they allow increasing the efficiency of the use of advertising resources and increasing the competitiveness of the bank in the market. The paper will consider both theoretical aspects of using linear programming problems and practical examples of their application based on real banking data.

The advertising budget is one of the key elements of the marketing strategy of any business, including the banking sector. Optimization of the distribution of the advertising budget allows you to increase the influx of new customers and increase profits, while not exceeding the specified financial limits. The use of linear programming methods becomes necessary to solve the problems of optimizing the bank's advertising budget, as this allows us to formalize the task and get an accurate answer to the question of how exactly the budget should be distributed in order to maximize profits[4-5]. In recent years, more and more attention has been paid to the task of optimizing the advertising budget of banks. Today, many researchers are working to propose effective methods for solving this problem [6-8]. Some of these studies are discussed in more detail below.

One of the largest studies in this field was the work [1]. The authors describe various approaches to optimizing the bank's advertising budget and consider their advantages and disadvantages. As a result of the study, it was revealed that the most effective methods are linear programming methods and methods based on machine learning algorithms. The paper analyzes the use of linear programming to optimize the advertising budget of the bank [1]. The article [2] provides a methodology for determining the share of bank marketing costs in revenue using correction coefficients depending on the marketing goal and industry. In the article [3] a discrete model of optimization of the advertising policy of the company is considered. The problem is solved by dynamic programming. The resulting solution allows you to optimize the company's profit.

Methods for calculating the advertising budget. To calculate the advertising budget, you can use the following methods:

1. The percentage of turnover method is calculated based on the percentage of the bank's total profit that will be allocated for advertising. The calculation is carried out according to the formula: $B_{\text{рекл}} = B * \Pi$, where $B_{\text{рекл}}$ is the budget; B - is the total revenue; Π -is the percentage.
2. The profit maximization method is based on the calculation of sales volume, which is necessary for the recoupment of advertising costs. It is calculated based on the formula: $S = \frac{Z+I}{F}$, where S -is sales volume; Z -is advertising costs; I - is fixed costs; F - is profit

per unit of production. Taking into account the volume of sales, you can calculate the budget for advertising.

3. The method of statistical analysis is based on the analysis of historical data of the company and its competitors. It is calculated based on the formula: $V = \frac{V_k * \alpha}{L_k}$, where V is the advertising budget; V_k is competitors' advertising expenses; L_k - competitors' share in the market; α - the bank's share in the market.

Thus, in order to find the optimal solution to the criterion of the quality of the bank's services, using advertising, it is necessary to use the above methods, defining the goal, variables, constraints, optimization problem and the solution of the problem.

According to the above studies [1-5], each bank uses the most familiar method. The main purpose for calculating the bank's advertising budget is not only to provide for advertising costs, but also to optimize it. Optimization is achieved by maximizing the profit that comes from advertising.

Based on the above, the optimization model can be formulated as a linear programming problem [9-12].

A mathematical model for solving the optimization problem of the bank 's advertising budget can be presented as follows:

Given: initial data on the budget, advertising channels and their effectiveness.

Desired parameters: optimal budget allocation between advertising channels, maximizing the number of bank customers.

Limitations:

- The advertising budget should not exceed the maximum value.
- The total number of bank customers attracted by advertising should not exceed the maximum allowable value.
- There is a limit on the available budget for each advertising channel.

The mathematical model of the problem is presented in the form:

$$\begin{aligned}
 F &= \sum_{i=1}^m c_i x_i \rightarrow \max \\
 \sum_{i=1}^m a_i x_i &\leq b \\
 d_i &\leq x_i \leq D_i \\
 x_i &\geq 0 \\
 d_i, x_i, D_i &- \text{ whole,} \\
 i &= 1, 2, \dots, m.
 \end{aligned}$$

Where F is the bank's profit from the entire advertising campaign;

- c_i - profit from advertising attracted through the i -th channel;
- x_i - the amount of money allocated to the advertising channel i ;
- a_i - the number of clients attracted through the i -th channel;
- D_i - the maximum budget allocated for advertising;
- b - budget amount;
- d_i - available budget for channel i .

Thus, solving this optimization problem, it is necessary to determine the optimal budget allocation between advertising channels, maximizing the number of bank customers while observing all restrictions.

To build a mathematical model of the optimization task of the bank's advertising budget, it is necessary to formulate the purpose and limitations of the task on a specific example, as well as to determine variables and parameters.

Let's consider an example of optimizing the advertising budget using the above models. All financial indicators will be considered, in a certain sense, conditional. We will calculate the optimal ratio in the use of various types of advertising in the bank's activities.

For an example of optimizing the bank's advertising budget, consider the following situation. Suppose a bank wants to use advertising in three different channels: television, radio and Internet advertising. He has a budget of 4 thousand somons per month to place these ads. Let's assume that the cost of each advertising channel is equal to the following values:

- Television: 100 somons per ad block
- Radio: 70 somons for an advertising series
- Online advertising: 40 somons per month

The purpose of this task is to maximize the overall effect of advertising from the invested funds.

Let x_1, x_2 and x_3 be the amount of money spent on television, radio and Internet advertising, respectively. Then the optimization problem can be written in the following form:

It is required to find the maximum of the function

$$F(X) = 130x_1 + 100x_2 + 80x_3 \rightarrow \max$$

under restrictions:

$$100x_1 + 70x_2 + 40x_3 \leq 4000$$

$$x_1 \leq 16$$

$$x_2 \leq 20$$

$$x_3 \leq 25$$

$$x_1 \geq 0, x_2 \geq 0, x_3 \geq 0$$

As basic variables, we can choose x_4, x_5, x_6, x_7 .

$$100x_1 + 70x_2 + 40x_3 + x_4 = 4000$$

$$x_1 + x_5 = 16$$

$$x_2 + x_6 = 20$$

$$x_3 + x_7 = 25$$

Let's solve the problem of linear programming by the simplex method, using a simplex table, with respect to the basic variables x_4, x_5, x_6, x_7 .

Assuming that the free variables are 0, we get the first reference plan:

$$X_0 = (0,0,0,4000,16,20,25)$$

Table 1.

№	Базис	Элем. св. столбца	x_1	x_2	x_3	x_4	x_5	x_6	x_7
1	x_4	4000	100	70	40	1	0	0	0
2	x_5	16	1	0	0	0	1	0	0
3	x_6	20	0	1	0	0	0	1	0
4	x_7	25	0	0	1	0	0	0	1
5	F	0	-130	-100	-80	0	0	0	0

Let's move on to the main algorithm of the simplex method.

Iteration №1.

Let's choose the column corresponding to the variable x_1 as the leading one, since this is the largest coefficient modulo.

Let's define the leading row by rows as a quotient of division: b_i / a_{i1} and choose the smallest of them:

$$\min(4000 : 100, 16 : 1) = 16$$

Therefore, the 2nd line is the leading one.

The resolving element is equal to 1 and is located at the intersection of the leading column and the leading row.

Table 2.

↓

№	Базис	Элем. св. столбца	x_1	x_2	x_3	x_4	x_5	x_6	x_7
1	x_4	4000	100	70	40	1	0	0	0
→ 2	x_5	16	1	0	0	0	1	0	0
3	x_6	20	0	1	0	0	0	1	0
4	x_7	25	0	0	1	0	0	0	1
5	F	0	-130	-100	-80	0	0	0	0

We form the next part of the simplex table. Instead of the variable x_5 , the variable x_1 will enter iteration 1.

We get a new simplex table:

Table 3.

№	Базис	Элем. св. столбца	x_1	x_2	x_3	x_4	x_5	x_6	x_7
1	x_4	2400	0	70	40	1	-100	0	0
2	x_1	16	1	0	0	0	1	0	0
3	x_6	20	0	1	0	0	0	1	0
4	x_7	25	0	0	1	0	0	0	1
5	F	2080	0	-100	-80	0	130	0	0

The current reference plan is not optimal, since there are negative coefficients in the index row.

Iteration №2.

As the leading column, we choose the corresponding variable x_2 , since this is the largest coefficient modulo.

Let's define the leading row by rows as a quotient of division: b_i / a_{i2} and choose the smallest of them:

$$\min (2400 : 70, 20 : 1) = 20$$

Therefore, the 3rd line is the leading one.

The resolving element is equal to 1 and is located at the intersection of the leading column and the leading row.

Table 4.

№	Базис	Элем. св. столбца	x_1	x_2	x_3	x_4	x_5	x_6	x_7
1	x_4	2400	0	70	40	1	-100	0	0
2	x_1	16	1	0	0	0	1	0	0
→ 3	x_6	20	0	1	0	0	0	1	0
4	x_7	25	0	0	1	0	0	0	1
5	F	2080	0	-100	-80	0	130	0	0

We form the next part of the simplex table. Instead of the variable x_6 , the variable x_2 will be included in the second iteration.

We get a new simplex table:

Table 5.

№	Базис	Элем. св. столбца	x_1	x_2	x_3	x_4	x_5	x_6	x_7
1	x_4	1000	0	0	40	1	-100	-70	0
2	x_1	16	1	0	0	0	1	0	0
3	x_2	20	0	1	0	0	0	1	0
4	x_7	25	0	0	1	0	0	0	1
5	F	4080	0	0	-80	0	130	100	0

Iteration №3.

The current reference plan is suboptimal, since there are negative coefficients in the index row. As the leading column, we choose the corresponding variable x_3 , since this is the largest coefficient modulo. Let's define the leading row by rows as a quotient of division: b_i / a_{i3}

and choose the smallest of them:

$$\min(1000 : 40, 25 : 1) = 25$$

Therefore, the 1st line is the leading one. The resolving element is 40 and is located at the intersection of the leading column and the leading row.

Table 6.

↓

№	Базис	Элем. св. столбца	x_1	x_2	x_3	x_4	x_5	x_6	x_7
→ 1	x_4	1000	0	0	1	-100	-70	0	25
2	x_1	16	1	0	0	0	1	0	0
3	x_2	20	0	1	0	0	0	1	0
4	x_7	25	0	0	1	0	0	0	1
5	F	4080	0	0	-80	0	130	100	0

Since there are several minimum elements of 25 in the last column, we select the row number according to the Kreko rule.

The Kreko method is as follows. The row elements having the same smallest values $\min = 25$, are divided into the intended resolving elements, and the results are entered in additional rows. For the leading row, the one in which the smallest quotient occurs first when reading the table from left to right across the columns is selected.

We form the next part of the simplex table. Instead of variable x_4 , iteration 3 will include variable x_3 .

We get a new simplex table:

Table 7.

№	Базис	Элем. св. столбца	x_1	x_2	x_3	x_4	x_5	x_6	x_7
1	x_3	25	0	0	1	1/40	-5/2	-7/4	0
2	x_1	16	1	0	0	0	1	0	0
3	x_2	20	0	1	0	0	0	1	0
4	x_7	0	0	0	0	-1/40	5/2	7/4	1
5	F	6080	0	0	0	2	-70	-40	0

Iteration №4.

The current reference plan is not optimal, since there are negative coefficients in the index row.

Let's choose the column corresponding to the variable x_5 as the leading one, since this is the largest coefficient modulo.

Let's define the leading row by rows as a quotient of division: b_i / a_{i5} and choose the smallest of them:

$$\min(-, 16 : 1, 0 : 5/2) = 0$$

Therefore, the 4th line is the leading one. The resolving element is 21/2 and is located at the intersection of the leading column and the leading row.

Table 8.

№	Базис	Элем. св. столбца	x_1	x_2	x_3	x_4	x_5	x_6	x_7
1	x_3	25	0	0	1	1/40	-5/2	-7/4	0
2	x_1	16	1	0	0	0	1	0	0
3	x_2	20	0	1	0	0	0	1	0
→ 4	x_7	0	0	0	0	-1/40	5/2	7/4	1
5	F	6080	0	0	0	2	-70	-40	0

We form the next part of the simplex table. Instead of variable x_7 , iteration 4 will include variable x_5 .

We get a new simplex table:

Table 9.

№	Базис	Элем. св. столбца	x_1	x_2	x_3	x_4	x_5	x_6	x_7
1	x_3	25	0	0	1	0	0	0	1
2	x_1	16	1	0	0	1/100	0	-7/10	-2/5
3	x_2	20	0	1	0	0	0	1	0
4	x_5	0	0	0	0	-1/100	1	7/10	2/5
5	F	6080	0	0	0	13/10	0	9	28

Since the last row in Table 9 does not contain negative elements, the found plan is optimal.

The optimal plan can be written as follows:

$$x_1 = 16, x_2 = 20, x_3 = 25, x_4 = 0, x_5 = 0, x_6 = 0, x_7 = 0$$

$$F(X) = 130 * 16 + 100 * 20 + 80 * 25 = 6080$$

this means that the final budget will be 6080 somons, and the budget distribution will be as follows: $x_1 = 16, x_2 = 20, x_3 = 25$.

The expected profit of the bank from investing in advertising will be $(6080-4000)/4000 * 100\% = 52\%$.

The results obtained confirm the need to use optimization models in calculating the bank's advertising budget in order to increase the communicative and economic effect of advertising.

In conclusion, it can be noted that optimization of the advertising budget is an urgent task in the conditions of a modern market economy. The developed mathematical model is a tool that can increase the efficiency of attracting and retaining customers, as well as strengthen the bank's competitive position in the market.

Thus, research in the field of optimization of the advertising budget of banks continues to develop, offering new effective methods for solving this problem. The use of linear programming and machine learning methods is the most promising and allows you to achieve maximum results at minimal cost. Based on the results of the study, it can be concluded that linear programming methods can effectively optimize the bank's advertising budget.

**REVIEWER: Shabozov M.Sh.,
Doctor of Physical and Mathematical Sciences,
Academician**

REFERENCES

1. Bobkov S.P., Optimization of advertising expenses in conditions of limited resources / S.P. Bobkov, O.A. Shirokaya, A.V. Filimonov // Modern high-tech technologies. Regional application. - No. 4. – 2010. – Pp. 20-25.
2. Shtezel A.Yu. Advertising costs in the structure of the marketing budget of a commercial bank / A.Yu. Shtezel // TERRAECONOMICUS (Economic Bulletin of Rostov State University). – 2009. – Volume 7. - No. 2. – Pp. 158-161.
3. Komarov E.G. Elements of bank marketing / E.G. Komarov // Personnel management. - 2007. – No. 10. – Pp. 24-26.
4. Miroshnikov D. Marketing of banking products from the point of view of the development of the banking system / D. Miroshnikov // Banking technologies. - 2006. – No. 8. – Pp. 46-48.

5. Matantsev A.N. Effectiveness of advertising / A.N. Matantsev // - M.: Finpress Publishing House. – 2002. – 416 p.
6. Shelobaev S.I. Mathematical methods and models in economics, finance, business: Textbook. Handbook for universities / Shelobaev S.I. // M.: UNITY-DANA. – 2000. – P. 367.
7. Intrigator M. Mathematical methods of optimization and economic theory / G.I. Zhukova, F.Ya. Kelman // M.: Iris-press. – 2002. – P.576.
8. Odinaev R. N. Mathematical model of cargo transportation of the republic of Tajikistan at the Premier Rogunskaya HPP using linear programming methods / R. N. Odinaev, S. H. Mavlonzoda // – 2020. – No. 4. – P. 5-15.
9. Odinaev R. N. Optimization methods / R. N. Odinaev // – Dushanbe: TNU, 2021. – p. 246.
10. Odinaev R.N. Optimization methods in examples and problems / R. N. Odinaev, F. Raimzoda, F. Raimzoda, N. Shermatov // Tajik National University. – Dushanbe: Er-graf. – 2020. – P. 148.
11. Yunusi M. Optimization methods / M. Yunusi, R.N. Odinaev // - Dushanbe: TNU, – 2014. – From 179.
12. Afzalshohi S., The best models of the banking system with one basis / S. Afzalshohi, M. Yunusi // Bulletin of the Tajik National University. Series contains Sciences. – 2021. – No. 3. – P p. 28 – 38.
13. Afzalshohi Safarkhon. Simplex method for solving the problem of written programming / Afzalshohi Safarkhon // Bulletin of the Nosir Khusrav BNU. Series of Humanities and Economic Sciences. – No.1-4. – 2020. - Volume 2.
14. Afzalshohi Safarkhon. Mathematical and computer model of automation of debt instruments in a bank / Afzalshohi Safarkhon // Bulletin of the Nosir Khusrav BNU. Series of Humanities and Economic Sciences. – № 2-3. – 2022.

USE OF LINEAR PROGRAMMING METHODS FOR SOLVING THE PROBLEMS OF OPTIMIZING THE ADVERTISING BUDGET OF A BANK

The advertising strategy is one of the most important components of optimizing the bank's business processes. It directly affects the level of profit, demand for services and strengthening the position of a financial organization in the market. This paper discusses the use of linear programming problems to optimize the advertising budget of the bank. To solve the problem of optimizing the bank's advertising budget, a mathematical model was proposed that determines the optimal distribution of the budget between advertising channels, maximizing the number of bank customers, subject to all restrictions. As a result of the experimental analysis, the effectiveness of this technique for optimizing the bank's advertising budget was proved. The main result of this work is the substantiation of the need to optimize the bank's advertising budget, as well as the development of a mathematical model for its implementation. The obtained results make it possible to increase the profitability of a financial institution, increase recognition and trust in the bank by customers.

Key words: mathematical model, advertising budget, advertising budget optimization, advertising profit, linear programming, simplex table, basic variables, basic plan, decisive element.

Information about the authors: **Odinaev Raim Nazarovich** – Tajik National University, Doctor of Physical and Mathematical Sciences, Professor, Head of the Department of Mathematical and Computer Modeling. **Address:** 734025, Dushanbe, Republic of Tajikistan, Rudaki Avenue 17. **E-mail:** raim_odinaev@mail.ru.

Afzalshohi Safarkhon - Bokhtar State University named after Nosiri Khusrav, Assistant of the Department of Information Technologies and Methods of Teaching Computer Science. **Address:** 735140, Bokhtar, Republic of Tajikistan, Aini street, 67. **E-mail:** sobirov.afzalsho@mail.ru

Article received 19.09.2023

Approved after review 19.02.2024

Accepted for publication 25.04.2024

MATHEMATICAL MODEL OF FUZZY DEFINITION OF SUBJECTS OF SCIENTIFIC ARTICLES USING SYNTACTICALLY RELATED WORDS

Murodov P.S., Prutskov A.V.

Introduction. The need for mathematical modeling of various natural languages led to the emergence of first mathematical and then, with the development of computer technology, computer linguistics. Mathematical modeling of morphological analysis and synthesis is described in [1-2]. The result of the modeling was a method for generating and determining word forms, applicable to natural languages of various groups and families [3].

The next object of mathematical modeling was scientific articles. The subject of the simulation was the topic of the articles.

The task of determining the topic of a scientific article can be used in the following cases:

- bibliographic affairs;
- information retrieval;
- searching for scientific articles on the same topic or similar to a given one;
- linguistic and statistical analysis of scientific articles on various topics.

Approaches to determining the topics of scientific articles

Several approaches have been proposed to determine the topics of scientific articles.

In [4] a digital portrait of the author's abstract (DPA) is proposed. The DPA is based on a discrete function of the sum of the frequencies of certain letters in the abstract. The distance between two DPAs is proportional to the maximum difference of discrete functions. Similar studies of abstracts on pedagogy and economics were carried out in [5-6].

In [7] reviews of books are classified. Experiments were conducted on dividing into 2 (positive, negative) and 3 (positive, negative and neutral) classes. The support vector machine was used for classification.

Descriptions of scientific research by individual authors or the titles of their scientific publications are classified into [8] using the nearest neighbor method. A vector representation of words is used. The paper raises the problem of the lack of established approaches to solving the problem of classifying scientific publications.

In [9] classification methods are studied: nearest neighbors, random forest, gradient boosting, logistic regression, support vector machine. Classification methods are applied to articles belonging to two classes: "Text Data Mining" and other computer science topics. The best classification results were shown by the gradient boosting method.

In [10] a method for classifying texts using machine learning algorithms is proposed. The results of computer experiments assessing the quality of algorithms for classifying dissertations by specialty are presented.

The classification of abstracts by topic proposed in [11] is as follows. The body of abstracts is preliminarily divided into classes. Key words are highlighted for each class. The decision rule is determined by the maximum likelihood estimation method.

Scientific articles in medicine, social sciences and engineering are classified into [12] "naive" Bayes classifier, random forest and support vector machines. A similar approach to the classification of scientific articles was proposed in [13]. It uses the nearest neighbors method instead of the random forest method.

[14] concluded that reference lists can classify scientific articles better than machine learning methods.

The reviews [15-16] list the following methods of text classification: “naive” Bayes classifier, nearest neighbors, decision trees, support vector machines, distribution of letter combinations (character -grams), logistic regression, based on artificial neural networks. In [] their advantages and disadvantages are identified, and a review of the results of comparison of classification methods is carried out.

The analysis showed great interest in determining the topics of scientific publications among scientists in Tajikistan [4,10].

Text classification is a rapidly developing field of computer science. This can be seen in the numerous reviews of text classification methods in recent years (see, for example, the 2022 reviews [17-18]).

The proposed methods for text classification continue to be researched and relate to modern computational linguistics. So far, none of them have become generally accepted. The reasons for this are the complexity of implementation and configuration.

Classical and modern computational linguistics and the mathematical apparatus they use

It is proposed to divide computer linguistics into classical and modern. The fundamental difference between these types of computational linguistics is the understanding of what a text is, but they solve the same problem of automatic text processing (AOT). Classical computational linguistics considers text as a carrier of meaning (the principle “Meaning \Leftrightarrow Text” [19]). Text processing is divided into processing levels: morphological, syntactic, semantic and sometimes pragmatic [20]. Modern computational linguistics considers text as a sequence of characters or words, as well as a sequence of words consisting of characters. Classical and modern computational linguistics use different concepts (Table 1) and mathematical apparatus (Table 2).

Table 1. Concepts of classical and modern computer linguistics

Classical computational linguistics	Modern computational linguistics
Morphological analysis and synthesis	Character -grams
Parsing and synthesis	Verbal -grams (shingles)
Semantic analysis and synthesis	Vector representation of the word
Meaning	Token
	Safe words

Table 2. Used mathematical apparatus of classical and modern computer linguistics

Classical computational linguistics	Modern computational linguistics
Theory of formal languages Logical model of knowledge representation Semantic model of knowledge representation (semantic networks)	Neural networks Vector distance Support Vector Machine Translation Memory

Read [15, 21] and you can easily determine what type of computational linguistics they belong to. Classical computational linguistics was unable to provide solutions to current problems, which led to the emergence of modern computational linguistics. However, the scientific potential of classical computational linguistics has not been exhausted..

The purpose of the work. Formalize the definition of the topics of scientific articles using syntactically related words using a mathematical model. We will use the approaches of classical computer linguistics, as well as the mathematical apparatus of set theory, propositional and predicate logic, fuzzy logic.

Abstract mathematical model of fuzzy classification by common objects

An abstract mathematical model of fuzzy classification based on common objects is proposed. Let there be objects:

$$B = \{b_1, b_2, \dots, b_{NB}\}.$$

Several objects make up an instance of a class:

$$E \subset B.$$

Objects can belong to one of the classes D_1, D_2, \dots, D_{ND} . Wherein

$$D_j \subset B; j = 1, 2, \dots, ND.$$

Each object belongs to at least one class:

$$\forall b_i \exists D_j (b_i \in D_j); i = 1, 2, \dots, NB.$$

Let us introduce a predicate that is true if it belongs to only one class:

$$C(b, D_i, D_1, D_2, \dots, D_{ND}) = \left((b \in D_i) \wedge \left(\bigwedge_{j=1}^{ND} \left((b \notin D_j) \vee (i = j) \right) \right) \right), i = 1, 2, \dots, ND.$$

Objects that belong to only one class are called class identifiers.

Введем функцию $h(D_i)$, возвращающее множество объектов H такое, что

$$H = h(D_i) = \{b: C(b, D_i, D_1, D_2, \dots, D_{ND})\}, H \subset D_i, H \subset B.$$

The degree of membership of a set to a class will be called a function:

$$\mu(E^*, D_i) = \frac{|E^* \cap h(D_i)|}{|h(D_i)|}, 0 \leq \mu(E^*, D_i) \leq 1.$$

The task of fuzzy classification is as follows. Let an instance of a class be given E^* . К какому классу D_1, D_2, \dots, D_{ND} копи E^* belongs to the greatest extent? Let us describe the classification function that solves this problem as:

$$MD = g(E^*, D_1, D_2, \dots, D_{ND}),$$

where MD – many sets D_1, D_2, \dots, D_{ND} .

Function $g(E^*, D_1, D_2, \dots, D_{ND})$ can be defined in several ways. For example, the classification result may be one class with the maximum membership degree:

$$g(E^*, D_1, D_2, \dots, D_{ND}) = \left\{ D: \max_{j=1,2,\dots,ND} (\mu(E^*, D_j)) \right\},$$

or a set of classes with a degree of membership greater than some value k :

$$g(E^*, D_1, D_2, \dots, D_{ND}) = \{D: \mu(E^*, D) > k\}, k = const, 0 < k < 1.$$

The classification result will be fuzzy and will be determined by the degree of membership.

Concretization of an abstract mathematical model of fuzzy classification with syntactically related words of the text of a scientific article as common objects

The following specification of an abstract mathematical model of fuzzy classification with syntactically related words of the text of a scientific article as common objects is proposed.

Let there be words:

$$W = \{w_1, w_2, \dots, w_{NW}\}.$$

Words used in the text. Text T is divided into sentences S :

$$T = \bigcup_{i=1}^N S_i, T \subset W.$$

There are various connections between words in a sentence. Let us determine the existence of a connection by numbered predicates:

$$r_k(w_i, w_j), i = 1, 2, \dots, NW, j = 1, 2, \dots, NW, k = 1, 2, \dots$$

One of the connections between words is the order of words in a sentence. Let us define it as the following predicate:

$$r_1(w_i, w_j) = \begin{cases} 1, & \text{если } w_j \text{ следует за } w_i, \\ 0, & \text{в противном случае.} \end{cases}$$

Predicate $r_1(w_i, w_j)$ can be used to determine whether a pair of words is a word bigram.

Another connection is the syntactic connection between words. For example, between subject and predicate. Let's define it by the predicate $r_2(w_i, w_j)$:

$$r_2(w_i, w_j) = \begin{cases} 1, & \text{если } w_i \text{ и } w_j \text{ связаны синтаксически,} \\ 0, & \text{в противном случае.} \end{cases}$$

Not all neighboring words are syntactically related:

$$\exists w_i \exists w_j (r_1(w_i, w_j) \wedge \overline{r_2(w_i, w_j)}).$$

Syntactic connection carries more information about words than the proximity of words, which is more promising in the study (Table 3). However, the syntactic connection is more difficult to highlight. We will use syntactically related words as common objects in an abstract mathematical model of fuzzy classification:

$$b = \langle w_i, w_j \rangle, r_2(w_i, w_j) = 1.$$

Table 3. Comparison of syntactically related words and word bigrams

Categories	Syntactically related words	Word bigrams
Receipt	Difficult, requires parsing	Simply, you need to divide the text into pairs
Example sentence "Computational linguistics is divided into classical and modern"	linguistics is divided computational linguistics divided into classical divided into modern	computational linguistics linguistics is divided shares the classic classic modern (without insignificant words)
Quality of the result	High, word pairs are syntactically related	Low, pairs of words are related by order in a sentence
Multilingual Suitability	Yes, pairs of words can be translated into another language while maintaining the syntactic connection	No, the order of words in sentences can be different in different languages.

DOSCUSSIONS

The proposed abstract mathematical model of fuzzy classification based on common objects is abstract. Common objects can be understood as objects from different subject areas. To solve the problem of fuzzy classification, syntactic related pairs of words of sentences in the text of a scientific article were selected. Syntactic connections between words carry more information than verbal bigrams, determined only by the order of words in a sentence.

The proposed abstract mathematical model of fuzzy classification by general objects and its specification are used in international research. The research proceeds according to the following plan:

1. Formation of a corpus of scientific articles on various topics.
2. Highlighting syntactically related words in the text.
3. Identification of syntactically related words specific to the topic.

4. Testing the classification function and, if necessary, modifying it.
In the future, it is planned to develop a method for classifying multilingual texts.

CONCLUSION

The article presents the following scientific results:

1. An analysis of methods for classifying scientific publications was carried out. The main methods are the "naive" Bayes classifier, -nearest neighbors, support vector machines. Some studies were carried out by scientists from Tajikistan. It is concluded that not a single method of text classification has become generally accepted.

2. It is proposed to divide computer linguistics into two types: classical and modern. Unlike modern computational linguistics, classical computational linguistics considers text as a carrier of meaning. For the selected types of computer linguistics, the concepts and mathematical apparatus used are defined.

3. An abstract mathematical model of fuzzy classification based on common objects has been developed. The model involves determining the degree of class membership by the ratio of the number of common objects of instances to the number of objects belonging to the class. To formalize the model, set theories, propositional and predicate logics, and fuzzy logic are used.

4. A specification of an abstract mathematical model of fuzzy classification based on common objects has been developed. It is proposed to use syntactically related pairs of words as common objects. It is concluded that syntactically related words are more promising in research than verbal bigrams, determined by the order of words in a sentence.

The formalization of an abstract mathematical model of fuzzy classification by general objects and its specification were carried out in an international study. In the future, the model and its specification will be applied practically to classify scientific articles.

**Reviewer: Komilien F.S.,
Doctor of Physical and Mathematical Sciences,
Professor**

REFERENCES

1. Prutzkow, A.V. Problems of automatic text processing in natural languages and possible mathematical approaches to their solutions / A.V. Prutzkow // Bulletin of the Ryazan State Radio Engineering University. – 2016. – No. 1 (55). – Pp. 81-86.
2. Prutzkow, A.V. Mathematical and algorithmic formalization of models of morphological analysis and synthesis of word forms in natural languages / A.V. Prutzkow // Cloud of Science. – 2018. – Vol. 5. – No. 4. – Pp. 729-748.
3. Prutzkow, A.V. Determination and generation of complex forms of words in natural languages in morphological analysis and synthesis / A.V. Prutzkow // News of the Taganrog State Radio Engineering University. – 2006. – Vol. 70. – No. 15. – Pp. 10-14.
4. Kosimov, A.A. Determining a specialty code using symbolic unigrams / A.A. Kosimov // Information exchange in interdisciplinary research: collection. tr. All-Russian scientific-practical conf. with international participation. – Ryazan: RGRTU, 2022. – 163 p.
5. Kurbonov, N.M. On automatic recognition based on unigrams of ciphers of abstracts on pedagogy / N.M. Kurbonov // Polytechnic Bulletin. Intelligence Series. Innovation. Investments. – 2021. – No. 3 (55). – Pp. 47-51.
6. Karimov A.A. On automatic recognition based on word forms of ciphers of abstracts in economics / A.A. Karimov // Polytechnic Bulletin. Intelligence Series. Innovation. Investments. – 2021. – No. 4 (55). – Pp. 54-58.

7. Polyakov, P.Yu. Study of the applicability of thematic classification methods in the problem of classifying book reviews / P.Yu. Polyakov, M.V. Kalinina, V.V. Pleshko // Computer linguistics and intellectual technologies: based on annual materials. International conf. Dialogue. – M.: IPI RAS, 2012. – Vol. 2. – Pp. 51-59.
8. Musidze, V.T. Application of methods for classifying text data in accordance with a given topic in contextual processing of general scientific information / V.T. Musidze, I.M. Lazareva // Problems of the Arctic region: tr. XVI International scientific conf. – Murmansk: Polygraphist, 2017. – Pp. 78-82.
9. Kozlov, P.A. Comparative analysis of binary classifiers on an array of scientific publications / P.A. Kozlov, A.S. Mokhov, N.A. Nazarov, Sh.I. Safin, V.O. Tolcheev // Factory laboratory. Diagnostics of materials. – 2022. – Vol. 88. – No. 7. – Pp. 79-87.
10. Maksudov, Kh. T. Comparative analysis of the “decision tree” and “random forest” methods - in determining the speciality of scientific texts / Kh. T. Maksudov, B. B. Inomov, N. M. Mullojanov // Bulletin of the Tajik National University. Natural Sciences Series. – 2019. – No. 3. – Pp. 23-29.
11. Leonova, Yu.V. On the approach to solving the problem of thematic classification of abstracts / Yu.V. Leonova, A.M. Fedotov // Bulletin of Novosibirsk State University. Series: Information technologies. – 2017. – Vol. 15. – No. 1. – Pp. 47-58.
12. Gürbüz, T. Research Article Classification with Text Mining Method // T. Gürbüz, Ç. Uluyol // Concurrency Computat Pract Exper. – 2023. – Vol. 35. – No. 1. – P.7437. DOI: 10.1002/cpe.7437.
13. Dien, T.T. et al. Article Classification Using Natural Language Processing and Machine Learning / T.T. Dien et al. // 2019 International Conference on Advanced Computing and Applications (ACOMP). – 2019. – Pp. 78–84.
14. Rivest, M. Article-Level Classification of Scientific Publications: A Comparison of Deep Learning, Direct Citation and Bibliographic Coupling / M. Rivest, E. Vignola-Gagne, E. Archambault // PLoS ONE. – 2021. – Vol. 16. – No. 5. – P.0251493. DOI: 10.1371/journal.pone.0251493.
15. Batura, T.V. Methods for automatic text classification / T.V. Batura // Software products and systems. – 2017. – Vol. 30. – No. 1. – Pp. 85-99.
16. Danilov, G.V. Comparative analysis of statistical methods for classifying scientific publications in the field of medicine / G.V. Danilov, V.V. Zhukov, A.S. Kulikov, E.S. Makashova, N.A. Mitin, Yu.N. Orlov // Computer research and modeling. – 2020. – Vol. 12. – Issue. 4. – Pp. 921-933. DOI: 10.20537/2076-7633-2020-12-4-921-933.
17. Li, Q. A Survey on Text Classification: From Traditional to Deep Learning / Q. Li, H. Peng, J. Li, C. Xia, R. Yang, L. Sun, P. Yu, L. He // ACM Trans. Intel. Syst. Technol. – 2022. – Vol. 13. – No. 2. – Art. 31 (April 2022). – 41 p. DOI: 10.1145/3495162.
18. Gasparetto, A. A Survey on Text Classification Algorithms: From Text to Predictions / A. Gasparetto, M. Marcuzzo, A. Zangari, A. Albarelli // Information. – 2022. – Vol. 13. – No. 83. – 39 p. DOI: 10.3390/info13020083.
19. Melchuk, I.A. Russian language in the “Meaning-Text” model. Semantics, syntax / I.A. Melchuk. – M.: Sch. “Languages of Russian culture”, 2005. – 682 p.
20. Artificial intelligence. In 3 books. Book 1. Communication systems and expert systems: a reference book / ed. E.V. Popova. – M.: Radio and Communications, 1990. – 464 p.
21. Gladky, A.V. Elements of mathematical linguistics / A.V. Gladky, I.A. Melchuk. – M.: Nauka, 1969. – Pp. 193.

MATHEMATICAL MODEL OF FUZZY RECOGNIZING OF THE TOPICS OF SCIENTIFIC ARTICLES USING SYNTACTICALLY RELATED WORDS

Mathematical methods are widely used to formalize the solution of problems of automatic text processing, including text classification. To classify texts, a “naive” Bayes classifier, methods of k -nearest neighbors, decision trees, support vector machines, distribution of letter combinations (character n -grams), logistic regression, and approaches based on artificial neural networks are used. These methods are used by modern computational linguistics. Classical computational linguistics considers text as a carrier of meaning. The purpose of the study is to formalize the definition of the topics of scientific articles using syntactically related words by a mathematical model, and therefore classical computer linguistics. We propose an abstract mathematical model of fuzzy classification based on common objects. The model assumes that some objects belong to only one class and are class identifiers. The result of a fuzzy classification can be one or more classes. For each class a degree of membership is determined. We propose a specification of the model with in which the common objects are syntactically related pairs of words. We conclude syntactically related words are more promising in research than verbal bigrams determined by sentence order. We propose the

model in our international study. The study involve the creation of a corpus of scientific articles and their distribution by topic. The corpus will be used to classify scientific articles by topic.

Key words: natural text processing, text classification, syntactic analysis, mathematical model, fuzzy classification, scientific article, text corpus.

Information about the authors: - **Murodov Parviz Saizhafarovich** – Tajik National University, Ph.D student of the Department of Informatics. **Address:** 734025, Dushanbe, Republic of Tajikistan, Rudaki Avenue, 17. **Phone:** (+992) 904-49-77-11. **E-mail:** mr.murodov93@mail.ru.

Prutzkow Alexander Viktorovich – Ryazan State Radio Engineering University named after V.F. Utkin, Doctor of Engineering, professor of the department of computational and applied mathematics. **Address:** 390005, Ryazan, Russian Federation, Gagarina str., 59/1. **Phone:** +7 (4912) 72-03-64. **E-mail:** mail@prutzkow.com.

Article received 19.12.2023
Approved after review 26.02.2024
Accepted for publication 29.03.2024

ON THE APPROXIMATION OF UNIFORM ALMOST PERIODIC FUNCTIONS BY CERTAIN SUMS AND INTEGRALS

Talbakov F.M.

Introduction. L_p ($1 \leq p < \infty$) space of measurable period 2π for each of the variable functions, $f(x, y)$, with norm

$$\|f\|_{L_p} = \left\{ \int_0^{2\pi} \int_0^{2\pi} |f(x, y)|^p dx dy \right\}^{\frac{1}{p}} < \infty,$$

and with $p = \infty$

$$\|f\|_{L_p} = \text{vraisup}_{x,y} |f(x, y)| < \infty.$$

The Fourier series of this function has the form

$$f(x, y) = \sum_{k=0}^{\infty} \sum_{l=0}^{\infty} A_{k,l}(x, y),$$

where the coefficients of this series are determined by the formulas

$$A_{k,l}(x, y) = a_{k,l} \cos kx \cos ly + b_{k,l} \sin kx \cos ly + c_{k,m} \cos kx \sin ly + d_{k,m} \sin kx \sin ly (k, l \leq 1),$$

$$A_{k,0}(x, y) = \frac{1}{2}$$

$$A_{0,l}(x, y) = \frac{1}{2}$$

$$A_{0,0} = \frac{1}{4} a_{0,0}.$$

In 1964, I. Martinkevich [4, p. 530] investigated the issue of deviation of sums of the form

$$\sigma_n(f; x, y) = (n+1)^{-1} \sum_{k=0}^m S_{k,k}(f; x, y),$$

where $S_{k,k}(f; x, y)$ – partial sums of order k for each variable of the Fourier series of the function $f(x, y) \in L_p$ ($1 \leq p \leq \infty$). In particular, he pointed out that $f(x, y)$ if the set of variables is continuous, then the estimate x, y , is fair

$$R_n(f)_{L_\infty} = \|f(x, y) - \sigma_n(f; x, y)\|_{L_\infty} \rightarrow 0 (n \rightarrow \infty).$$

In the work of L.V. Zhizhiashvili [5, p. 527] some estimates were obtained about the rate at which the quantity tends to zero

$$R_n(f)_{L_p} = \|f(x, y) - \sigma_n(f; x, y)\|_{L_p} (1 < p \leq \infty).$$

Behavior of the deviation of a function of two variables from sums of the form

$$W_r(f; x, y) = (1-r) \sum_{k=0}^{\infty} r^k S_{k,k}(f; x, y)$$

at $0 < r < 1$ и $r \rightarrow \infty$, and and were studied in the work of R. Tabersky [6, p. 310]. Some clarifying assessments of the results of L.V. Zhizhiashvili and R. Tabersky are given in the work of M.F. Timan and G. Gaimnazarov [7] in 1972. M.F. Timan and V.G. Ponomarenko [8, p. 61-63] investigated the question of the behavior of the quantity

$$R_n(f; \nu)_{L_p} = \left\| f(x, y) - \sum_{k=0}^n \nu_{k,k}(f; x, y) \right\|_{L_p} \quad (1)$$

for classical triangular matrices $\{\mu_{k,n}\}$

$$\{\mu_{k,n}\} = \begin{cases} \frac{A_{n-k}^{\alpha-1}}{A_k^\alpha}, & k \leq n; \\ 0, & k > n. \end{cases}$$

For quantity (1), an upper estimate is given in [5], and a lower estimate for this quantity is established in [7]. In [8], some estimates from the works of L.V. were also refined. Zhizhiashvili [5] and R. Taberski [6]. And also for any natural r in [3, p. 562] obtained exact order equalities for a triangular matrix

$$\{\mu_{k,n}\} =$$

It has been established that if $f(x, y) \in L_p$ (2), then the $\{\mu_{k,n}\}$ are defined in the form of a triangular matrix

$$R_n(f; \nu)_{L_p} \leq c_r (n+1)^{-r} \sum_{\nu=0}^n (\nu+1)^{r-1} E_{\nu,\nu}(f)_{L_p},$$

where

$$E_{\nu,\nu}(f)_{L_p} = \inf_{T_{k,k}} \|f(x, y) - T_{\nu,\nu}(x, y)\|_{L_p},$$

$T_{\nu,\nu}$ - trigonometric polynomials of order no higher than n in each of the variables, and the constant c_r depends only on r .

If $f(x, y) \in L_p$ ($1 < p \leq \infty$) and $\{\mu_{k,n}\}$ are defined by relation (2), then in [5, p. 549-550] estimates were obtained using continuity modules, that is

$$R_n(f; \nu)_{L_p} \leq c_{p,k} \left(\omega_k^{(1)}\left(f; \frac{1}{n}\right)_{L_p} + \omega_k^{(2)}\left(f; \frac{1}{n}\right)_{L_p} \right),$$

where

$$\omega_k^{(1)}(f; u)_{L_p} = \sup_{|h| \leq u} \|\Delta_{x,h}^k f\|_{L_p}, \quad \omega_k^{(2)}(f; u)_{L_p} = \sup_{|h| \leq u} \|\Delta_{h,y}^k f\|_{L_p},$$

$$\Delta_{x,h}^k f = \sum_{\nu=0}^k (-1)^{k-\nu} \binom{k}{\nu} f(x + \nu h, y),$$

$$\Delta_{h,y}^k f = \sum_{\nu=0}^k (-1)^{k-\nu} \binom{k}{\nu} f(x, y + \nu h) \quad (u > 0, k \in \mathbb{N}),$$

$c_{p,k}$ - constant depending on p и k .

In $1 < p < \infty$ в [8, с. 60] the following results were also obtained:

$$a) \omega_k^{(1)} \leq M_{p,k} R_n(f; \mu)_{L_p}, \quad \omega_k^{(2)} \leq M_{p,k} R_n(f; \mu)_{L_p},$$

where $M_{p,k}$ – constant depending on p и k ;

$$b) R_n(f; \mu)_{L_p} \leq \omega_k^{(1)}\left(f; \frac{1}{n}\right)_{L_p} + \omega_k^{(2)}\left(f; \frac{1}{n}\right)_{L_p};$$

$$c) \|f(x, y) - W_r(f; x, y)\|_{L_p} \leq c_p \left(\omega_1^{(1)}(f; 1-r)_{L_p} + \omega_1^{(2)}(f; 1-r)_{L_p} \right);$$

$$d) \omega_1^{(1)}(f; 1-r)_{L_p} \leq M_p \|f(x, y) - W_k(f; x, y)\|_{L_p};$$

$$e) \omega_1^{(2)}(f; 1-r)_{L_p} \leq M_p \|f(x, y) - W_k(f; x, y)\|_{L_p}.$$

In the work of Yu.Kh. Khasanova [11, p. 83] obtained analogues of the above results on the behavior of deviations of functions of two variables $f(x, y)$, given on the plane from the integral averages of their Fourier transforms in the space metric $L_p(R^2)$ ($1 \leq p < \infty$).

$f(x, y) \in L_p(R^2)$ - space of measurable functions $f(x, y)$, for which

$$\|f\|_{L_p} = \left\{ \int_{-\infty}^{\infty} \int_{-\infty}^{\infty} |f(x, y)|^p dx dy \right\}^{\frac{1}{p}} < \infty$$

and almost everywhere there is a Fourier transform

$$F(t, z) = \frac{1}{2\pi} \int_{-\infty}^{\infty} \int_{-\infty}^{\infty} f(u, v) \exp(-i(tu + zv)) dudv,$$

где $F(t, z) \in l_q(R^2)$ ($\frac{1}{p} + \frac{1}{q} = 1$).

In $\sigma > 0$ consider private sums

$$S_{\sigma, \sigma}(f; x, y) = \int_{-\sigma}^{\sigma} \int_{-\sigma}^{\sigma} F(t, z) e^{i(tx+zy)} dt dz = \int_{-\sigma}^{\sigma} S_{u, u}(f; x, y) du, \quad (3)$$

where

$$S_{u, u}^*(f; x, y) = \int_{-u}^u A(t, u) dt + \int_{-u}^u A(t, -u) dt + \int_{-u}^u A(u, z) dz + \int_{-u}^u A(-u, z) dz.$$

We investigate the order of behavior of the deviation value

$$R_{\sigma, r} \quad (4)$$

where

$$U_{\sigma, r} f(x, y) = \int_0^{\sigma} \left(1 - \frac{u^r}{\sigma^r}\right) S_{u, u}(f; x, y) du.$$

The following statements hold [11]:

Theorem A. If $f \in L_p(R^2)$ ($1 < p \leq 2$), then the following assessment is fair

$$R_{\sigma, k}(f; L_p) \leq c_{p, k} \left(\omega_k^{(1)} \left(f; \frac{1}{\sigma} \right)_{L_p} + \omega_k^{(2)} \left(f; \frac{1}{\sigma} \right)_{L_p} \right),$$

where $c_{p, k}$ - constant that depends only on u и k .

Theorem B. In $f(x, y) \in L_p(R^2)$ ($0 < p \leq 2$). Then it holds

$$\omega_k^{(v)} \left(f; \frac{1}{\sigma} \right)_{L_p} \leq M_{p, k} R_{\sigma, k}(f)_{L_p} \quad (v = 1, 2),$$

$M_{p, k}$ - constant that depends only p и k .

From Theorems A and B it follows that if the conditions of Theorem B hold, then for any natural k , number the estimate is

$$R_{\sigma, k}(f; L_p) \leq c_{p, k} \left(\omega_k^{(1)} \left(f; \frac{1}{\sigma} \right)_{L_p} + \omega_k^{(2)} \left(f; \frac{1}{\sigma} \right)_{L_p} \right).$$

In $p = \infty$ и $k = 1$ similar results were obtained in [9], and for the case of periodic functions, in work [5].

MAIN RESULTS

Now we present the results of this section of the upper estimate for the deviation of functions $f(x) \in B$ from sums of Marcinkiewicz type, when the Fourier exponents have a single limit point at infinity.

In $B(R)$ – space of all bounded functions $f(x) \in B$ with the norm (см., for example, [1], [2])

$$\|f\|_B = \sup_{x \in R} |f(x)|$$

and the function $f(x) \in B$ has a Fourier series of the form

$$f(x) = \sum_{k=-\infty}^{\infty} A_k \exp(i\lambda_k x), \quad (8)$$

with odds

$$A_k = \lim_{T \rightarrow \infty} \frac{1}{2T} \int_{-T}^T f(x) \exp(-i\lambda_k x) dx,$$

where numbers $\{\lambda_k\}$ – are Fourier exponents that have a single limit point at infinity, that is (see, for example, [14, p. 814] and, [14, c. 814] и [15, c. 55])

$$\lambda_0 = 0, \lambda_{-n} = -\lambda_n, |\lambda_n| < |\lambda_{n+1}|, \lim_{n \rightarrow \infty} \lambda_n = \infty.$$

Let us introduce into consideration

$$S_\sigma(f; x)_B = \sum_{|\lambda_n| \leq \sigma} A_n \Phi_\sigma(\lambda_n) e^{i\lambda_n x},$$

where $\Phi_\sigma(t) \in R$ continuous and even function such that $\Phi_\sigma(0) = 1, \Phi_\sigma(t) = 0$ in $|t| \leq \sigma$;

$$\psi_\sigma(t) \in L(-\infty, \infty), \quad (9)$$

where

$$\psi_\sigma(u) = \frac{1}{2\pi} \int_{-\infty}^{\infty} \Phi_\sigma(t) e^{-iut} dt.$$

First, we prove the following auxiliary statement, which has an independent character.

Lemma 1. *If the function $f(x) \in B$, then*

$$S_\sigma(f; x) = U_\sigma(f; \varphi; x) = \int_{-\infty}^{\infty} f(x+t) \Phi_\sigma(t) dt.$$

Proof.

$$f_\sigma(x) = \int_{-\infty}^{\infty} f(x+t) \Phi_\sigma(t) dt$$

Then, by virtue of (9), we obtain that

$$\begin{aligned} |f_\sigma(x+\tau) - f_\sigma(x)| &\leq \int_{-\infty}^{\infty} |f(x+t+\tau) - f(x+t)| |\psi_\sigma(t)| dt \leq \\ &\leq \sup_x |f(x+\tau) - f(x)| \int_{-\infty}^{\infty} |\psi_\sigma(t)| dt. \end{aligned}$$

The integral on the right side of the last inequality converges and

$$|f(x+t+\tau) - f(x+t)| < \varepsilon.$$

Therefore, from the last inequality it follows that the function $f(x) \in B$.

Let us denote $D(\lambda_n)$ the Fourier coefficients of the functions $f_\sigma(x) \in B$, that correspond to the exponents λ_n . Then we have

$$\begin{aligned} \frac{1}{2T} \int_{-T}^T f_\sigma(x) e^{-i\lambda_n x} dx &= \frac{1}{2T} \int_{-T}^T \int_{-\infty}^{\infty} f(x+t) \psi_\sigma(t) e^{-i\lambda_n x} dt dx = \\ &= \int_{-\infty}^{\infty} \psi_\sigma(t) dt \frac{1}{2T} \int_{-T}^T f(x+t) e^{-i\lambda_n x} dx = \end{aligned}$$

$$\begin{aligned}
& \int_{-\infty}^{\infty} \psi_{\sigma}(t) \left(\frac{1}{2T} \int_{-T}^T f(x+t) e^{-i\lambda_n x} dx \right) dt = \\
& \int_{-\infty}^{\infty} \psi_{\sigma}(t) \left(\frac{1}{2T} \int_{-T+t}^{T+t} f(x) e^{-i\lambda_n(x+t)} dx \right) dt = \\
& + \int_{-\infty}^{\infty} \psi_{\sigma}(t) \left(\frac{1}{2T} \int_{-T+t}^{T+t} f(x) e^{-i\lambda_n x} e^{-i\lambda_n t} dx \right) dt = \\
& \int_{-\infty}^{\infty} \psi_{\sigma}(t) e^{-i\lambda_n t} \left(\frac{1}{2T} \int_{-T+t}^{T+t} f(x) e^{-i\lambda_n x} dx \right) dt.
\end{aligned}$$

The internal integral in the latter is the pre-limit expression of the Fourier coefficients of the function. Hence, according to the Fourier inversion formula

$$\int_{-\infty}^{\infty} \psi_{\sigma}(t) e^{-i\lambda_n t} dt = \Phi_{\sigma}(\lambda_n).$$

That's why $D(\lambda_n) = A_n \Phi_{\sigma}(\lambda_n)$ and

$$f_{\sigma}(x) = \sum_{|\lambda_n| \leq \sigma} A_n \Phi_{\sigma}(\lambda_n) e^{i\lambda_n x}.$$

If $f(x) \in B$, then the statement of the lemma follows from the latter.

Let $B(R)$ – space of all bounded functions $f(x) \in B$ with the norm (for example see, [1], [2])

$$\|f\|_B = \sup_{x \in R} |f(x)|.$$

Let's consider the quantity

$$R(f; x) = \|U_{\sigma}(f; \varphi; x) - f(x)\|_B, \quad (10)$$

in which

$$U_{\sigma}(f; \varphi; x) = \int_{-\infty}^{\infty} f(x+t) \Phi_{\sigma}(t) dt, \quad \Phi_{\sigma}(t) = \frac{1}{2\pi} \int_0^{\infty} \varphi_{\sigma}(u) K_m(t) du, \quad (11)$$

where, $\varphi_{\sigma}(u)$ – some absolutely integrable on the interval $(0, \infty)$ function for every fixed $\sigma > 0$, then

$$\int_{-\infty}^{\infty} |\Phi_{\sigma}(t)| dt = 1. \quad (12)$$

depending on the speed of approaching zero $E_{\sigma}(f)$ ($\sigma \rightarrow \infty$) for the cases when

$$\varphi_{\sigma}(u) = \varphi_{\sigma,a}(u) = \begin{cases} 1, & |u| \leq a \quad (0 < a < \sigma); \\ \frac{\sigma - |u|}{\sigma - a}, & a < |u| < \sigma; \\ 0, & |u| \geq \sigma, \end{cases} \quad (13)$$

Let us study the behavior of quantity (10). It is known that [8] (see [8, p. 60], Theorem 1)

$$\int_{-\infty}^{\infty} |\Phi_{\sigma,a}(t)| dt \leq C \frac{\sigma + a}{\sigma - a}, \quad (14)$$

where C – constanta.

Theorem 1. Let $f(x) \in B(R)$ and function $\varphi_{\sigma}(u) = \varphi_{\sigma,a}(u)$ is determined by relation (13). Then for any Λ ($0 < \Lambda < a < \sigma$) there is an assessment

$$R(f; \varphi_{\sigma}) \leq C \frac{\sigma + a}{\sigma - a} E_{\Lambda}(f)_B, \quad (15)$$

where C – is an absolute constant.

Proof. We write relation (12) in the form

$$\int_0^{\infty} \Phi_{\sigma}(t) dt = \frac{1}{2}.$$

Multiply both sides of the latter by $f(x)$ and subtract the resulting equality from (11) at $\Phi_{\sigma}(t) = \Phi_{\sigma,a}(t)$, then we would have

$$\begin{aligned} \Delta_{\sigma,a}(f; x) &= U_{\sigma}(f; \varphi; x) - f(x) = \\ &= \int_{-\infty}^{\infty} (f(x+t)\Phi_{\sigma,a}(t) - f(x)\Phi_{\sigma,a}(t)) dt = \\ &= \int_0^{\infty} [f(x+t) - f(x-t)]\Phi_{\sigma,a}(t) dt - 2 \int_0^{\infty} f(x)\Phi_{\sigma,a}(t) dt = \\ &= \int_0^{\infty} [f(x+t) - f(x-t) - 2f(x)]\Phi_{\sigma,a}(t) dt = \\ &= \int_0^{\infty} \Omega_x(f; t)\Phi_{\sigma,a}(t) dt, \end{aligned}$$

where $\Omega_x(f; t) = f(x+t) + f(x-t) - 2f(x)$.

In

$$T_r = \sum_{|\lambda_m| \leq r} A_m e^{i\lambda_m x}$$

an arbitrary trigonometric polynomial and $0 < \Lambda < a < \sigma$. Then (see [14, p. 14], Theorem 3)

$$T_{\Lambda}(x) = \int_{-\infty}^{\infty} \sum_{|\lambda_m| \leq r} T_{\Lambda} f(x+t)\Phi_{\sigma,a}(t).$$

It is easy to show that for the polynomial $T_{\Lambda}(x)$

$$\int_0^{\infty} \Omega_x(T_{\Lambda}; f; t)\Phi_{\sigma,a} dt = 0.$$

Indeed, by virtue of estimate (12), we obtain

$$\begin{aligned} & \int_0^{\infty} \Omega_x(T_{\Lambda}; f; t)\Phi_{\sigma,a}(t) dt = \\ &= \int_0^{\infty} [T_{\Lambda}(x+t) + T_{\Lambda}(x-t) - 2T_{\Lambda}(x)]\Phi_{\sigma,a}(t) dt = \\ &= \int_{-\infty}^{\infty} T_{\Lambda}(x+t)\Phi_{\sigma,a}(t) dt - \int_{-\infty}^{\infty} T_{\Lambda}(x)\Phi_{\sigma,a}(t) dt = \\ &= T_{\Lambda}(x) - T_{\Lambda}(x) \int_{-\infty}^{\infty} \Phi_{\sigma,a}(t) dt = 0 \end{aligned}$$

So,

$$\Delta_{\sigma,a}(f; x) = \int_0^{\infty} \Omega_x[(f - T_{\Lambda}); t]\Phi_{\sigma,a}(t) dt. \quad (16)$$

In

$$\|f(x) - T_{\Lambda}(x)\| = E_{\Lambda}(f)_B,$$

where $T_r(x)$ –trigonometric polynomial that provides the best approximation of the order Λ , then

$$\|\Omega_x[(f - T_{\Lambda}); t]\|_B = 4E_r(f)_B. \quad (17)$$

From (14), (17) and (16) estimate (15) follows. Theorem 1 is proven.

Theorem 2. *If $f(x) \in B$, whose Fourier exponents have a unique limit point at infinity, that is $\lambda_m \rightarrow \infty$. Then the estimate is valid*

$$\left\| f(x) - (n+1)^{-1} \sum_{k=0}^n S_k(f; x) \right\|_B \leq M(n+1)^{-1} \sum_{k=0}^n E_\Lambda(f)_B, \quad (\text{B})$$

where M – constanta and

$$E_\Lambda(f; x)_B = \inf_{A(\lambda_n)} \left\| f(x) - \sum_{|\lambda_n| \leq k} A_n e^{i\lambda_n x} \right\|_B$$

- value of the best approximation of the function $f(x)$ trigonometric polynomials of degree not higher than Λ .

Proof. If $n \in [2^m; 2^m + 1]$. Then

$$\begin{aligned} R_n(f)_B &= \left\| f(x) - (n+1)^{-1} \sum_{k=0}^n S_k(f; x) \right\|_B = \\ &= \left\| (n+1)^{-1} \sum_{k=0}^n (f(x) - S_k(f; x)) \right\|_B = \\ &= (n+1)^{-1} \left\| \sum_{k=0}^{m-1} \sum_{k=2^v}^{2^{v+1}-1} (f(x) - S_k(f; x)) + f(x) - S_0(f; x) + \sum_{r=2^m}^n (f(x) - S_k(f; x)) \right\|_B \leq \\ &\leq (n+1)^{-1} \left\| \sum_{v=0}^{m-1} 2^v \cdot \frac{1}{2^v} \sum_{k=2^v}^{2^{v+1}-1} (f(x) - S_k(f; x)) \right\|_B + \\ &\quad + (n+1)^{-1} \|f(x) - S_0(f; x)\|_B + \\ &\quad + (n+1)^{-1} \left\| \sum_{k=2^m}^n (f(x) - S_k(f; x)) \right\|_B. \quad (18) \end{aligned}$$

By Theorem 1 we have

$$\left\| 2^{-v} \sum_{k=2^v}^{2^{v+1}-1} (f(x) - S_k(f; x)) \right\|_B \leq M E_{2^{v+1}-1}(f)_B, \quad (19)$$

$$\left\| \sum_{k=2^v}^m (f(x) - S_k(f; x)) \right\|_B \leq M(n-2^m) E_{2^{m-1}}(f)_B. \quad (20)$$

Substituting (19), (20) into (18), we obtain

$$\begin{aligned} R_n(f)_B &\leq M(n+1)^{-1} \sum_{v=0}^{m-1} 2^v E_{2^{v+1}-1}(f)_B + (n+1)^{-1} E_0(f)_B + \\ &\quad + M(n+1)^{-1} (n-2^m) E_{2^{m-1}}(f)_B \leq \\ &\leq M(n+1)^{-1} \sum_{v=0}^{m-1} 2^v E_{2^{v+1}-1}(f)_B + (n+1)^{-1} E_0(f)_B + \\ &\quad + M(n+1)^{-1} E_{2^{m-1}}(f)_B \leq \\ &\leq M_1(n+1)^{-1} \sum_{k=0}^{2^m} E_k(f)_B \leq M_1(n+1)^{-1} \sum_{k=0}^n E_k(f)_B. \end{aligned}$$

This implies inequality (B), which completes the proof of Theorem 2. An analogue of Theorem 2 for periodic functions was established in the work of M.F. Timan and V.G. Ponomarenko [8], and for the class of almost periodic functions in the sense of Bohr and Besicovich in [11]-[16].

**REVIEWER: Abdugarimov M.F.,
Doctor of Physical and Mathematical Sciences,
Associate Professor**

REFERENCES

1. Besicovitch A.S. Almost periodic functions / A.S Besicovitch. – Cambridge. – 1932. – 180 p.
2. Bohr G. Almost periodic functions / G. Bohr. – M.: LIBROKOM, 2009. –128 p.
3. Bernshtein S.N. Collected Works / S.N. Bernstein // – M.: Publishing house. USSR Academy of Sciences. – 1954. –T. 2. – 627 p.
4. Marcinkewisz I. Sur une metode remarquable de sommation des series doubles de Fourier / I. Marcinkewisz // Collected papers, Warszawa. – 1964. – Pp. 527-538.
5. Zhizhiashvili L.V. On the summation of double Fourier series / L.V. Zhizhiashvili // Sib. Mat. Magazine. - T. VIII. – No. 3. – 1967. – Pp. 548-564.
6. Taberski R. Abel summability of double Fourier series / R. Taberski // Bull. Acad. Polon. Sci. Ser. Sci. Msth. Astron. Et phys., Vol. 18. – No. 6. – 1970. – Pp.307-314.
7. Timan M.F., Deviation of periodic functions of two variables from some polynomials / M.F. Timan, G. Gaimnazarov // Reports of the Taj Academy of Sciences. SSR. - 1972. – T.15. - No. 5. – Pp. 6-8.
8. Timan M.F., On the approximation of functions of two variables by sums of Martsinkevich type / M.F. Timan, V.G. Ponomarenko // News of universities. Mathematics. - 1975. - No. 9. – Pp. 59–67.
9. Timan M.F., On the absolute convergence of Fourier series of almost periodic functions [Text] / M.F. Timan, Yu.H. Khasanov // Fourier series: theory and applications. Kyiv, Institute of Mathematics of the Academy of Sciences of Ukraine. - 1992. – Pp. 142-146.
10. Titchmarsh E. Theory of functions [Text] / E. Titchmarsh // - M.: Nauka, - 1980. – P. 464.
11. Khasanov Yu.Kh. On the approximation of almost periodic functions of two variables / Yu.Kh. Khasanov // News of universities. Mathematics. - 2010. - No. 12. – Pp. 82-86.
12. Khasanov, Yu.Kh. On the absolute convergence of Fourier series of almost periodic functions / Yu.Kh. Khasanov // Matem. notes. – 2013. –T.94. – No. 5. – Pp. 745-756.
13. Talbakov F.M. An analogue of the theorem of S.N. Bernstein on the best approximation of almost periodic functions / Yu.Kh. Khasanov, F.M. Talbakov // DAN RT. - 2016. - T.59. - No. 1-2. – Pp. 11-18.
14. Talbakov, F.M. On the absolute convergence of Fourier series of almost periodic Besicovitch functions / F.M. Talbakov, Yu.Kh. Khasanov // DAN RT. – 2018. - T.61. – No. 1-2. – Pp. 813-821.
15. Talbakov, F.M. On the absolute convergence of Fourier series of uniform almost periodic functions and some questions of their approximation / F.M. Talbakov. Dissertation for the degree of candidate of physical and mathematical sciences NAST Institute of Mathematics named after. A. Juraeva. – 2020. – P. 84.
16. Talbakov, F.M. On the absolute convergence of double Fourier series of almost periodic functions in the uniform metric / F.M. Talbakov // News of higher educational institutions. Mathematics. - 2023. – № 4. – Pp. 65-75.

ON THE APPROXIMATION OF UNIFORM ALMOST-PERIODIC FUNCTIONS BY SOME SUMS AND INTEGRALS

The paper investigates some issues of approximation of almost-periodic Bohr functions from partial sums of the Fourier series and the Marcinkevich averages, when the Fourier exponents (the spectrum of the function) of the functions under consideration have a limit point at infinity. The question of the deviation of a given function $f(x)$ from its partial sums of the Fourier series is investigated, depending on the rate of tendency to zero of the magnitude of the best approximation by a trigonometric polynomial of bounded degree. Here, when determining the Fourier coefficients, instead of the function under consideration, some arbitrary, real, continuous function $\Phi_\sigma(t)$ ($\sigma > 0$), is taken, which in a given interval is equal to one, and in other cases is zero. Then, similarly, the upper estimate of the deviation of the almost-periodic in the sense of the Bohr function by the Marcinkevich averages is established.

Keywords: uniform almost-periodic functions, Fourier series, function spectrum, Fourier coefficients, limit point at infinity, Marcinkevich averages, trigonometric polynomial, best approximation.

Information about the author: – Talbakov Farkhodjon Makhmadshoevich - Tajik State Pedagogical University named after. S. Aini, Candidate of Physical and Mathematical Sciences, Associate Professor,

Head of the Department of Geometry and Higher Mathematics. **Address:** 734003, Dushanbe, Republic of Tajikistan, Rudaki, 121. E-mail: talbakov_90@mail.ru.

Article received 25.12.2023
Approved after review 13.01.2024
Accepted for publication 07.03.2024

POVERTY LINE, POVERTY THRESHOLD, POVERTY FORECASTING, METHODS

Pejman Jafari

INTRODUCTION. In today's economy, understanding and measuring poverty is crucial for policymakers, researchers, and organizations working to address economic disparities and improve the well-being of individuals and communities. One common method used to calculate poverty thresholds is the Slack Base method, which helps determine the upper and lower limits of poverty and forecast future trends. By using this method, stakeholders can gain valuable insights into the extent of poverty and make informed decisions on resource allocation and intervention strategies.

The Slack Base method is a widely recognized approach for calculating poverty thresholds, which are income levels below which individuals or households are considered to be living in poverty [1]. The method involves setting a base poverty line, known as the slack base, and adjusting it based on various factors such as inflation, cost of living, and changes in household composition. By applying these adjustments, researchers can estimate the upper and lower limits of poverty for different demographic groups and geographic areas.

To determine the upper limit of poverty using the Slack Base method, researchers start with the base poverty line and make adjustments to account for factors that may increase the cost of living or income requirements [2]. This allows for a more comprehensive understanding of the income levels at which individuals or households may be at risk of falling into poverty. On the other hand, calculating the lower limit of poverty involves identifying the minimum income needed to meet basic needs and avoid deprivation. By considering both the upper and lower limits, policymakers can develop targeted interventions to support those most in need [3].

In addition to calculating current poverty thresholds, the Slack Base method can also be used for forecasting future trends in poverty rates [4]. By analyzing historical data, economic indicators, and demographic changes, researchers can project how poverty levels may evolve over time and anticipate potential challenges or opportunities for intervention. This proactive approach enables stakeholders to plan ahead and implement policies that address emerging issues before they escalate [5].

In today's economy, accurate and up-to-date information on poverty is essential for guiding decision-making and promoting social justice. By using methods like the Slack Base approach to calculate poverty thresholds, policymakers can better understand the root causes of poverty, identify vulnerable populations, and tailor interventions to meet specific needs. This data-driven approach helps ensure that resources are allocated efficiently and effectively, leading to more targeted and impactful anti-poverty initiatives [6].

Furthermore, in the wake of global economic challenges such as the COVID-19 pandemic, the importance of poverty threshold calculation has become even more pronounced. As unemployment rates rise and income inequality widens, it is crucial to have reliable data on poverty levels to inform recovery efforts and support those most affected by economic downturns. By using robust methods like the Slack Base approach, policymakers can assess the impact of external shocks on poverty rates, prioritize assistance programs, and monitor progress towards reducing disparities.

In conclusion, the Slack Base method offers a systematic and comprehensive approach to calculating poverty thresholds, finding upper and lower limits, forecasting future trends, and informing policy decisions in today's economy. By leveraging this method effectively, stakeholders can gain valuable insights into the dynamics of poverty, target resources where they are most needed, and work towards creating a more equitable and inclusive society. As we navigate complex economic challenges and strive for sustainable development, understanding and addressing poverty remains a critical priority for building a more resilient and prosperous future [7].

POVERTY THRESHOLD CALCULATION THROUGH SBM METHOD

There are two types of models in DEA: radial and non-radial. Radial models are represented by the CCR (Charnes–Cooper–Rhodes) model. Basically, they deal with proportional changes of inputs or outputs. On the other hand, non-radial models, e.g., the slacks-based measure of efficiency (SBM) model, handle input or output slacks directly, and do not assume proportional changes of inputs or outputs. In this chapter, we introduce the SBM model and its extensions.

To calculate the poverty line through fuzzy linear programming using the SBM (Slacks-Based Measure) method, we need to follow these steps;

- Step 1: Normalize the data (Dimensionless)
- Step 2: Determine the input and output variables
- Step 3: Formulate the fuzzy linear programming model
- Step 4: Solve the model using the SBM method

These are data entries for poverty line calculation for 3 years respectively.

Table1. Data entry

Years	Income	Education	Healthy care	Basic needs
2020	2300	65	234000	540
2021	2350	72	241000	620
2022	2500	83	249000	745

Step 1: Normalize (Dimensionless) the data to a common scale through $n_{ij} = r_{ij} / \sqrt{\sum_{1-m} r^2_{ij}}$. Normalized data shown as follow [8];

Table 2. Normalized data

Years	Income	Education	Healthy care	Basic needs
2020	0.557	0.509	0.560	0.487
2021	0.569	0.564	0.576	0.559
2022	0.605	0.650	0.595	0.671

- Step 2:** Determine the input and output variables
 Input Variables (X): Income – Education – Healthcare – Basic Needs
 Output Variable (Y): Poverty Line

Step 3: For the fuzzy Super SBM model, we aim to minimize the output variable (Poverty Line) by considering the input variables (Income, Education, Healthcare, and Basic Needs) and their corresponding slacks. The objective is to find the optimal weights (λ) for each input variable that maximize the output variable [9]. The fuzzy linear programming model can be formulated as follows;

$$\delta^* = \min_{\lambda, \bar{y}, \bar{s}} \frac{(1/m) \sum_{i=1}^m (\bar{x}_i / x_{io})}{(1/s) \sum_{r=1}^s (\bar{y}_r / y_{ro})}$$

St.

$$\bar{x}_i \geq \sum_{j=1, j \neq o}^n x_{ij} \lambda_j \quad (i = 1, \dots, m),$$

$$\bar{y}_r \leq \sum_{j=1, j \neq o}^n y_{rj} \lambda_j \quad (r = 1, \dots, s),$$

$$\bar{x} \geq x_o, \quad \bar{y} \leq y_o, \quad \bar{y} \geq 0, \quad \lambda \geq 0.$$

Where;

m = input coefficient factor

s = output coefficient factor

x-bar i = Normalized value of input variable j

y-bar r = Output variable (Poverty Line)

λ_j = Weight for input variable i

X_j^- = Lower bound of input variable j

X_j^+ = Upper bound of input variable j

For simplicity, let's assume the lower bounds are all set to zero and the upper bounds are all set to one. Substitute the values into the formula;

$$\text{Maximize } Y_{2020} = \lambda_{\text{Income}} * (0.557 - 0) / 1 + \lambda_{\text{Education}} * (0.509 - 0) / 1 + \lambda_{\text{Healthcare}} * (0.560 - 0) / 1 + \lambda_{\text{Basic Needs}} * (0.487 - 0) / 1$$

St.

$$\lambda_{\text{Income}} + \lambda_{\text{Education}} + \lambda_{\text{Healthcare}} + \lambda_{\text{Basic Needs}} = 1$$

$$\lambda_{\text{Income}} + \lambda_{\text{Education}} + \lambda_{\text{Healthcare}} + \lambda_{\text{Basic Needs}} = Y$$

This formulation represents the fuzzy linear programming model that aims to find the optimal weights for each input variable to maximize the output variable (Poverty Line) while considering the slacks and normalized values of the input variables. The actual solution involves solving this model iteratively using the SBM method to determine the optimal weights that define the poverty line based on the given data and constraints.

Step 4: Solve the model using the SBM method. At the first, we need to calculate the slacks for each input variable and then determine the (λ) for each variable through **1-normalize data**.

4-1. Calculate the slacks for each input variable. The slack for each input variable can be calculated using the normalized values provided earlier (2020) as follows;

$$\text{- Normalized Income} = 0.557 \rightarrow \text{Slack} = 1 - 0.557 = 0.443$$

$$\text{- Normalized Education} = 0.509 \rightarrow \text{Slack} = 1 - 0.509 = 0.491$$

$$\text{- Normalized Healthcare} = 0.560 \rightarrow \text{Slack} = 1 - 0.560 = 0.440$$

$$\text{- Normalized Basic Needs} = 0.487 \rightarrow \text{Slack} = 1 - 0.487 = 0.513$$

Table 3. SlacksYears	Income	Education	Healthy care -	Basic needs -
2020	0.443	0.491	0.440	0.513
2021	0.431	0.436	0.424	0.441
2022	0.395	0.350	0.405	0.329

4-2. Calculate the weights for each input variable. Let's assume we have calculated the weights for each input variable as follows;

$$\lambda_{\text{Income}} = \text{Slack-2020}_{\text{Income}} / \Sigma \text{Slacks} = 0.443 / (0.443 + 0.491 + 0.440 + 0.513) = 0.235$$

$$\lambda_{\text{Income}} = \text{Slack-2021}_{\text{Income}} / \Sigma \text{Slacks} = 0.431 / (0.431 + 0.436 + 0.424 + 0.441) = 0.249$$

$$\lambda_{\text{Income}} = \text{Slack-2022}_{\text{Income}} / \Sigma \text{Slacks} = 0.395 / (0.395 + 0.350 + 0.405 + 0.329) = 0.267,$$

$$\vdots$$

$$\lambda_{\text{Education}} = \text{Slacks}_{\text{Education}} / \Sigma \text{Slacks} = \dots (2020-2022)$$

$$\lambda_{\text{Healthcare}} = \text{Slacks}_{\text{Healthcare}} / \Sigma \text{Slacks} = \dots (2020-2022)$$

$$\vdots$$

$$\lambda_{\text{Basic Needs}} = \text{Slacks-2022}_{\text{Basic Needs}} / \Sigma \text{Slacks} = 0.329 / (0.395 + 0.350 + 0.405 + 0.329) = 0.222,$$

Table 4. Weights

Years	Income	Education	Healthy care	Basic needs
2020	0.235	0.260	0.233	0.272
2021	0.249	0.252	0.245	0.255
2022	0.267	0.237	0.274	0.222

After calculating the weights for each input variable, we can determine the poverty line (Y) based on these weights and normalized values of the input variables. To determine the poverty line (Y) based on the above calculation, we need to follow;

4-3. Substitute the weights and normalized values of the input variables into the formula;

$$Y = \lambda_{\text{Income}} * (\text{Norm. Income}) + \lambda_{\text{Education}} * (\text{Norm. Education}) + \lambda_{\text{Healthcare}} * (\text{Norm. Healthcare}) + \lambda_{\text{Basic Needs}} * (\text{Norm. Basic Needs}),$$

$$Y_{2020} = (0.235 * 0.557) + (0.260 * 0.509) + (0.233 * 0.560) + (0.272 * 0.487)$$

$$Y_{2020} = 0.131 + 0.132 + 0.131 + 0.133$$

$$Y_{2020} = \mathbf{0.527}$$

$$Y_{2021} = (0.249 * 0.569) + (0.252 * 0.564) + (0.245 * 0.576) + (0.255 * 0.559)$$

$$Y_{2021} = 0.142 + 0.142 + 0.141 + 0.143$$

$$Y_{2021} = \mathbf{0.568}$$

$$Y_{2022} = (0.267 * 0.605) + (0.237 * 0.650) + (0.274 * 0.595) + (0.222 * 0.671)$$

$$Y_{2022} = 0.162 + 0.154 + 0.163 + 0.149$$

$$Y_{2022} = \mathbf{0.628}$$

Therefore, based on the calculated weights for each input variable and the normalized values of the input variables, the poverty line (Y) is determined to be 0.527, 0.568, and 0.628 from 2020 up to 2022 respectively.

Poverty threshold calculations have numerous applications in poverty alleviation efforts and policy-making. By establishing clear and objective poverty thresholds, policymakers can accurately identify individuals and households living below the poverty line, enabling targeted interventions to reach those most in need. These thresholds also serve as a benchmark for measuring progress towards poverty reduction goals, evaluating the impact of social programs, and monitoring changes in poverty levels over time. Additionally, poverty threshold calculations help in the allocation of resources and prioritization of interventions, ensuring that limited resources are directed towards areas with the highest levels of need. Overall, poverty threshold calculations play a crucial role

in guiding evidence-based decision-making and shaping effective strategies for combating poverty and promoting inclusive development.

POVERTY LIMITS CALCULATION

Because transfer of poverty line to poverty threshold, we must calculate the upper limit and lower limit to make a bound. To calculate the upper and lower limits for the poverty line using the SBM (Slack-Based Method) approach, we need to use the weights (λ) for each input variable that we calculated earlier. The upper and lower limits will help in defining a range within which the poverty line can vary based on the sensitivity of the input variables. Here's how you can calculate the upper and lower limits in detail [10];

1. Define the formula for calculating the upper and lower limits:

The upper limit (UL) and lower limit (LL) for the poverty line can be calculated using the following formulas;

- UL = Poverty Line + (λ_{\max} * Sum of Slacks)

- LL = Poverty Line - (λ_{\min} * Sum of Slacks)

2. Determine the maximum and minimum weights (λ) among all input variables;

- Maximum weight (λ_{\max}) = max (λ_{Income} , $\lambda_{\text{Education}}$, $\lambda_{\text{Healthcare}}$, $\lambda_{\text{Basic Needs}}$)

- Minimum weight (λ_{\min}) = min (λ_{Income} , $\lambda_{\text{Education}}$, $\lambda_{\text{Healthcare}}$, $\lambda_{\text{Basic Needs}}$)

3. Calculate the upper and lower limits for the poverty line;

- UL 2020 = 0.527 + (0.272 * 1.888) \approx 0.527 + 0.514 \approx **1.041**

- LL 2020 = 0.527 - (0.233 * 1.888) \approx 0.527 - 0.440 \approx **0.087**

Bound width: **0.954**

- UL 2021 = 0.568 + (0.255 * 1.732) \approx 0.568 + 0.442 \approx **1.010**

- LL 2021 = 0.568 - (0.245 * 1.732) \approx 0.568 - 0.424 \approx **0.144**

Bound width: **0.866**

- UL 2022 = 0.628 + (0.274 * 1.478) \approx 0.628 + 0.405 \approx **1.033**

- LL 2022 = 0.628 - (0.222 * 1.478) \approx 0.628 - 0.328 \approx **0.300**

Bound width: **0.733**

Bandwidth is considered an indicator of the intensity of poverty development or its slowness. In addition to the increase in the amount of poverty, which indicates the penetration of poverty into the upper classes of society, the intensity of poverty shows the speed and depth of the development of poverty. The poverty bandwidth will be a professional and practical indicator for those responsible for fighting poverty in any society.

Author proposed a new heuristic bound width date group as follow formula;

$$UL = \left(\sum_{i=1}^n x_i / n \right) + \sqrt[3]{\text{Max}(x_i) - \text{Min}(x_i)}$$

$$LL = \left(\sum_{i=1}^n x_i / n \right) - \sqrt[3]{\text{Max}(x_i) - \text{Min}(x_i)}$$

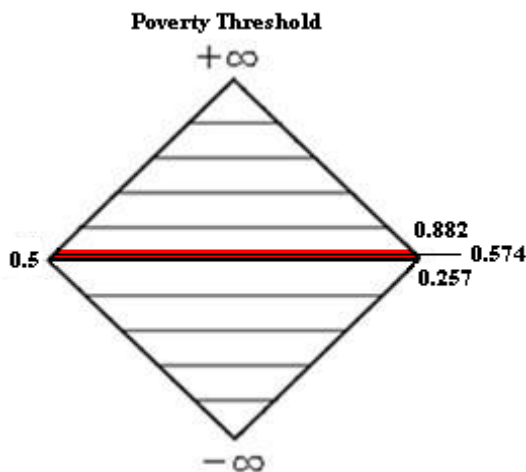
Poverty threshold with above formula from 2020 up to 2022 calculated as follow;
Where;

$\Sigma x_i/n = 0.574$, $\text{Max}x_i - \text{Min}x_i = 0.101$ and $\sqrt[3]{\text{Max}x_i - \text{Min}x_i} \approx 0.318$

So, UL = 0.574 + 0.318 = 0.882 and LL = 0.574 - 0.318 = 0.257

Also, Author proposed a new heuristic Poverty Threshold shape as follow;

Fig.1: Poverty Threshold



Poverty limits calculation and poverty bound width are important tools used in poverty forecasting to estimate the range of potential poverty levels within a given population. These calculations are crucial for setting realistic targets, monitoring progress, and evaluating the effectiveness of poverty alleviation efforts. By determining poverty limits, policymakers can establish thresholds for measuring poverty reduction goals and identifying areas where interventions are most needed. Additionally, understanding the poverty bound width helps policymakers assess the uncertainty in poverty forecasts and make informed decisions on resource allocation and program implementation. These tools provide valuable insights into the dynamics of poverty and enable stakeholders to develop evidence-based strategies for addressing the root causes of poverty and promoting sustainable development.

POVERTY THRESHOLD FORECASTING

To forecast the poverty line for the fourth, fifth, and sixth years based on the given data for the first three years (0.527, 0.568, and 0.628), we can use various methods such as simple linear regression, exponential smoothing, or time series analysis. In this case, I will demonstrate how to use a simple linear regression model to forecast the poverty line for the next three years [11].

Step 1: Calculate the Average Annual Growth Rate

First, we need to calculate the average annual growth rate based on the data for the first three years. Average Annual Growth Rate (AAGR) = $[(\text{Ending Value} / \text{Beginning Value})^{(1 / \text{Number of Years})}] - 1$

- Beginning Value (Year 1): 0.527
- Ending Value (Year 3): 0.628
- Number of Years: 3

$$\text{AAGR} = [(0.628 / 0.527)^{(1 / 3)}] - 1 = [(1.1917)^{(0.3333)}] - 1 = 0.09 \text{ or } 9\%$$

Step 2: Forecasting Poverty Line for Years 4, 5, and 6 using Linear Regression

Now that we have the average annual growth rate, we can use a simple linear regression model to forecast the poverty line for the next three years. The formula for forecasting the poverty line using linear regression is;

$$\text{Forecasted Value} = \text{Previous Value} + (\text{Previous Value} * \text{AAGR})$$

For Year 4- 6 respectively;

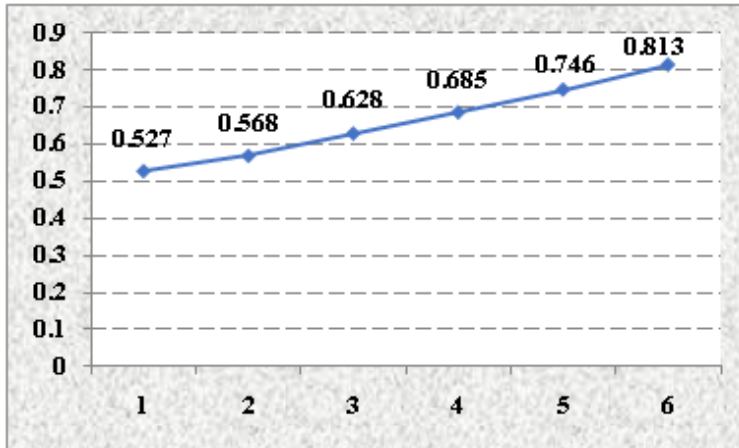
Forecasted Value (Year 4) = $0.628 + (0.628 * 0.09) = 0.628 + 0.05652 \approx 0.685$

Forecasted Value (Year 5) = $0.68452 + (0.68452 * 0.09) = 0.68452 + 0.06161 \approx 0.746$

Forecasted Value (Year 6) = $0.74613 + (0.74613 * 0.09) = 0.74613 + 0.06715 = \approx 0.813$

These values are based on the assumption of a linear growth pattern determined by the calculated average annual growth rate of 9%.

Diagram 1. Poverty line forecasting



Last result of this paper is diagnostic of poverty as progressive because average annual growth rate of 9% and poverty rate from 2020 up to 2022.

Poverty forecasting plays a crucial role in informing policy decisions and designing targeted interventions to address the needs of vulnerable populations. By accurately predicting changes in poverty levels over time, policymakers can proactively allocate resources, implement effective social programs, and monitor the impact of interventions. For example, governments can use poverty forecasts to adjust social welfare programs, such as cash transfer schemes or food assistance programs, to reach those most in need. Additionally, businesses and non-profit organizations can leverage poverty forecasts to tailor their services and products to cater to low-income populations. By incorporating poverty forecasting into decision-making processes, stakeholders can work towards reducing poverty, promoting economic development, and fostering social inclusion.

CONCLUSION

In this article, we have explored the intricate process of calculating the poverty line using the Slack Base method for the years 2020-2022, which resulted in values of 0.527, 0.568, and 0.628 respectively. The poverty line serves as a crucial benchmark for identifying individuals or households living below the poverty threshold, enabling policymakers to target interventions effectively.

Furthermore, we have delved into the forecasting of poverty levels through the Annual Average Growth Rate (AAGR) method for the same period, yielding values of 1.041-0.087, 1.010-0.144, and 1.033-0.300. By analyzing historical trends and projecting future growth rates, policymakers can anticipate changes in poverty levels and plan sustainable interventions accordingly.

Additionally, we have discussed the concept of progressive poverty, with values of 0.685, 0.746, and 0.813 projected for the years 2023-2025. Progressive poverty takes into

account the dynamic nature of poverty and provides a nuanced understanding of poverty dynamics over time, enabling policymakers to tailor interventions to address specific challenges faced by vulnerable populations.

One of the key innovations presented in this article is the construction of the poverty intensity index based on changes in the poverty bandwidth, with values of 0.954, 0.866, and 0.733 observed. This index offers a comprehensive view of poverty dynamics by capturing variations in the depth and severity of poverty as it increases, resulting in a decrease in the bound width.

In conclusion, based on the data and quantities presented in this article, we propose three key recommendations for policymakers:

1. Utilize the Slack Base method and AAGR forecasting to continuously monitor and update poverty lines and thresholds to ensure accurate targeting of interventions.

2. Incorporate the concept of progressive poverty in policy planning to address the evolving needs of vulnerable populations and implement targeted strategies to alleviate poverty sustainably.

3. Leverage the poverty intensity index to gain deeper insights into the changing nature of poverty, adjust intervention strategies to effectively combat poverty, and promote inclusive development.

By following these recommendations and leveraging data-driven approaches, policymakers can make informed decisions and design effective interventions to combat poverty and create a more equitable society for all individuals and communities.

**REVIEWER: Saidzoda I.M.,
Candidate of Technical Sciences**

REFERENCES

1. Tone, K. A slacks-based measure of efficiency in data envelopment analysis/*European Journal of Operational Research*, 2001. 130(3). – Pp.498-509.
2. Cooper, W.W., ET. Al. *Data envelopment analysis: History, models, and interpretations/ Handbook on data envelopment analysis*, Springer, 2007. – Pp. 1-39.
3. Cancian, M., W. W., ET. Al. *Changing poverty, changing policies*, Russell Sage Foundation, (2009).
4. Emrouznejad, A., W. W., ET. Al. A survey and analysis of the first-order SBM-DEA models. *Omega*, 2018, 80. – Pp. 274-284.
5. Ravallion, M. *The economics of poverty: History, measurement, and policy/ Oxford University Press*. 2016.
6. Brady, D., W. W., ET. Al. *The Oxford Handbook of the Social Science of Poverty/Oxford University Press*, 2018
7. Deaton, A. *The analysis of household surveys: A micro-econometric approach to development policy/ World Bank Publications*, 1997.
8. Asgharpour, M. J. *Multiple Criteria Decision Making*. - Tehran University Publication, 1998. ISBN 96-4-03-9320-7. – P.194.
9. Fodor, J. *Fuzzy preference modeling and multi-criteria Decision-Support*. - Kluwer Academic publication, 1995
10. Chen, S. J., ET. Al. *Fuzzy Multiple Attribute decision-making/ Springer- verlag*, 1992.
11. Lai Hwang, Ching, ET. Al. *Multi Objective Decision-making-methods and Applications/Springer- verlag*. – Berlin Heidelberg, 1979
12. Goedhart, Th., ET. Al, *the Poverty Line: Concept and Measurement, Journal of Human Resources, | Th., ET. AL Goedhart|| Vol. 12, (1977) . – Pp.503-520.*
13. Kapteyn, A., ET. Al, *Family Composition and Family Welfare*, in: Simon, J. and J. DaVanzo (eds), *Research in Population Economics*, 11, JAI-Press, Greenwich, \ A., ET. Al \ \ (1980). – Pp.77-97.
14. Jasso, G., Et Al, *Distributive Justice and Earned Income*, *American Sociological Review*\ G. Jasso\ 1977. Vol.42. – Pp.639-651.

15. Wu, D. D., ET. All..A comparison of three methods for selecting values of input variables in the analysis of output from a computer code/Journal of Statistical Computer Simulation, 2002. 72 (2). – Pp.119–139

POVERTY LINE, POVERTY THRESHOLD, POVERTY FORECASTING, METHODS

In this article, the author focuses on poverty and its consequences. The SBM method was used to calculate the poverty threshold, which helped to determine the upper and lower limits of poverty and forecast the poverty rate for the next three years. The data set entries included income, education, healthcare, and basic needs from 2020 to 2022. These inputs were used to calculate the poverty threshold. The problem-solving steps included making the dataset dimensionless, finding slacks, calculating variable weights, and then calculating poverty through $Y = \lambda_{\text{Income}} * (\text{Norm. Income}) + \dots + \lambda_{\text{Basic Needs}} (\text{Norm. Basic Needs})$. The poverty lines (Y) were determined to be 0.527, 0.568, and 0.628 from 2020 to 2022, respectively. The next part focused on calculating the poverty limits. The upper limits (UL) were calculated as “Poverty Line + (λ max * Sum of Slacks)” and the lower limits (LL) were calculated as “Poverty Line - (λ min * Sum of Slacks).” The results from 2020 to 2022 were 1.041, 0.087, 1.010, 0.144, and 1.033, 0.300, respectively. The innovation at this stage was to find bandwidth as an indicator of the intensity of poverty. Finally, the last stage focused on forecasting the Poverty threshold. The average annual growth rate (AAGR) was used to calculate the increasing coefficient of the regression line through $[(\text{Ending Value} / \text{Beginning Value}) ^ (1 / \text{Number of Years})] - 1$ formula and found to be 0.09 or 9%. By this stage, 0.685, 0.746, and 0.813 were forecasted as the poverty rates for the years 2023-2025. The kind of poverty diagnosed at this stage was progressive.

Key words: Slack Based Method, Data bound, Average Annual Growth Rate (AAGR)

Information about the author: Pejman Jafari – Tajik National University, post-doctoral. **Address:** 734025, Dushanbe, Tajikistan, Rudaki Ave., 17. **Phone:** (+992)001016655. **E-mail:** jafaripejman3@gmail.com.

Article received 12.10.2023

Approved after review 24.12.2023

Accepted for publication 15.04.2024

PHYSICS

doi.org/10.62965/tnu.sns.2024.2.5

UDC: 531.42

CAUSAL PHYSICS: CROSS-SECTIONAL AREA INSTEAD OF MASS

Rajabov T.M.

The issue under consideration requires some philosophical digression. From a philosophical point of view, establishing the cause in the origin of phenomena and processes is an important part of logical thinking in establishing scientific and other truth. However, it should be recognized that at present the principle of causation, as a universal principle in the logical connection of things and phenomena and the most important mechanism of cognition, has lost its relevance within the causal field of thought itself - in physical science, within which all processes and phenomena should be considered in close interrelation. We are talking about the methodological basis of modern physics. Modern physics, using the example of special and general relativity, quantum physics and other approaches, has become predominantly mathematical, with abstract propositions and a postulative character. The methodological basis of modern physics is devoid of visual representations. This is how it differs from traditional classical physics, which has been developing for more than three centuries with visual representations that meet the conditions of the principle of causation.

Modern physics has created concepts that do not fit within the framework of human perception. There are difficulties in interpreting quantum physics [1-4]. The abstractness of representations within its framework is a consequence of its probabilistic nature, which a priori implies problems in its interpretation. It is another matter when it comes to representations within the framework of relativity theories [5-8]. Within their framework, unusual concepts were introduced, such as space-time relationship, relativity of mass, time, size of objects and much more. Clarity has been lost in determining one of the important physical quantities - mass.

Meanwhile, the lack of clarity regarding the fundamental issues of physical theory – the mechanism of physical interaction, the question of gravitational shielding, the unified field theory, the question of the luminiferous ether, the nature of the force of inertia and other issues related to them, again and again creates the need to return to the initial positions in order to try to create an acceptable physical picture of the phenomena. This work is devoted to demonstrating the presence of unrealized arguments and possibilities within the framework of traditional causal physics to obtain results, including new ones. Taking into account previously unaccounted-for circumstances, an acceptable physical picture is proposed regarding fundamental questions of physics that are somehow related to mass.

In the classical view, the gravitational interaction is associated with mass, in the framework of Newton's theory [9], and with size, in the framework of the kinetic theory of Le Sage [10]. The size factor is an important characteristic of objects in their physical existence and manifestation of properties. However, within the framework of the new physics, this factor is not considered as such, which causes inevitable problems. It can be shown that in the description of physical phenomena, the size factor, as a quantitative characteristic of an object, is a more fundamental quantity compared to mass, and mass is only a special case of its manifestation.

2. The evolution of the concept of mass. For thousands of years, mass has been a quantity characterizing the amount of matter. From the early stages of the development of scientific ideas, it entered science as such. The discovery of the laws of mechanics by Newton revealed the property of inertia of mass. Mass is included in the equations of accelerated motion and gravitational interaction

$$F_a = ma \quad (1)$$

$$F_g = G \frac{m_1 m_2}{r^2}. \quad (2)$$

In expressions (1) and (2), F_a is the force acting on the body, m is the mass of the body, a is acceleration, F_g is the force of gravitational interaction, m_1 and m_2 are the masses of interacting bodies, r is the distance between them, G is the gravitational constant.

The mass began to differ into gravitational and inert. Experiments have shown that they have almost identical values.

The study of the properties of the atomic nucleus has discovered a new phenomenon related to mass - a mass defect, which is described by the expression

$$\Delta M = M_p + M_n - M, \quad (3)$$

where M is the mass of the atomic nucleus, M_p and M_n are the mass of protons and the mass of neutrons in the atomic nucleus, respectively.

With the advent of new concepts since the beginning of the 20th century, within the framework of the special theory of relativity (SRT), two more properties have been added to mass - the relativity of mass and the equivalence of mass and energy. The relativity of mass is represented by the dependence of the mass of a body on its kinematic state: mass can grow when the speed of the body approaches the value of the speed of light in a vacuum, and there is no limit to growth. The concepts of rest mass and relativistic mass appeared. For the relativistic mass, a dependence is proposed in the form

$$m = \frac{m_0}{\sqrt{1 - \frac{v^2}{c^2}}}, \quad (4)$$

where m_0 is the mass of a body in its own coordinate system, which is called the rest mass, v is the velocity of a body relative to a stationary coordinate system, c is the speed of light in a vacuum.

For the equivalence of mass and energy, the expression is proposed

$$E = mc^2. \quad (5)$$

Thus, the properties of inertia of mass, the phenomenon of mass defect and relativistic properties of mass were added to the primary idea of mass as a quantity of matter. If the properties of mass inertia and mass defect are considered by specialists within the framework of reality, then the idea of mass within the SRT causes their ambiguous opinion. Many works are devoted to the criticism of the SRT. The mathematical and logical inconsistency of the foundations of SRT is shown in one of the latest works [11]. It is shown that the principle of interval invariance, accepted as the basic position of SRT, is incorrect and has nothing to do with the reality of physical phenomena and states. It is shown that expression (5) can be obtained in an alternative way within the framework of the classical approach.

With the discovery of new properties, mass has ceased to be considered as a measure of the amount of matter. There is a need to find out what the mass is and how it is related to the amount of matter? The fact that in certain cases mass can be considered as a measure of the amount of matter is true and indicates that mass is a special case of another physical quantity that needs to be determined.

3. Mass, as the area of impact on an object. A new idea of mass was proposed in [12]. In this work, within the framework of traditional causal physics, mass-area equivalence is proposed in the form

$$m = kS, \quad (6)$$

where S is the cross-sectional area of a physical object (elementary mass-forming particles - nucleons and systems consisting of them are considered in this work by physical objects), k is the proportionality coefficient.

The rationale and method of obtaining expression (6) can be considered in the concepts of the effect of ether particles on physical bodies. Suppose that as a result of the external action of force F , the body receives acceleration a (Fig.1). The relative velocity of ether particles relative to the body varies from opposite sides along the direction of motion. The body experiences additional pressure against movement from the particles of segment Δl_2 , and a decrease in pressure from behind by the same amount. A resistance force arises, the magnitude

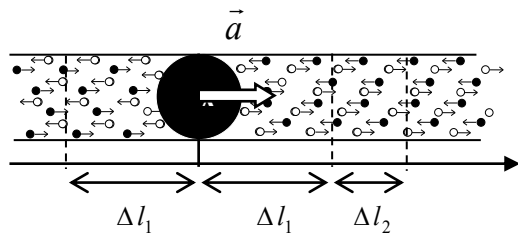


Fig.1. The picture of the accelerated movement of the physical body and the increase in pressure on it from the ether particles against the direction of movement

of which determines the acceleration of the body. The acceleration of a body is recorded as a consequence of the action of force F according to Newton's second law $a = \frac{F}{m}$, on the one hand, and as a consequence of the pressure difference on the object from opposite sides $a \sim \Delta p$, according to Le Sage's representation, on the other. The other hand. Expressing Δp by definition $\Delta p = \frac{F}{S}$, where S is the cross-sectional area of the object, we can write

$$\frac{F}{S} = k \frac{F}{m} \quad (7)$$

where k is the proportionality coefficient.

From this expression we get $m = kS$.

In expression (6), the mass of an object is replaced by a physical quantity proportional to its cross-sectional area. This substitution represents a transition from one quantitative characteristic of an object to another – from mass to size. This transition is dictated by the mechanism of interaction in accordance with the kinetic theory of gravity of Le Sage, where the main argument for interaction is the size of interacting objects. It is shown in [12-15] that this transition makes it possible to describe many physical phenomena more broadly and on a causal basis.

In expression (6), S represents the effective area of interaction of a physical object. If there is a system of two objects with cross-sectional areas S_1 and S_2 and an area of mutual overlap ΔS (Fig.2), then the effective area of interaction of such a system is determined by the ratio

$$S = S_1 + S_2 - \Delta S. \quad (8)$$

For the effective area of interaction of a system of N identical spherical elements located at a certain distance from each other, a mathematical expression is proposed in the form:

$$S = S_b \left[1 - \left(1 - \frac{S_l}{S_b} \right)^N \right]. \quad (9)$$

In this expression, S_l is the cross-sectional area of one element, S_b is the area of the base of the cube, in the center of which there is one interaction element.

The nature of the dependence of S on the number of interaction elements N in expression (9) is shown in Fig.3.

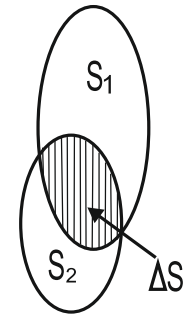


Fig. 2. Mutual spatial overlap of two bodies

It is known that mass, as an argument, appears both in the description of the gravitational and in the description of the nuclear interaction, which indirectly indicates the presence of a commonality between these interactions. It is shown in [15] that gravitational and nuclear interactions have a single mechanism and a common nature. It is shown that expression (9) is applicable both to describe the macrocosm and to describe the microcosm. In the representations of mutual shielding of interaction elements, the gravitational and nuclear interactions differ in the values of the mutual shielding parameter $\delta = \frac{S_l}{S_b}$ in expression (9). At $\delta \geq 1$, expression (9) describes the close mutual shielding, which is typical for the mutual shielding of nucleons in the atomic nucleus. At $\delta \ll 1$, it describes far shielding, which is the mutual shielding of atomic nuclei in ordinary substances.

4. Mass in the gravitational interaction. Newton's law of universal gravitation in terms of mass-area equivalence is written as:

$$F = G' \frac{S_1 S_2}{r^2}. \quad (10)$$

The areas S_1 and S_2 in expression (10) represent the effective areas of interaction of celestial bodies. G' is the areal constant of the gravitational interaction. In general, the areas S_1 and S_2 are defined by the expression

$$S = S_a \left[1 - \left(1 - \frac{S_n}{S_a} \right)^N \right], \quad (11)$$

where $S_a = r_a^2$, in which r is the radius of the atom, S_n is the cross-sectional area of the atomic nucleus, N is the value associated with the number of atomic nuclei in the object.

The work [12] was carried out in the development of the kinetic theory of Le Sage, taking into account the size and relative position of elementary mass-forming elements for ordinary substances - atomic nuclei. The gravitational interaction is presented as a result of mutual shielding of atomic nuclei in the path of ether particles.

The mutual shielding of atomic nuclei in the path of ether particles leads to the phenomenon of gravitational shielding. Gravitational shielding is a mass defect for the

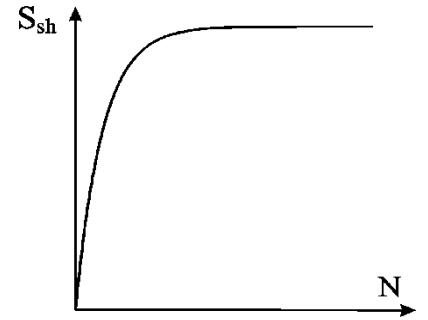


Fig. 3. A general view of the area of mutual shielding of interacting elements, depending on the number of shielding elements

macrocosm. In [12-15], based on the mechanism of mutual shielding of objects, the results are presented that justify the presence of gravitational shielding for massive celestial bodies.

The use of expression (10) made it possible to establish the manifestation of gravitational shielding depending on the size of celestial bodies. Due to the small size of the shielding elements – atomic nuclei and the large distance between them in comparison with their size, gravitational shielding is manifested for celestial bodies with a sufficiently large size. Ordinary bodies are quite transparent to the passage of tiny particles through them. This explains the passage of neutrinos through massive celestial objects. It has been established that the Moon is not capable of gravitational shielding due to its insufficient size, the Earth, as a planet, shields gravitational effects, depending on its thickness up to 50%. Giant planets shield from gravitational influence by 100%.

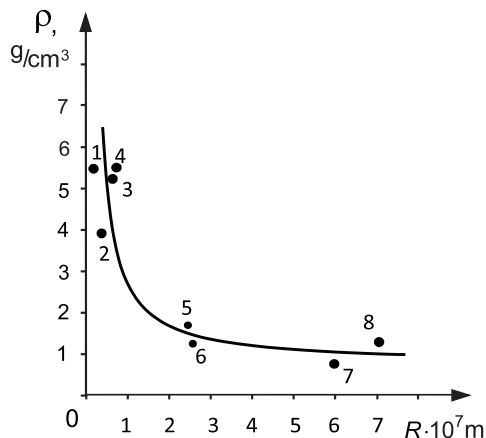


Fig.4. The density of the planets of the Solar system depending on their size: 1 - Mercury, 2 – Mars, 3 – Venus, 4 – Earth, 5 – Uranus, 6 – Neptune, 7 – Saturn, 8 – Jupiter.

The presence of gravitational shielding leads to the conclusion that there is a hidden mass in massive celestial bodies: due to the shielding of one part of their remaining parts, not all the substance of the object participates in gravitational interaction. As a result, calculations to determine the mass and density of massive celestial bodies by gravitational interaction result in underestimated values. It turns out a dependence where a smaller density value will correspond to the larger sizes of celestial bodies, which is confirmed for the planets of the Solar system (Fig.4). The values obtained in this way for mass and density are not true. In the matter of determining the true values of the mass and density of giant planets, the impossibility of determining their solid surface creates difficulty. For these reasons, the statement that the giant

planets are gaseous is not correct.

The presence of gravitational shielding provides an acceptable interpretation of a number of physical phenomena, such as the diurnal variation of gravity, precession of the perihelion of Mercury and features of tidal processes.

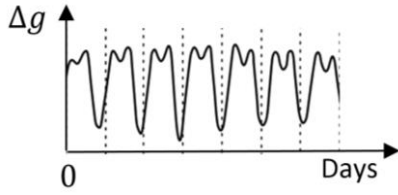


Fig. 5. A fragment of the curve of the daily variation of gravity with minima in the upper part of the maxima [16]

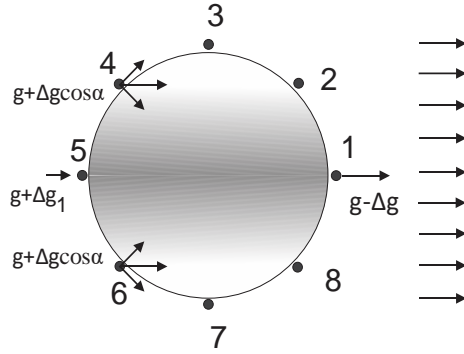


Fig. 6. The daily variation of vertical gravity depending on the gravitational structure of the Earth in the gravitational field of the star located on the right.

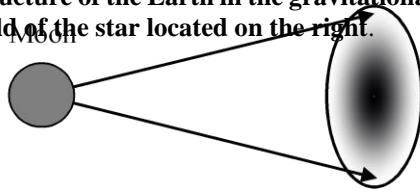


Fig. 7. Diagram of the gravitational effect of the Moon on the Earth's zones in the form of a cross-section of the Earth. The degree of gravitational shielding from the Earth is expressed by the degree of darkness in the figure

It is shown that the manifestation of semi-daily effects, which are reflected by small minima at the top of the maxima of the curve of the daily variation of gravity (Fig.5), is due to the manifestation of gravitational shielding from the Earth. These minima are manifested as a result of the weakening of the influence of the luminaries – the Sun and the Moon - by the factor of shielding the Earth in its equatorial part due to its greater thickness (Fig.6).

Regarding the peculiarities of the manifestation of tidal processes, it has been established that tidal forces are more peripheral in nature than volumetric. Due to the small thickness of the peripheral regions of the planet, the shielding factor in these areas is not significant (Fig.7). Consequently, the influence of the luminaries on the peripheral waters is greater than on the waters of the equatorial part. This factor provides a justification for the interpretation of the two-time manifestation of tides per day, as well as the factor of the six-hour delay of tidal processes.

The presence of gravitational shielding indicates the cause of Mercury's perihelion precession. Mercury, as the smallest planet and located close to the Sun, when rotating around the Sun, regularly falls into the field of mutual shielding of large planets. Since the planets are located on the opposite side of the Sun, the effect of mutual shielding of large planets leads to a decrease in their impact on Mercury. As a result, the resulting force from the Sun becomes greater. This leads to precession of the perihelion of Mercury.

5. Mass in nuclear physics.

Mass defect. Nuclear interaction is also considered in the form of mutual shielding of mass-forming elements - nucleons in the path of motion of cosmic particles. The results are obtained using the dependence (1) in the form $M = kS_{nc}$, where M is the mass of the atomic nucleus, S_{nc} is the cross-sectional area of the nucleus, k is the proportionality coefficient.

In the representations of mass-area equivalence, the mutual spatial overlap of nucleons in the path of the movement of ether particles is a mass defect in the atomic nucleus. The mass defect is defined as a value proportional to the difference between the cross-sectional area of the atomic nucleus and the sum of the cross-sectional areas of the nucleons of the atomic nucleus

$$\Delta S = \sum S_p + \sum S_n - S_{nc}, \quad (12)$$

Using expression (1) allows to obtain an expression for the mass defect:

$$\Delta M = M_p + M_n - M. \quad (13)$$

In (13) M_p is the mass of all protons, M_n is the mass of all neutrons, M is the mass of the atomic nucleus.

The energy of communication. The expression for the binding energy is obtained from (2) using the expression for the mass-area equivalence (1).

$$E = mc^2[1 - (1 - \delta)^N]. \quad (14)$$

In this expression, the mutual shielding parameter $\delta \geq 1$. Roughly, we can assume that the parameter δ is the ratio of the square of the radius of the nucleon to the square of the distance between the nucleons.

The repulsive Coulomb force between protons increases with the number of protons, which increases the distance between the nucleons. The change in distance can be seen as a correction of μ multiplied by δ . At $\mu = e^{-0,02N}$ the theoretical curve will be coordinated with experimental.

$$.E = mc^2[1 - (1 - \delta e^{-0,02N})^N]. \quad (15)$$

6. On gravitational and inert masses. As noted above, the acceleration of a body can be written as a result of the effect of force on the one hand, and as a result of the pressure difference on the body from opposite sides.

Within the framework of the above presentation, we can talk about the equality of gravitational and inert masses. Since mass is determined by the effective area of interaction - the size of a physical object, it remains unchanged, both in gravitational interaction and in accelerated motion. When moving with acceleration, the pressure on a physical object increases due to an increase in the velocity of the body to meet other particles, but the size remains unchanged. Hence, the gravitational and inert masses are identical.

7. Additivity in determining mass.

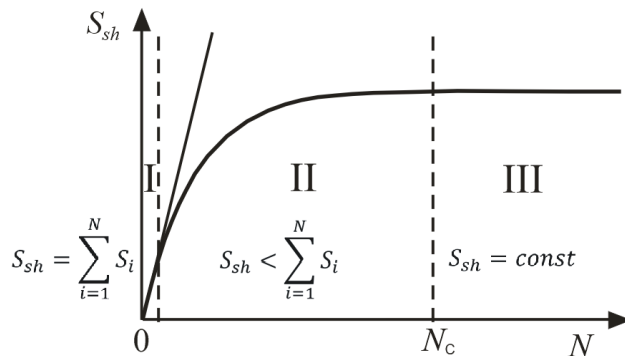


Fig.8. Areas of mutual shielding depending on the number of interaction elements

The mass of the system, considered in the form of expression (1) as a value depending on the mutual shielding of its elements, satisfies the principle of additivity only in the special case. The mutual shielding curve can be divided into three areas: I, II, III (Fig.8). In the initial region I, the curve has a linear character in a narrow range. There is no mutual shielding of elements in this area, the total area of interaction of the system is equal to the sum of the areas of interaction of individual elements $S =$

$\sum S_i$ and in accordance with expression (6) $M = \sum m_i$. The presence of mutual shielding of interaction elements corresponds to area II. In this area, the sum of the mass of the individual elements will be greater than the mass of the system: $M < \sum m_i$. In this case, there is a mass defect. The complete mutual overlap of the elements takes place in area III. In this area, $S = const$, accordingly, $M = const$. This result leads to the conclusion that as the size of the

object increases, the amount of matter above the critical thickness remains hidden. In mass representations, the mass no longer increases with increasing thickness.

Based on this approach, it is possible to explain the difference in the calculated density of the planets of the Earth group and the giant planets by an average of 5 times. If all the elements of interaction – atomic nuclei at a critical thickness of the object would be in one layer and would not overlap each other, then the total area of interaction would exceed the area of interaction in the presence of mutual shielding by 5 times (Fig.9).

A violation of additivity occurs for the mass of the atomic nucleus, which is associated with the mutual spatial overlap of nucleons. For ordinary substances, mutual shielding of mass-forming elements – atomic nuclei occurs with a sufficiently large size of objects - massive celestial bodies. According to experimental data, the Moon does not exhibit gravitational shielding, the Earth in the equatorial part shields by about 50% [14]. The diameter of the Moon is 3 475 m, the diameter of the Earth is 12 742 m. From Figure 10, it is possible to estimate the maximum thickness of the object, up to which the principle of mass additivity is maintained. This is the linear part of the curve, which takes place up to a thickness of the order of $5 \cdot 10^6$ m. Up to these thicknesses, there is practically no mutual shielding of the interaction elements – atomic nuclei. In the field of chemical transformations, the condition of mass additivity is always fulfilled and mass remains a measure of the amount of matter.

In the case of ordinary substances, the mutual shielding parameter $\delta \sim 10^{-10}$

8. Mass and energy. In the framework of modern physics, the relationship between mass and energy is expressed by the relations

$$E = mc^2. \quad (16)$$

Taking into account the mass-area equivalence, expression (5) can be written as

$$E = kSc^2.$$

According to the principles of causal physics, the energy of the universe is in the motion of ether particles. Since the mass-forming elements are nucleons and systems consisting of them - atomic nuclei, changing their sizes upsets the equilibrium: the amount of particle influx differs from the amount of outflow. This is manifested during the fission of atomic nuclei, when the cross-sectional area of the system changes.

Consider the division of nuclei into two equal parts. Let its volume be equal to V_1 , radius R , and cross-sectional area S_1 before division.

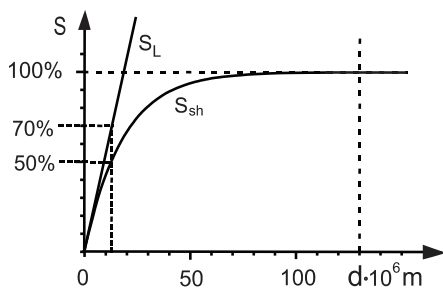


Fig.10. On the definition of the hidden mass of the Earth.

Then $V_1 = \frac{4}{3}\pi R^3$, $S_1 = \pi R^2$. After dividing into two equal parts, the volume of each part will be V_2 , radius r , cross-sectional area S_2 . Accordingly, we have $V_2 = \frac{4}{3}\pi r^3$ and $S_2 = \pi r^2$. From the condition $2V_2 = V_1$ we find

$$\frac{2S_2}{S_1} = 1,26.$$

Thus, when the atomic nucleus is divided, the cross-

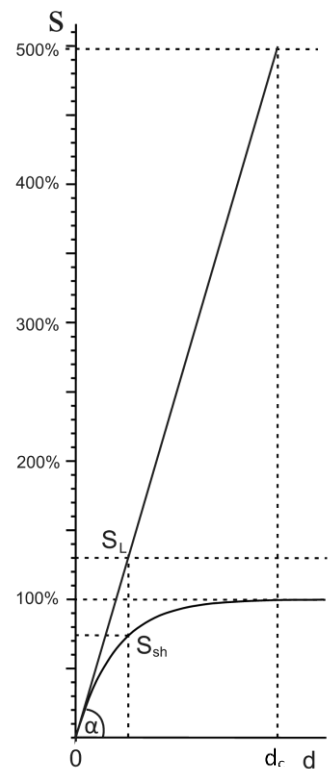


Fig. 9. To the calculation of the hidden mass of objects with dimensions where there is mutual shielding of elements.

sectional area of the system increases by 1.26. This is a significant amount of energy when it comes to strong interaction. The release energy is 26% of the total energy.

9. Determination of mass. The described interaction scheme allows to determine which physical quantity is taken as mass. Mass is a quantity proportional to the area of a physical object or system that is under pressure from falling cosmic particles. According to Le Sage, these particles are particles of ether. Although in a particular case they can be mistaken for ether particles, however, in the general case, the picture concerning ether is somewhat unusual. This is described in detail in [17-18]. At the same time, this does not change the concept of mass under consideration.

10. Conclusion

Considering the cross-sectional area of the object and the system instead of the mass allows to:

- create a clear and causal picture of the mechanism of physical interaction.
- to justify the presence of gravitational shielding;
- to determine the presence of hidden mass (matter) in massive celestial bodies and in the entire universe as a whole.
- to propose a causal picture of the mass defect;
- describe and interpret the abnormal manifestation in the diurnal change in gravity;
- to substantiate the cause of the precession of the perihelion of Mercury and artificial Earth satellites;
- describe the features of tidal processes.

It should be noted that each of the above issues is fundamental. In matters of physical interaction, the representation of mass as an area of interaction involves the participation of an intermediate material substance that physically connects objects with each other. We are talking about a classic broadcast. Regarding the ether, a work was published [18], where an analogue of the classical ether, based on the ideas of P. Dirac, is presented as a classical ether [19]. The substantiation of the existence of an analogue of the classical ether, coupled with the stated idea of mass, ensures the integrity of the causal doctrine of the mechanism of physical interaction.

**REVIEWER: Sharipov J.G.,
Candidate of Physical and Mathematical Sciences,
Associate Professor**

REFERENCE

1. Bell. J. S., On the Problem of Hidden Variables in Quantum Mechanics / J. S. Bell // *Rev. Mod. Phys.* - 1966. - T. 38. - Pp. 447–452.
2. Ballentine L. E. The Statistical Interpretation of Quantum Mechanics / L. E. Ballentine. // *Rev. Mod. Phys.* - 1970. -T. 42. - Pp. 358–381.
3. Cramer J. G., The transactional interpretation of quantum mechanics / J. G. Cramer // *Rev. Mod. Phys.* - 1986.- T. 58. - Pp. 647–687.
4. Omnès R., Consistent interpretations of quantum mechanics / R. Omnès. // *Rev. Mod. Phys.* - 1992. - T. 64. - Pp. 339–382.
5. Einstein A. Relativity: The Special and General Theory (Translation 1920). - New York: / A. Einstein. // H. Holt and Company
6. Einstein A. Time, Space, and Gravitation / A. Einstein // *The Times.* - 28 November 1919.
7. Greene B. The Theory of Relativity, Then and Now / B. Greene // Retrieved 26 September 2015.
8. Taylor E.F. Space-time physics: Introduction to Special Relativity (2nd ed.) / E. F. Taylor, John Archibald Wheeler //New York: W.H. Freeman, 1992. - Pp. 84–88. ISBN 978-0-7167-2327-1.
9. Newton I. The Principia: Mathematical Principles of Natural Philosophy / I. Newton // University of California Press, 1999.

10. Evans J. C. Gravity in the century of light: sources, construction and reception of Le Sage's theory of gravitation", in Edwards, M.R. (ed.), Pushing Gravity: / J. C. Evans. // *New Perspectives on Le Sage's Theory of Gravitation*, Montreal: C. Roy Keys Inc, 2002. – Pp. 9–40
11. T.M. Radzhabov. On the distinction between corpuscular and wave processes and the arbitrariness in the basis of special relativity theory / T.M. Radzhabov. // *Physics Essays*. 2023. V. 36-4.– Pp. 405-410,
12. Radzhabov T.M., Mass-area equivalence in classical physics and aspects of mutual shielding of objects. / Radzhabov T.M., // *Physics Essays*, 2022, V.35. 2. – Pp.175-180. DOI.org/10.4006/0836-1398-35.2.175.
13. Radzhabov T.M., Consideration of the daily variation of gravity on the manifestation of gravitational shielding. / T.M. Radzhabov // *Journal of Geoscience and Environment Protection*. Vol.10 No.7. – Pp. 31-47. July 11, 2022. DOI: 10.4236/gep.2022.107003.
14. Radzhabov T.M., On the gravitational shielding, gravitational permeability and hidden matter / T.M. Radzhabov//*International Journal of Geosciences*. Vol.13. – Pp.531-546. Jul.18, 2022. DOI: 10.4236/ijg.2022.137028.
15. Radzhabov T.M., On the Common Nature and Unified Mechanism of Gravitational and Nuclear Interactions / T.M. Radzhabov // *Mathematical Statistician and Engineering Applications*. ISSN: 2094-0343 2326-9865 Vol. 71 No. 4 (2022). – Pp.10784-10794. <http://philstat.org.ph>
16. Melchior P. (1966). The Earth tides. / P. Melchior // Pergamon press Oxford-London-Edinburgh-New-York-Paris-Frankfurt. – 483 p.
17. Radzhabov T.M., On the missed opportunities of classical physics. *Physics Essays*, 2021, V. 34. – Pp. 475-479. [<http://dx.DOI.org/10.4006/0836-1398-34.4.475>]
18. Radzhabov T.M. On The Analogue of The Classical Ether And Its Physico-Philosophical Interpretation. / T.M. Radzhabov. // *JJR*. 2023. DOI: 10.33425/2690-8077.1076.
19. Dirac P.A. (1963). The Evolution of the Physicist's Picture of Nature / Dirac P.A. // *Scientific American*. Vol. 208. No. 5. – Pp. 45–53.

CAUSAL PHYSICS: CROSS-SECTIONAL AREA INSTEAD OF MASS

A review and analysis on the topic of mass and physical interaction within the framework of causal physics is presented. Mass is considered as a special case of a quantity that is proportional to the cross-sectional area of physical objects. Replacing the mass with this quantity allows further development of the kinetic theory of gravity by Le Sage. Physical interaction is considered as a result of mutual shielding of elementary mass-forming elements - nucleons and systems consisting of them - atomic nuclei in the path of movement of cosmic ether particles. It is shown that the applied approach makes it possible to create a visual and causal picture of physical interaction, both in the microcosm and in the macrocosm, leading to completely new results. The existence of gravitational shielding is substantiated, a visual picture of the mass defect is created, the presence of hidden mass in massive celestial bodies is revealed, the reason for the precession of the perihelion of Mercury and artificial Earth satellites is indicated, semi-daily behavior in the diurnal variation of gravity is described and interpreted, features in the manifestation of tidal processes are described. The applied approach allows to consider the issues of interaction in the micro and macrocosm from a single mechanism.

Keywords: mass, hidden mass, gravitational shielding, Le Sage theory, mass defect, diurnal variation of gravity, tidal processes.

Information about the author: Rajabov Toir Makhsudovich - Tajik National University, Candidate of Physical and Mathematical Sciences, Associate Professor. **Address.**734025, Dushanbe, Republic of Tajikistan, Rudaki ave., 17. **Phone:** + 992 93 9995602. **E-mail:** buny_r@mail.ru

Article received 07.12.2023
 Approved after review 15.01.2024
 Accepted for publication 11.04.2024

EFFECT OF BARRIER DISCHARGE ON GERMINATION ENERGY AND GERMINATION OF "NAVRUZ" WHEAT SEEDS IN THE OPEN FIELD

Solikhova M.I., Kurzina I.A., Khojazoda T.A,
Khodzhaev A.T., Daybova E.B.

Wheat is considered to be one of the vital foodstuffs in Central Asian countries and is one of the strategically important agrarian crops - it provides the highest number of calories and nutrients in the diet of the inhabitants of the region. The area under wheat cultivation in Central Asia has been growing since 1991 in the territories of Uzbekistan, Turkmenistan and Tajikistan [1].

The trend towards more environmentally friendly practices in agriculture emphasizes the importance of considering the environment when developing and implementing new technologies. This includes the use of practices that minimize negative impacts on soil, water and air, and reduce the use of chemical fertilizers and pesticides. Organic produce grown using sustainable practices contributes to food safety and consumer welfare. Seed treatment with various methods can improve seed properties such as germination, disease and stress resistance, which ultimately affects the quality and quantity of the crop. Environmentally sound seed treatment methods can help to reduce the risk of disease and reduce the need for chemical defenses. Such approaches promote sustainable agriculture, which is a key aspect of food security and environmental conservation [2].

Physical treatment is one of the most effective methods to determine the potential yield and quality of products. In recent years, the factors of physical treatment of seeds of various crops to accelerate germination and increase field germination have been increasingly studied, and the main criterion for assessing all types of productivity is considered to be the yield of agricultural crops [3].

The principle of seed treatment before sowing by physical factors to stimulate seed development and increase yield has a significant history. According to literature sources, this issue was dealt with by A.V. Sirotnina, M.F. Trifonova, I.F. Borodin. More than 40 physical methods are known to act on seeds, resulting in increased germination, enhanced light scattering and increased germination energy. These methods can act on a variety of physical and biochemical processes in plants, ultimately leading to improved plant growth, development and productivity. Yield increases of 15-30%, accelerated maturation and improved product quality are significant, especially in the context of improving agricultural efficiency and food security [4].

According to studies, pre-sowing irradiation of wheat seeds with short-wave ultraviolet radiation resulted in suppression of growth, decreased transpiration intensity, while medium-wave irradiation on the contrary stimulated growth, and increased transpiration intensity of leaves of wheat plants [5].

Exposure to radiation, ultraviolet lasers causes various changes in metabolism and energy. The effects of physical methods on plants can lead to various changes in their physiology and biochemistry. Disruption of membrane integrity, changes in compound content, accumulation of free radicals, genetic damage, changes in protein synthesis and regulation of genomic expression can be a consequence of such exposure. These changes can have both positive and negative effects on plant growth and development. Including some physical

methods can stimulate growth and improve product quality as mentioned earlier. While other methods may cause stress and damage to plants, which can negatively affect their survival and productivity [6].

In order to increase field germination, quality and yield of agricultural crops, various pre-sowing seed treatments are used today, including irradiation with electromagnetic fields in the radio range from decimeters to millimeters [7-8-9]. Some researchers suggest that millimeter waves can influence cellular structure and metabolism through their effect on biochemical processes in tissues [10]. One of the most important directions of scientists is to study the effects of low-intensity millimeter waves on plants and their vitality.

Taking into account environmental safety, these waves can have a positive effect on the growth and development of plants, which can bring considerable benefit to agriculture. However, it is important to keep in mind that any technology, even if it aims to improve plant growth, must be evaluated in terms of its full environmental impact. In order to consider methods environmentally sound, it is necessary to consider not only the impact on plants, but also the potential impacts on soil, water and other elements of the ecosystem [11-12].

Electromagnetic radiation covers a wide range of different frequencies and wavelengths. From extremely low frequencies such as radio waves to gamma rays and X-rays, which are ionizing and can cause ionization of atoms and molecules.

The effects of radiation on biological objects such as seeds depend on the dose of radiation. Low doses of radiation can have a stimulating effect on enzymatic reactions and other biological processes. On the other hand, high doses, especially of ionizing radiation, can cause damage to DNA and other cellular structures, which can lead to inhibitory effects or even cell death. [8-13]. Stimulating doses promote growth and change the physicochemical state of the cell, membrane permeability and other metabolic reactions. The dose effect causes disturbances of intracellular structures, the restoration of which is costly [8-10].

Studies have shown that certain electromagnetic field parameters can positively influence plant growth and yield, improve photosynthesis and metabolic processes. However, the effects may be sensitive to specific growing conditions and require certain optimal parameter values [14-15]. According to researchers' observations, practical scientific experiments have increased seed integrity, density and germination [16], and ozonation has a positive effect on the progress of seed properties of seeds in particular, germination energy and laboratory germination.

Ozone stimulates seed germination and, as a consequence, plant growth and improved enzymatic properties of seeds involved in the breakdown of endosperm reserves and providing energy for germination. Exposure of seeds to ozone can accelerate metabolism, activating enzymes responsible for the hydrolysis of carbohydrates such as glucose and starch. This in turn promotes more efficient germination and plant development. However, it is worth noting that the effects of ozone can also be dual and concentration dependent. High concentrations of ozone can stress plants and lead to negative effects such as damage to cell structures and reduced photosynthesis.

The purpose of many studies is to determine the appropriate parameters of pre-sowing treatment of wheat seeds with physical influences, to increase germination energy, germination, productivity, yield and improve grain quality [2]. As the literature review shows in the course of most experiments the positive effect of physical methods on the seeds of technical crops was established: the quality of seed sowing, bioindicators of plants is improved, the number of their diseases is reduced, germination energy is increased, yield and quality of products are increased.

It is proved that the influence of physical methods increases the solubility of salts and acids, which leads to changes in pH and bioelectric potential of plant cells.

Thus, the permeability of cell membranes increases, which facilitates the diffusion of molecules and ions through the cell membrane. As a result, seeds absorb more water. In addition, the diffusion rate of oxygen molecules through the cell membrane increases, the spore formation processes of phytopathogenic fungi are inhibited, ion transport is enhanced, which causes an increase in the concentration of mineral elements entering the cell, [17] the process of increasing the volume of cytoplasm is accelerated, the intensity of oxidative and photosynthetic reactions is increased [18].

One of the most important elements of technical crops research is represented by pre-sowing seed treatment, which allows taking advantage of potential opportunities. In practical crop production, seed treatment has an effective significance for finding ways to increase plant productivity and its resistance to a variety of negative environmental conditions. One of the successful ways to increase the yield and quality of crop production is the application of physical factors for pre-sowing seed treatment [19-20]. This treatment is aimed at improving the biological properties of seeds, stimulating and enhancing their development, protection from diseases and pests, and resistance to stress conditions. Improvement of seed properties can be achieved by various physical methods [21].

The harm caused to the environment by physical factors in seed treatment is much less. Such methods include ultrasound, ionizing radiation, electromagnetic fields, as well as thermal, photoenergetic or optical influence, including coherent radiation by barrier discharges, gamma and X-rays.

Indeed, research into the effects of electric shocks and electromagnetic fields on plant seeds has attracted the attention of scientists and agronomists.

These techniques are often considered as alternative ways to improve seed germination, plant growth and consequently yields. The application of electric and magnetic fields can influence various biological processes such as activation of enzyme systems, changing the physicochemical state of cells, stimulating metabolism and other metabolic reactions.

The interest in these techniques is not only related to yield improvement, but also to their potential impact on environmental sustainability and product quality. However, despite some positive results, the efficacy and applicability of these techniques may depend on various factors including plant type, growing conditions, parameters of electric and magnetic fields and others.

In order to reduce the influence of unfavorable factors acting on agricultural production, it is necessary to search for methods that improve its qualitative and quantitative indicators in different climatic conditions, regardless of the condition of the seed. One of the widely used techniques in this area is pre-sowing seed treatment [22]. Due to the fact that under the influence of pre-sowing seed treatment with physical method physiological and biochemical processes flow better, high yields increase and product quality improves.

Various factors, such as electric discharges and electromagnetic fields, can act as catalysts for growth processes and metabolic directionality, consistent with current research in agrophysics and plant biology. The effects of physical influences on plant growth and development are being studied to increase yields, improve product quality, and create more efficient agricultural practices. Physical factors such as electric fields and magnetic fields can affect various aspects of plant physiology: germination, root and stem growth, flowering and fruiting. However, it is worth noting that the effects may depend on the specific parameters of these fields, such as frequency, intensity and duration of exposure.

The present study shows that in order to increase yield with minimum economic and energy costs while maintaining high quality traits, it is extremely important to select common plant-stimulating interacting factors that cause positive changes in physiological and biochemical processes in plants. According to literature data, high intensity of physiological-biochemical processes associated with increased plant productivity can lead to micronutrient deficiency. The increase in seed germination energy during laboratory germination under the influence of barrier discharges leads to better rooting and development of leaf apparatus of seedlings, which, in turn, leads to an increase in plant mass and productivity [19-20].

The research work was carried out by setting up field experiments in accordance with the established methods of conducting such experiments with the influence of barrier discharge. This field experiment was conducted to improve the germination energy and germination of wheat seeds after treatment with electric barrier discharge.

EXPERIMENTAL PART

The object of the experiment was wheat seeds of "Navruz" variety. Type of plasma source treatment - barrier discharge at atmospheric pressure. Before sowing treatment of wheat seeds by barrier discharge was conducted on 01.04.2023 in the laboratory of the Institute of High Current Electronics SB RAS. The treatment time was 4 and 6 minutes.

The main argument of the source was a glass cuvette of 10 ml volume, the walls of which were a dielectric barrier dividing the electrodes of the discharge system.

The pulse repetition rate was 71 kHz. The duration of the current pulses was presumably 1 μ s, with an amplitude of almost 12 mA, and with a voltage amplitude of approximately 290V. Consequently, we can put the average power invested in the discharge over the pulse period: $2 \times 950 \text{ V} \times 0.012 \text{ A} \times 10^{-6} \text{ s} \times 71 \times 10^3 \text{ Hz} \approx 1.6 \text{ W}$.

Tale 1. Parameters of plasma treatment of wheat seeds

Mode number	Pulse frequency, kHz	Current pulse duration, μ s	Voltage amplitude, V	Current amplitude, mA	Exposure time, min.
1	71	1	950	12	4
2	71	1	950	12	6

The coaxial electrode system is formed by a multi-axial central electrode immersed in the cuvette cavity and a cylindrical electrode covering the outer surface of the cuvette. The experiments revealed the optimal treatment conditions. During plasma treatment of wheat seeds, samples were loaded into the cuvettes. Two treatment modes were applied, the parameters of which are given in Table 1 [23].

RESULTS

Analysis of the investigated data shows that treatment of seeds before sowing with different physical methods leads to obtaining good and stable crop yields. Under certain influence of external factors, in particular electric barrier discharge, there is a positive effect on

their sowing qualities. The effectiveness of seed and planting object treatment before sowing depends largely on seed moisture and atmospheric conditions. Physical influences appear to be an effective method of seed treatment before sowing. With proper selection of treatment, all types of physical influences lead to an increase in yield of each object under study [24].

The seeds of wheat variety "Navruz" were used as an object of research. Research works of field experiment of influence of pre-sowing seed treatment with barrier discharge on growth processes of wheat plants of "Navruz" variety were conducted in the Republic of Tajikistan (Rudaki district, Dehkan site "Murajan"). For reliable explanation of the results of all conducted experiments the processes of germination energy and total germination of wheat in the open ground were carefully observed.

Table 2. Results of the field experiment before and after treatment

№	Barrier discharge 48h and 72 h	Date of processing	Date of sowing	Bookmark seeds	Emergence of seedlings after seed placement (days)				Germination	% - Energy . germination to contro	% - Total germination to control
					3	4	5	6			
		01.04.2023	03.04.2023	With cooling for 48 hours after treatment						63.4	6.4
1	Control			920	41	153	302	332	828		
2	Processed 4 min			920	77	196	325	285	883		
3	Control			920	51	155	304	324	834		
4	Processed 6 min	920	61	188	311	285	843	16.3	1.07		
		01.04.2023	04.04.2023	With cooling down for 72 hours after treatment						47.6	4.07
5	Control			920	42	149	298	321	810		
6	Processed 4 min			920	62	185	314	282	843		
7	Control			920	48	148	295	319	810		
8	Processed 6 min	920	50	173	306	297	826	4.1	1.9		

From the experimental data obtained, it can be said that treatment of wheat seeds with barrier discharge on germination energy and total plant germination gives indicative results. As can be seen from Table 2. Pre-sowing treatment of wheat seeds with electric barrier discharge with time of 4 and 6 minutes stimulates germination energy and total germination. According

to the data obtained, the germination energy of treated samples at 4 min with cooling 48h after treatment increased by 63.4% and total germination by 6.4% compared to control, while the germination energy and germination of wheat at 6 min with cooling 48h was 16.3% and total germination was 1.07% compared to control. The treated variant of 4 min with cooling 72h compared to control showed the following results: 47.6% germination energy, 4.07% total germination, germination energy, and total germination, treated wheat with time 6 min with cooling 72h compared to control variant were 4.1% and 1.9%.

As can be seen from Fig.1 positive results of germination energy and total germination yielded treated variant with treatment time 4 min with cooling 48 h, and 6 min with cooling 48 h was almost identical to the control.

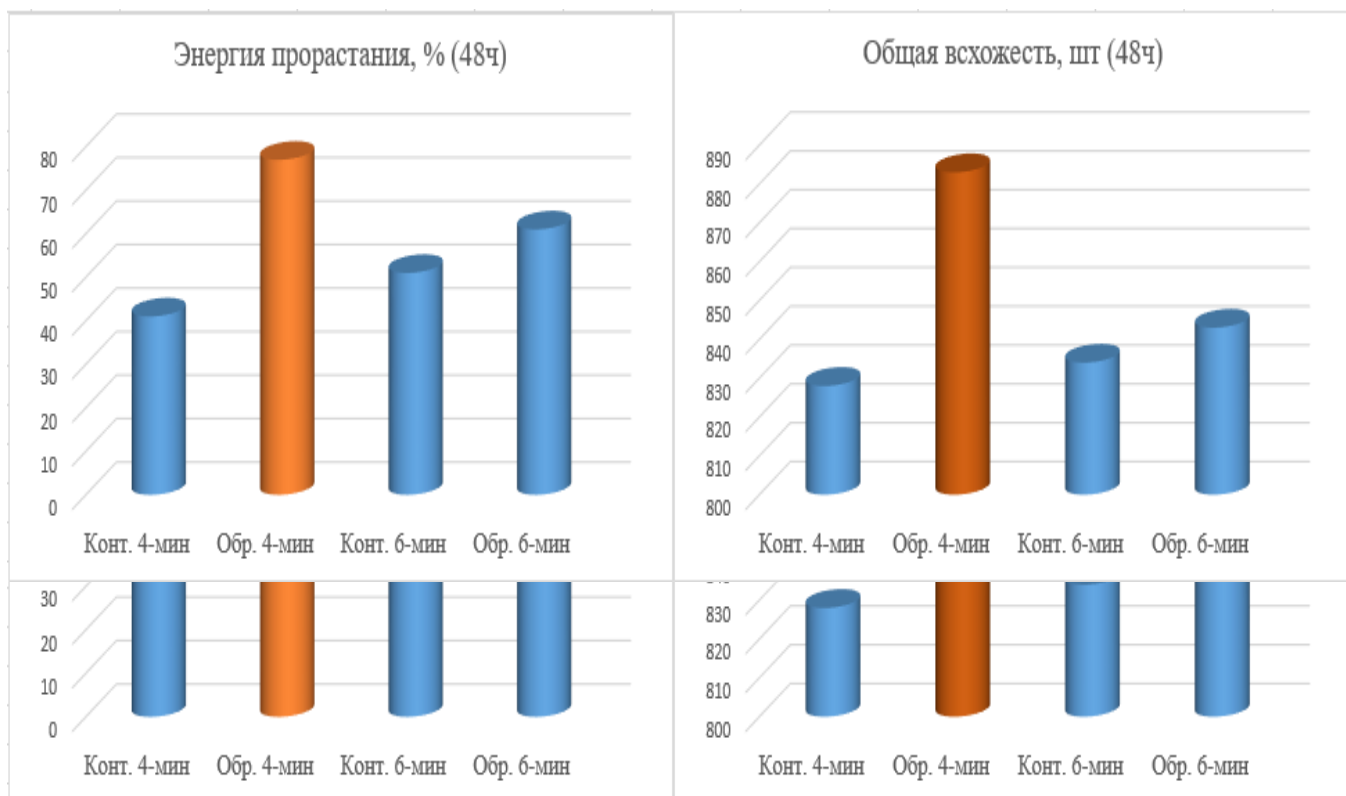


Fig.1. The appearance of the first shoots and overall germination, control and barrier-discharge treated wheat seeds of the “Navruz” variety with cooling for 48 hours

In Fig.2. the results of a study of germination energy and general germination are presented, which were processed with a time of 4 minutes and 6 minutes, with a cooling period of 72 hours. The results vary slightly from the control variant.

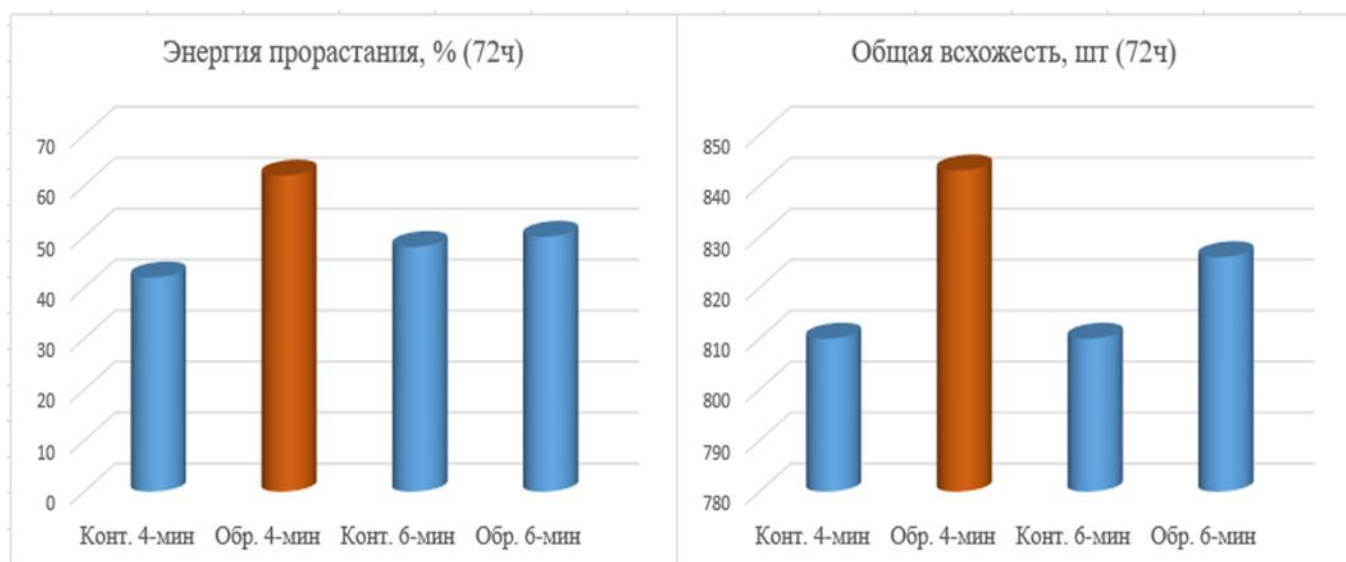


Figure 2. Appearance of first sprouts and total germination, control and barrier discharge treated seeds of wheat variety "Navruz" with cooling 72h

CONCLUSION

The aim of the experiment was to investigate the effect of electric discharge on the acceleration of germination energy and total germination of wheat variety "Navruz". The experimental data obtained show that higher treatment with time of 6-i min, cooling at 48h decreased field germination energy by 47.1%, and total seed germination relative to the control decreased by 5.33%.

The results of the research allow us to conclude that low treatment of seed material before sowing had a positive effect on the field germination energy and germination of industrial crops. One of the main indicators characterizing the biological properties of seeds is their ability to germinate and rooting of seedlings, which affects the increase in a number of physiological and biochemical processes: seed qualities improve, germination energy and total germination increases.

The best result of the present field study under the influence of electric barrier discharge on wheat seeds was shown by a group of seeds treated with barrier discharge operating in 4-minute mode with cooling 48 hours. In biomass growth, the length of sprouts and roots emerged from wheat seeds treated in this mode was more than 60%. Seed treatment with electric barrier discharge, in the mode of 6 min with cooling 72 hours, gave negative results and showed similar results to the control.

**REVIEWER: Kudryashov S.V.
Doctor of Chemical Sciences**

REFERENCES

1. <https://cabar.asia/ru/diversifikatsiya-rynka-pshenitsy-vopros-prodovolstvennoj-bezopasnosti-kyrgyzstana>
2. Creation and study of spring soft wheat source material in the conditions of Amur region for obtaining high-yielding food purpose varieties of spring wheat. <https://apknet.ru/sozdanie-i-izuchenie-ixodnogo-materi/>
3. Krasilnikov V.V. Effect of pre-sowing seed laser treatment on spring wheat yield. 2019. / V.V. Krasilnikov., O.G. Dolgovykh., A.B. Spiridonov. // <file:///C:/C:/Users/admin/Documents/Downloads/vliyanie-predposevnoy-obrabotki-semyan-lazerom-na-urozhaynost-yarovoy-pshenitsy.pdf>

4. Klochkov A.V. Seed germination in a magnetic field. / A.V. Klochkov., O. S. Klochkova., O. B. Solomko // Belarus, 2020. – Pp.163-168. <https://elib.baa.by/xmlui/bitstream/handle/123456789/2542/%D0%9A%D0%BB%D0%BE%D1%87%D0%BA%D0%BE%D0%B2%20163-168.pdf?Sequence=1&isallowed=y>
5. Safaralikhonov A.B. Effect of pre-sowing UV-irradiation of wheat plant seeds on their subsequent growth and intensity of leaf transpiration / A.B. Safaralikhonov., F.N. Khudoyorbekov., O.A. Aknazarov // Plant Physiology. 2016, T. 59, №7-8. – Pp.344-349.
6. Lakhanova K.M. The effect of different doses of X-rays and gamma rays on Ural licorice / K.M. Lakhanova., M.U. Sarsembaeva. // Uspekhi sovremennoi naukhnoostroiznaniya. 2015. № 6. – Pp.119-122.
7. Shein A.G. Experimental study of the effect of low-intensity microwave radiation on germination / A.G. Shein., R.N. Nikulin., I.A. Kovalev., D.G. Artemova., L.H. Chang., M.P. Nikulina // Biomedical Radioelectronics, No. 4. - 2009. – Pp. 77-121.
8. Savelyev V.A. Laser improves seeds / V.A. Savelyev., Kulikov V. // Uralskie niv. - 1984. - №12. – Pp.28-29.
9. Ragha L. Effects of low power microwave fields on seed germination and growth rate / L. Ragha., S. Mishra., V. Ramachandran M. S. Bhatia. // Journal of Electromagnetic Analysis and Applications, – 2011. –Vol. 3. – Pp. 165-171.
10. Devyatkov N.D. Features of interaction of low intensity millimeter radiation with biological objects / N.D. Devyatkov, O.B. Betsky // Collection of reports: Application of low intensity millimeter radiation in biology and medicine / M.: 1985. – Pp.6-20.
11. Sidortsov I.G. Increasing the efficiency of the effect of a permanent magnetic field on the seeds of grain crops during their pre-sowing treatment / I.G. Sidortsov // Zernograd, 2008. – P. 19.
12. Dresvyannikova E.V. Possibilities of regulation of heat and moisture treatment processes in mass-exchange apparatuses under the influence of electric field / E.V. Dresvyannikova., P.L. Lekomtsev., A.V. Savushkin. // Engineering bulletin of Don. 2014. №1. URL: ivdon.ru/en/magazine/archive/n1y2014/2235.
13. Dolgovykh O.G. Ecologically safe pre-sowing seed treatment of spring wheat / O.G. Dolgovykh., V.N. Ognev. // Engineering Bulletin of Don, 2014, No. 4 URL: ivdon.ru/en/magazine/archive/n4y2014/2565.
14. J. C. Evaluating scientific literature on biological effects of microwave radiation / J. C. Evaluating, J. C. Lin // IEEE Microwave Magazine, - 2004. - Vol. 5. - № 1. – Pp.34-37
15. Karpovich V. A. Application of microwave energy in modern biotechnologies / V. A. Karpovich., V. N. Rodionova., G. Ya. Lepyan // Symposium Proceedings, Kharkov, 2001. – Pp. 909-910.
16. Ivanovna A.S. Application of physical method in protection of spring wheat from diseases in the Middle Volga region / A.S. Ivanovna // Saratov, 2013. <https://earth.papers.net/prominence-fizicheskogo-metod-v-zaschite-yarovoy-pshenitsy-ot-bolezney-v-srednem-povolzhie>
17. Zhiltsov A.V. Presowing treatment of seeds in magnetic / A.V. Zhiltsov., V. V. Savchenko., A. Y. Sinyavskiy. // Kyiv, 2019. – Pp.243-245. <https://core.ac.uk/download/pdf/212954909.pdf>
18. Gorelov M.V. Installation for pre-sowing treatment and drying of seeds by microwave energy / M.V. Gorelov., T.N. Bastron. // Krasnoyarsk. 2020, – Pp.195-198. <file:///C:/C:/Users/admin/Documents/Downloads/ispolzovanie-svch-energii-dlya-predposevnoy-obrabotki-semyan.pdf>
19. Reshetnikova S.N. Yield and quality of spring wheat depending on ionizing radiation and microelements in the forest-steppe of the Volga region. 2002, / S.N. Reshetnikova // Ulyanovsk. – P.150.
20. Khodzhazoda T.A., Influence of barrier discharge on germination energy and germination of cotton seeds / T.A. Hodzhazoda., I.A. Kurzina., S.V. Kudryashov., A.Yu. Ryabov, D.N.Lytkina., M. I. Solikhova., A. T. Hodjaev // Tomsk, - 2022. - № 28. – Pp. 65-75.
21. Isupov A.N. Laser treatment of seeds-results of field trials in Udmurtia. 2020. / A.N. Isupov., O. N. Krylov., M. M. Kiselev., A. E. Reshetnikov. // <https://agbz.ru/articles/lazernaya-obrabotka-semyan/>.
22. Krylov O. N. Laser treatment of seeds. / O. N. Krylov., M. M. Kiselev., A. N. Isupov // <https://agbz.ru/articles/lazernaya-obrabotka-semyan-rezultaty-polevykh-ispytaniy-v-udmurtii/>
23. Khodjaev A.T., Treatment of wheat seeds of "Navruz" variety by barrier discharge plasma at atmospheric pressure / A.T. Khodjaev., M.I. Solikhova., K.P.Savkin// – P.70. https://conf-prfn.org/Files/2023/program_2023.pdf
24. Khodjazoda T.A. Effect of pre-sowing barrier discharge treatment on germination energies and germination of maize seeds / T.A. Khodjazoda., I.A. Kurzina., R.S. Makhmadbegov., A.T. Khodjaev., M.I. Solikhova., D.N. Lytkina // Kishovarz. – 2023. - №1. – Pp. 22-26.

EFFECT OF BARRIER DISCHARGE ON GERMINATION ENERGY AND GERMINATION OF "NAVRUZ" WHEAT SEEDS IN THE OPEN FIELD

The paper presents the treatment of wheat seeds with barrier discharge for 4 and 6 minutes. Laying of treated seeds on research field was carried out with chilling at 48h and 72h after barrier discharge treatment. Treatment of plants with barrier discharge affects growth stimulation, germination energy, germination and, as a consequence, the increase in wheat yield and seed quality. In recent years, methods aimed at stimulating (accelerating growth, increasing yield, improving crop quality) electrophysical effects on plants and seeds of grain crops have been increasingly introduced into the practice of effective land management. Among various electrophysical methods used in crop production, a special place is occupied by discharge treatment. Many scientists have confirmed high efficiency and exceptional environmental friendliness of pre-sowing treatment of agricultural seeds, including seeds of technical crops. The present task is to investigate new ways of seed treatment, for example, by physical factors. Characterization of the effects of energy discharges on germination vigor and germination of wheat is reviewed. Some of the most important plasma parameters include the treatment time of the main tissues, which should be carefully chosen, to optimize the efficiency. This experiment was conducted under field condition. Results of field experiments showed that the barrier discharge treatment affected germination rate and had a positive effect on germination of wheat seeds. This paper presents the results of field experiment on the effect of barrier electric discharge on seed germination energy and total germination rate.

Key words: wheat, seeds, physical effects, barrier discharge, pre-sowing treatment, open ground, germination energy, germination.

Information about the authors: Solihova Mahina Imomalievna - Institute of Biology, Tomsk State Research University, graduate student. **Address:** 634050, Tomsk, Russia. **Phone:** +79234231995, +992988701187. **E-mail:** solihovamahina@gmail.com

Kurzina Irina Aleksandrovna - Tomsk State Research University, doctor of physics and mathematics, head of the department of natural compounds, pharmaceutical and medical chemistry. **Address:** 634050, Tomsk, Russia. **Phone:** +79138821028. **E-mail:** kurzina99@mail.ru

Khojazoda Tohir Abdullo – Tajik National University, Doctor of Physics and Mathematics, Professor of the Department of Physical Electronics, Faculty of Physics. **Address:** 734025 Dushanbe, Tajikistan, 17 Rudaki Ave. **Phone:** +992900526352. **E-mail:** toir.khodzhaiev.62@mail.ru

Khojaev Abdullo Toirovich - Institute of Biology, Tomsk State Research University, graduate student. **Address:** 634050, Tomsk, Russia. **Phone:** +79234336452, +992009770532. **E-mail:** abdullo1997asa@gmail.com

Daybova Elena Borisovna - Scientific Research Institute of Crops and Peat of Siberia - branch of RASS of the Russian Federation, candidate of chemical sciences, head of the laboratory. **Address:** 634050, Tomsk, Russia. **Phone:** +79234203876. **E-mail:** edaibova@eandex.ru

Article received 18.12.2023

Approved after review 20.01.2024

Accepted for publication 28.03.2024

INFLUENCE OF SURFACTANT CONCENTRATION ON CHANGES IN THE PLANE OF POLARIZATION OF LIGHT WHEN PASSING THROUGH THE LCD MEDIUM

Maksudov B.I., Egamovb M.Kh., Rakhimova W. J.

Although over the past half century significant progress has been made in the study of the structure and properties of liquid crystals related to optical electronics, holography and information security [1-3], some issues in this aspect still remain unresolved. Such problems include orientational order relationships in nematics in the presence of cationic surfactants. In essence, this problem is quite multifaceted and its solution is largely determined by the type of microparticles introduced into the nematic volume as an impurity, their nature, as well as a number of external destabilizing factors [4]. In nematics, the phenomenon of birefringence anisotropy is observed, which is controlled by external fields (electric, magnetic, light, sound or mechanical). This effect makes it possible to simulate light radiation in the optical range according to important physical parameters such as phase, amplitude and polarization. When studying nematic liquid crystals (NLCs) in the absence of external forces, due to the anisotropy of the refractive index (Δn), it is possible to change the orientation of the plane of polarization of light radiation passing through the cell. Accordingly, they can be used as media for passive optical phase shifters and serve as an alternative for aqueous dye-based solutions [5,6].

There is a similar method for developing LC elements designed to polarize light radiation under the influence of an electric field (active mode) or in their absence (passive mode). To do this, in order to improve brightness, contrast and performance, special orienting surfaces with a pre-selected morphology are used [7], and the volume of the LC cell is filled with surfactants. When a surfactant is introduced into an LC medium, the anisotropy of the refractive index (Δn) changes greatly. Consequently, the last argument affects the magnitude of the change in the plane of polarization between the incident rays and those directly passing through the LC cell

$$\Delta\varphi = \frac{2\pi d}{\lambda} \cdot \Delta n = \frac{2\pi d}{\lambda} \cdot (n_e - n_0) \quad (1)$$

where d is the thickness of the LC layer; n_0 – refractive index for an ordinary beam; n_e is the refractive index for the extraordinary ray. In equation (1), the value of n_0 is a constant value for the LC material under study, and n_e strictly depends on the degree of director orientation (the predominant direction of molecular orientation along the main optical axis) of the LC. Changes in the polarization plane $\Delta\varphi$ in equation (1) negatively affect the operation of LCD devices in both passive and active modes. Therefore, in order to reduce undesirable losses in the intensity of the simulated light beam, it is necessary to solve the problem of matching the LC elements with the optical design of the device according to the position of the polarization plane. This work is devoted to solving exactly this kind of problem. To solve this problem, we studied the influence of the concentration of surface-active media (surfactants) in the form of nanoparticles from the cationic surfactant - cetyltrimethylammonium bromide (CTAB) on the magnitude of the change in the polarization plane of light in the nematic liquid crystal (NLC) 4-pentyl-4-cyanobiphenyl (5CB). This allows the liquid crystal cell and the polarizer to be matched in terms of the degree of orientation of the polarization plane not only due to the thickness of the layer, but also due to the concentration of CTAB.

EXPERIMENTAL PART

The liquid crystal cell was created in a twist-nematic configuration, consisting of two parallel glass plates, on one side of which conductive metal coatings based on indium tin oxides (ITO) were applied. The latter had a thickness of ~ 200 nm with a triple content of 74% (In), 18% (O₂) and 8% (Sn) by weight [8,9]. In thin layers of coating, ITO becomes transparent and colorless, so in the IR region of the spectrum it acts like metallic glass. ITO thin films were deposited on the surface of glass substrates via physical vapor deposition. To prepare and mix the liquid crystal mixture, a magnetic stirrer was used with a rotation speed of 3500 rpm. The thickness of the LC layer was controlled using Teflon gaskets. To determine the rotation of the polarization plane, a Ge-Ne laser with a wavelength of $\lambda=0.633$ nm at room temperature was used. The initial position of the polarizer and analyzer was chosen in such a way that when placing two oppositely located glass plates with an LC cell thickness of 8–10 μm , maximum light transmission was achieved [10]. The signal transmitted through the cell was recorded on an FD-10-GB photodetector.

RESULTS AND DISCUSSION

A surfactant (surfactant) in the form of ionic surfactant cetyltrimethylammonium bromide (CTAB), dissolving in a mixture of nematic liquid crystal (NLC), dissociates into a positive surfactant ion CTA⁺ and negative ions Br⁻. CTA⁺ ions are adsorbed on substrate substrates and determine the homeotropic adhesion of the nematic [11-13]. As mentioned above, the formation of a homeotropic or twisted director configuration under rigid perpendicular coupling depends on the coupling coefficient ρ . The critical value ρ_c corresponding to the transition between these structures is determined by the ratio of the elastic modulus of the liquid crystal and is about unity for the PVA polymer matrix.

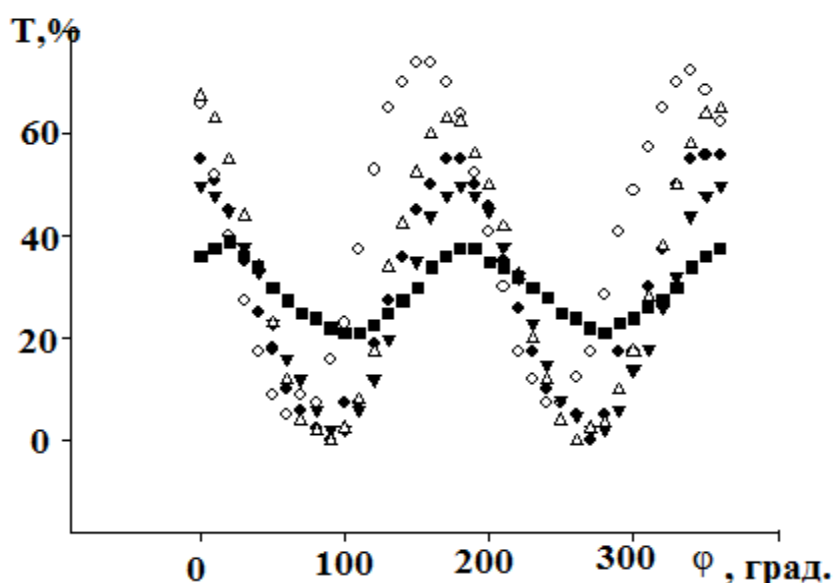


Fig. 1 Dependence of the light transmission of NLC 5SV cells on the angle of rotation of the polarizer (■) – initial; (◆) – 0.05 wt.%; (◇) – 0.1 wt.%; (▼) – 0.3 wt.%; (△) – 0.5 weight.%

The observation results showed that the configuration of the cells we studied with the introduction of a surfactant consists of a combination of two components: due to the concentration of the surfactant and a change in the plane of polarization in the lateral limiting planes. The latter makes almost no contribution to the effect we are studying, so they can be ignored. Figure 1 illustrates the dependence of the light transmittance of 5SV LC cells with different surfactant concentrations on the angle of rotation of the samples relative to the analyzer and polarizer. An experimental setup to determine the dependence of the light transmittance of LC cells with different concentrations on the relative position between the analyzer and the polarizer was assembled in such a way that the maximum transmission was observed between 0 and 180°, and the minimum transmission was observed at 90 and 270°. Then it is possible to identify the position of the maximum transmittance coefficients based on Malus's law. These shifts are clearly visible when analyzing the values given in Table 1.

Fig. 1. Changes in the plane of polarization in an LC cell

Transmittance extremum position	Concentration of CTAB in the composition of NLC 5 SV, wt.%				
	0	0,05	0,1	0,3	0,5
90°	86,1	85,7	66,4	94,8	101,5
180°	173,8	174,3	155,0	181,9	186,6
270°	266,1	266,0	245,4	172,1	279,8
360°	255,5	353,4	338,1	361,8	375,5

As can be seen, with increasing concentration of the CTAB surfactant, a shift in all maxima is observed, except for samples containing 0.1% CTAB, relative to the maximum light transmittance for the original 5SV NLC. Moreover, the average deviation of the position of the extrema in relation to the initial NLC 5SV for concentrations of 0.05 and 0.1% is negative (by -0.5° and -19.2°, respectively), and for concentrations of 0.3% and 0.5% is positive (at 7.3° and 15.5°, respectively). It was shown in [14] that a concentration of 0.1% corresponds to the concentration condition at which the transition from the nematic to the smectic state occurs. In our case, such a transition manifests itself in a change in the polarization properties of the films under study. From Fig. 1 we can determine the ratio of the amplitudes of the radiation intensity passing through the liquid crystal cell relative to the ox and oy axis. The main condition for determining the amplitude of the radiation intensity along the x axis must be the maximum transmittance, and along the y axis, on the contrary, the minimum. Then, using the shift of extrema $\Delta\varphi$ and the ratio I_{ox}/I_{oy} , it is possible to determine the azimuthal angle α and the elliptical angle ε , which explain the radiation with elliptical polarization [8];

$$\operatorname{tg}(2\alpha) = \frac{2\sqrt{\frac{I_{ox}}{I_{oy}}}}{1 - \left(\frac{I_{ox}}{I_{oy}}\right)} \cdot \cos(\Delta\varphi) \quad (2)$$

$$\sin(2\varepsilon) = \frac{2\sqrt{\frac{I_{ox}}{I_{oy}}}}{1 + \left(\frac{I_{ox}}{I_{oy}}\right)} \cdot \sin(\Delta\varphi) \quad (3)$$

It turned out that for the initial 5CB NLC and a cell with a concentration of 0.05% CTAB-a, the light radiation passing through the cells can be perceived as polarized, since the ratio I_{ox}/I_{oy} is greater than 100; in cells containing NLC 5SV and concentrations of 0.1 and 0.3 wt.% CTAB-a, light radiation can be considered linearly polarized, since the conditions $10 < I_{ox}/I_{oy} < 100$ are met; and a cell containing 0.5 wt.% surfactant serves as a means for obtaining elliptical polarization of light. In the latter case, the condition is I_{ox}/I_{oy} less than 100. To interpret the results obtained, we took into account the influence of the surfactant CTAB on the director of NLC 5SV. To do this, the z axes were chosen so that the conditions of perpendicularity to the plane of the glass substrate were satisfied [15, 16]. In this case, the dependence of the refractive index (n_e) on the displacement angle θ of the extrema is written by the expression.

$$n_e(\theta) = \frac{n_{\perp} n_{\parallel}}{\sqrt{n_{\perp}^2 (\cos \theta(z))^2 + n_{\parallel}^2 (\sin \theta(z))^2}} \quad (4)$$

Here, in passive mode (in the absence of an external field), the cells $n_e = n_{\parallel}$, where $\Delta n = n_{\parallel} - n_0$, and in active mode (i.e. in the presence of an external electric field) - $n_e = n_{\perp}$, where $\Delta n = n_{\perp} - n_0$. This means that under the influence of an external electric field, a reorientation of the director of the 5SV NLC and local fluctuations of dipoles in the volume of a liquid crystal drop relative to the introduced CTAB surfactants are observed. The results obtained can also be explained by changes in the anisotropy of the refractive index (n_e) and are in good agreement with the results of [17], where similar parameters for the performance of LC cells were studied. Having analyzed experimental data on changes in the state of the plane of polarization in cells made of 5SV NLC and surfactant concentration CTAB, the following conclusions are put forward. At CTAB surfactant concentrations of 0.3 and 0.5 wt. %, you can change the position of the plane of polarization relative to the original cell of the NLC 5SV by 7.3 and 15.5°, respectively. Similar results can be obtained at concentrations of 0.1 wt. % by a value of 19.2°, and for 0.05 wt. % by only 0.5°, which we attribute to the error of the measuring equipment and minor fluctuations in the optical properties of concentrated NLCs in relation to the original cells.

CONCLUSION

Changes in the concentration of CTAB contribute to not changing the thickness of the LC cells and not resorting to the use of additional mechanisms and devices such as polarization plane rotators to match the NDC elements with external optical circuits. This fact is of valuable practical interest for display technologies, since it is possible to integrate an NLC composite with the addition of a CTAB surfactant, with improved spectral and dynamic characteristics, and install a thickness fixation device into the body. The studied LC composites can be used as passive rotators of the plane of polarization, the magnitude of rotation of which is adjusted by changing the concentration of the CTAB surfactant and the thickness of the cell layer. For laser technology, this relationship is beneficial in conditions where it is not possible to change the thickness of the layer or it is impossible to change the position of the polarizer. The work was carried out within the framework of the project “Study of the structure, mechanical and optical properties of new optoelectronic elements based on polymer-liquid crystal composites” for 2021-2025, under state no. registration 0121TJ1107 dated March 10, 2021 and financed from the budget of the Republic of Tajikistan.

Conflict of interest. The authors declare that they have no conflict of interest.

**REVIEWER: Abdulloev Kh.M.,
Doctor of Physical and Mathematical Sciences,
Professor**

REFERENCES

1. P.G. de Gennes, *The Physics of Liquid Crystals.* / P.G. de Gennes, J. Prost. // Clarendon Press, Oxford, - 1993. – 597 p.
2. Valkov A.Yu. Fluctuations and light scattering in liquid crystals / Valkov A.Yu., Romanov V.P., Shalaginov A.N. // *UFN* -1994.- Volume 164. No. 2. – Pp.149-193
3. Egamov M.Kh. The structural transformation of polymer dispersed liquid crystalline films in external deformation field -*Journal of Physics: / M.Kh. Egamov // Conference Series,* - 2018. – P.012013
4. Popov V.A., Gilev V.G., Zakhlevnykh A.N. The influence of weak adhesion on the magnetic Fredericks transition in a ferromagnetic liquid crystal / V.A. Popov, V.G. Gilev, A.N. Zahlevnykh // *Solid State Physics.* – 2018. – Volume 60. ISSUE. 7. – Pp.1445-1450
5. Krizhanovskii D.N./ D.N. Krizhanovskii, D. Sanvitto, I.A. Shelykh, M.M. Glazov, G. Malpucchi, D.D. Solnyshkov, A. Kavokin, S. Ceccarelli, M.S. Skolnick, J.S. Roberts // *Phys. Rev. B.* 2006, V. 93, No 7. – P.073303
6. Warsi S.S. / S.S.A. Warsi, R. Manohar // *Ind. J. Sci. Technol.*, 2022, Vol. 15, No.21. – Pp.1052-1059
7. Chausov D.N. / D.N. Chausov, A.D. Kurilov, R.N. Kucherov, A.V. Simakin, S.V. Gudkov // *J. Phys.: Condens. Matter.* 2020. – Vol.32. NO. 39. – P. 395102
8. Egamov M.Kh. Polarizing properties of an elongated film of polymer-encapsulated liquid crystal with an admixture of surfactant / M.Kh. Egamov, V.P. Gerasimov, M.N. Krakhalev, O.O. Prishchepa, V.A. Loiko, V.Ya. Zyryanov // *Optical Journal* - 2014. - T. - 81, №7. – Pp.67-71
9. Egamov M.Kh. Light polarizers based on composite “polymer-LC-surfactant” films as anisotropic scattering media / M.Kh. Egamov, O.O. Prishchepa, V.P. Gerasimov, M.N. Krakhalev, V.A. Loiko // *News of Universities. Physics Series.* – 2013. – Vol.56, - No. 2-2. – Pp. 258-263
10. Egamov M.Kh., Light scattering effect of polymer-liquid crystal composites with spontaneous self-organization of structure / M.Kh. Egamov, U. J. Rakhimova // *News of the National Academy of Sciences of Tajikistan.* – 2022. - No. 3 (188). – Pp.78-84
11. Makhsudov B.I., Influence of injection laser radiation power on the optical properties of composites based on “polymer-liquid crystal” / B.I. Makhsudov, M.Kh. Egamov, I.Kh. Faizulloev // *Bulletin of the Tajik National University. Natural Sciences Series.* - 2019. - No. 3. – Pp. 83-89
12. Egamov M.Kh., Conformational transitions in polymer-encapsulated liquid crystal films / M.Kh. Egamov, S.K. Karimov, A. Abdumanovov // *Reports of NAST,* - 2022. – T. - 65, No. 1-2. – Pp.75-80
13. Makhsudov B.I., Temperature dependence of optical properties in composites based on a polymer-nematic liquid crystal under uniaxial deformation / B.I. Makhsudov, I.Kh. Faizulloev, M.Kh. Egamov // *Reports of NAST,* - 2021. - Volume 64, No. 9-10. – Pp.536-541
14. Kalitaevsky N.I. *Wave optics* / N.I. Kalitaevsky // *Textbook. Manual for universities.* Ed. 2nd, rev. and additional. – M.: Higher School, - 1978. – P.383.
15. Egamov M.Kh. Modifications of the structure of polymer-liquid-crystal films for the production of polarizers / M.Kh. Egamov, U. J. Rakhimova // *Reports of the National Academy of Sciences of Tajikistan,* - 2021. - Volume 64. No. 11-12. – Pp.682-686
16. Makhsudov B.I. Nonlinear optical phenomena in the interaction of laser radiation with composites based on polymer-nematic liquid crystal under uniaxial deformation / B.I.Makhsudov, M.Kh.Egamov, I.Kh. Faizulloev // *Bulletin of the Tajik National University. Natural Sciences Series.* - 2022. No. 1. – Pp. 104-115
17. Makhsudov B.I. Optical hysteresis in composites based on a polymer-nematic liquid crystal under uniaxial deformation / B.I. Makhsudov, I.Kh. Faizulloev, M.Kh. Egamov // *News of Universities. Physics series.* – 2022. –T.65, № 3 (772). – Pp.88-91. DOI: 10.17223/00213411/65/3/88

THE EFFECT OF SURFACTANT CONCENTRATION ON CHANGES IN THE PLANE OF POLARIZATION OF LIGHT PASSING THROUGH THE LCD MEDIUM

The effect of surfactants in the form of cetyltrimethyl ammonium bromide (CTAB) in nematic liquid crystal cells of type 5CB have been studied by the polarization-optical method. The relationship between the concentrations of the introduced surfactant and the angle of rotation of the polarization plane is established.

The clear boundaries of the linear and elliptical polarization of the light transmitted through the cell are indicated, depending on the concentration of surface-active substances (surfactants). Possible applications of such materials in semiconductor and solid-state laser technology and display technologies are proposed.

Keywords: surface-active substance (surfactant), liquid crystal, light transmission, orientation, optical anisotropy, polarization plane.

Information about the authors: Makhsudov Barot Isломovich – Tajik National University, doctor of Physical and Mathematical Sciences head of the nuclear physics, professor. **Address:** 734025, Dushanbe, Republic of Tajikistan, Rudaki Avenue, 17. **Phone:** +992-907-74-33-83. **E-mail:** maksudov_barot@mail.ru

Egamov Mukhtor Khasanovich – Khujand Scientific Center of the National Academy of Sciences of the Republic of Tajikistan, Candidate of Physical and Mathematical Sciences. **Address:** 735730, Khujand, Republic of Tajikistan, Kosmonavtov st., 2-42. **Phone:** (+992) 939-83-93-53. **E-mail:** egamov62@mail.ru.

Rahimova Umedakhon Juraboevna - Tajik state university of Law, Business and Policy, assistant of the information and communication technologies and programming department. **Address:** 735700, Khujand, Tajikistan, 19 micro district. **Phone:** (+992) 925-55-55-20. **E-mail:** rakhimova0508@mail.ru.

Article received 29.09.2023

Approved after review 04.12.2024

Accepted for publication 02.03.2024

RESEARCH OF THE STATIONARY PHENOMENON OF HEAT TRANSFER IN A SPHERICAL CONDENSED MEDIA

Juraev Kh.Sh., Juraeva G.Kh.

Thermal processes are common in various cylindrical condensed media, in the particular case of production: metals, their heat treatment, mechanical engineering, oil refining, chemical, food industry, production of building materials. In any industry or science and technology, there are necessarily many heat exchangers. For example, in machine-building plants, thermal energy is used to power a number of technological processes: heating water in baths, drying molds in dryers. In addition, heat exchangers are often auxiliary devices in boiler houses and compressor stations. At machine-building plants there are boiler installations in which hot water is prepared for industrial and domestic needs. At the outlet of thermal or heating furnaces, recuperative heat exchangers are installed to heat the blast air with exhaust flue gases. Chemical industry enterprises also have a lot of thermal equipment: reactors, evaporation and distillation units, evaporators. At food industry enterprises there are many cooking machines, refrigeration units, vacuum and drying units. In the production of building materials, drying units, drum dryers for drying sand, gravel, and refrigeration units are used. Heat exchanger is a device for transferring heat from one medium to another, or from one to several, or from several to one. All these processes are engineering and technical objects that are constantly under the direct influence of climatic factors, one of which is thermodynamic conditions. In this regard, heat transfer and mass transfer processes are becoming increasingly important.

As is known [1-6], any condensed medium serves as a material structural structure; according to their physicochemical composition, they form a set of interconnected and interdependent phases. Various processes occur in them separately and together, the energy and direction of which depend on the thermodynamic conditions of the environment. With cyclical changes in air temperature, the temperature of the layers of condensed matter changes. This leads to cyclical changes in moisture content, structure and stability of the condensed medium. The reliability and efficiency of promising energy facilities largely, and sometimes to a large extent, depends on how well the system of structural energy materials is organized, which ultimately determines the reliability of engineering methods for calculating heat transfer. For the correct and justified design of measures aimed at regulating thermal processes in various tasks in order to eliminate their influence on the durability, reliability and efficiency of structural materials in natural conditions and when using various thermal insulation materials. In this case, calculation models are also used to determine the thickness of thermal insulation devices and cladding structures. The process of heat transfer and mass transfer of a cylindrical condensed medium is spatial in nature; to obtain a complete picture, it is necessary to proceed from the solution of the problem of spatial thermodynamics. A number of mathematical models and methods for their application have been developed for engineering calculations of traditional problems. However, with the development of the technological structure, which constantly poses new and diverse tasks for specialists in this field and requires their study, an approximate method for considering one-dimensional heat flow, based on determining the temperature layer, was specified.

In the general case, when the mathematical model is of the type of singularly perturbed differential equations of the second order, the number of singular points will change and the phase plane can be divided into regions with different behavior of stable and unstable solutions

of the system of equations. For the problem of heat flow and temperature considered in [7-9], this occurs when a small parameter describing the behavior of temperature and heat flow (a nonlinear function of variable coordinates) changes its structure compared to some parameters included in the equation or system of equations .

In many physical problems, a model study of stationary (steady-state) solutions is of interest [6, 7, 10-14]. In this case, the singular perturbed ordinary differential equations of the second order, that is, the stationary heat equations with one spatial variable, turn into a boundary value problem for a system of ordinary differential equations of the first order with unknown functions of temperature and heat flow (see [10-15]). Since the boundary value problem is generated by transforming the stationary heat equation, an important aspect of its study is the analysis and assessment of the behavior of solutions to the boundary value problem in the form of certain phase structures.

The method of model representation of an analytical solution for analyzing a problem can be considered as a type of geometric forms (graphics), which is used at such stages of computational experiment technology as model construction and its verification [15-20]. This work is devoted to the development of these methods, its application to the model representation, and the problems of stationary heat transfer processes in cylindrical condensed media are studied. The perturbed and unperturbed proximity of the solution under the action of the initial approximation was numerically determined with acceptable accuracy.

In works [6-8], the process of diffusion-reactive transfer in a medium with a volumetric and flat heat source and a thermal conductivity coefficient depending on a small parameter is studied. Temperature distribution within the framework of problems of model representation of stationary heat transfer in a cylindrical medium is carried out using the following equation:

$$\varepsilon^2 \frac{d^2 T(r, \varepsilon)}{dr^2} + \frac{2\varepsilon^2}{r} \cdot \frac{dT(r, \varepsilon)}{dr} - g(r)T(r, \varepsilon) = f(r), \quad (1)$$

where is ε - a small parameter; r - radius sphere; the functions $g(r)$ and $f(r)$ are given, the multiplier and the heat source, respectively, and are $[0, a]$, at least continuous on the interval $[0, a]$, and $g(r) \geq 0$.

Assuming that the functions $g(r)$, $f(r)$ are known, we will consider finding a solution to equation (1) in accordance with the fulfillment of the boundary conditions:

$$\left(\gamma_1 \frac{dT(r, \varepsilon)}{dr} + \gamma_2 T(r, \varepsilon) \right) \Big|_r = \begin{cases} |T(0, \varepsilon)| < \infty & \text{npu } r = 0, \\ \psi & \text{npu } r = a. \end{cases} \quad (2)$$

Here γ_1, γ_2 - numerals, and ψ - specified number.

To refine the solution obtained from the model, a type of perturbation method is used to clarify the errors of this solution, and there is an extensive literature devoted to it [21-24]. Effective model selection for the intact and perturbed solution must be carried out in many situations, even under the influence of the initial approximation, in order to obtain a solution with satisfactory error at relatively low research costs.

Let us be interested in disturbances described by mathematical models as expressions of the form (1), under given boundary conditions (2). If we place $\varepsilon = 0$, that is, discard the disturbance in formula (1), then in this case we have:

$$g(r)v(r) + f(r) = 0. \quad (3)$$

In this case, the limit conditions (2) may be arbitrarily known and not correspond to equation (3) within the boundaries $r = 0$ or environment $r = a$. If the unperturbed formula (3) is within the limits $r = 0$ or $r = a$ does not satisfy the implementation of condition (2), then in this case the possibility of the inertial force at a given time differs from zero, that is, at the so-called stage of relaxation of motion, the first term in equation (1) cannot be neglected.

This means that any differential equation is approximate and not completely adequate to the process it describes. Therefore, some factors whose influence on the process under study is assumed to be "small" are reduced to studying the dependence of solutions of differential equations on small parameters. In the mathematical formulation of applied problems, the question arises about the behavior of solutions to problem (1)-(2) for values of coefficients characterized by "small" parameters. Solving a problem with a small parameter due to its applied importance (application of the theory of these equations in hydrodynamics, nonlinear mechanics, chemical and biological kinetics, ecology, shell theory and many other areas) has become one of the main directions in the field of differential equations and mathematical physics (see [6, 7, 15, 22-25]).

In [7-9, 25], the problem of finding approximate solutions of the boundary value problem for differential equations with a small parameter at higher derivatives, which are close to the solution of the boundary value problem for the secondary (unperturbed) equation, is considered. In this regard, it is of interest to find an approximate solution to problem (1)-(2), which is close to the solution to problem (3)-(4).

3. Model representation of the stationary phenomenon of heat transfer in a spherical condensed medium. First of all, we note that in most cases it is possible to construct a good mathematical model containing only two or three first-order equations. In our presentation, according to [7, 25], changes in temperature and heat flux density along the radius coordinate of the axis are described by a system of equations:

$$\begin{cases} \frac{dT(r, \varepsilon)}{dr} = q(r, \varepsilon) - \mathcal{G}_1 T(r, \varepsilon), \\ \varepsilon^2 \frac{dq(r, \varepsilon)}{dr} = f(r) - \mathcal{G}_2 q(r, \varepsilon), \end{cases} \quad (4)$$

where $T(r, \varepsilon)$ - temperature within radius r ; $q(r, \varepsilon)$ - heat flux density in radius r ; λ - coefficient of thermal conductivity

$$\mathcal{G}_1 = -\frac{1}{2r} \left(1 + \sqrt{1 + \left(\frac{r}{\varepsilon}\right)^2 g(r)} \right) \left(\mathcal{G}_1 = -\frac{1}{2r} \left(1 - \sqrt{1 + \left(\frac{r}{\varepsilon}\right)^2 g(r)} \right) \right)$$

and

$$\mathcal{G}_2 = \frac{\varepsilon^2}{2r} \left(3 - \sqrt{1 + \left(\frac{r}{\varepsilon}\right)^2 g(r)} \right) \left(\mathcal{G}_2 = \frac{\varepsilon^2}{2r} \left(3 + \sqrt{1 + \left(\frac{r}{\varepsilon}\right)^2 g(r)} \right) \right)$$

- the number of components characterizing the coefficients of equation (1).

As is known from [7-9, 25], in the vicinity of the equilibrium point, that is, the singular point $(q(r, \varepsilon), T(r, \varepsilon))$, phase transformations occur, either a phenomenon occurs in the

medium or it does not occur. There is a need to control the process of the phenomenon of condensed matter in the vicinity of a given point.

In this regard, let us consider the process of heat propagation in the positive direction of the coordinate system $((q(r, \varepsilon), T(r, \varepsilon)))$. In this case, boundary conditions (2) for temperature and heat flux density can be written as:

$$\begin{aligned} T(r, \varepsilon) \Big|_{r=0} &= |T(0, \varepsilon)|, & q(r, \varepsilon) &= |T(0, \varepsilon)|; \\ T(r, \varepsilon) \Big|_{r=a} &= \psi, & q(r, \varepsilon) \Big|_{r=a} &= \psi. \end{aligned} \quad (5)$$

To determine the dependence of heat flow on the temperature of spherical condensed media, we divide the second equation of system (1) by the first. As a result we get:

$$\varepsilon^2 \frac{dq(r, \varepsilon)}{dT(r, \varepsilon)} = \frac{f(r) - \mathcal{G}_2 q(r, \varepsilon)}{q(r, \varepsilon) - \mathcal{G}_1 T(r, \varepsilon)}. \quad (6)$$

To simplify further calculations, we denote:

$$A(T) = \frac{f(r) - \mathcal{G}_2 q(r, \varepsilon)}{\varepsilon^2 (q(r, \varepsilon) - \mathcal{G}_1 T(r, \varepsilon))}. \quad (7)$$

Then equation (6) takes the form:

$$\frac{dq(r, \varepsilon)}{dT(r, \varepsilon)} = A(T). \quad (8)$$

The solution to equation (8) has the following form:

$$q(r, \varepsilon) = \frac{A(T) \varepsilon^2 \mathcal{G}_1}{A(T) \varepsilon^2 + \mathcal{G}_2} T(r, \varepsilon) + \frac{f(r)}{A(T) \varepsilon^2 + \mathcal{G}_2}. \quad (9)$$

As can be seen from expression (9), the dependence $q(T)$ is complex: a) according to the first term, as the temperature increases, the heat flux density increases linearly; b) according to the second term, with increasing temperature, the heat flux density decreases linearly. Therefore, to clarify the nature of the dependence $q(T)$, we will conduct a computational experiment based on expression (9).

Of particular interest are the definitions of the coordinates of a stationary point, that is, the main isoclines $\frac{dq(r, \varepsilon)}{dT(r, \varepsilon)} = 0$ - horizontal isocline and $\frac{dq(r, \varepsilon)}{dT(r, \varepsilon)} = \infty$ - vertical isocline.

According to (7), the equation of horizontal isoclines ($A(T) = 0$) has the form:

$$f(r) - \mathcal{G}_2 q(r, \varepsilon) = 0, \quad (10)$$

and the equation of vertical isoclines ($A(T) = \infty$)

$$q(r, \varepsilon) - \mathcal{G}_1 T(r, \varepsilon) = 0. \quad (11)$$

At the point where both the numerator and the denominator (7) simultaneously become zero, or at the point of intersection of the main isoclines (10) and (11), the direction of the tangent becomes uncertain. Since in this case the value of the derivative becomes uncertain

$$\frac{dq(r, \varepsilon)}{dT(r, \varepsilon)} = \frac{f(r) - \mathcal{G}_2 q^*(r, \varepsilon)}{\varepsilon^2 (q^*(r, \varepsilon) - \mathcal{G}_1 T^*(r, \varepsilon))}. \quad (12)$$

The point of intersection of the main isoclines, or a singular point, has the most important property that at it the derivatives of the heat flow $q(r, \varepsilon)$ and the temperature with $T(r, \varepsilon)$ to r :

$$\frac{dq(r, \varepsilon)}{dr} = 0, \quad \frac{dT(r, \varepsilon)}{dr} = 0. \quad (13)$$

Obviously a special point $M(q^*(r, \varepsilon), T^*(r, \varepsilon))$ corresponds to a stationary state in the system, and its coordinates $(q^*(r, \varepsilon), T^*(r, \varepsilon))$ are stationary values of variables $q(r, \varepsilon)$ and $T(r, \varepsilon)$. It should be emphasized that the system can, of course, have several stationary states, since the main isoclines can intersect at several points.

Let us now see how we can determine the nature of the stability of singular points on the phase plane from the properties of the right-hand sides of equations (4).

We will proceed from the same ideas about the properties of stable states as in [14, 15] when studying the stability of stationary points in the case of an equation with one variable. Let be $(q^*(r, \varepsilon), T^*(r, \varepsilon))$ - the coordinates of the singular point of system (4) on the phase plane, and let our system undergo a slight deviation from the stationary position. The magnitude of this offset from the point $(q^*(r, \varepsilon), T^*(r, \varepsilon))$ is specified as follows:

$$T(r, \varepsilon) - T^*(r, \varepsilon) = \mu_1; \quad q(r, \varepsilon) - q^*(r, \varepsilon) = \mu_2. \quad (14)$$

где $\|\mu_1\| \ll \|T^*\|$, $\|\mu_2\| \ll \|q^*\|$.

Substituting (14) into equations (4) and taking advantage of the smallness of the quantities μ_1 , μ_2 , let's expand the functions $\Theta_1(T, q) = \varepsilon^2 (q(r, \varepsilon) - \mathcal{G}_1 T(r, \varepsilon))$ и $\Theta_2(T, q) = f(r) - \mathcal{G}_2 q(r, \varepsilon)$ in a Taylor series near a stationary point $(q^*(r, \varepsilon), T^*(r, \varepsilon))$ limited to the first terms of the expansion:

$$\begin{aligned} \Theta_1(T, q) = \varepsilon^2 (q^*(r, \varepsilon) - \mathcal{G}_1 T^*(r, \varepsilon)) + \mu_1 \cdot \left(\frac{\partial \Theta_1}{\partial T} \right)_{T=T^*, q=q^*} + \\ + \mu_2 \cdot \left(\frac{\partial \Theta_1}{\partial q} \right)_{T=T^*, q=q^*} + \dots, \end{aligned} \quad (15)$$

$$\begin{aligned} \Theta_2(T, q) = f(r) - \mathcal{G}_2 q^*(r, \varepsilon) + \mu_1 \cdot \left(\frac{\partial \Theta_2}{\partial T} \right)_{T=T^*, q=q^*} + \\ + \mu_2 \cdot \left(\frac{\partial \Theta_2}{\partial q} \right)_{T=T^*, q=q^*} + \dots \end{aligned} \quad (16)$$

Denoting the values of partial derivatives at a point $(q^*(r, \varepsilon), T^*(r, \varepsilon))$:

$$\begin{aligned} \left. \frac{\partial \Theta_1}{\partial T} \right|_{T=T^*, q=q^*} = \varepsilon^2 \mathcal{G}_1; \quad \left. \frac{\partial \Theta_1}{\partial q} \right|_{T=T^*, q=q^*} = \varepsilon^2; \\ \left. \frac{\partial \Theta_2}{\partial T} \right|_{T=T^*, q=q^*} = 0; \quad \left. \frac{\partial \Theta_2}{\partial q} \right|_{T=T^*, q=q^*} = \mathcal{G}_2; \end{aligned}$$

and using expressions (15) and (16), we rewrite the Taylor series in the form:

$$\begin{aligned} \Theta_1(T, q) = \varepsilon^2 \mathcal{G}_1 \mu_1 + \varepsilon^2 \mu_2, \\ \Theta_2(T, q) = \mathcal{G}_2 \mu_2. \end{aligned} \quad (17)$$

Substituting (15), (16) and (17) into the original equations (4), we obtain a system of differential equations

$$\begin{cases} \frac{d\mu_1}{dx} = \varepsilon^2 \mathcal{G}_1 \mu_1 + \varepsilon^2 \mu_2, \\ \frac{d\mu_2}{dx} = 0 \cdot \mu_1 + \mathcal{G}_2 \mu_2. \end{cases} \quad (18)$$

Consequently, equations (18) describe the nature of the change in quantities μ_1 , μ_2 on the x coordinate or the behavior of the original system (4) near the singular point $(q^*(r, \varepsilon), T^*(r, \varepsilon))$.

To determine the nature of the stability of a singular point, it is necessary to find out how the quantities behave μ_1 , μ_2 depending on parameter values $\varepsilon^2 \lambda \mathcal{G}_1$, $\varepsilon^2 \mathcal{G}_2$, $\lambda \mathcal{G}_2$ on the right sides of equation (4). To solve system (18), we apply procedures for finding eigenvalues using the matrix method (see [9,17]). We will look for a solution in the form:

$$\mu_1 = C \exp(\omega x), \quad \mu_2 = D \exp(\omega x). \quad (19)$$

where C, D are the values of the initial deviations μ_1 , μ_2 at $x=0$.

$$\begin{cases} \omega C = \varepsilon^2 \mathcal{G}_1 C + \varepsilon^2 D, \\ \omega D = \mathcal{G}_2 D. \end{cases} \quad (20)$$

Next, we write system (20) in matrix form:

$$\begin{pmatrix} \varepsilon^2 \mathcal{G}_1 - \omega & \varepsilon^2 \\ 0 & \mathcal{G}_2 - \omega \end{pmatrix} \cdot \begin{pmatrix} C \\ D \end{pmatrix} = 0. \quad (21)$$

If you enter a column vector

$$\delta_k = \begin{pmatrix} C_k \\ D_k \end{pmatrix}, \text{ где } -\infty < k < \infty$$

and coefficient matrix

$$F = \begin{pmatrix} \varepsilon^2 \mathcal{G}_1 - \omega & \varepsilon^2 \\ 0 & \mathcal{G}_2 - \omega \end{pmatrix}$$

then (21) can be written as

$$\delta_k = F \cdot \delta_{k-1} = F^2 \cdot \delta_{k-2} = \dots = F^k \cdot \delta_0. \quad (22)$$

Let us assume that there are characteristic numbers of the matrix of system (21), that is, the roots of the characteristic equation

$$\omega^2 - (\varepsilon^2 \mathcal{G}_1 + \mathcal{G}_2) \omega + \varepsilon^2 \mathcal{G}_1 \mathcal{G}_2 = 0. \quad (23)$$

Solving equations (23), we determine the roots of the characteristic equation:

$$\omega_1 = \varepsilon^2 \mathcal{G}_1, \quad \omega_2 = \mathcal{G}_2. \quad (24)$$

Using expressions (24), we analyze the dependence ω_1 and ω_2 on the system parameters:

and if

$$\varepsilon^2 > -r^2 g(r),$$

then the roots ω_1, ω_2 are real, their product is equal to

$$\omega_1 \cdot \omega_2 = \frac{\varepsilon^4}{r^2} (1 - \varepsilon^2 - r^2 g(r))$$

Hence, if

$$|\omega_1| > \frac{\varepsilon^2}{r} \left(1 + \sqrt{\varepsilon^2 + r^2 g(r)} \right)$$

Then

$$|\omega_2| < \frac{\varepsilon^2}{r} \left(1 - \sqrt{\varepsilon^2 + r^2 g(r)} \right)$$

and vice versa. Then $F^k \cdot \delta_0$ when $k \rightarrow \infty$ or $k \rightarrow -\infty$ increases without limit, then the corresponding value ω is not an eigenvalue;

b) if

$$\varepsilon^2 < -r^2 g(r),$$

then the roots ω_1, ω_2 are complex conjugate:

$$|\omega_1| = |\omega_2|.$$

In this case, the coefficient $F^k \cdot \delta_0$ matrix remains limited for any δ_0 given value. Moreover, each solution to the system of equation (21) is an eigenfunction, and the corresponding values ω are doubly degenerate eigenvalues;

c) if

$$\varepsilon^2 = -r^2 g(r), \text{ Then}$$

$$\omega_1 = \omega_2 = \frac{\varepsilon^2}{r}.$$

In this case, there is at least one vector δ_0 satisfying the equality $F \cdot \delta_0 = \pm \delta_0$. In this case, they do not depend ω_1, ω_2 on T .

Therefore, the solution to system (18) can be represented in the form

$$\begin{aligned} \mu_1(x) &= C_1 \exp(\omega_1 x) + D_1 \exp(\omega_2 x), \\ \mu_2(x) &= C_2 \exp(\omega_1 x) + D_2 \exp(\omega_2 x). \end{aligned} \quad (25)$$

Here, C_i, D_i ($i = 1, 2$) - the integral constants depend on the boundary conditions (5) and on the coefficients of the system of equation (18) (or (4)). Thus, the nature of behavior μ_1, μ_2 near a singular point $(q^*(r, \varepsilon), T^*(r, \varepsilon))$ depends in a certain way on the value of ω_1, ω_2 .

Computational experiment

To study the model presented solutions to problem (4)-(5), the parameters of a specific environment were taken from the works [7, 8, 10, 15]. Depending on the initial distribution of stationary temperature and the type of boundary conditions, different evolution of the temperature signal is observed.

Let's create structures in the phase plane that determine the behavior when solving boundary value problems. By setting the values of A and performing a numerical calculation using expression (9) with respect to the heat flow ω , we obtain the coordinates of the branches depending on the temperature u .

In Figure 1, isoclines are created for values $\frac{d\omega}{du} = A$ equal to 0.0; 0.5; 1.5; 2 and integral curves are obtained by connecting the corresponding isocline points.

From Figure 1 it follows that the dependence of heat flow $q(r, \varepsilon)$ on temperature $T(r, \varepsilon)$ is represented by families of isoclines. An isocline of a first-order differential equation (6) (or (8)) is a curve on the plane $(q(r, \varepsilon), T(r, \varepsilon))$, along which the cylindrical field specified by the differential equation (cylindrical temperature field) has the same slope. Typically, isoclines are horizontal and vertical tangents, and the coordinates of a stationary point can be determined. The isocline family is a series of straight lines, the general solution of which is in the phase plane.

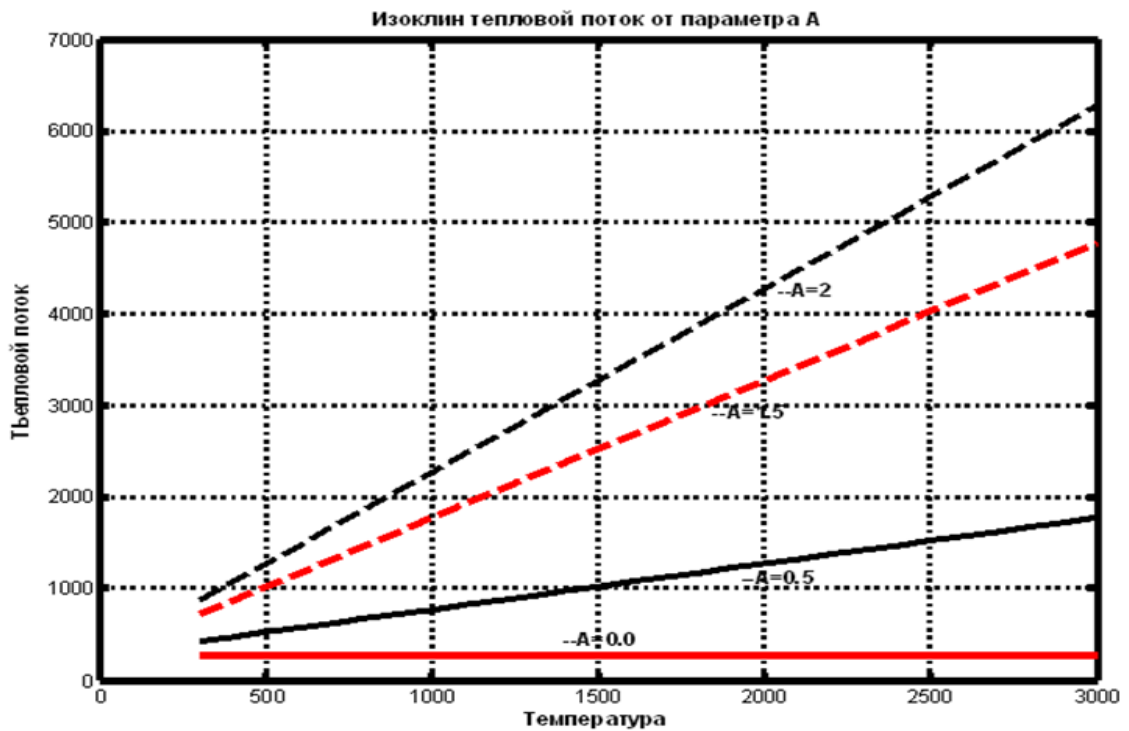


Fig. 1. The isocline family for equation (6).

Figure 2 shows the structure of the phase portrait of a stationary system (4) depending on the small parameters ε .

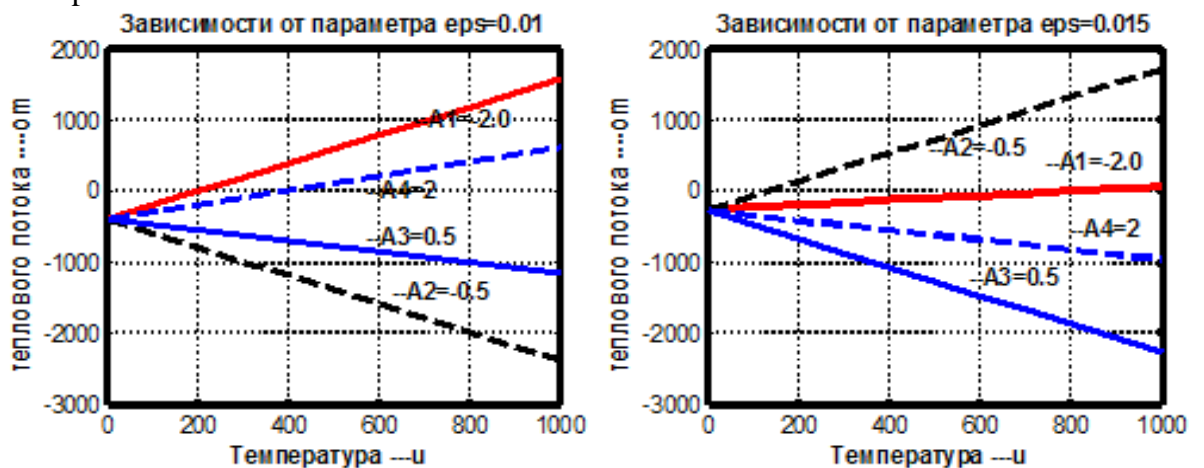


Fig. 2. Temperature dependence of heat flow at different parameter values ε

From Figure 2 it follows that the range of possible solutions to the stationary problem (4)-(5) is limited by straight line segments, the initial distribution of variables with parametric expressions (9) and (10) relative to ε and A , and the corresponding segments of u - temperature branches.

Figures 3 and 4 show a model solution of the form (19) (25) depending on the coordinate x for given different values of small parameters ε .

In Figure 3, the change in stationary temperature for known small parameters ε is plotted, and the integral curves are obtained by connecting the corresponding points of the x coordinate.

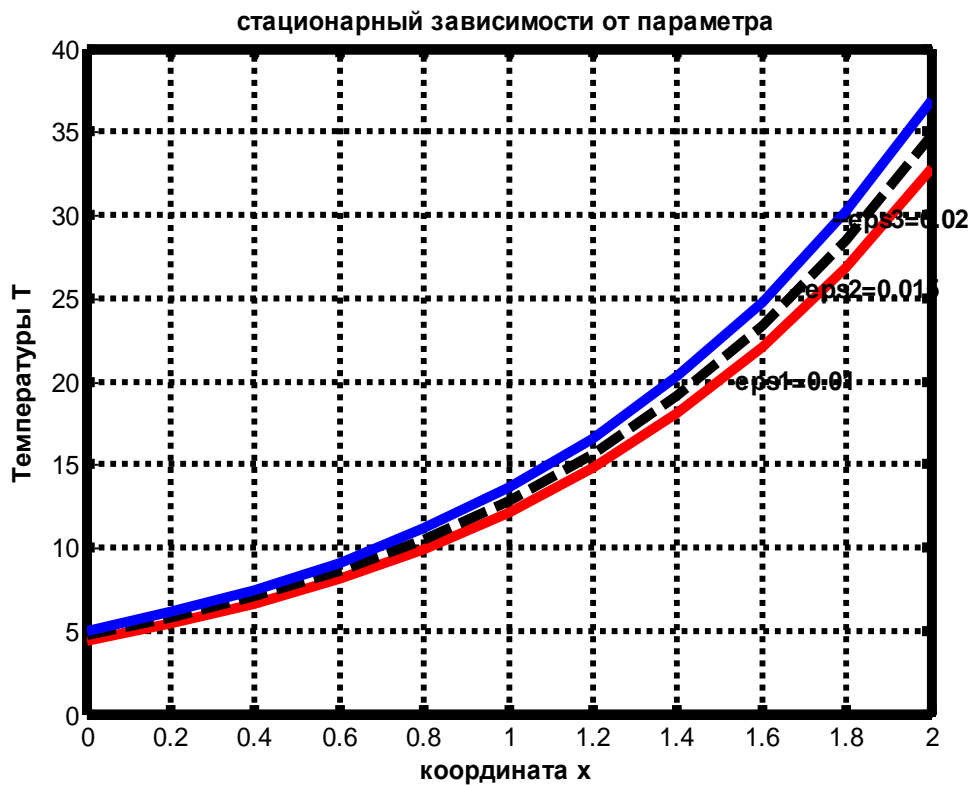


Fig.3. Change in steady-state temperature at different parameter values ε : eps1 =0.01; eps2=0.015; eps3=0.02

From Figure 3 it follows that the stationary temperature (solution of the form (19)), depending on the parameter ε , increases nonlinearly with increasing coordinate length x . The class of such solutions is a series of nonlinear lines, the general equation of which is based on the phase cylindrical geometry.

Figure 4 shows the change in heat flow depending on the x coordinate for given different values of small parameters ε .

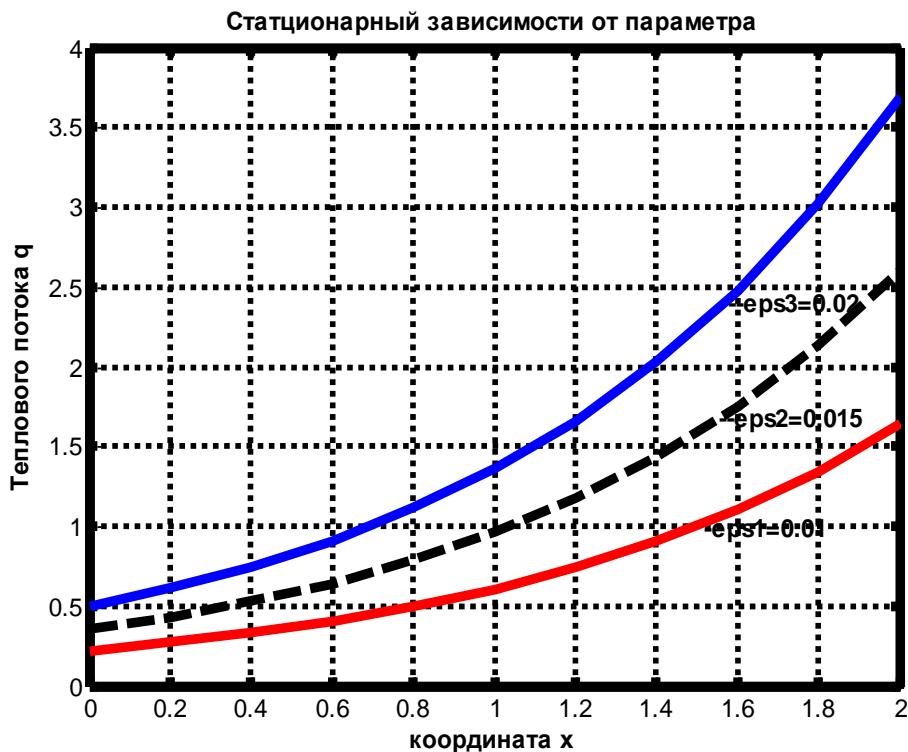


Fig.4. Dependences of heat flow on the value of coordinates x and the number of small parameters ε : $\varepsilon_1 = 0.01$; $\varepsilon_2 = 0.015$; $\varepsilon_3 = 0.02$

From Figure 4 it is clear that the heat flux density is formed from the initial propagation, continuously filling the specified area until it completely coincides with the solution of the boundary layer problem.

From solutions (25) and graphs it follows that a certain approximate solution to problem (1)-(2) in the form (25) is close to the solution to problem (3)-(4).

5. Conclusion. In general, when the type of singularly perturbed second-order differential equations changes in the type of system of equations, the number of singular points will change. Consequently, in the general case, the phase plane can be divided into regions with different behavior of stable and unstable solutions of the system of equations. For the heat flow and temperature problem discussed above, this occurs when a small parameter describing the behavior of temperature and heat flow (a nonlinear function of coordinate variables) changes its structure compared to some parameters included in the equation or system of equations.

In many physical problems, it is of interest to model the study of stationary (steady-state) solutions. In this case, the singular perturbed ordinary differential equations of the second order, that is, the stationary heat equations with one spatial variable, turn into a boundary value problem for a system of ordinary differential equations of the first order with unknown functions of temperature and heat flow. Since the boundary value problem is generated by transforming the stationary heat equation, an important aspect of its study is the analysis of the behavior of solutions to the boundary value problem in the form of certain phase structures, rather than phase points.

The method of model representation of an analytical solution for problem analysis can be considered as a type of cognitive graphics, which is used at such stages of computational experiment technology as model construction and its verification.

**REVIEWER: Hamrokulov R.,
Candidate of Physical and Mathematical Sciences,**

REFERENSEC

1. Luikov A.V. Theory of thermal conductivity / A.V. Lykov // - M.: Higher School. - 1967. – P. 600.
2. Luikov A.V. Thermal conductivity of porous systems / A.V. Luikov, A.G. Shashkov, L.L. Vasiliev, Yu.E. Fraiman // International Journal of Heat and Mass Transfer. - 1968. - Vol.11. - Issue 2. – Pp. 117-140.
3. Alekseev V.P. System design of heat-resistant radio devices and systems / V.P. Alekseev // - Tomsk: Publishing House of the Institute of Atmospheric Optics SB RAS. - 2004. – P. 316.
4. Petukhov B.S. Heat exchange in nuclear power plants. /B.S. Petukhov, L.G. Genin, S.A. Kovalev // - M: Publishing house MPEI. -2003. – P. 470.
5. Achilov B.M. Harmonic analysis of daily fluctuations in outside air temperature and solar radiation intensity / B.M. Achilov. V.V. Chigunkov // - Tashkent: Solar engineering. - 1981. - No. 2. - P.54-59.
6. Sklyar S.N. Projection method for constructing difference schemes for problems with boundary layers / S.N. Sklyar, Zh.Zh. Bakirov // News of the National Academy of Sciences of the Kyrgyz Republic. Echo of Science. - 1997. - No. 2-3. – Pp. 36-47.
7. Juraev H.Sh. On the approximate analytical solution of boundary value problems for the singularly perturbed equation of stationary heat conduction. / Kh.Sh. Juraev, G.Kh. Juraeva // Problems of automation and control. -2021. No. 1 (40). – Pp.31-38.
8. Juraeva G.Kh. On the analytical solution of boundary value problems for a singularly perturbed stationary heat equation / G.Kh. Juraeva // Materials of the International conference on the topic “The role of physics in the development of science, education and innovation”, dedicated to the “Twentieth anniversary of the study and development of natural, exact and mathematical sciences in the field of science and education (2020-2040)” and the 80th anniversary of the memory of the Honored worker of science and technology of Tajikistan, corresponding member of the National Academy of Sciences of Tajikistan, Doctor of Physical and Mathematical Sciences, Professor Boboev Toshboy Boboevich (October 27, 2022). - Dushanbe: TNU Publishing House.– Pp. 107-109.
9. Juraeva G.Kh., Model study of a singularly perturbed stationary heat transfer process in condensed media / G.Kh. Juraeva // Materials of the Republican scientific and practical conference on the topic “Mathematical and computer modeling of physical processes” dedicated to the 20th anniversary of the study and development of natural, exact and mathematical disciplines in the field of science and education (February 9, 2023). – Dushanbe: TNU. - 2023. – Pp.55-64.
10. Juraev Kh.Sh. Stationary heat distribution in an infinite strip / Kh.Sh. Juraev // Bulletin of the Tajik National University. Natural Sciences Series. - 2017. - No. 1/5. – Pp. 83-87.
11. Juraev Kh.Sh. Stationary heat distribution using a mathematical model of the thermal conduction process. / Kh.Sh. Juraev // Problems of automation and control. -2017. -No. 2 (33). – Pp. 10-20.
12. Juraev Kh. Sh. Study of heat flow distribution in an unbounded environment in the presence of an external source / Kh.Sh. Juraev, K. Komilov, Z.S. Normatov // Scientific and technical bulletin of the Volga region. - 2015. - No. 6. – Pp. 10-13.
13. Juraev Kh.Sh. Study of thermal conductivity in a limited environment by the method of artificial hyperbolization / Kh.Sh. Juraev, K. Komilov, Z.S. Normatov // Bulletin of the Tajik National University. Natural Sciences Series. -2015. -No1/5 (188). – Pp. 53-61.
14. Juraev Kh.Sh. Study of the dependence of the stationary distribution of heat flow on temperature in condensed media / Kh.Sh. Juraev, K. Komilov, A.M. Najmiddinov // Bulletin of the Tajik National University. Natural Sciences Series. -2016. -No1/1 (192). – Pp. 114-120.
15. Juraev Kh.Sh. The phenomenon of energy and mass transfer in condensed matter: mathematical modeling, optimization, practical applications / Kh.Sh. Juraev // - Dushanbe: ER-graph. – 2021. – P. 236.
16. Yakubov B. Model study of the dependence of the concentration of substances on system parameters / B. Yakubov, Kh. Sh. Juraev, K. Komilov // Materials of the Thirteenth International Thermophysical School “Thermophysics and Information Technologies” dedicated to the 60th anniversary Doctor of Technical Sciences, Professor, Corresponding Member. NAST Kabuliev Zainalobuddin Valievich (Kobuli Zainalobuddini Vali) and the 70th anniversary of the Honored Worker of Science and Technology of Tajikistan, Doctor of Technical Sciences, Professor, Academician of the Institute of Arts of the Republic of Tajikistan, Academician of the MIA, Academician of the Academy of Arts Safarov Mahmatali Mahmadiyevich (October 17-20, 2022 Dushanbe) – Dushanbe-Tambov. – Pp. 218-221.
17. Komilov, K. Model study of stationary heat transfer processes in condensed media / K. Komilov, B. Yakubov, Kh.Sh. Juraev, Z.S. Normatov // Materials of the Republican scientific and practical conference on the topic “Mathematical and computer modeling of physical processes” dedicated to the 20th anniversary of the study

and development of natural, exact and mathematical disciplines in the field of science and education (February 9, 2023). – Dushanbe: TNU. – 2023. – Pp.4-12.

18. Juraev Kh. Sh. Model representation of the analytical solution of the dependence of the stationary state of the nonlinear distribution of heat flow on temperature in condensed media / Kh.Sh. Juraev, A.M. Najmiddiniyon, D.K. Solikhov // Bulletin of the Tajik National University. Natural Sciences Series. -2023. -No. 1. – P. 28.

19. Juraev Kh.. Sh. Model representation of the analytical solution of the dependence of the stationary state of the nonlinear distribution of heat flow on temperature in condensed media / Kh.Sh. Juraev, A.M. Najmiddiniyon, D.K. Solikhov // Materials of the Republican scientific and practical conference on the topic “Mathematical and computer modeling of physical processes” dedicated to the 20th anniversary of the study and development of natural, exact and mathematical disciplines in the field of science and education (February 9, 2023). –Jushanbe: TNU. -2023. – Pp. 20-30.

20. Juraev H. Sh. Investigation of Conductivity of Nanostructures Using A Mathematical Model / H.Sh. Juraev, G. Kh. Juraeva // Journal of Physics: Conf. Ser. -2022. –Volume 2270. –012015

21. Vasilyeva, A.B. Singularly perturbed equations in critical cases. / A.B. Vasilyeva, V.F. Butuzov // – M.: Moscow State University Publishing House. -1987. – P. 108.

22. Bogolyubov N.N. Asymptotic methods in the theory of nonlinear oscillations. / N.N. Bogolyubov, Yu.F. Mitropolsky // M.: Nauk. -1974. – P.410.

23. Mishchenko, E.F. Differential equations with a small parameter and relaxation oscillations. / E.F. Mishchenko, N.Kh. Rozov // M.: Science. -1975. – P.227.

24. Butuzov V.F. Singular disturbances/ V.F. Butuzov // Mathematics, cybernetics. -1988. No. 1. – P. 50.

25. Sklyar S.N. Difference schemes for solving heat transfer problems in different coordinate systems / S.N. Sklyar, O.S. Khlybov // AUCA Academic Review. Section IV. Natural Science sanding formational Ethnology. -2006. – Pp.219-229.

26. Krutov, Yu.M. Modeling the combustion of dusty coke particles in the presence of water vapor / Yu.M. Krutov, D.V. Reshetnyak, I.I. Tokarev // Energy saving. Energy. Energy audit. 2013. - No. 5 (111). – Pp. 47-57.

27. Shepakina E.A. Critical conditions for self-ignition in porous media. / E.A. Shepakina // Chemical physics. -2001. No. 7. – Pp. 3-9.

28. Juraeva G. Kh. Study of mathematical models and corresponding boundary value problems with singular coefficients. Monograph. / G. Kh. Juraeva // - Dushanbe: ER-graph. -2021. – 100 p.

INVESTIGATION OF THE STATIONARY PHENOMENON OF HEAT TRANSFER IN A CYLINDRICAL CONDENSED MEDIUM

A method for investigating approximate analytical solutions of boundary value problems of singularly perturbed equations of stationary heat transfer processes in a spherical condensed medium, close to solving the boundary value problem for an undisturbed equation, is presented. The main task in which the structure of the article is defined is the development of mathematical and computer models of the stationary phenomenon of heat transfer in flat condensed media and a model of diffusion-reactive energy transfer depending on the thermal conductivity of materials.

Key words: aisle, singular perturbed, small parameter, boundary and transition layers, heat flux, temperature.

Information about the authors: Juraev Khayrullo Sharofovich– Tajik National University, Doctor of physical and mathematical sciences, Head of the Department of Computing Machines, Systems and Networks. **Address:** 734025, Dushanbe, Republic of Tajikistan, Rudaki Avenue, 17. **Phone:** (+992) 917-30-70-60. **E-mail:** hayrullo_58@mail.ru.

Juraeva Gulshan Khairulloevna – Tajik State Pedagogical University named after S. Aini, Candidate of Physical and Mathematical Sciences, Associate Professor of the Department of Higher Mathematics and Geometric. **Address:** 734025, Dushanbe, Republic of Tajikistan, Rudaki Avenue, 121. **Phone:** (+992) 911-11-04-31. **E-mail:** hayrullo_58@mail.ru.

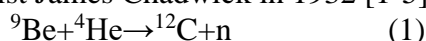
Article received 31.10.2023
Approved after review 11.01.2024
Accepted for publication 01.03.2024

**STUDY OF SCINTILLATION RESPONSE OF NEUTRONS AND GAMMA QUANTA
BY THE METHOD OF REMOVING SUPERPOSED PULSE**

Imom M. Sh., Romodanov V.L., Rahimi F.,
Odinaev S.F.

The main characteristics of a particle are charge, stability over time, mass, spin and magnetic moment. However, the charge of a neutron is usually allowed to be zero. A similar hypothesis about the magnitude of the charge is proven by most studies on the interaction of neutrons with various nuclei. The neutron, like the proton and electron, has a certain spin and magnetic moment. The neutron as a source of radiation can be used in all nuclear reactions that use neutron emission reactions.

The neutron was first obtained through the reaction of irradiating beryllium with alpha particles by the English scientist James Chadwick in 1932 [1-5]:



Finding and regulating nuclear fissile materials (NFM) is possible using their own radiation of neutrons and gamma rays. NFM most often include those materials in which there are one or more types of nuclides capable of fission by thermal neutrons. The production of nuclear fuel in industry is increasing day by day, which is caused by the large energy needs of the national economy. In today's nuclear energy, ${}^{235}\text{U}$ and ${}^{239}\text{Pu}$ nuclides are mainly used as fuel elements. In this regard, government and international standards for accounting and control of their composition pay special attention.

Accounting and control of NFM consist of the collection, registration and analysis of data on the quantity, quality and transportation of fissile materials and are implemented through continuous documentary accounting of all processes with NFM. The main tasks of accounting and control of nuclear materials are the implementation of control over fissile materials, safety, identification and elimination of violations in the accounting and control of nuclear materials, illegal use and theft of NFM [6-11].

Practical tasks of finding the mass and composition of NFM are focused primarily on their processing and production of materials. Such control objects are various technological installations, transport containers, fuel elements and irradiated fuel assemblies. Significant radioactivity, the ability to form a chain reaction, and relatively high cost require accurate descriptive accounting of NFM and materials, adherence to established technological and sustainable standards, and physical protection from unauthorized personnel actions. Accordingly, the observed quantities and parameters, the range of errors, and suitable methods and means are determined [12-14].

Today, nuclear materials are produced and analyzed using nuclear reactors, radiation detectors, radiometers, spectrometers, etc. In most cases, ionizing radiation detectors with a specific research method are used to analyze nuclear materials. Radiation detectors are considered to be installations designed to convert the absorbed energy of nuclear radiation into a signal, that is, restore the properties of radiation from the responses at the detector output. According to classifications, ionizing radiation detectors are divided into proportional (gas), semiconductor, scintillation, track detectors, etc., which have their own advantages and disadvantages [15].

To determine neutron pulses, proportional helium counters are used, which are considered the gold standard in the field of detection. However, the significant use of

proportional detectors based on ^3He has led to a decrease in their reserves and the need for costly technologies for their production in the world [16-18]. Hence the task arises of looking for alternative methods of replacing these detectors with modernized ones both in terms of price and analysis of new radiation detectors.

Scintillators are devices that emit a flash of light when they absorb fissile radiation. That is, processes of scintillation of particles of fissile substances with high energy in the range from several KeV to tens of MeV into many gamma rays with significantly lower energies occur in them. The scintillation method was proposed by William Crookes together with Ernest Rutherford. Later, Wilhelm Roentgen used a crystal scintillator to determine rays, which were later named after him. Scintillation detectors have been widely used in recent centuries.

The main characteristics demonstrating the positive properties of scintillators are their light output, which determines the number of gamma rays emitted by the scintillator when particles with an energy of 1 MeV are absorbed and the time of emission of the scintillator, in which it is less.

Scintillation detectors are divided into: organic, inorganic, liquid, plastic and combined [19-21].

Description of a digital method for removing superimposed neutron and gamma ray pulses using scintillation detectors

Today, there are various digital methods for detecting and monitoring nuclear fuel. Most of the digital methods are based on pulse shape recognition and its application. The proposed work examines one of these methods, the digital method for removing superimposed separate scintillation pulses of neutrons and gamma rays [22-24].

The modeling response from the output of the photomultiplier tube (PMT) goes to the input of an analog-to-digital converter (ADC), which converts it into a numerical sequence at a set frequency. This sequence will be recorded in the memory of a personal computer for further processing. The queue length is set by the measurement time and digitization frequency. Pulse processing does not require additional electronic modules or units. All you need is an ADC. Also, the presented method does not require shift registers or special software, which demonstrates the advantages of digital separation technology [25-26].

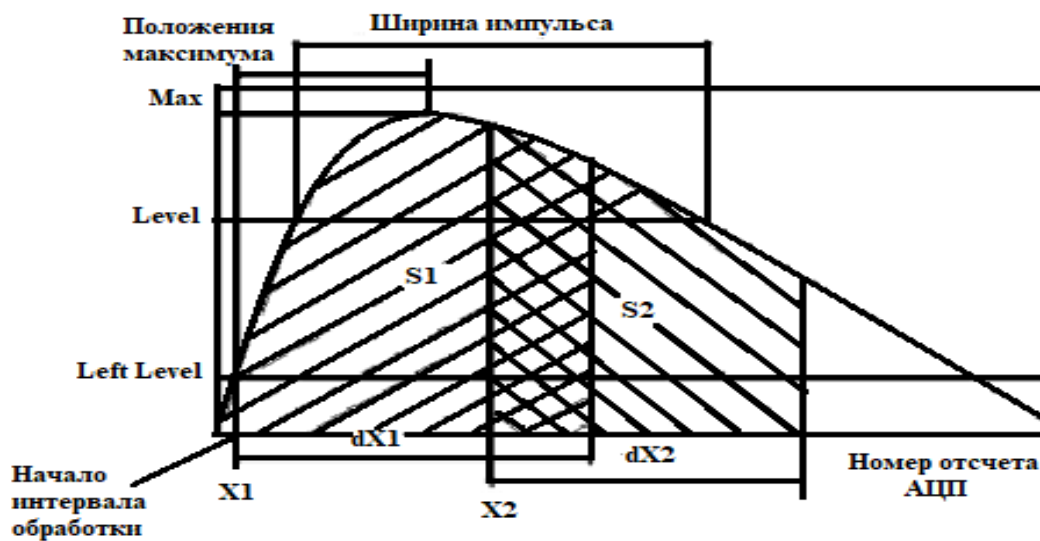
The method for removing superimposed neutron pulses involves software to process the resulting data. Practical data is recorded in a separate file. It is designed for repeated processing of digitized amplitude-time distributions of combined radiation pulses and pulse recognition by shape. By using the difference in the shape of the momenta of various charged particles, for example, recoil protons (neutrons) and electrons (gamma quanta), it is possible to obtain their distributions according to the separation parameters in the form of a curve, which can be seen in Fig. 1.

Fig. 1. Separation of particles of different types according to the shape of their scintillation pulses



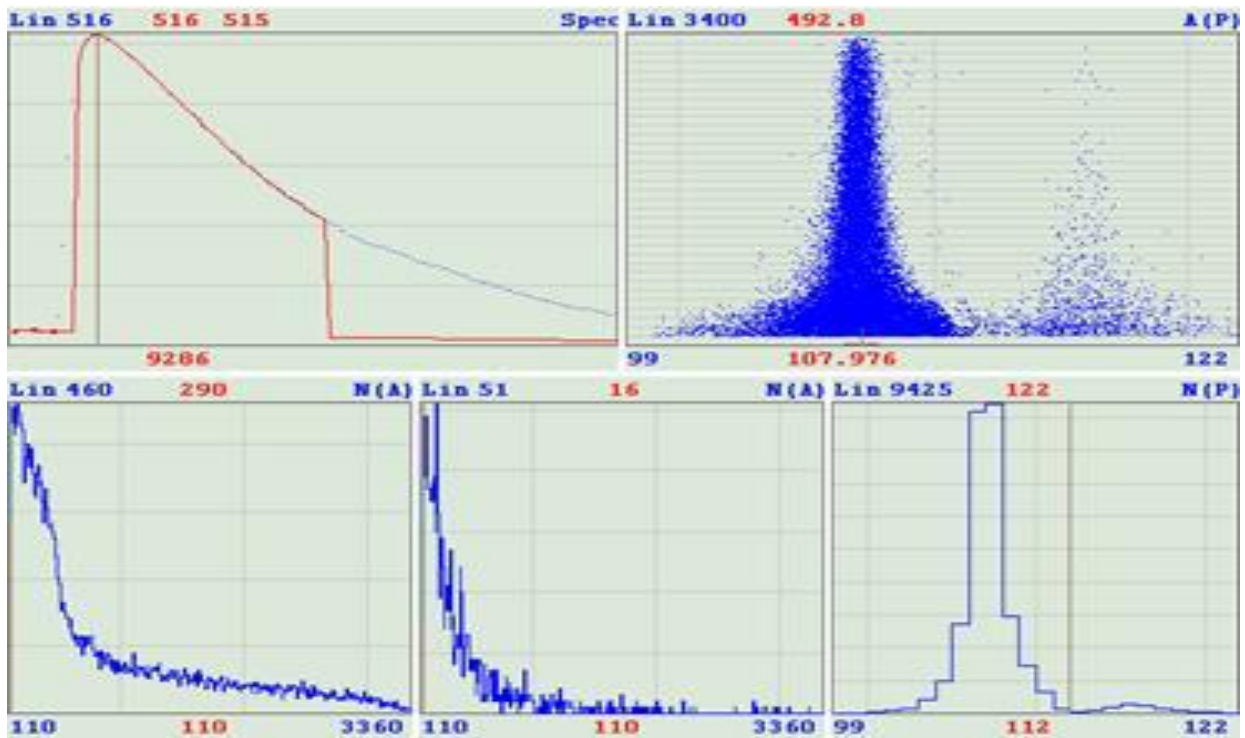
To recognize the detected particles for each pulse, the separation parameter was calculated using the program, which is determined by the ratio of the two areas of a specific pulse section to its amplitude (S_1 , S_2).

Fig. 2. Description of the pulse shape parameter count



In order to study the obtained experimental results using the software, the possibilities of graphical and numerical description of the processing results are provided. At the end of processing the results, the program gives the amplitude distribution of neutron and gamma quanta pulses in a separate graphic window, the time distribution of neutron and gamma quanta pulses, the amplitude loading level, the number of recorded gamma ray and neutron pulses and the value of the separation parameter [27].

Fig. 3. Amplitude distribution of neutron and gamma-ray pulses, removal of superimposed pulses and correction of responses



When measuring neutrons and gamma quanta, they are carried out programmatically under conditions of high load on the measuring path; it is possible to superimpose pulses on each other. Also, using the program, you can clarify the proportion of doubtful impulses between peaks and remove them from the total number. The results of the work performed are saved to the computer memory for re-processing.

The superimposed pulse removal method consists of the following principles for analyzing and processing radiation pulses:

- drawing a line of separation boundaries of neutron and gamma quanta peaks;
- removal of doubtful pulses between peaks;
- correction of neutron and gamma ray pulses.

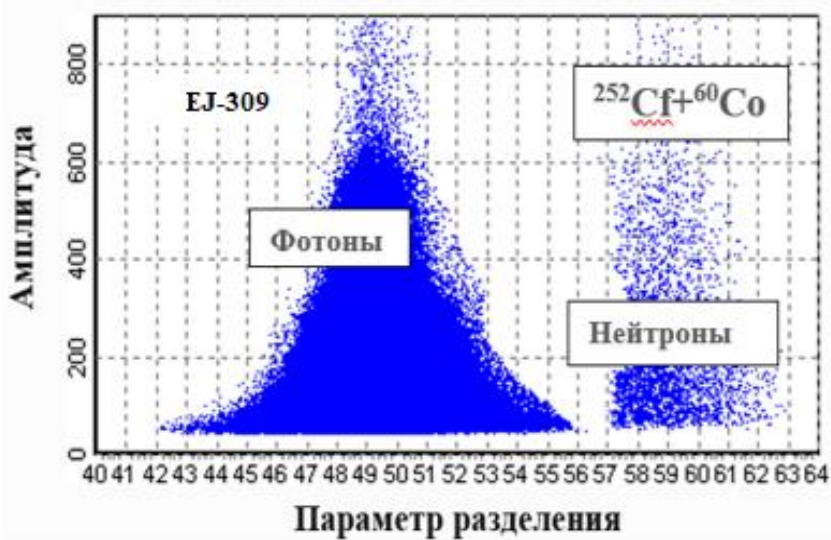
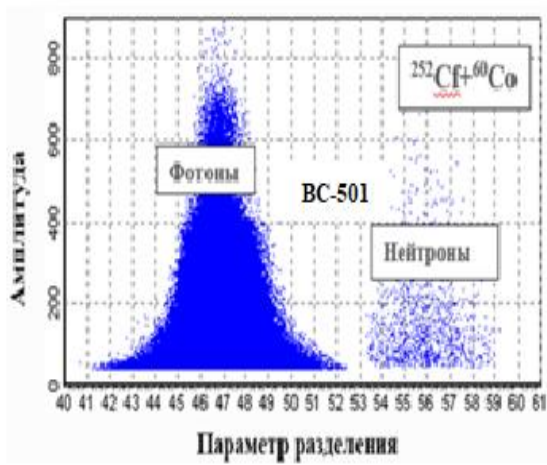
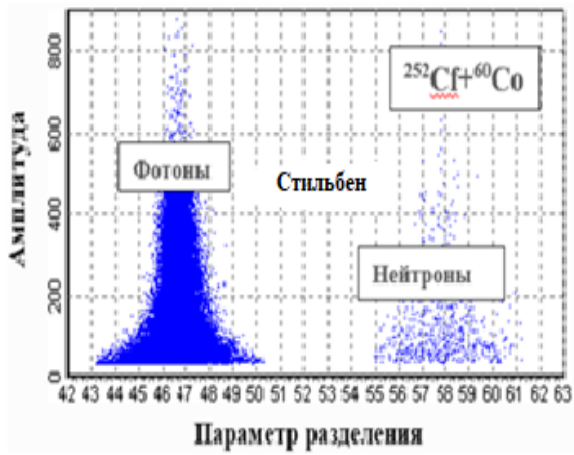
Experimental work and results obtained

In order to determine the applicability of the proposed technique, a special algorithm, liquid scintillators (BC-501 and EJ-309) and a crystalline scintillator (stilbene) were used, with the help of which certain tasks in the presented work were carried out.

Neutron Channel Loads for Liquid and Crystalline Scintillation Detectors

The work was carried out to determine the load on the neutron channel of various types of scintillators. The task involved placing a Californian source at a certain distance from the installation; at the same time, a cobalt source (a source of gamma rays) was used. The experiments performed are similar for all scintillators, through which the yield of neutron and gamma ray responses was established [28].

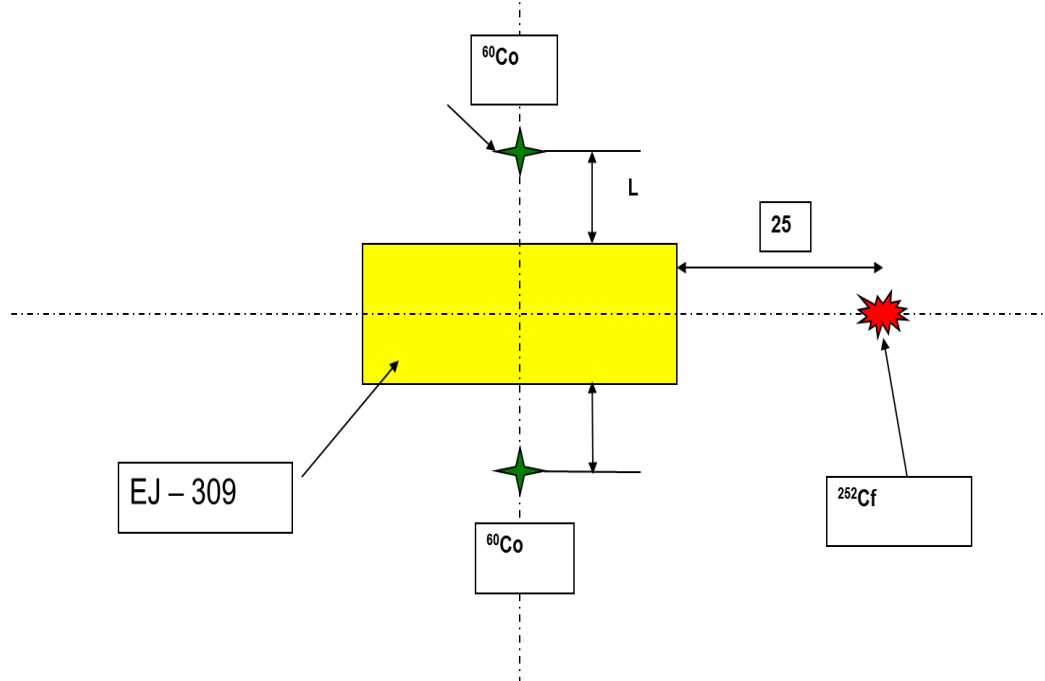
Fig. 4. Neutron channel loading results for BC-501 and EJ-309 liquid scintillators and stilbene crystal scintillator



Ratio of the number of neutrons in response to changes in the distance of gamma ray sources

The objective of the experiment in the presented work was to measure scintillator loads, at which the number of neutron pulses remains continuous depending on the change in the distance of gamma ray sources from the scintillator. The stilbene crystalline scintillator showed the best loading quality in terms of separation of gamma ray and neutron pulse peaks.

Fig. 5. Ratios between the number of neutron pulses from the scintillator load created by the source of gamma rays



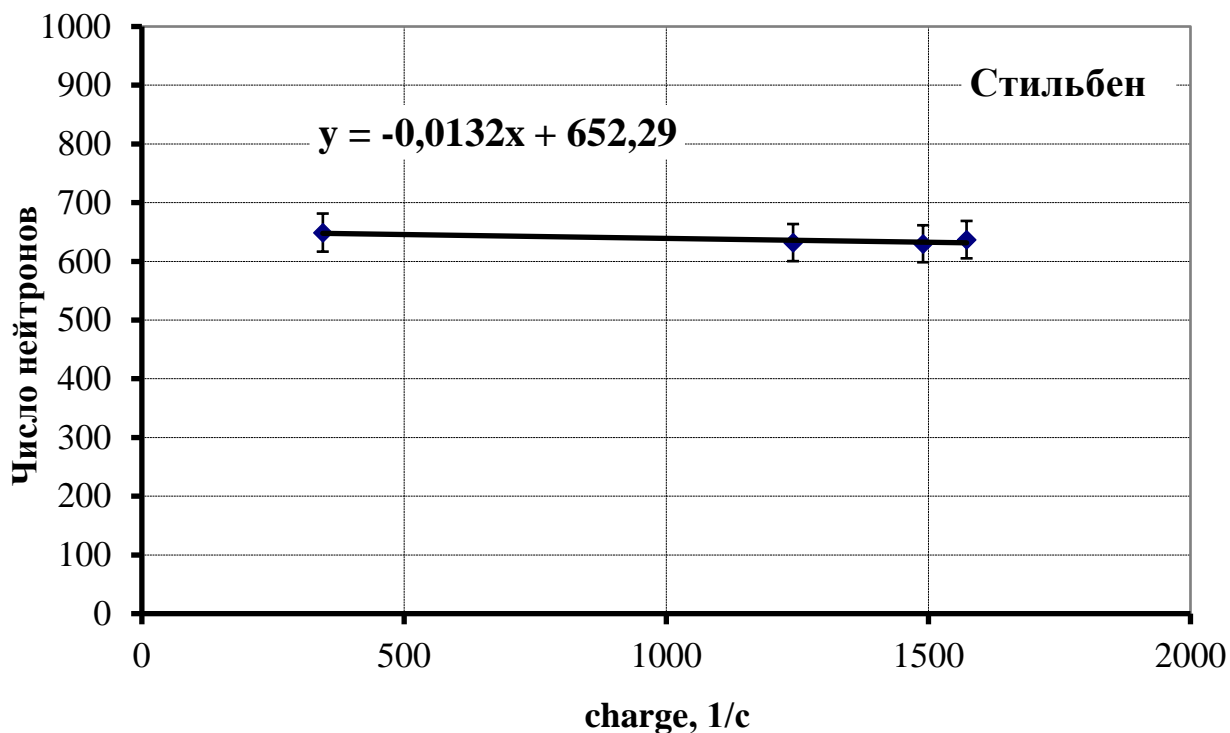
Liquid scintillators BC-501 and EJ-309 and crystalline stilbene scintillator were also used in this experiment. The results of the work carried out are given in the tables and figures below:

Crystal scintillator stilbene

Table 1. The ratio of the number of neutron pulses in the signal from the loading of the stilbene crystal scintillator, created by the source of gamma quanta

№	Source type	Loading, imp/s	Distance, cm	Number of gamma quanta	Number of neutrons
	^{252}Cf	345	-	9258 ($\pm 96,21$)	649 ($\pm 25,47$)
1	$^{252}\text{Cf} + ^{60}\text{Co}$	1490	1	52340 ($\pm 228,77$)	630 ($\pm 25,09$)
2	$^{252}\text{Cf} + ^{60}\text{Co}$	1573	2	45715 ($\pm 213,81$)	637 ($\pm 25,23$)
3	$^{252}\text{Cf} + ^{60}\text{Co}$	1242	3	23254 ($\pm 152,49$)	632 ($\pm 25,13$)

Fig. 6. The ratio of the number of neutron pulses in the stilbene crystal scintillator signal from loading

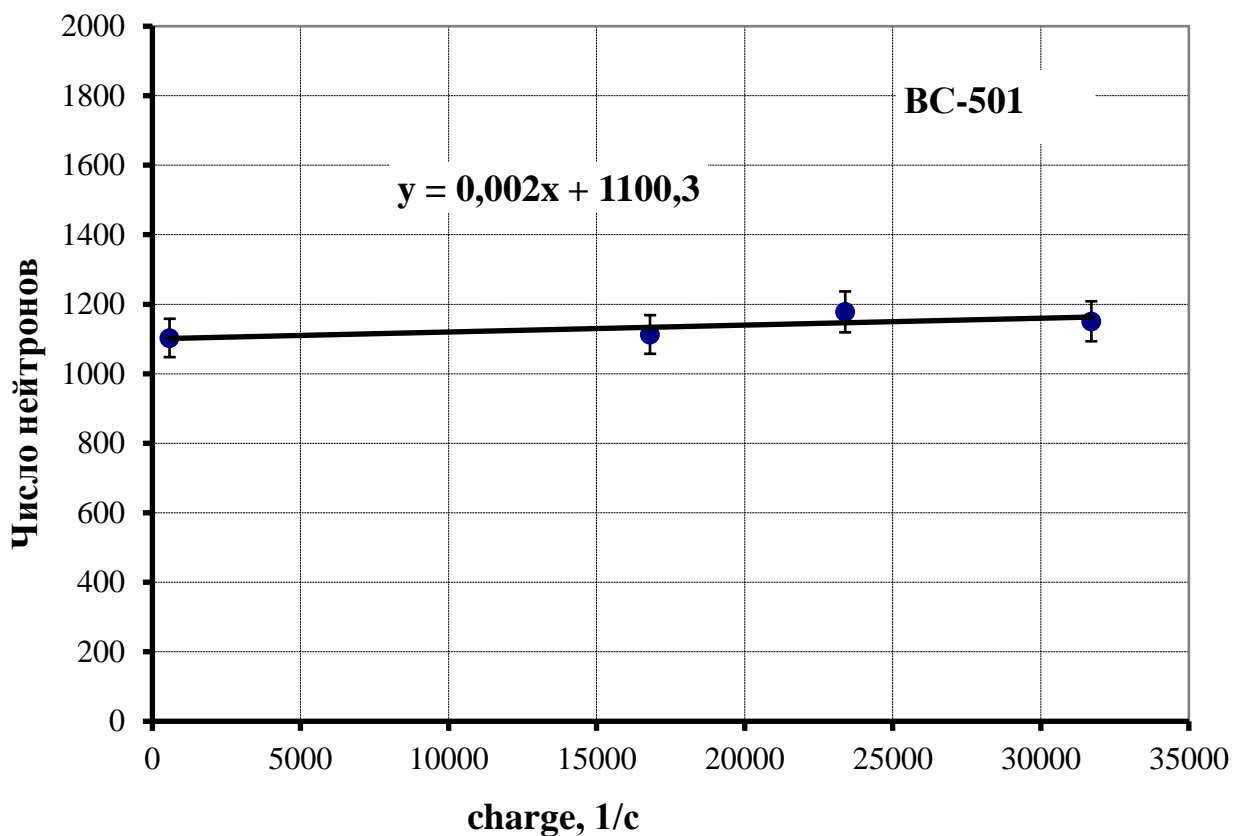


Liquid scintillator VS-501

Table 2. The ratio of the number of neutron pulses in the signal from the load of the liquid scintillator BC-501, created by the source of gamma rays

№	Source type	Loading, imp/s	Distance, cm	Number of gamma quanta	Number of neutrons
	^{252}Cf	584	-	14704 ($\pm 121,26$)	1103 ($\pm 33,21$)
1	$^{252}\text{Cf} + ^{60}\text{Co}$	31707	0,5	904817 ($\pm 951,21$)	1151 ($\pm 33,92$)
2	$^{252}\text{Cf} + ^{60}\text{Co}$	23394	3,5	668472 ($\pm 817,60$)	1178 ($\pm 34,32$)
3	$^{252}\text{Cf} + ^{60}\text{Co}$	16808	6	481883 ($\pm 694,17$)	1113 ($\pm 33,36$)

Fig. 7. The ratio of the number of neutron pulses in the signal of the liquid scintillator BC-501 from loading

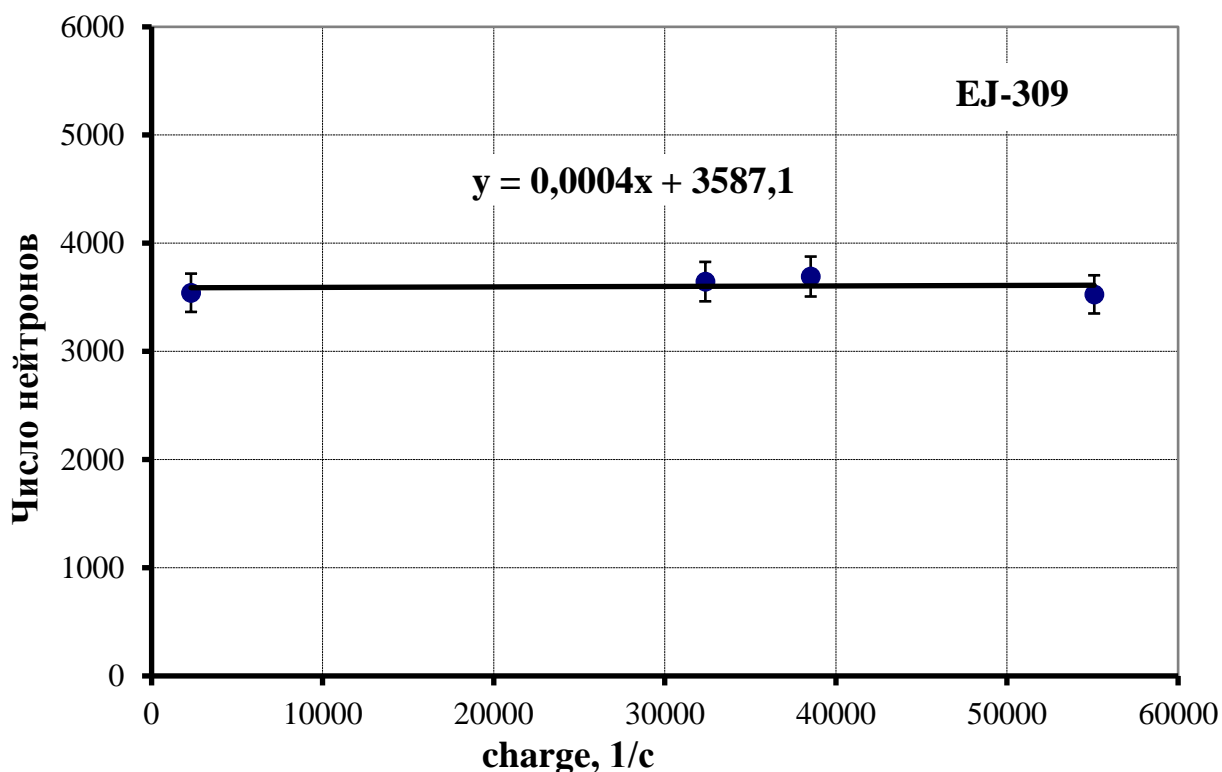


Liquid scintillator EJ-309

Table 2. The ratio of the number of neutron pulses in the signal from the liquid scintillator load created by the source of gamma rays

№	Тип источника	Загрузка, имп/с	Расстояние, см	Количество гамма-квантов	Количество нейтронов
	^{252}Cf	2303	-	49259 ($\pm 221,94$)	3542 ($\pm 59,51$)
1	$^{252}\text{Cf} + ^{60}\text{Co}$	55093	0	1486490 ($\pm 1219,21$)	3527 ($\pm 59,38$)
2	$^{252}\text{Cf} + ^{60}\text{Co}$	38526	3	1100009 ($\pm 1048,81$)	3692 ($\pm 60,76$)
3	$^{252}\text{Cf} + ^{60}\text{Co}$	32361	5	925519 ($\pm 962,03$)	3645 ($\pm 60,37$)

Figure 8. The ratio of the number of neutron pulses in the signal of the liquid scintillator EJ-309 from loading

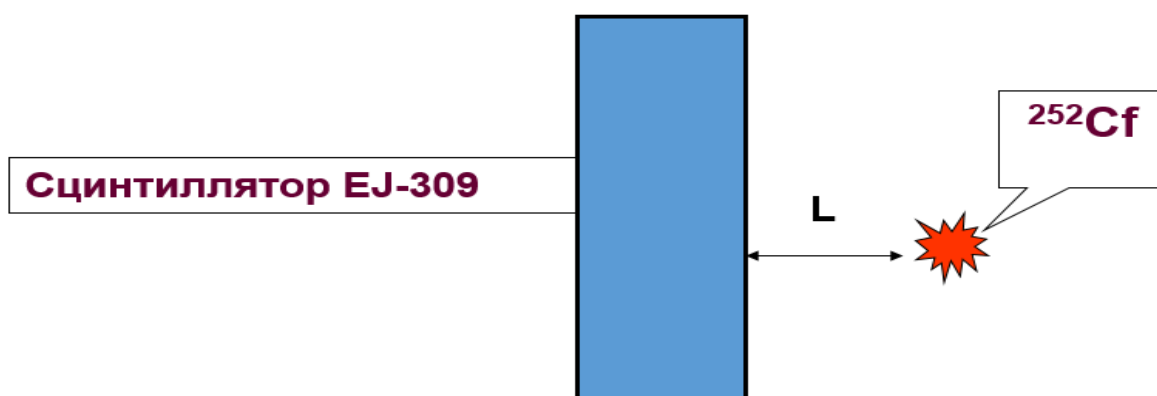


The results of the experimental work carried out on all scintillators demonstrate that when the loading of the scintillator channel with gamma ray sources changes, the number of gamma quanta pulses increases, but the number of neutron pulses remains unchanged, which required clarification during practical work. This raises the problem of changing the distance of the neutron source from the scintillator used [29].

Ratios of neutron and gamma quanta momenta for various scintillator loads

In this experiment, an analysis of scintillation pulses of neutrons and gamma rays from the spontaneous decay of the californium source was carried out. The task was to carry out digital analysis of neutron and gamma ray pulses with varying distances of a neutron source with a high neutron yield from the EJ-309 scintillator.

Fig. 9. The ratio of neutron and gamma quanta pulses for various scintillator loads



The distance of the neutron source in the presented experiment was changed from 4 cm to 20 cm and, accordingly, the load changed from this. The energy thresholds were chosen to be 300 KeV and 400 KeV.

Table 3. Ratio of scintillation pulses of neutrons and gamma quanta at different loadings of the scintillation tract

Расстояние, см	Загрузка, 1/с	Время измерения, с	Порог, 300 КэВ			Порог, 400 КэВ		
			Нейтрон ы	Гамма	Нейтроны / Гамма	Нейтроны	Гамма	Нейтроны / Гамма
0	$2.28 \cdot 10^4$	10	28840 (169)	179251 (423)	0.161 (0,0010)	27866 (166)	16480 (128)	0.169 (0,0166)
4	$6.18 \cdot 10^3$	15	12595 (112)	73265 (270)	0.172 (0,0016)	12170 (110)	67131 (259)	0.181 (0,0017)
8	$2.20 \cdot 10^3$	20	6192 (78)	34578 (185)	0.175 (0,0024)	5979 (77)	31707 (178)	0.189 (0,0026)
12	$1.13 \cdot 10^4$	30	5006 (70)	26443 (162)	0.189 (0,0029)	4811 (69)	24185 (155)	0.198 (0,0031)
20	476	0	2118 (46)	11076 (105)	0.191 (0,0045)	2046 (45)	10200 (100)	0.201 (0,0048)

Fig. 10. Determination of the error in the ratio of the number of neutron pulses to the pulses of gamma rays from the distance of the neutron source to the scintillator

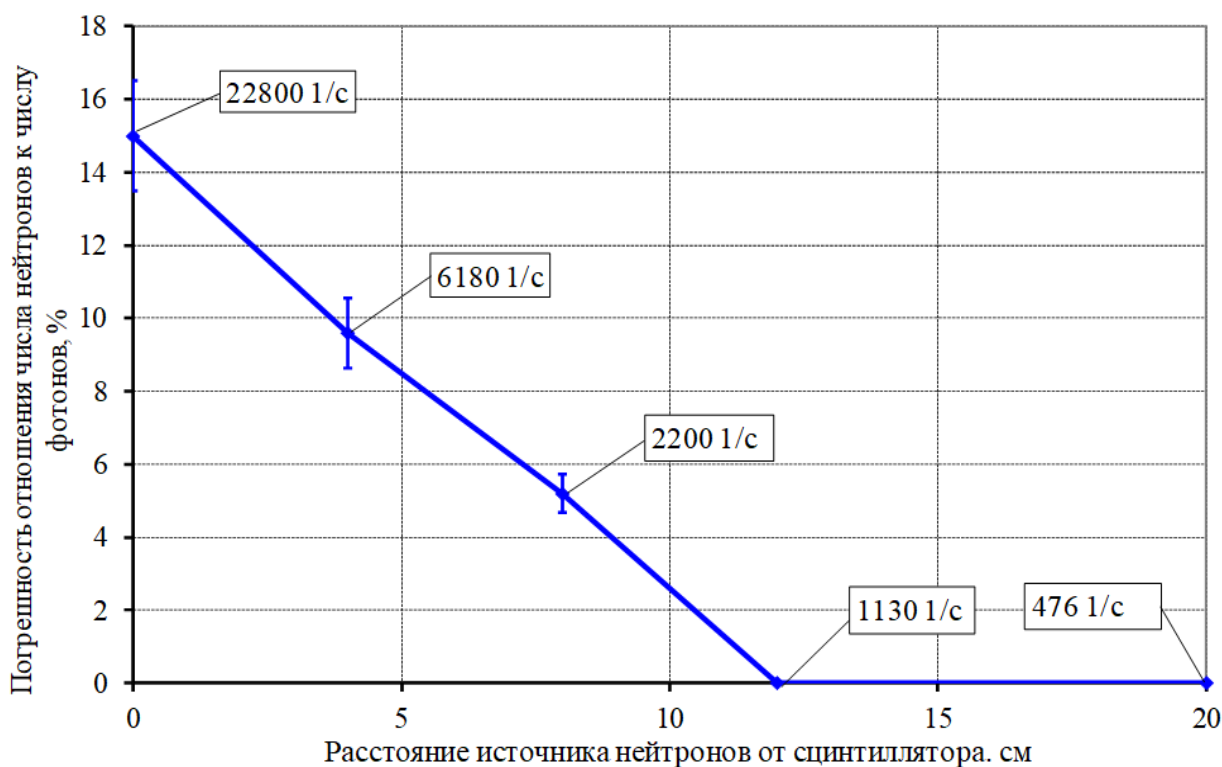
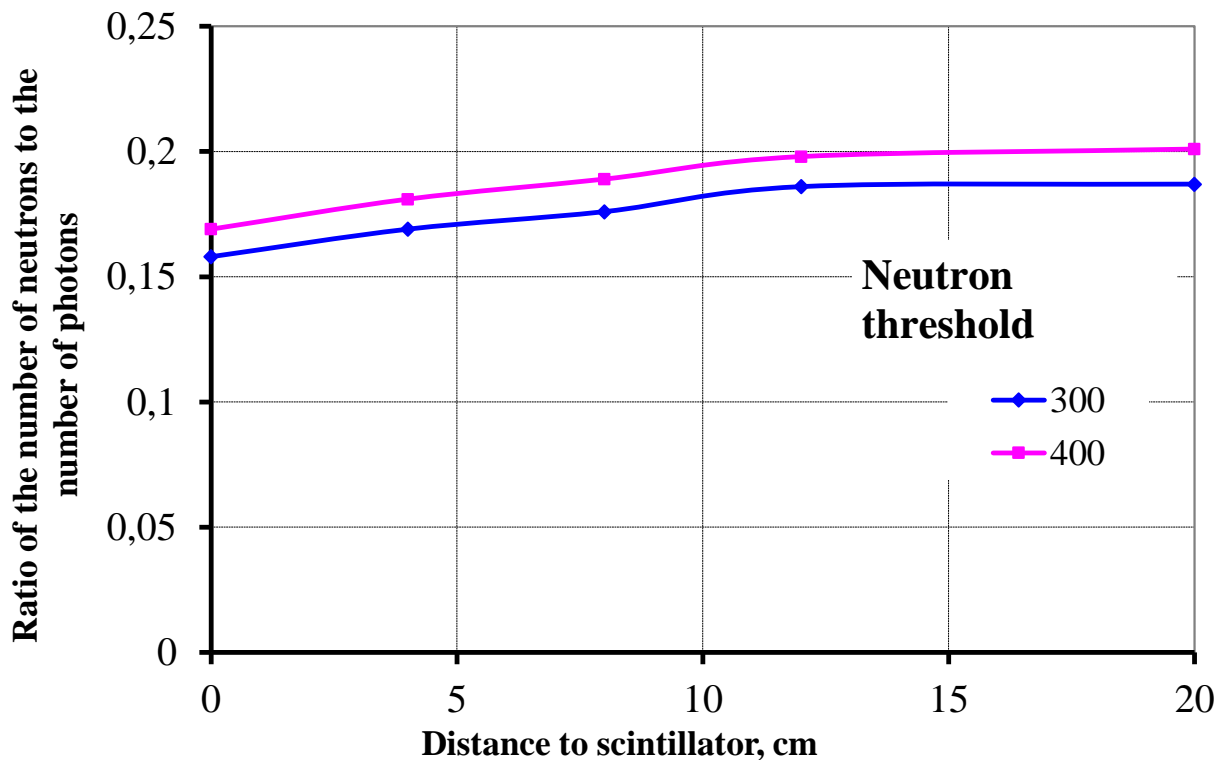


Fig. 11. Dependence of the number of neutron pulses on the number of gamma quanta on the distance to the scintillator for different energy thresholds



The results of research work demonstrate that when using a californium source, the number of neutron pulses increases, but the number of gamma rays remains unchanged. It was also determined that when the distance changes up to 12 cm, the number of neutron pulses increases, however, from a distance of 12 cm to 20 cm, the number of neutron pulses remains constant, which is subject to further study (Table 4, Figure 10 and Figure 11) [30].

CONCLUSION

In this work, various types of ionizing radiation detectors, the main properties and disadvantages of the studied detectors were investigated. A digital method for removing superimposed (doubtful) pulses is presented to determine the number of neutron and gamma ray pulses.

Some experimental work was carried out to determine the quality of scintillation detectors, the ratio of neutron pulses to gamma quanta pulses, and measurements were also carried out with changing the distance of the neutron source from the scintillator to determine the dependence of the number of neutrons on gamma quanta.

When conducting experiments to determine the quality of scintillators, it was determined that the crystalline stilbene scintillator, compared with the liquid scintillators EJ-309 and BC-501, showed the best pulse separation performance.

In an experiment on the relationship between the number of neutrons and the load of various scintillators created by gamma ray sources, it was determined that when the distance of gamma quanta sources changes, the load of gamma quanta up to $3 \cdot 10^4$ pulses/s does not affect the efficiency of neutron detection, which shows the reliability non-impact of neutron pulses and their separation.

In the work to determine the ratio of the number of neutrons to gamma quanta of the scintillator load created by the gamma quanta source, it was determined that changing the

distance of the gamma quanta source increases the number of gamma quanta, but the number of neutrons remains unchanged. Therefore, we can assume that loading the scintillation path to a level of $5 \cdot 10^4$ n/s does not provide an error in measuring the number of neutrons of more than a few percent.

GRATITUDE

The author expresses deep gratitude to Professor of the National Research Nuclear University "Moscow Engineering Physics Institute" A.G. Belevitin, Doctor of Physical and Mathematical Sciences V.L. Romodanov for assistance in digital processing of experimental data, as well as the late NAST academician Kh.Kh. Muminov for a profitable discussion of the results obtained.

**REVIEWER: Makhsudov B.I. doctor
physical and mathematical sciences,
Professor**

REFERENCES

1. Bak, M. Neutron / M. Bak, Y.F. Romanov // M.: Atomizdat 1960. - Pp. 12-21.
2. Bolozdinya, A.I., - Experimental nuclear physics. / A.I. Bolozdinya // -M.: NRNU MEPhI, 2018. - Pp. 26-30.
3. Vyaltsev, A.N. - Neutron background discovery consequences. / A.N. Vyaltsev // -M.: Nauka. - 1975. - Pp. 69-109.
4. Frolov, V.V. Nuclear-physical methods of control of fissile substances / V.V. Frolov // -M.: Energoatomizdat, 1989. - Pp. 7-15.
5. Frank, AI, - Fundamental properties of the neutron. / AI. Frank // M.: Uspekhi fizicheskikh nauk. Volume 137. Issue 1, 1982. - Pp.5-18.
6. Rakobolskaya I.V. Nuclear physics. / I.V. Rakobolskaya // M.: Publishing House of Moscow University, 1971. - Pp. 190-198.
7. Kadilin, V.V. Applied neutron physics / V.V. Kadilin, E.V. Ryabeva, V.T. Samosadny // -M.: NRNU MEPhI, 2011. - Pp.24-26.
8. Goncharova, N.G. Particles and atomic nuclei / N.G. Goncharova, B.S. Ishkhanov, I.M. Kapitonov // -M.: Fizmatlit, 2013. - Pp.370-386.
9. Nozik, Y.Z. Neutrons and solids. Structural neutronography / Nozik, Y.Z. Ozerov R.P., Hennig K. // -M.: Atomizdat, Volume 1, 1979. - Pp.12-14.
10. Stogov Y.V. Fundamentals of neutron physics / Y.V. Stogov // M.: NRNU MEPhI, 2008. - Pp. 5-40.
11. Federal norms and rules in the field of the use of atomic energy "Basic rules for accounting and control of nuclear materials" (NP-030-19), Moscow: Rostekhnadzor, April 10, 2020. - Pp. 2-7.
12. Dolgoplov, S.V. Determination of the neutron-physical properties of moderating media / Dolgoplov, S.V. Nesterov, V.N., Chertkov, Y.B. // - Tomsk: Publishing House of the Tomsk Polytechnic University, 2008. - Pp. 6-15.
13. DOE Fundamental handbook Instrumentation and Control. / U.S. Department of Energy, Washington D.C. 20585, FSC-6910, Volume 2 of 2, June 1982. - Pp. 8-19.
14. Doug Reilly. Passive Nondestructive Assay of Nuclear Materials / Norbert Ensslin, and Hastings Smith, Jr. / Doug Reilly // The Superintendent of Documents U.S. Government Printing Office, Washington, D.C. 20013-7082. March 1991. - Pp. 379-404.
15. Groupen, K. Particle Detectors / K. Groupen, Borer, A., Smolik L. // Research Center "Siberian Chronograph". 1999. - Pp. 56-81.
16. Richard T. Kouzes. Neutron detection alternatives to ^3He for national security applications / Richard T. James H. Ely, Luke E. Erikson, Warnick J. Kernan, Azaree T. Lintereur, Edward R. Siciliano, Daniel L. Stephens, David C. Stromswold, Renee M. Van Ginhoven, Mitchell L. Woodring // Science Direct. Elsevier. <https://doi.org/10.1016/j.nima.2010.08.021>. Volume 623. Pp. 1035-1045.
17. Pikar, V.A. Portable devices for the search and identification of radioactive materials / V.A. Pikar, A.V. Rodigin // Youth in science: collection of reports of the 11th scientific and technical conference. 2013. No. 11. - Pp. 342-246.

18. Marunin, P.V. Modernization of the electronic unit of the neutron detector for portable equipment for radiation monitoring / Rodigin A.V. // Federal State Unitary Enterprise "RYaFTs-VNIIEF", Sarov.: 2015. – Pp. 224-228.
19. Akimov, Y.K. Nuclear radiation detectors based on plastic scintillators / Y. K. Akimov // Physics of elementary particles and the atomic nucleus, 1994. Volume 25, Issue. 2. – Pp.496-500.
20. Shendrik, R.Yu. Methods of experimental physics of condensed matter. Part 3. Introduction to the physics of scintillators. Textbook / R. Yu. Shendrik // Irkutsk: Irkutsk State University Publishing House, 2013. – Pp. 9-15.
21. Swank, R.K. Characteristics of scintillators / R.K. Swank // Uspekhi fizicheskikh nauk, 1956. Volume 58, Issue. 3, – Pp. 519-530.
22. Demenkov, V. G. Beginnings of electronic methods of nuclear physics. Textbook / V.G. Demenkov // St. Petersburg: Publishing house "Lan", 2016. – Pp. 26-39.
23. Romodanov, V. L. Physical methods and installations for active control of fissile materials: a textbook for students of higher educational institutions / V. L. Romodanov // –M.: NRNU MEPhI, 2007. P. 66-77.
24. Romodanov, V. L. Method for reducing the loading of scintillation tracts in installations with pulsed neutron sources / V. L. Romodanov, V.K. Sakharov, D.N. Chernikova // –M.: 2010. Devices and experimental technique. No. 3. – Pp. 38-49.
25. Romodanov, V. L. Laboratory work on active methods of non-destructive testing of fissile materials: a textbook for students of higher educational institutions / V. L. Romodanov // –M.: NRNU MEPhI, 2007. – Pp. 4-9.
26. Chernikova, D. N. Computational and experimental studies of the installation for detecting fissile materials at airports / D. N. Chernikova, V.L. Romodanov, V.K. Sakharov, I.V. Mukhamadyarov, V.V. Afanasiev, A.G. Belevitin // –M.: Atomic energy, 2008, No. 105. – Pp. 102-118.
27. Romodanov, V. L. Complex for digital data processing in installations for the detection of radioactive and fissile materials / V.L. Romodanov, V.V. Afanasyev, A.G. Belevitin, R. Yu. Ryabov // –M.: MEPhI preprint, 2005. – Pp. 32-43.
28. Imom, M. Sh. Development of qualitative digital analysis of neutron and gamma-ray responses with different scintillation counters / M.Sh. Imom, V.L. Romodanov, Kh.Kh. Muminov, F. Rakhimi, S.F. Odinaev // Izvestiya of NANT.: 2019. No. 1 (174). – P.125.
29. Imom, M. Sh. Investigation of the effectiveness of the digital method for analyzing the loading of a neutron channel for various scintillation counters / M. Sh. Imom, V.L. Romodanov, Kh.Kh. Muminov, F. Rakhimi, S. F. Odinaev // Izvestiya of NANT, 2020. No. 1 (178). – P. 44.
30. Imom M.Sh., Digital method for determining the ratio of neutron pulses to gamma-quantum pulses for various scintillator loads / M. Sh. Imom, V.L. Romodanov, Kh.Kh. Muminov, F. Rakhimi, S.F. Odinaev // Izvestiya of the NAST, 2020 No. 4. – P. 84.

INVESTIGATION OF THE SCINTILLATION RESPONSE OF NEUTRONS AND GAMMA-QUANTS BY THE METHOD OF REMOVING SUPERIMPOSED PULSES

The presented research work is devoted to the problems of studying the digital method for analyzing neutron and gamma ray pulses by eliminating superimposed responses. This method consists of scintillation detectors, photomultiplier tubes, an analog-to-digital converter and an appropriate algorithm. The method was used to analyze the loading of neutron channels in liquid and crystalline scintillation detectors, the ratio of the number of neutrons in the response with a change in the distance of the gamma-ray source, as well as the ratio of neutron and gamma ray pulses for various scintillator loads. Liquid and crystal scintillators were used as analytical instruments.

Keywords: digital method, scintillator, neutron, gamma-quantum, detector, separation parameter, removal of superimposed pulses, counter, detection and control.

Information about the authors: Imom Mirahmadi Sharofiddin - S.U.Umarov Physical and Technical Institute of the National Academy of Sciences of Tajikistan, senior researcher. **Address:** 734063, Dushanbe, Republic of Tajikistan, Aini Avenue, 299/1. **Phone:** (+992) 933-77-22-11. **E-mail:** emmirshar@gmail.com.

Romodanov Vadim Leonidovich – National Research Nuclear University Moscow Engineering Physics Institute, Professor, Doctor of Physical and Mathematical Sciences. **Address:** 115409, Moscow, Russia, Kashirskoe highway, 31. **Phone:** +7 (495) 788-56-99. **E-mail:** vlromodanov@mephi.ru.

Farhod Rahimi - National Academy of Sciences of Tajikistan, Doctor of Physical and Mathematical Sciences, Professor, Corresponding Member. **Address:** 734025, Dushanbe, Republic of Tajikistan, Rudaki Avenue, 33. **Phone:** (+992) 900-00-44-99. **E-mail:** frahimi-2002@mail.ru.

Odinaev Subkhonjon Fatkhulloevich - S.U.Umarov Physical and Technical Institute of the National Academy of Sciences of Tajikistan, senior researcher. **Address:** 734063, Dushanbe, Republic of Tajikistan, Aini Avenue, 299/1. **Phone:** (+992) 938-01-32-01. **E-mail:** emmirshar@gmail.com.

Article received 11.12.2023
Approved after review 25.01.2024
Accepted for publication 13.03.2024

STRUCTURAL CHANGES IN CdTe SINGLE CRYSTALS UPON IRRADIATION WITH HEAVY IONS OF INERT GASES

Sultonov N., Akobirova A.T., Naimov U.R.,
Rahmatov B.A., Hamrokulov R.B.

Polycrystalline films of A^2B^6 compounds, mainly cadmium telluride, are increasingly used in the main areas of electronic engineering, microelectronics, optoelectronics, and solar energy [1-3].

Cadmium telluride, due to the large atomic numbers of the components, as well as the large band gap ($\Delta E=1,5 \text{ eV}$), is currently one of the most promising materials for the creation of dosimeters and counters of γ - quanta [4-6].

The possibility of creating instruments and devices based on polycrystalline CdTe films is determined by the level of technology for synthesizing films with reproducible and controllable properties.

Based on this, increasing reproducibility in the technology of polycrystalline film structures is the most important task of microelectronics and optoelectronics. Its solution is determined by the ability to predict the influence of technological factors on the structure and electrical properties of films, which requires modeling of technological processes and interoperational control [3,7].

The growing need for polycrystalline films is also caused by the fact that in single crystals, due to the peculiarities of growth mechanisms, it is impossible to obtain the spectrum of structures that is inherent in polycrystalline disorder.

This paper presents results on the production of polycrystalline films by irradiation of single-crystalline cadmium telluride with ions of inert gases of different radii.

Progress in micro- and optoelectronics, optics and other fields of technology, which has transformed the information world in a short period, is directly related to the development of thin-film technologies. When growing films, experimenters and technologists are forced to control a number of parameters, such as the material and structure of the substrate, its temperature, vapor composition, and the intensity of its supply [8-11]. Typically, these parameters are selected empirically to obtain the desired structures and film composition [12, 13].

Fundamental research into the kinetics of first-order phase transitions is underway. It has been shown that the kinetics of first-order phase transitions is a complex multistage process that is accompanied by various nonlinear phenomena [14, 15]. Such stages usually include the stages of nucleation, separate growth of nuclei of a new phase, coalescence and the late stage, that is, Ostwald ripening, in which the growth of larger islands occurs due to the dissolution of smaller ones.

The main goal of thin-film technologies is to obtain continuous film structures of a given composition, thickness and structure. Depending on the application, films can be amorphous, polycrystalline or epitaxial (monocrystalline). Polycrystalline films, as a rule, are formed on non-orienting substrates or on orienting ones, but under conditions far from equilibrium. To obtain amorphous, that is, frozen, metastable structures, it is necessary to use special techniques for creating high saturations or supercoolings. The question of what is the main guiding growth factor remains open today. It is believed that a necessary condition for the growth of oriented structures is the proximity of the lattice parameters of the substrate and the film (usually it is

sufficient that this difference between them does not exceed 15%). However, this is far from a sufficient condition, since the islands of the new phase participate in various evolutionary processes. It is quite difficult to determine which of them has the main influence on orientation. Some models of oriented growth are considered in [12, 13].

An essential feature of the nucleation of a new phase on the surface of substrates in comparison with a homogeneous formation in the bulk is that the substrate contains various defects. Defects are usually divided into point and linear, which include steps, dislocation exits and scratches. Even an ideal substrate contains defects such as Tamm levels, formed by the incompleteness of crystalline planes. A rigorous theory of the heterogeneous nucleation of a new phase on the surface has not yet been developed.

Growth modes of thin films are usually divided into layer-by-layer, island, and intermediate [12].

The layer-by-layer mode, or Frank-van der Merwe mode, is realized if the atoms of the deposited substance are bonded to the substrate more strongly than to each other. Monatomic layers are filled in this mode one by one, that is, two-dimensional nuclei (one atom thick) of the next layer are formed on the top of the nuclei of the previous layer after its filling.

The island mode, or Volmer-Weber mode, is realized in the opposite case, when the atoms of the deposited substance are bonded more strongly to each other than to the substrate.

In the intermediate regime, or Stranski-Krastanov regime, layer-by-layer growth is first realized, then, after filling one or two layers, the island growth regime begins. There may be several reasons for the change in growth mechanisms. The main one is that the lattice parameter cannot remain unchanged when filling the next layer. Its change leads to a strong increase in the energy of the adsorbate-intermediate layer interface, which ensures the fulfillment of the island regime criterion.

On the surface, according to modern concepts [16], the following main methods of migration of atoms and distribution of energy, in particular heat, are distinguished: three-dimensional or volumetric diffusion of atoms and three-dimensional heat removal; two-dimensional diffusion of atoms over the surface of the substrate and two-dimensional heat removal; one-dimensional diffusion of atoms along substrate steps, dislocation exits and other linear defects. Islands can also grow due to the direct supply of atoms from the vapor to their surface.

Among the variety of processes that accompany the growth of thin films, the main one, of course, is the process of nucleation of islands of a new phase, that is, the first-order phase transition itself. It is at this initial stage of condensation that it is determined how many islands of the new phase will appear, and the foundations for the formation of the structure of a thin film are laid.

It is easiest to control the film growth parameters at the OS stage, when the nucleation of new islands does not occur and a continuous film has not yet formed. The possibility of control is based on the fact that at this stage the ensemble of islands of the new phase enters into a peculiar interaction with the generalized diffusion-thermal fields formed on the surface of the substrate and the flows of atoms incident on it. In this case, the asymptotic size distribution of islands and their composition do not depend on the initial distribution, but depend on the mechanism of mass and heat transfer realized during the growth of islands, and on the intensity of the supply of matter and heat to the substrate.

An original technique for obtaining highly oriented films was proposed in [19]. As a rule, such films are obtained at elevated temperatures (to ensure the required mobility of adatoms) under conditions close to equilibrium. For example, CdTe films are usually grown at

substrate temperatures of the order of 500-650 K [19]. This work also describes a method for producing epitaxial films at a temperature of 228 K. Moreover, changing the substrate temperature both up and down led to a deterioration in the structure of the films. This is due to a two-dimensional layer of liquid on the surface of the substrate, formed either immediately or due to the appearance of liquid CdTe droplets directly at the surface of the substrate. An increase in the substrate temperature leads to the destruction of this two-dimensional layer, and a decrease in it leads to the creation of large supercooling and disruption of the OS stage. With a further decrease in temperature, amorphous films begin to grow.

It is well known that the properties of films mainly depend on their composition. It is the composition that determines most of the electrophysical, optical, strength and other properties. Understanding how the composition of films evolves in order to be able to control it during film growth is one of the most important tasks in the physics of thin films. It was shown in [17, 18] that at a certain stage a one-to-one relationship is established between the radius of islands of solid solutions and their composition.

Various processes can occur inside continuous films under the influence of external factors. This is due to the fact that the substrate-film system is significantly nonequilibrium. This disequilibrium is a consequence of the stresses present in the film and substrate. In the presence of a proper mass transfer mechanism, these stresses relax, resulting in a loss of film continuity. In addition, in polycrystalline films, the grains of which are stressed in different ways, recrystallization processes can occur. A rigorous theory of such processes has not yet been constructed, but all these processes, to one degree or another, can be attributed to first-order phase transitions.

RESULTS AND DISCUSSION

In this work, the influence of the ion radius on the resistivity and intensity of the strongest X-ray reflection (111) was studied. X-ray studies were carried out using the DRON-2 installation. To measure the film resistance, a P4053 direct current bridge was used. The samples were irradiated with neon, argon and xenon ions of the same dose (250 mrad) with radii of 38, 71 and 108 picometers (10-12 m), respectively [11, 12]. As follows from Fig. 1, as the ion radius increases, the intensity of the (111) reflection decreases and the X-ray diffraction patterns in all cases take on the shape characteristic of polycrystalline bodies. The difference in the half-width of the reflections, which determine the crystallite sizes for all three types of irradiated ions, does not exceed 10%. The half-width of the reflection for the irradiated sample according to the strongest reflection (III) is $\sim 42^\circ$, which corresponds to the size of the crystallites (grains). The half-width of another reflection (220) of the irradiated single crystal is also characteristic of polycrystalline substances.

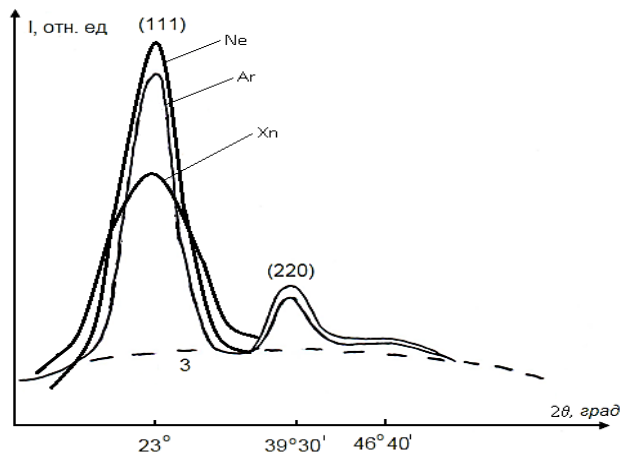


Figure 1. Effect of the radius of the argon ion on the intensity of the X-ray reflection (111)

The dependence of resistivity on the radius of irradiated ions is shown in Fig. 2. It is shown that, in accordance with X-ray data, as the ion radius increases, the resistivity increases, and the larger the ion radius, the greater the growth rate ρ . Irradiation transforms a single crystal into a polycrystalline state with the formation of a large number of defects, which are sources of current carrier capture, which leads to an increase in ρ .

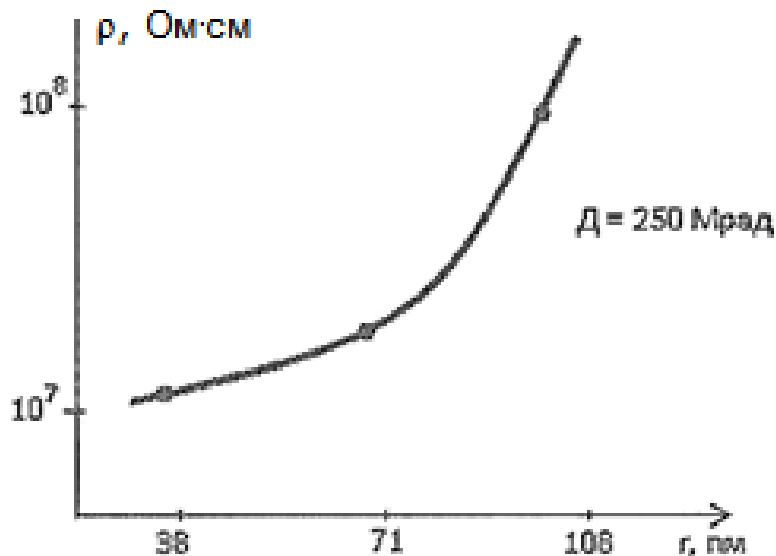


Figure 2. Dependence of the resistivity of CdTe films on the radius of the argon ion

It is obvious that irradiation leads to a change in the crystal structure of the sample and their partial amorphization. The increasing decrease in ρ with increasing ion radius is apparently due to the fact that ions with a large radius have a significantly larger effective cross section for interaction with the crystal, and much more defects are formed along their track (compared to ions with a smaller radius) - vacancies, dislocations, the escape of atoms into interstices, which subsequently become centers of the amorphous region.

In order to clarify the mechanism of amorphization of single crystals, studies of the structural and electrical changes in CdTe single crystals were carried out at doses lower or higher than the already considered dose of 250 MeV.

The objects of study for these experiments were chosen single-crystal films of cadmium telluride 80 microns thick. In Fig.3 shows the change in the diffraction pattern of the film as the irradiation dose with argon ions increases. As can be seen, for the original non-irradiated film, four diffraction maxima are observed with a gradual decrease in intensity. At a dose of 150 mrad, the 400 reflection disappears and three clear reflections with a broadening of the half-width compared to the original are observed in the diffraction pattern; at a dose of 250 MeV, reflection 311 turns into a plateau and two reflections are observed on the x-ray diffraction pattern - (111) and (220); at a dose of 400 MeV, all reflections disappear and two blurred maxima, characteristic of amorphous bodies, are observed in the diffraction pattern (Fig. 2, curve 4).

From the analysis of Fig. 3 it follows that during irradiation the single crystal first transforms into a polycrystal, as evidenced by the expansion of the half-width of the reflections, then at $D > 350$ MeV. crystallites are destroyed and the polycrystalline film becomes amorphous.

From the analysis of the reflection intensities it follows that the most stable planes are those corresponding to large values of d (interplanar distance), i.e. small values of the angular position of the maximum ($\theta = 23^\circ$ и $30^\circ 30'$), while the crystal planes corresponding to large values of θ ($\theta = 23^\circ$ и $30^\circ 30'$) are destroyed. Thus, atomic planes with a small value of d , when destroyed, form pockets of amorphous regions.

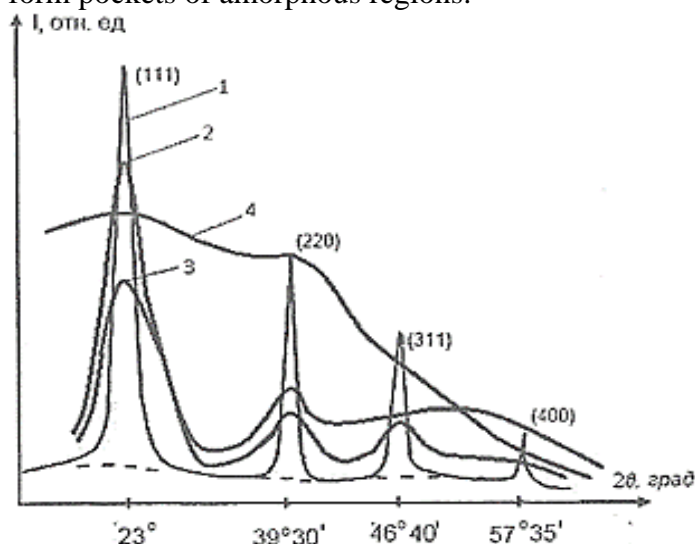


Figure 3. Effect of irradiation dose of a single-crystal CdTe film with argon ions on X-ray diffraction patterns: 1 - initial, 2 - 150, 3 - 250, 4 - 400 MeV

From Figure 3 shows that the decrease in the intensity of crystalline reflections with increasing dose is accompanied by the disappearance of long-range reflections; first, the most distant reflection (400) disappears, then (011) and then (220) and (111).

In Figure 4 shows the dependence of the film resistivity (ρ) on the irradiation dose D , where it is clear that initially, with increasing dose, ρ increases linearly (section AB, Fig. 4), which is associated with the transition of the single crystal to the polycrystalline state, and in section BC (Fig. 4) There is a sharper increase in ρ , which is associated with the gradual transition of the polycrystalline state to the amorphous one. The SD region, where constancy of ρ is observed with increasing D , refers to the transition of the polycrystalline state to a completely amorphized one.

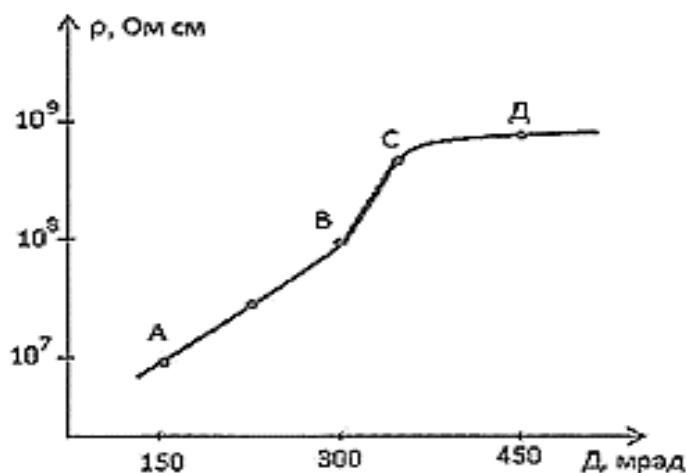


Fig. 4. Dependence of resistivity on the dose of irradiation with argon ions of cadmium telluride films

Moving on to a discussion of the results, it should be noted that the bombardment of crystals by ions is accompanied by the accumulation of vacancy complexes (enriched in vacancies) and the formation of an interstitial atom.

The spatial separation of defects, namely the spatial separation of primary defects and interstitial atoms, allows the accumulation of defects to a high concentration. At the initial moment of time, each individual disordered region (RD) is a region with enriched vacancies in the center, surrounded by a cloud of interstitial atoms. Next, the radiation region goes through a number of stages caused by the occurrence of secondary processes: a) the departure of defects from the RO due to diffusion; b) interaction of defects with each other with the formation of stable defects that are immobile at a given temperature. The named processes act towards each other, the effectiveness of one or another process depends on the mass of the bombarded particle and the temperature of the substrate.

An increase in the mass of the ion promotes more efficient complex formation. Since with increasing ion mass the concentration of displacements in the PO increases and the size of the PO in the plane perpendicular to the beam direction increases, this increases the probability of interaction of defects with each other with the formation of complexes immobile at a given temperature. Conversely, a decrease in mass promotes the occurrence of the first process, i.e. removal of defects from the RO.

When a semiconductor was irradiated with even small doses of heavy ions, VV centers were observed. The concentration of primary displacements in this case was apparently sufficient to transform the polycrystal into an amorphous state in the region of the particle track; at least the inner part of the disordered region is amorphous.

At high energies, an amorphous layer is formed in the bulk of the semiconductor, and the transition to the amorphous state of the surface layer occurs only with a further increase in the dose. Irradiation of semiconductors with light ions leads to the formation of two amorphous layers: near-surface and bulk.

The introduction of an ion into a crystal provides a sufficient concentration of defects to form a separate amorphous zone. It was also believed that the formation of such a zone requires a certain characteristic time τ , during which defects diffuse from the disordered region (DR). The more defects that leave the PO as a result of diffusion, the smaller the size of the amorphous zone (PO is an accumulation of point defects formed when crystals are irradiated with ions, fast neutrons and high-energy electrons (>10 MeV)).

Defects (vacancies, interstitial atoms) that go deep into the crystal form complexes with impurities there or are captured by dislocations. Another part of the defects, moving towards the surface, accumulates at the surface layer, forming complexes that are stable at the selected temperature of irradiation of objects.

In the process of bombardment by ions, PO is superimposed, which gives a layer enriched with vacancies in the region of maximum of other elastic collisions.

The vacancy layer is surrounded by a region with an increased concentration of interstitial complexes. The flow of defects to the surface contributes to the formation of a near-surface region of defects. Depending on the conditions on the surface, this region contains defects of either vacancy or interstitial type.

The mass of the incident ion has a strong influence on secondary processes in the bombarded layer. This is especially clearly manifested in the dose dependence of the amorphization of the irradiated layer, as well as in the depth distribution of defects introduced by heavy ions at elevated temperatures.

Even when heavy ions are introduced into a semiconductor, the amorphous phase is formed as a result of secondary processes - the interaction of defects with each other during irradiation.

We assume that amorphous zones are formed as a result of primary processes when the following conditions are met: 1) irradiation is carried out at temperatures when the thermal movement of the components of Frenkel pairs is inhibited; 2) the thermal realization time of RO is much less than the characteristic times of interaction of defects with each other; 3) Between the layer amorphized by ion bombardment and the single-crystalline substrate there is a transition region saturated with defects. A single crystal is destroyed especially intensively when bombarded with heavy particles. The limiting case of accumulation of defects during ion bombardment is the complete destruction of the crystalline structure with the formation of a continuous amorphous layer. Recovery occurs after annealing at a sufficiently high temperature.

CONCLUSION

The influence of the ion radius on the resistivity and structure of the (111) layer of a single crystal of cadmium telluride has been studied. The samples were irradiated with neon, argon and xenon ions with radii of 38, 71 and 108 picometers (10-12 m), respectively. The radiation dose for all ions was 250 Mrad.

It has been shown that ions with a large radius have the strongest influence on structural transformations; at the same dose (250 Mrad), the drop in intensity of the (111) reflection under the influence of xenon ions is twice as high as that of neon ions. In accordance with X-ray data, as the radius of the ion increases, the resistivity increases, and the larger the radius of the ion, the greater the rate of increase ρ . Irradiation transforms a single crystal into a polycrystalline state with the formation of a large number of defects, which are sources of current carrier capture, which leads to an increase in ρ . The increasing growth of ρ with increasing ion radius is apparently due to the fact that ions with a larger radius have a significantly larger effective cross section for interaction with the crystal.

**REVIEWER: Makhsudov B.I.,
Doctor of Physical and Mathematical Sciences,
Professor**

REFERENCES

1. Akobirova A.T. Surface morphology of cadmium telluride films obtained by vacuum deposition on silicon and cadmium telluride substrates / A.T.Akobirova, V.I. Golovchuk, M.G.Lukashevich, N. Sulonov,

- R.B. Khamrokulov // Journal of the Belarusian State University. Physics. – Minsk, 2017. No. 2. – Pp. 69–75.
2. Sultonov N. Development of technology for producing polycrystalline cadmium telluride films and study of their structure and electrical properties / N.Sultonov, A.T. Akobirova, R.B. Khamrokulov // Bulletin of the Tajik National University. Series of natural sciences. – Dushanbe, 2020. No. 4. – Pp. 130-146.
 3. Chopra K.L. Thin film solar cells / K.L. Chopra, R.D. Suchit // - M.: Publishing house "Mir", 1986. – Pp. 80-89.
 4. Schieber M. Theoretical and experimental sensitivity to X-rays of single and polycrystalline HgI₂ compared with different single-crystal detectors / M. Schieber, H. Hermon, A. Zuck, L. Melekhov, R. Shatunovsky, E. Meerson, H. Saado // Nuclear Instruments and Methods in Physics Research. 2001. – Pp. 41-46. [doi.org/10.1016/S0168-9002\(00\)00849-4](https://doi.org/10.1016/S0168-9002(00)00849-4).
 5. Stephane R. CdTe end CdZnTe detector in X ray computed tomography conditions / R.Stephane, G. Francis, G. Michel//Nuclear instruments and Mechods Research. 2000. –Pp.45-52. [doi.org/10.1016/S0168-9002\(99\)01198-5](https://doi.org/10.1016/S0168-9002(99)01198-5).
 6. Zaveryukhin Sh.A. Mirsagitov N.N. Volodarsky V.V. Film detectors of nuclear radiation from cadmium telluride / Zaveryukhin Sh.A. Mirsagitov N.N. Volodarsky V.V. // Letter to the ZhTF, 2003. - T.29, No. 22. – Pp. 80-85.
 7. Chopra K.L. Electrical phenomena in thin films / K.L. Chopra // – M.: Publishing house "Mir", 1982. – Pp. 260-264.
 8. Sultonov N. Preparation of polycrystalline CdTe films and study of their electrical characteristics / N.Sultonov, A.T.Akobirova, K.D. Azizov // Proceedings of the international conference on modern problems of physical and mathematical properties of condensed matter. – Khujand, 2002. – Pp. 60-65.
 9. Sultonov N. X-ray determination of sliding planes of amorphous-crystalline polymers / N.Sultonov, B.M. Ginzburg, R.B. Khamrokulov // Journal "Reports of the Academy of Sciences of the Republic of Tajikistan". – Dushanbe, 2003. – T.46. – No. 9. – Pp. 71-80
 10. Sultonov N. Structural changes in cadmium telluride single crystals upon irradiation with argon ions / N.S.Sultonov, A.T. Akobirova, R.B. Khamrokulov // Bulletin of the National University– Dushanbe, "SINO", 2006, – No. 2. . – Pp. 55-58.
 11. Sultonov N., Akobirova A.T., Khamrokulov R.B. Study of the structure of cadmium telluride films obtained on single-crystal substrates. Bulletin of the National University (scientific journal). - Dushanbe: "SINO", 2006. – No. 2. – Pp. 96-102.
 12. Sultonov N. Effect of the thickness of cadmium telluride films on their supramolecular structure / N. Sultonov, A.T. Akobirova, K. Azizov // Proceedings of the international conference “Modern problems of condensed matter physics and astrophysics”, dedicated to the 70th anniversary of Professor Sultonov N. - Dushanbe, 2010. – Pp.10-14.
 13. Sultonov N. Study of conductivity and photosensitivity of CdTe films on sapphire / N. Sultonov, A.T. Akobirova, K.Azizov// Proceedings of the international conference “Modern problems of condensed matter physics and astrophysics” dedicated to the 70th anniversary of Professor Sultonov N. - Dushanbe, 2010. – Pp.15-17.
 14. Sultonov N. Structure and electrical properties of CdTe films. / N. Sultonov, A.T. Akobirova, K. Azizov // Bulletin of the Tajik National University (scientific journal) (Special issue dedicated to the 20th anniversary of Independence of the Republic of Tajikistan), - Dushanbe: "SINO", 2011, - No. 6 (70). pp. 26-31. ISSN 2074-1847.
 15. Sultonov N. Influence of film structure on the mechanism of their conductivity / N. Sultonov, A.T. Akobirova, K. Azizov, U. Naimov, R.B. Khamrokulov // Proceedings of the international conference “Modern issues of molecular spectroscopy of condensed matter” dedicated to the 50th anniversary of the Department of Optics and Spectroscopy. – Dushanbe, 2011. – Pp. 39-41.
 16. Sultonov N. On the mechanism of current transfer in polycrystalline films of cadmium telluride / N. Sultonov, A.T. Akobirova, K. Azizov, R.B. Khamrokulov // News of the Academy of Sciences of the Republic of Tajikistan. – Dushanbe, 2011. – No. 3 (144). – Pp. 72-77.
 17. Sultonov N. Structure, morphology and electrical properties of cadmium telluride films / N. Sultonov, A.T. Akobirova, M.G. Lukashevich, V.I. Golovchuk // Proceedings of the international conference “Modern problems of condensed matter physics”, dedicated to the 90th anniversary of the Honored Worker of Science and Technology of the Republic of Tatarstan, Doctor of Physics and Mathematics. Sciences, Professor Narzulloev B.N. – Dushanbe, 2019. – Pp. 29-36.
 18. Naimov U.R. Study of the structure of CdTe films obtained by vacuum deposition in a quasi-closed volume / U.R. Naimov, N. Sultonov, A.T. Akobirova, R.B. Khamrokulov // Bulletin of Tambov State Technical University. – Tambov, 2019. – No. 4. –T.25. – Pp. 500-506

19. Sultonov N. Synthesis of polycrystalline cadmium telluride films on single-crystal substrates / N. Sultonov, A.T. Akobirova, B.A. Rakhmatov, R.B. Khamrokulov // Bulletin of the Tajik National University. Series of natural sciences. – Dushanbe, 2020, – No. 3. – Pp. 113-119.

STRUCTURAL CHANGES IN CdTe SINGLE CRYSTALS UPON IRRADIATION WITH HEAVY IONS OF INDERENT GASES

The paper presents the results of studies on the production of a polycrystalline or amorphous layer by irradiation of single-crystalline cadmium telluride with ions of inert gases differing in radii. The influence of the ion radius on the resistivity and structure of the (111) layer of a single crystal of cadmium telluride has been studied. The samples were irradiated with neon, argon and xenon ions with radii of 38, 71 and 108 picometers (10-12 m), respectively. The radiation dose for all ions was 250 Mrad. It has been shown that ions with a large radius have the strongest influence on structural transformations; at the same dose (250 Mrad), the drop in intensity of the (111) reflection under the influence of xenon ions is twice as high as that of neon ions. In accordance with X-ray data, as the radius of the ion increases, the resistivity increases, and the larger the radius of the ion, the greater the rate of increase ρ . Irradiation transforms a single crystal into a polycrystalline state with the formation of a large number of defects, which are sources of current carrier capture, which leads to an increase in ρ . The increasing growth of ρ with increasing ion radius is apparently due to the fact that ions with a larger radius have a significantly larger effective cross section for interaction with the crystal.

Key words: structure, irradiation, ion radius, conductivity, resistivity, single crystal, polycrystal, defect, charge carriers

Information about the authors: **Sultonov Nizom** – Tajik National University, Doctor of Physical and Mathematical Sciences, Professor of the Department of Physical Electronics. **Address:** 734025, Dushanbe, Republic of Tajikistan, Rudaki Avenue, 17. **Phone:** 988003588. **E-mail:** sultonov_nizom@mail.ru

Akobirova Aziza Toshpulatovna – Tajik National University, Ph.D., Associate Professor, Department of Physical Electronics, Tajik National University. **Address:** 734025, Dushanbe, Republic of Tajikistan, Rudaki Avenue, 17. **Phone:** (+992) 907917626. **E-mail:** aziza.akobirova@mail.ru

Naimov Umedjon Rozibekovich – Tajik National University, Ph.D., Art. teacher Department of Physical Electronics. **Address:** 734025, Dushanbe, Republic of Tajikistan, Rudaki Avenue, 17. **Phone:** (+992) 918697984. **E-mail:** umed87-88@mail.ru

Rahmatov Badurdin Amirulloevich – Tajik National University, Ph.D., Art. teacher Department of Physical Electronics. **Address:** 734025, Dushanbe, Republic of Tajikistan, Rudaki Avenue, 17. **Phone:** (+992) 981006951. **E-mail:** badriddin.rakhmatov.91@mail.ru

Hamrokulov Rajabmurod Badriddinovich – Tajik National University, Ph.D., Associate Professor of the Department of Physical Electronics. **Address:** 734025, Dushanbe, Republic of Tajikistan, Rudaki Avenue, 17. **Phone:** (+992)904160775. **E-mail:** h.rajabmurod@mail.ru.

Article received 20.09.2023

Approved after review 16.12.2023

Accepted for publication 29.02.2024

CHEMISTRY

doi.org/10.62965/tnu.sns.2024.2.11

UDC: 661.48:66.011.014.06.08:54.03.05.06.08

STUDY OF THE TECHNOLOGY FOR OBTAINING A MIXTURE OF SILICOFLUORIDE AND SODIUM FLUORIDE FROM A BY-PRODUCT OF HYDROFLUORIC ACID PRODUCTION

Shokarimov S.M., Naimov N.A., Ruziev J.R., Rafiev R.S.

Aslonov A.A., Safiev H.

Taking into account the importance of the industrial production sphere in raising the socio-economic status of the population and creating additional jobs, accelerated industrialisation of the country has been declared a priority strategic direction in the Republic of Tajikistan [1].

It is known that hydrofluoric acid is produced mainly by sulphuric acid decomposition of fluorite in a reaction furnace, whereby as a result of absorption of silicon tetrafluoride released during sulphuric acid decomposition of fluorite concentrate containing a small amount of residual silica [2], a by-product – fluorosilicic acid (FSA) is formed [3].

In addition, with the growing demand for fertiliser and the consequent start-up of more and more phosphoric acid production facilities, the need to utilise by-products (FSA) is increasing [4-8]. Currently, FSA is used either for fluoridation of drinking water or for the production of low bulk density aluminium fluoride, cryolite, silicon tetrafluoride, sodium fluoride and fluorosilicates [9-15]. Considering that phosphoric acid production exceeds 64 million tonnes per year [16], more than 2.2 million tonnes of FSA need to be utilised.

Currently, an enterprise for the production of hydrofluoric and sulphuric acid, as well as fluoride salts (Talco Chemical LLC) operates in the territory of the Republic of Tajikistan [17]. At maximum capacity, approximately 4 thousand tonnes of FSA and hydrofluoric acid mixture is formed as a by-product per year, the storage of which requires large

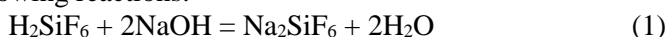
Thus, recycling of production waste from the chemical industry, and in particular, the production of fluoride salts, using local resources, from the point of view of economics and ecology is an urgent task.

The simplest way to process a mixture of FSA and hydrofluoric acid is neutralisation using caustic and soda ash, resulting in the formation of sodium fluorosilicate (SFS) and sodium fluoride [18-22].

The purpose of the present work is utilisation of by-product of hydrofluoric acid production – mixture of FSA and hydrofluoric acid using sodium hydroxide and sodium chloride (local mineral raw materials) to obtain fluoride salts – SFS and sodium fluoride.

Specialists of the State Institution «Research Institute of Metallurgy» JSC «Tajik Aluminum Company» carried out laboratory studies on utilisation of acid mixture in order to extract fluorine-containing components. The utilisation process was investigated in two variants, using sodium hydroxide and sodium chloride, depending on the temperature and duration of the process, as well as the concentration of sodium hydroxide and sodium chloride [23].

When a mixture of FSA and hydrofluoric acid interacts with sodium hydroxide, a mixture of SFS and sodium fluoride is formed by the following reactions:



The results of the conducted studies to determine the dependence of the yield of SFS and sodium fluoride on temperature, process duration and concentration of sodium hydroxide are presented in Table 1.

Table 1. The dependence of the yield of SFS and sodium fluoride on temperature, process duration and sodium hydroxide concentration

№	Process parameters			Yield of components, %
	Temperature, °C	Duration, min.	Concentration of NaOH, %	Mixtures of Na ₂ SiF ₆ and NaF
1	25	15	25	91,2
2	65	15	25	89,8
3	75	15	25	88,1
4	85	15	25	87,7
5	95	15	25	87,5
6	25	5	25	85,6
7	25	10	25	86,3
8	25	20	25	89,1
9	25	25	25	88,6
10	25	30	25	87,3
11	25	15	15	76,1
12	25	15	20	85,2
13	25	15	30	93,3
14	25	15	35	95,1
15	25	15	40	96,3
16	25	15	45	97,5

As can be seen from Table 1, the yield of SFS and sodium fluoride decreases as the temperature rises above 65 °C, which is associated with an increase in the solubility of these components, as well as with the evaporation of the acid mixture. Proceeding from the fact that the interaction of the mixture of FSA and hydrofluoric acid with sodium hydroxide is an exothermic reaction with temperature increase up to 65-75 °C, the process is started at 25 °C. It was found that the solubility of fluoride salts increases when the duration of treatment is increased above 20 min, while the yield of the mixture of SFS and sodium fluoride decreases to 87.3%. The influence of sodium hydroxide concentration on the yield of the specified fluoride salt mixture has been studied. It was determined that with increasing the concentration of sodium hydroxide more than 25% there is an increase in the yield of fluoride salts up to 97.5%, but due to the formation of thick and sticky pulp difficult pumping and filtering processes. Thus, the optimum parameters of the process are the following: temperature 25 °C, duration of the process up to 20 minutes, concentration of sodium hydroxide 25%. Thus, the degree of extraction of a mixture of fluoride salts makes 91,2 %. It should be noted that dissolved mixtures of fluoride salts are not lost, as the filtrate is used back in the preparation of sodium hydroxide solution.

Chemical analysis of the investigated sample obtained by processing the mixture of FSA and hydrofluoric acid with sodium hydroxide showed that the mixture of fluoride salts contained 67.8% SFS (Na₂SiF₆) and 31.5% sodium fluoride (NaF).

X-ray phase analysis (XRD) was carried out to confirm the results of the research, chemical analysis, as well as to determine the mineralogical composition of the fluoride salt mixture obtained during the treatment of the acid mixture with sodium hydroxide (Fig.1).

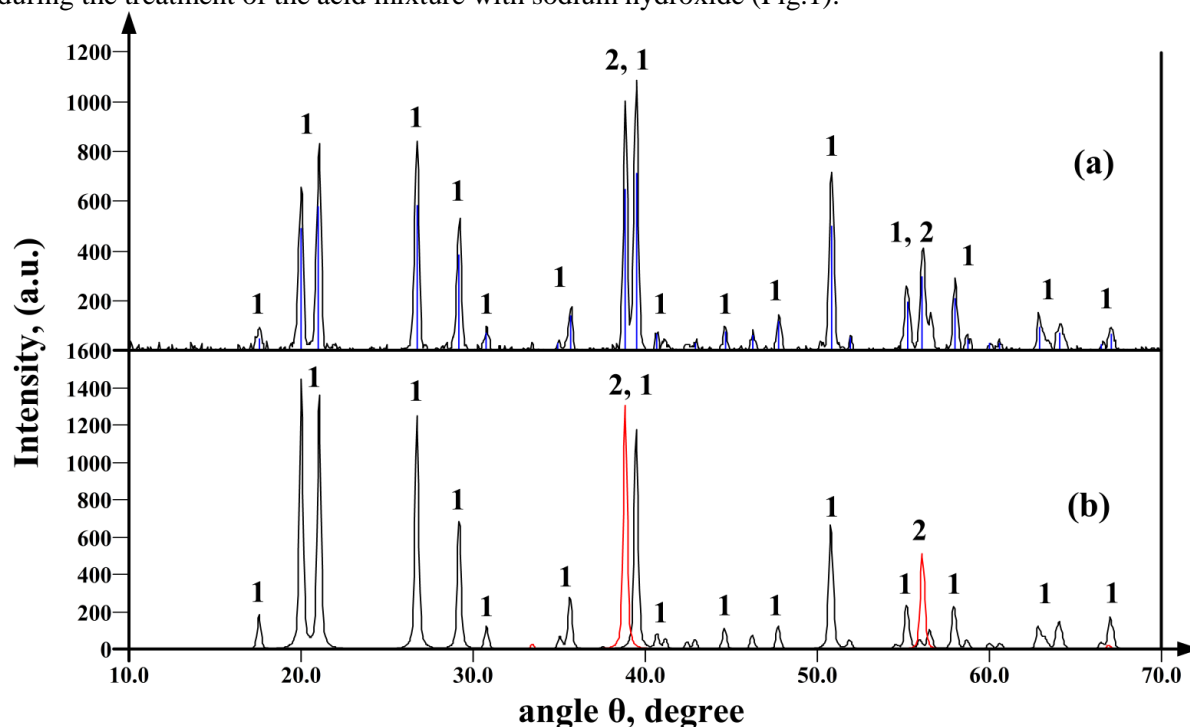


Fig. 1. X-ray of a mixture of fluoride salts (a) and a standard sample (b): 1-malladrite (Na_2SiF_6), 2-villiaumite (NaF)

Table 2 shows the XRD data of the investigated sample of fluoride salts, by which it is determined which mineral corresponds to the peaks of the X-ray diagram (Fig. 1).

Table 2. Indicators of X-ray examination of a mixture of fluoride salts (A-malladrite, B-villiaumite)

2-Theta	D-Spacing	Intensity	Width	Confidence	Matches
1	2	3	4	5	6
17.584	5.0396	51	0.188	99.9%	A
20.034	4.4285	492	0.192	100%	A
1	2	3	4	5	6
21.077	4.2116	580	0.189	100%	A
26.770	3.3275	585	0.184	100%	A
29.225	3.0532	383	0.190	100%	A
30.823	2.8985	73	0.195	100%	A
34.977	2.5632	28	0.183	98.3%	A
35.699	2.5130	140	0.198	100%	A

38.871	2.3149	649	0.172	100%	B
39.506	2.2792	713	0.180	100%	A
40.707	2.2147	68	0.170	100%	A
42.967	2.1032	32	0.170	99.5%	A
44.668	2.0270	75	0.193	100%	A
46.301	1.9593	61	0.195	100%	A
47.821	1.9005	117	0.193	100%	A
50.868	1.7936	502	0.189	100%	A
51.978	1.7578	51	0.176	100%	A
55.264	1.6608	198	0.221	100%	A
56.156	1.6366	299	0.195	100%	B
58.048	1.5876	208	0.188	100%	A
58.782	1.5695	42	0.218	100%	A
60.064	1.5391	32	0.177	99.8%	A
60.612	1.5265	28	0.173	99.5%	A
62.936	1.4756	95	0.195	100%	A
64.086	1.4518	70	0.254	100%	A
66.561	1.4037	27	0.158	99.3%	A
67.108	1.3936	67	0.195	100%	A

As can be seen from the X-ray diagram (Fig. 1) and Table 2, the peaks of the obtained mixture of fluoride salts (upper graph), coincide with the peaks of the X-ray diagram of the reference sample (lower graph), which indicates the presence of the minerals malladrite and villiaumite in the studied sample.

A study on acid mixture recycling using sodium chloride was carried out similarly to the use of sodium hydroxide:



From the reaction equations (3 and 4), it can be seen that the processing of acid mixture using sodium chloride, produces mixtures of SFS, sodium fluoride and hydrochloric acid. The results of the conducted research are given in Table 3.

Table 3. Dependence of the yield of SFS and sodium fluoride on temperature, duration of the process and concentration of sodium chloride

№	Process parameters			Yield of components, %
	Temperature, °C	Duration, min.	Concentration of NaCl, %	Mixtures of Na ₂ SiF ₆ and NaF

1	2	3	4	5
1	25	5	25	78,58
2	35	5	25	72,77
3	50	5	25	73,81
4	65	5	25	73,52
5	80	5	25	73,66
6	25	10	25	76,79
7	25	15	25	73,06
8	25	20	25	71,22
9	25	25	25	71,37
10	25	30	25	71,42
11	25	5	5	67,58
1	2	3	4	5
12	25	5	10	68,72
13	25	5	15	70,86
14	25	5	20	73,10
15	25	5	25	78,58

Table 3 shows that with increasing temperature above 25 °C and process duration of more than 5 min, the degree of fluoride salts extraction decreases, which is probably associated with an increase in their solubility in hydrochloric acid. It is important to note that as the concentration of sodium chloride decreases and the formation of dilute hydrochloric acid increases the solubility of fluoride salts, which contributes to a decrease in the degree of their extraction - on this basis, it is advisable to use a concentrated solution of table salt.

Thus, the optimal parameters of the process of acid mixture processing using sodium chloride are: temperature 20-25 °C, duration 5-10 min, concentration of sodium chloride 20-25 %. Thus, the maximum degree of extraction of a mixture of fluoride salts makes 78,58%.

However, chemical analysis of the investigated sample obtained by processing the mixture of FSA and hydrofluoric acid with sodium chloride showed that the composition of the mixture of fluoride salts contains 95.8% of SFS (Na_2SiF_6) and 3.5% of sodium fluoride (NaF). Apparently, this situation is associated with good solubility of sodium fluoride in the formed hydrochloric acid, which determines the low content of sodium fluoride in the mixture of fluoride salts. To confirm the above chemical analyses, XRD of fluoride salts was carried out (Fig. 2.).

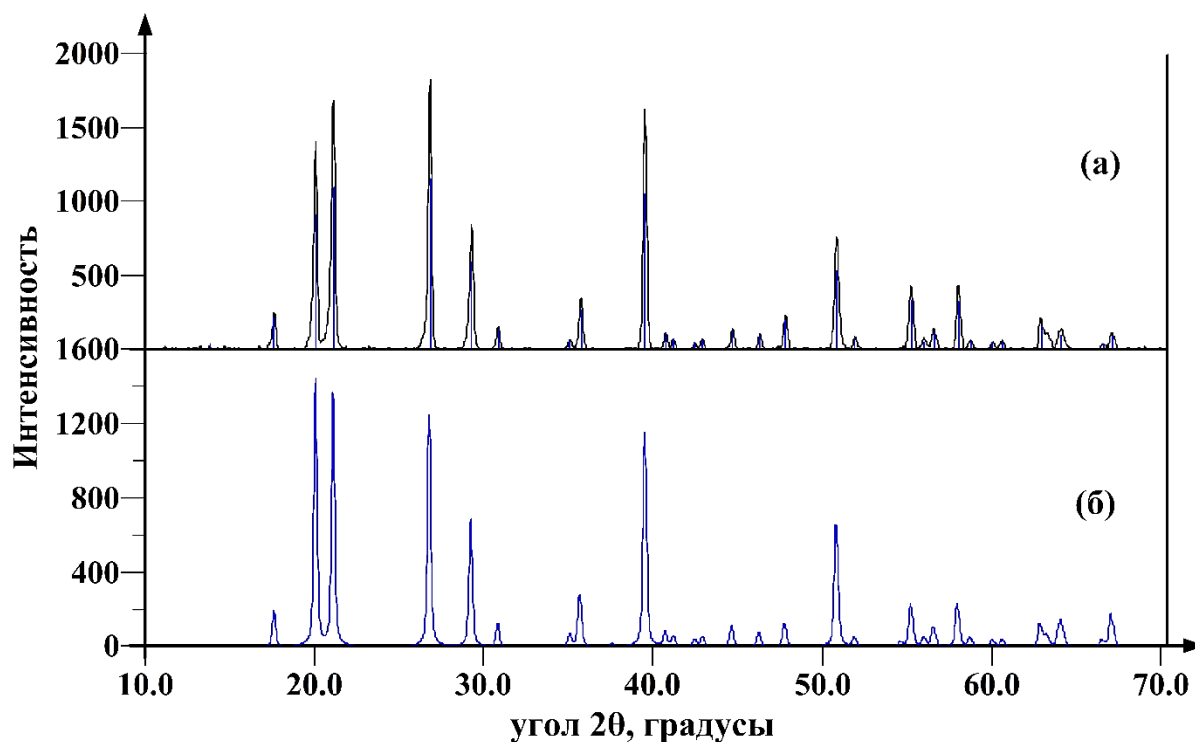


Fig. 2. X-ray diffraction of a mixture of fluoride salts (a) and a standard sample of the mineral malladrite (b)

Table 4 shows the XRD data of the investigated sample of fluoride salts, by which it is determined to which mineral the peaks of the X-ray diagram correspond (Fig. 2).

Table 4. Indicators of XRD of a mixture of fluoride salts (A-malladrite)

2-Theta	D-Spacing	Intensity	Width	Confidence	Matches
1	2	3	4	5	6
17.607	5.0330	213	0.169	100%	A
20.046	4.4257	911	0.159	100%	A
21.101	4.2068	1096	0.162	100%	A
26.819	3.3215	1153	0.155	100%	A
29.268	3.0489	590	0.165	100%	A
1	2	3	4	5	6
30.842	2.8968	133	0.171	100%	A
35.092	2.5551	56	0.179	100%	A
35.741	2.5101	262	0.171	100%	A
39.518	2.2785	1054	0.159	100%	A
40.751	2.2124	103	0.168	100%	A
41.235	2.1875	74	0.160	100%	A

42.924	2.1052	64	0.167	100%	A
44.703	2.0255	123	0.177	100%	A
46.321	1.9585	98	0.171	100%	A
47.834	1.9000	199	0.178	100%	A
50.862	1.7938	536	0.174	100%	A
51.937	1.7591	74	0.168	100%	A
55.254	1.6611	334	0.184	100%	A
56.027	1.6400	47	0.242	100%	A
56.595	1.6249	107	0.192	100%	A
58.053	1.5875	325	0.176	100%	A
58.774	1.5697	58	0.206	100%	A
60.059	1.5392	47	0.174	100%	A
60.629	1.5261	46	0.182	100%	A
62.925	1.4758	154	0.171	100%	A
64.101	1.4515	93	0.212	100%	A
66.580	1.4034	36	0.170	99.9%	A
67.132	1.3932	86	0.193	100%	A

As can be seen from the X-ray diagram (Fig. 2) and Table 4, the peaks of the obtained mixture of fluoride salts (upper graph), coincide with the peaks of the X-ray diagram of the reference sample (lower graph), which indicates the presence of the mineral malladrite in the studied sample, as the content of villiaumite in the composition of the analysed sample is less than 5%.

In order to separate the remaining dissolved sodium fluoride from hydrochloric acid, the mixture was evaporated in natural conditions (in the open air), since at temperatures above 60 °C sodium fluoride interacts with hydrochloric acid with the release of gaseous fluoride hydrogens and obtaining sodium chloride in the residue. The obtained salt after natural evaporation was also subjected to XRD (Fig. 3.).

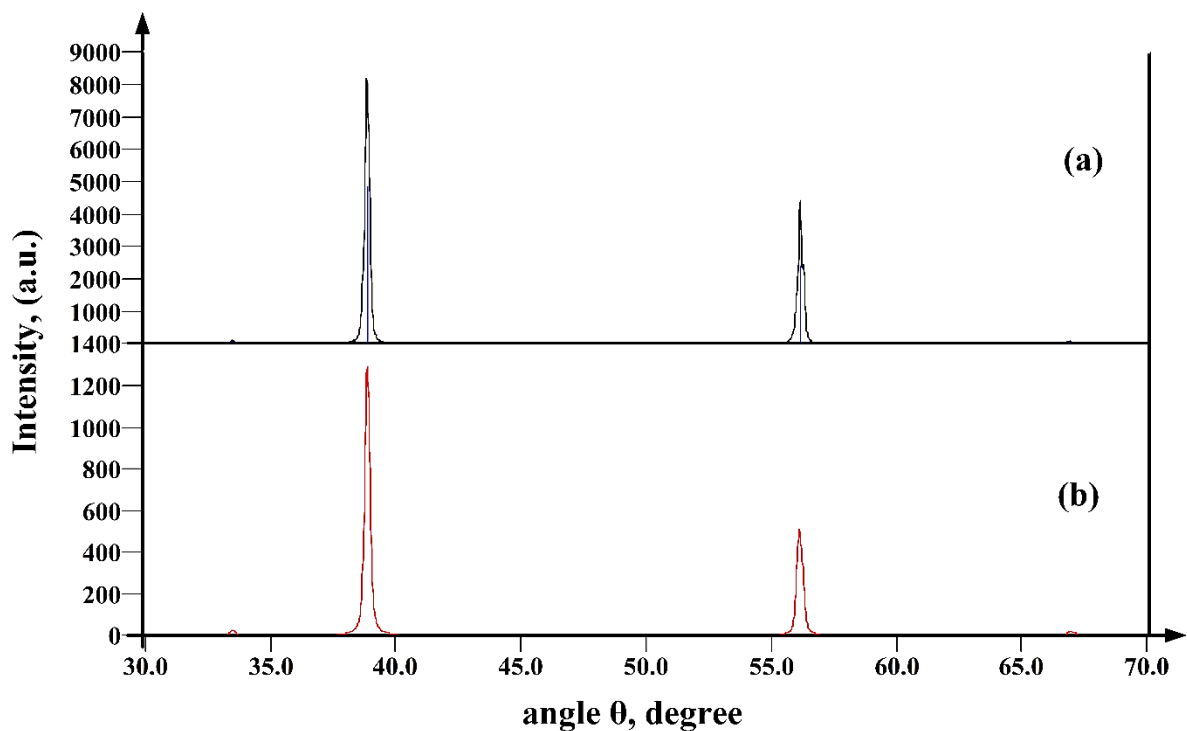


Fig. 3. XRD of the evaporated solution of hydrochloric acid and sodium fluoride mixture (a) and a standard sample of villiaumite mineral (b)

Also, in table 5 the data of XRD of the investigated sample are given, by which it is determined what minerals correspond to the peaks of X-ray diagram (fig. 3).

Table 5. Indices of radiographic study of the evaporated salt of a mixture of hydrochloric acid and sodium fluoride (A-villiaumite)

2-Theta	D-Spacing	Intensity	Width	Confidence	Matches
33.491	2.6735	89	0.169	100%	A
38.864	2.3153	4857	0.155	100%	A
56.172	1.6361	2408	0.164	100%	A
66.940	1.3967	51	0.190	100%	A

According to the performed XRD (Fig. 3.) and Table 5, the peaks of the analysed salt correspond only to the mineral villiaumite, which confirms the dissolution of sodium fluoride in hydrochloric acid.

It should be noted that mixtures of hydrochloric acid and sodium fluoride can be directly applied as an acid composition to treat the bottomhole zone of hot water reservoirs, or can be used back in the processing of a mixture of FSA and hydrofluoric acid to produce of SFS.

On the basis of laboratory studies, the basic technological scheme for obtaining a mixture of SFS and sodium fluoride from a mixture of FSA and hydrofluoric acid by two variants was developed (Fig. 2).

According to the basic technological scheme, to the prepared 20% solution of sodium hydroxide or 25% solution of sodium chloride a mixture of FSA and hydrofluoric acid is added according to the stoichiometric calculation. The resulting pulp is filtered with a single washing. The water can be reused in the preparation of sodium chloride or sodium hydroxide solutions. The filtered salt mixture is then dried – the resulting product can be directly used in the electrolysis industry to produce alumina-silicon alloy (silumin) and electrolyte melt, as well as for fluoridation of drinking water and in the production of acid-resistant cements.

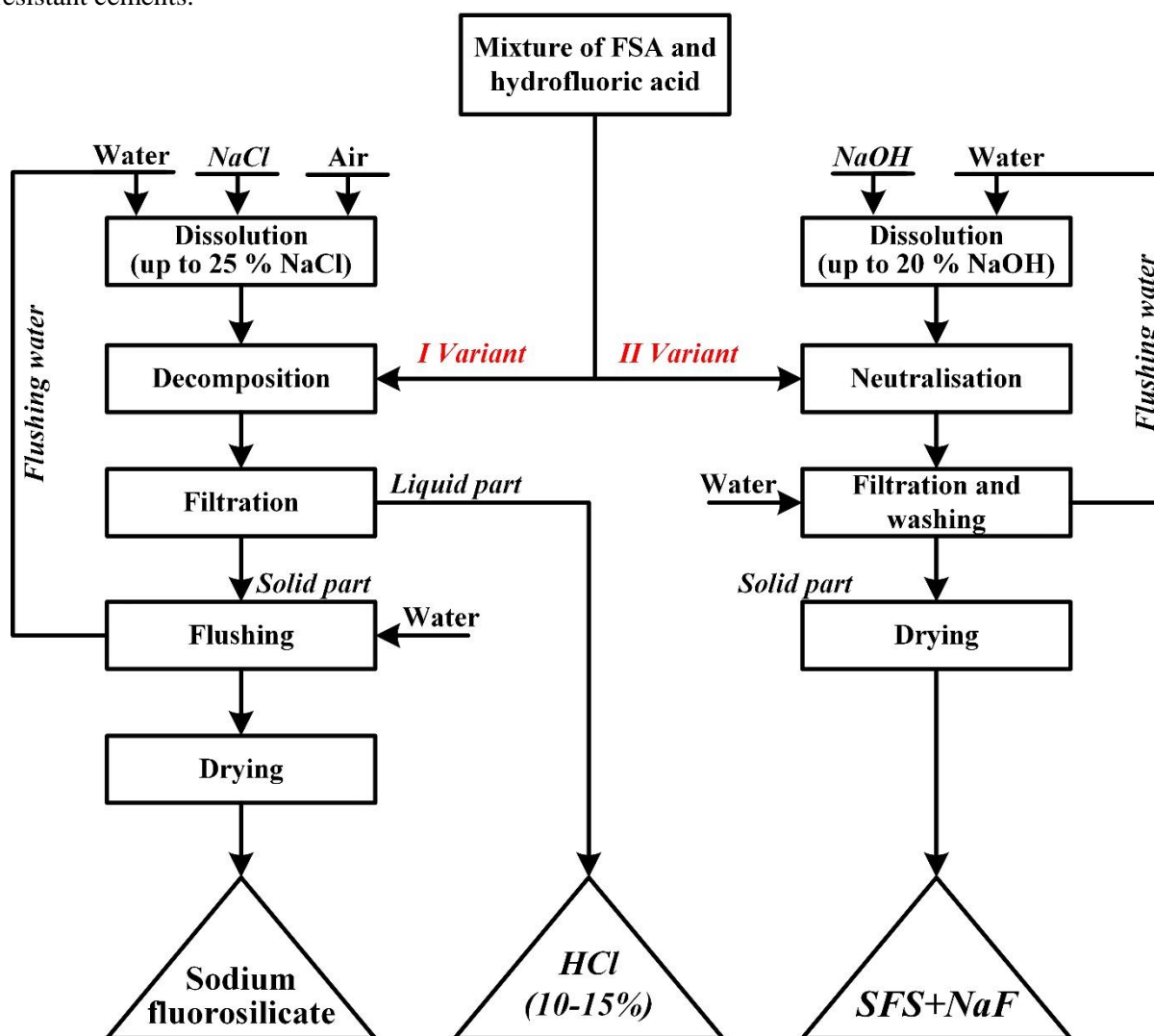


Fig. 2 – Basic technological scheme for the production of a mixture of SFS and sodium fluoride from a mixture of FSA and hydrofluoric acid using chloride and sodium hydroxide.

As it was noted, the application of sodium chloride produces a solution of 10-15% hydrochloric acid, which can be used as a composition for treatment of bottomhole zone of different reservoirs or evaporated in vivo to obtain sodium fluoride in the precipitate, as well as reused in the processing of a mixture of FSA and hydrofluoric acid to obtain SFS.

In the process of laboratory research and corresponding stoichiometric calculations it has been established that when treating 100 kg of acid mixture consisting of 33,36% FSA and 21,44% hydrofluoric acid with sodium hydroxide the following components are consumed: sodium hydroxide – 42,99 kg (including 14,27 kg or 33,19% for formation of SFS; 28,72 kg or 66,80% for formation of sodium fluoride), water consumption – 171,96 kg (or 214,95 kg of 20% NaOH solution). At the same time, 33.53 kg (52.64%)

of Na_2SiF_6 and 30.16 kg (47.35%) of NaF (totalling 63.69 kg of the mixture of the said salts) and 200 kg of water are formed. It should be taken into account that under these conditions up to 4 % of sodium fluoride and up to 1.65 per cent of SFS remain dissolved in water.

As a result of the conducted research, it has been established that the technology of neutralisation of the mixture of FSA and hydrofluoric acid in order to obtain a mixture of fluoride salts according to both variants is simple in implementation and environmentally safe, as well as economically efficient due to the use of local mineral raw materials and low.

**REVIEWER: Sherov M.,
Candidate of Chemical Sciences
Assistant Professor**

REFERENCES

1. Eshonkulova L. The fourth goal–industrialization. http://www.narodnaya.tj/index.php?option=com_content&view=article&id=12647:2020-12-24-05-19-35&catid=53:ekonomika&Itemid=58. 24.12.2020.
2. Pozin M. E. Technology of mineral salts (fertilizers, pesticides, industrial salts, oxides and acids): monograph / M. E. Pozin // Part 2; 4th ed. - Leningrad: Chemistry, 1974. – 768 p.
3. Production of HF from H_2SiF_6 / Thomas Dahlke, Olivier Ruffiner, Roderick Cant // *Procedia Engineering*, Volume 138, 2016. – Pp.231-239 <https://doi.org/10.1016/j.proeng.2016.02.080>.
4. Technical Report No. 26, Mineral Fertilizer Production and the environment: Part 1: The fertilizer Industry's Manufacturing processes and environmental issues, United Nations Publication.
5. Zaitsev V.A., Production of fluoride compounds in the processing of phosphate raw materials / V.A. Zaitsev., A.A. Novikov, V.I. Rodin // *M. Chemistry*, 1972. – 246 p.
6. Production of Fluorosilicic Acid from Phosphoric Acid Slurry of a Fertilizer Manufacturing Plant / Se-Won Kim, Woo-Kyun Moon, Hung-Suck Park // *Journal of the Korea Academia-Industrial cooperation Society* 13(2). February 2012. DOI:10.5762/KAIS.2012.13.2.926
7. Yuldashev Kh., Zhuraev A., Rakhmonov O. Methods of obtaining sodium hexafluorosilicate from waste gases of phosphorus fertilizers production (review) / Kh. Yuldashev, A. Zhuraev, O. Rakhmonov // *Universum: technical sciences: electronic scientific journal*. 2020. No8 (77). URL:<https://7universum.com/ru/tech/archive/item/10648>
8. Sharipov T.V. Processing of Karatau phosphorites into sodium hexafluorosilicate: / T.V. Sharipov // *dis. candidate of technical sciences: 05.17.01 / Bashkir State University*. - Ufa, 2014. – 178 p.
9. Research and development of low-waste production of mineral salts [Text]. Issue 57 / UNICHIM; resp. ed. K. V. Tkachev - Sverdlovsk: UNIKhim, 1984. – 144 p.
10. Dreveton, A., Manufacture of Aluminum Fluoride of High Density and Anhydrous Hydrofluoric Acid from Fluosilicic Acid/A. Dreveton//*Procedia Engineering* 46 (2012). – Pp. 255-265.
11. Sarawade P.B. et al, Recovery of a high surface area mesoporous silica from waste hexafluorosilicic acid (H_2SiF_6) from fertilizer industry / P.B. Sarawade // *Journal of hazardous materials* 173 (2010). – Pp.576-580.
12. Tumanov V.V. The problem of processing fluorosilicic acid into basic fluorine-containing products / V.V. Tumanov, S.V. Ostrovsky, A.G. Starostin // *Bulletin of the Perm National Research Polytechnic University. Chemical technology and biotechnology*. - 2017. - No. 1. – Pp.138-148.
13. Improving the quality of sodium fluorosilicate / T.I. Myzovskaya, S.R. Masakbaeva // *Science and Technology of Kazakhstan*. No. 4, 2020. <https://doi.org/10.48081/UGRM6297>
14. Shayakhmetov D.I. Processing of fluorosilicic acid with obtaining sodium fluoride / D.I. Shayakhmetov, A.G. Mustafin, T.V. Sharipov // *Bashkir Chemical Journal* 2013. Vol. 20. No. 2.
15. Mamchenkov E.A., Prokofiev V.Yu. Obtaining sodium silicate from modified silica gel, a by-product of aluminum fluoride. *Proceedings of universities / E.A. Mamchenkov, V.Yu Prokofiev//Chemistry and chemical technology*. 2019. Vol. 62. 3. – Pp.89-93.
16. International Fertilizer Industry Association, Production and International Trade figures for phosphoric acid and phosphate rock, 2020
17. Igor Sattarov. National treasure of Tajikistan. To the 45th anniversary of the Tajik Aluminum Company / Igor Sattarov // March 31, 2020. <https://asiaplustj.info/ru/news/tajikistan/society/20200331/natsionalnoe-dostoyanie-tadzhikistana-k-45-letiyu-tadzhikskoi-alyuminievoi-kompanii>.
18. Arianpour, F. Characterization and Properties of Sodium Hexa-Fluorosilicate and its Potential Application in the Production of Sodium Fluoride / F.Arianpour, A.Ç. Arianpour, B. Aali// *Silicon* (2020). doi.org/10.1007/s12633-020-00755-0
19. Marwan M. Batiha, Mohammad Al-Harashseh. The effect of reaction conditions on the precipitation of sodium hexafluorosilicate produced from waste hexafluorosilicic acid / M. Marwan.Batiha, Mohammad Al-Harashseh. // *Polish Journal of Chemical Technology*, 2011, 13, 2. – Pp.23-28.
20. Patent CN (China) No. 102923713A, C 01B 33/10. Method for sanitary production of sodium fluosilicate / Liu Hai; - No. 201210446052.2; application 09.11.2012; publ. 13.02.2013. - 4 p.
21. Sharipov T.V. RF patent No. 2604236C1, C01B 33/10. Method of obtaining sodium silicofluoride / T.V. Sharipov, A.G. Mustafin, G.S. Kinzyabulov and E.R. Safaryanov // No. 2015136833/05; application 08/28/2015; publ. 10.12.2016, Bul. No. 34. – 7 p.

22. Takeshi Fujiwara. JP patent (Japan) No. 2015224162A, C 01B 33/10, C 02F 1/58, C 02F 1/60. Production method of sodium silicofluoride, and waste liquid treatment system / Takeshi Fujiwara, Yuto Shimizu, Takao Nakaseko, Masato Morita, Kenichi Sakurai, Masaru Yamazaki // –No. 2014110234 (P2014-110234) application. 05/28/2014; publ.12/14/2015.-8 p. URL: <https://patents.google.com/patent/JP2015224162A/en?q=sodium+silicofluoride&oq=sodium+silicofluoride>

23. Rajabzoda N.H. Small patent of the Republic of Tajikistan No. TJ 1319. Method for obtaining a mixture of silicofluoride and sodium fluoride / N.H. Rajabzoda, H. Safiev, A. MirpochoevKh, A. Murodiyov, N.A. Naimov, J.R. Ruziev, S.M. Shokarimov, Sh. AhmadshoevI, R.S. Makhkambaev N.P. Mukhamediev // IPC C01B33/10. No. 2201672; declaration 28.04.2022; registered 21.11.2022, Bul.189, 2022. – 3 p.

STUDY OF THE TECHNOLOGY FOR OBTAINING A MIXTURE OF SILICOFLUORIDE AND SODIUM FLUORIDE FROM A BY-PRODUCT OF HYDROFLUORIC ACID PRODUCTION

The article presents the results of research on the technology of processing and utilization of by-product of hydrofluoric acid production – a mixture of fluorosilicic and hydrofluoric acids using sodium hydroxide and sodium chloride (local mineral raw materials) to obtain fluoride salts – a mixture of silicofluoride and sodium fluoride. As a result of laboratory studies, the optimal parameters of the process of acid mixture processing using sodium hydroxide and sodium chloride to obtain a mixture of SSF and sodium fluoride were determined: temperature – 20-25 °C, duration – 10-20 min, concentration of sodium hydroxide and sodium chloride – 20-25%; in this case the maximum degree of extraction of SSF and sodium fluoride is achieved. The product obtained when sodium hydroxide was used under these optimum conditions was chemically analyzed and found to consist of 67.8% Na₂SiF₆ and 31.5% NaF. In the case of sodium chloride, the resulting mixture contains 95.8% of Na₂SiF₆ and 3.5% of NaF. To confirm the reliability of the results of chemical analysis and the found optimal parameters, as well as to determine the mineralogical composition of the obtained fluoride salts, X-ray phase analysis was carried out using an upgraded Dron-2 unit. The obtained product can be used in electrolysis production for obtaining aluminosilicon alloy (silumin) and electrolyte melt, as well as for fluoridation of drinking water and in the production of acid-resistant cements. On the basis of the conducted laboratory studies, the basic technological scheme of processing of the mixture of FSA and hydrofluoric acid with the use of sodium hydroxide and sodium chloride was developed.

Keywords: fluorosilicic acid, hydrofluoric acid, sodium hydroxide, sodium chloride, fluoride salts, sodium silicofluoride, sodium fluoride, utilization.

Information about the authors: Shokarimov Sirojiddin Mirzoevich – Tajik National University, Ph.D student of Department of inorganic substances. **Address** 734025, Republic of Tajikistan, Dushanbe, Rudaki Avenue, 17. **Phone:** (+992) 901-10-16-63. **E-mail:** sirojshokarimov@mail.ru.

Naimov Nosir Abdurahmonovich – Tajik National University, candidate of technical sciences, doctoral student of the Department of Applied Chemistry, Faculty of Chemistry, **Address:** 734025, Republic of Tajikistan, Dushanbe, Rudaki Avenue, 17. **Phone:** (+992) 901-11-65-12. **E-mail:** nosser2016@outlook.com.

Ruziev Jura Rahimnazarovich – Tajik National University, Doctor of Technical Sciences, Prof., Professor of Applied Chemistry Department, Faculty of Chemistry. **Address:** 734025, Republic of Tajikistan, Dushanbe, Rudaki Avenue, 17. **Phone:** (+992) 917-36-15-13. **E-mail:** gyra71@mail.ru.

Rafiev Rustam Safaralievich – Tajik National University, Candidate of Chemical Sciences, Head of the Department of Applied Chemistry, Faculty of Chemistry. **Address:** 734025, Republic of Tajikistan, Dushanbe, Rudaki Avenue, 17. **Phone:** (+992) 939-06-69-59. **E-mail:** rustam.rafiiev@mail.ru.

Aslonov Azim Abdulhusaynovich – Tajik National University, Ph.D student of inorganic substances. **Address:** 734025, Republic of Tajikistan, Dushanbe, Rudaki Avenue, 17. **Telephone:** (+992) 935-32-97-97. **E-mail:** aslonov04061997@mail.ru.

Safiev Haidar – State Institution «Research Institute of Metallurgy» JSC «Tajik Aluminum Company», Doctor of Chemical Sciences, Professor, Academician of the National Academy of Sciences of Tajikistan.

Article received 16.11.2023

Approved after review 19.03.2024

Accepted for publication 11.04.2024

COMPLEXATION OF SILVER (I) C 2-ETHYLIMIDAZOLE

Sodatdinova A.S., Akimbekova Kh.A., Usacheva T.R.,

Safarmamadodzoda S.M.

The five-membered cycle of imidazole is a component of histidine, a structural fragment of histamine, purine bases, and a number of drugs [1,2]. Imidazole derivatives are used to treat diseases of the gastrointestinal tract and bladder, peripheral vascular patency, myocardial ischemia, heart failure, glaucoma, and thyroid disease [3,4,2]. 2-methylimidazole is widely used in the production of ionic liquids [5,6]. Benzimidazole derivatives are known as inhibitors of selective corrosion of brass in aqueous solutions [7].

Acid-base characteristics of organic compounds are very important physicochemical parameters and are widely used in the calculation of equilibrium constants of complexation reactions [8]. The paper [9] presents data on ionization constants (pKa) of some imidazole derivatives in aqueous solutions: imidazole 7.05; 2-phenylimidazole 6.48; 2-aminobenzimidazole 6,11; benzimidazole 5.53; 2-Phenylbenzimidazole 5,23. The authors [10,11] showed that the introduction of a mercaptogroup into the imidazole molecule leads to a sharp weakening of its basic properties (pK a for 2-mercaptoimidazole is 2.97, and 1-methyl-2-mercaptoimidazole is 2.11).

Imidazole and its derivatives have pronounced complexing properties and form coordination compounds with mild, intermediate, and less often hard acids [12-14]. In [15], on the basis of synthesized malates of cobalt (II), copper (II) and zinc MMalat·3H₂O at pH 6.5-8.7, imidazol malates of the composition MIm_xMalat·nH₂O (x = 1.3; n = 0-3) were obtained. Chemical analysis, analysis of IR spectra of salts in comparison with spectra of ligands, as well as analysis of the process of thermal decomposition of salts were carried out, which confirmed the formation of mixed ligand salts. Photo- and spectrophotometrically in an aqueous solution at pH 6.5-7.3 for Co²⁺, Cu²⁺, the compositions of monoligand complexes [MIm 2]₂⁺, [MMalat] were determined, the stability of biligand imidazol malate complexes [MImMalat], [MIm 2Malat] was determined, and electron absorption spectra of solutions containing a complexing agent and ligands were obtained. [16,17] presents data on the complexation of silver(I) with imidazole derivatives in water and aqueous organic solvents. In [18], the complexation of H[AuCl₄] with 2-methylimidazole at 288-318K was studied by the potentiometric method. It is shown that when there is an excess of 2-methylimidazole in the solution, three chloride ions from the composition of H[AuCl₄] are replaced. The values of the general stability constants at different temperatures are calculated. It has been established that as the temperature increases, the values of the total stability constants increase.

In [19] the process of complexation of silver(I) with heterocyclic amines was investigated. In particular, it has been shown that silver(I) reacts with imidazole in a stepwise manner. The stability of the saturated complex form of AgL₂⁺ was determined, which was lgβ₂=6.93. The authors [11, 20, 21] investigated the process of complexation of silver(I) with 2-mercaptoimidazole in water, hydroalcoholic and water-DMSO solvents. The step-by-step nature of the complexation process has been proved and the stability constants of sequentially formed complex forms have been determined: lgβ₁=6.84±0.03; lgβ₂ =10,56±0,03; lgβ₃ =12,27±0,04. It has been shown that the introduction of a mercapto group into the imidazole molecule leads to an increase in the stability of its coordination compounds with silver (I).

The aim of this work was to study the protolytic equilibria of 2-ethylimidazole (EM), the complexation of Ag(I) with 2-ethylimidazole and to establish the effect of the ethyl group on the acid-base and complexing characteristics of imidazole.

EXPERIMENTAL PART

To study the complexation of silver(I) with 2-ethylimidazole, a galvanic cell with transfer was used, where a plate of pure silver was used as an indicator electrode, and a silver chloride electrode served as a reference electrode. The initial concentration of AgNO_3 was $1 \cdot 10^{-4}$ mol/L, the initial concentration of 2-ethylimidazole was $1 \cdot 10^{-2}$ mol/l. The potential of the galvanic system was measured using a RNS-25 pH meter. The equilibrium value of the potential on the indicator electrode was set for 5-10 min. The temperature in the cell was kept constant using a water thermostat of 298.1 ± 0.1 K. Equilibrium concentrations of silver(I) and 2-ethylimidazole formed complex forms and stability constants were determined according to the KEV program [22]. Acid-base titration of 2-ethylimidazole was carried out using a technique similar to that described in the paper [21].

OUTCOMES

It is known that nitrogen atoms in the composition of heterocyclic compounds have a great influence on their acid-base and complexing properties. The ability of a proton to attach also depends on the structure and nature of the functional groups that make up the heterocyclic compounds. Analysis of the literature data showed that the introduction of substituents into the imidazole molecule has a significant effect on the acid-base properties of imidazoles, which, as a result, affects the complexing properties of these compounds [18, 21, 23]. In this regard, the acid-base equilibria of 2-ethylimidazole were studied in this work (Fig. 1, Table 1).

Figure 1 shows the pH v- V_{HCl} for 2-ethylimidazole, Built according to potentiometric titration.

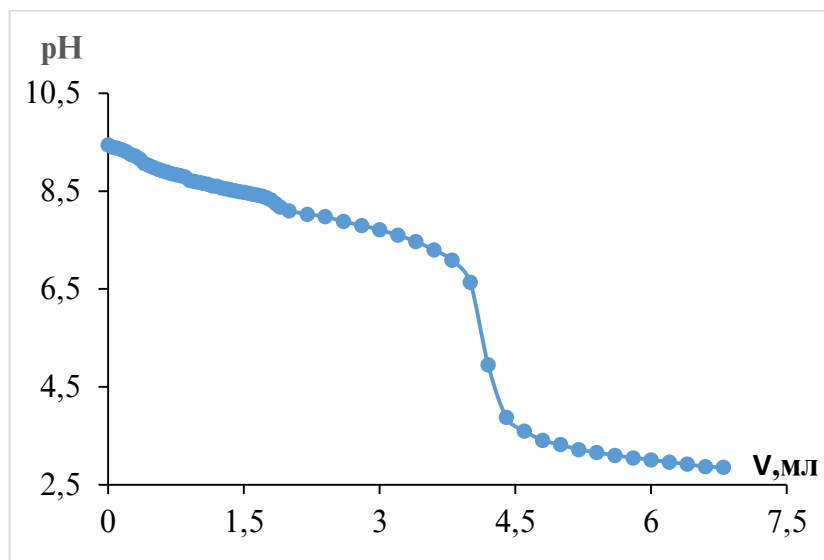


Fig.1. pH of V_{HCl} for aqueous solution of 2-ethylimidazole at 298.1K

As can be seen from Figure 1, there is one jump in the EM titration curves, which is typical for weak bases. One of the most reliable methods for calculating protonation constants from data potentiometric titration is an online computer program KEV. To calculate the EM protonation constants, the data of potentiometric titration (E,mV), the concentration of titrant and EM at each titration point, as well as the EM protonation reaction in the form of a matrix were entered into the KEV program:

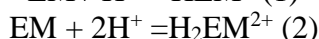
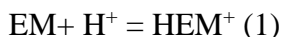


Table 1 shows an example of experimental results of pH-metric titration of an EM solution with an HCl solution.

Table 1. Results of pH-metric titration of 2-ethylimidazole at 298.1K, $C_{\text{HCl}}=0.1\text{N}$, $\text{EM}=0.01\text{mol/L}$

E,mV	pH	$[\text{EM}] \cdot 10^3$, mol/l	$[\text{HEM}^+] \cdot 10^4$, mol/l
62	9,48	10,00	0
64	9,45	9,895	1,050

66	9,4	9,824	1,660
68	9,38	9,736	2,440
70	9,35	9,639	3,320
71	9,31	9,537	4,240
74	9,25	9,432	5,180
76	9,22	9,327	6,130
79	9,16	9,221	7,100
84	9,07	9,114	8,060
86	9,03	9,008	9,030
88	8,99	8,901	10,000
91	8,95	8,794	10,970
93	8,92	8,688	11,940
94	8,89	8,581	12,910
96	8,86	8,474	13,870
98	8,84	8,368	14,840
99	8,82	8,262	15,810
101	8,79	8,156	16,770
102	8,72	8,050	17,730
104	8,7	8,944	18,690
106	8,68	7,839	19,650
107	8,66	7,733	20,610
~	~	~	~
446	2,87	0,00003690	88,340
448	2,86	0,00003280	88,030

It should be noted that the processing of potentiometric titration data by the program KEV gives satisfactory results when a protonated form of imidazole is formed in the system by reaction (1). The onset of the EM proton attachment turned out to be equal to 7.93 ± 0.06 log.units.

Figure 2 shows the distribution diagrams of different EM forms as a function of the pH of the solution. It has been established that the maximum share of accumulation of the molecular form falls on the region of $\text{pH} = 9.0 \div 10.0$.

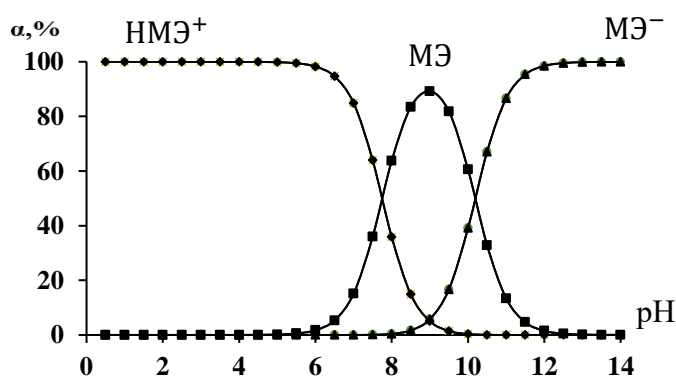


Fig.2. Fractional distribution of protonated, molecular, and deprotonated forms of EM at 298.1K

Our studies have shown that Ag^+ with 2-ethylimidazole enters into stepwise complexation (Fig. 3).

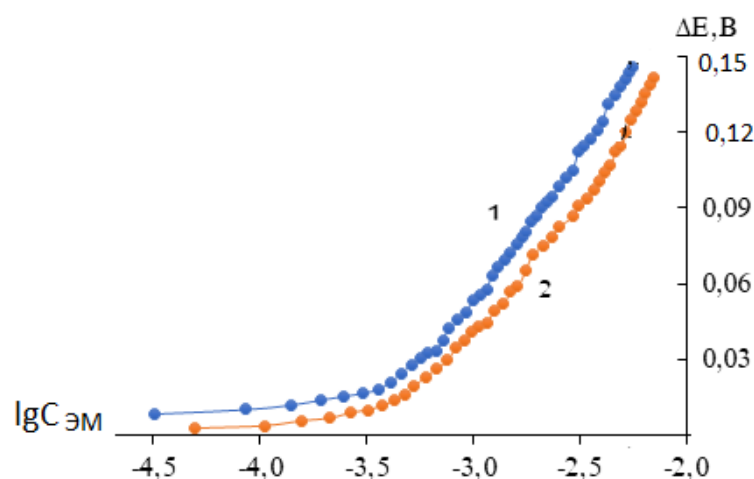


Fig.3. EM dependence ΔE on $\lg C$ for silver(I) 2-ethylimidazole complexes: 1-298.1; 2-308.15K.

Processing of KEV potentiometric titration results [22] gives satisfactory results for the formation of mono and two-substituted complexes by reactions:

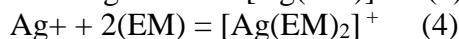
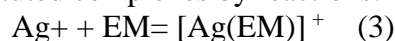


Table 2 illustrates the results of potentiometric titration of an AgNO_3 solution with an EM solution at 298.1 K and the equilibrium concentrations of starting substances and reaction products at each titration point calculated using the KEV program.

Table 2. Results of potentiometric titration of AgNO_3 solution with EM solution at $T = 298.1 \text{ K}$, $I = 0.1 \text{ mol/l NaClO}_4$

E, mV	$C_L \cdot 10^3$, mol/l	$C_{\text{Ag}^+} \cdot 10^5$, mol/l	$[\text{Ag}^+] \cdot 10^5$, mol/l	$[\text{L}] \cdot 10^3$, mol/l	$[\text{AgL}]$ $\cdot 10^5$, mol/l	$[\text{AgL}_2] \cdot 10^5$, mol/l
565,3	10,00					
556,6	0,0598	9,960	9,321	0,520	0,5018	0,1371
554,8	0,119	9,921	8,557	0,101	0,8915	0,4714
553,0	0,178	9,881	7,773	0,148	1,187	0,9198
551,0	0,236	9,843	7,009	0,194	1,404	1,427
549,5	0,294	9,804	6,286	0,239	1,557	1,957
548,4	0,352	9,766	5,624	0,285	1,660	2,486
546,8	0,409	9,728	5,016	0,331	1,720	2,994
543,9	0,465	9,690	4,469	0,378	1,749	3,472
540,4	0,521	9,653	3,983	0,425	1,753	3,915
537,1	0,577	9,615	3,557	0,473	1,740	4,323
534,5	0,632	9,579	3,177	0,521	1,713	4,689
532,2	0,687	9,542	2,845	0,570	1,677	5,018
531,7	0,741	9,506	2,557	0,619	1,636	5,317
527,1	0,795	9,470	2,302	0,668	1,590	5,578
522,5	0,849	9,434	2,078	0,717	1,542	5,810
519,4	0,929	9,381	1,796	0,792	1,471	6,114
516,3	1,007	9,328	1,563	0,866	1,400	6,367
511,3	1,085	9,276	1,369	0,940	1,332	6,578
509,1	1,162	9,225	1,208	10,15	1,268	6,754
507,4	1,239	9,174	1,071	10,89	1,206	6,893
501,6	1,314	9,124	0,9562	11,62	1,150	7,014

498,1	1,388	9,074	0,8586	12,35	1,097	7,114
495,8	1,486	9,009	0,7503	13,32	1,033	7,226
492,8	1,583	8,945	0,6601	14,27	0,9747	7,305
489,3	1,679	8,881	0,5860	15,22	0,9225	7,372
486,2	1,772	8,818	0,5236	16,15	0,8750	7,421
484,3	1,865	8,757	0,4708	17,08	0,8317	7,457
480,4	1,957	8,696	0,4257	17,99	0,7921	7,482
478,3	2,069	8,621	0,3776	19,12	0,7468	7,496
475	2,179	8,547	0,3379	20,22	0,7068	7,505
472,3	2,288	8,475	0,3038	21,32	0,6698	7,496
470,4	2,416	8,389	0,2699	22,60	0,6311	7,489
466,3	2,624	8,251	0,2250	24,69	0,5747	7,450
462,8	2,825	8,117	0,1909	26,71	0,5277	7,401
460,5	3,019	7,987	0,1643	28,68	0,4874	7,338
452,8	3,208	7,862	0,1430	30,58	0,4525	7,264
450,5	3,339	7,740	0,1260	32,42	0,4225	7,192
447,6	3,654	7,564	0,01058	35,08	0,3838	7,070
444,5	3,905	7,396	0,09047	37,63	0,3522	6,957
440,6	4,146	7,236	0,07842	40,06	0,3250	6,837
433,5	4,377	7,082	0,06873	42,40	0,3014	6,710
430,5	4,669	6,887	0,05867	45,36	0,2753	6,556
426,6	4,946	6,702	0,05077	48,16	0,2529	6,396
424,3	5,209	6,527	0,04457	50,82	0,2343	6,251
421,2	5,458	6,361	0,03949	53,34	0,2179	6,103
419,0	5,695	6,203	0,03533	55,74	0,2037	5,961

DISCUSSION OF THE RESULTS

When comparing the protonation constants of imidazole and 2-ethylimidazole, it was found that the introduction of an ethyl radical into the imidazole molecule leads to an increase in its basic properties, which is most likely due to an increase in the electron density on the pyridine nitrogen atom of the imidazole molecule. Using the literature data and our own results, we have established a number of changes in the acid-base properties (pKa) of imidazoles: ethylimidazole (7,93) > imidazole (7,05) > 2-phenylimidazole (6,48); >2-aminobenzimidazole (6,11); benzimidazole (5,53); >2-phenylbenzimidazole (5,23); >2-mercaptoimidazole (2,97); >1-methyl-2-mercaptoimidazole (2,11).

Earlier in [20] The stability constant of the saturated complex form of silver(I) with imidazole (AgL) was determined by potentiometric titration₂₊, which amounted to 6.96 log units. The authors of the study [20] were unable to determine the stability of the mono-complex of silver(I) with imidazole. In addition, complexation was studied at a temperature of 298 K and there is no information about the influence of enthalpy and entropy factors on the spontaneous course of the complexation reaction.

In Table. Figure 3 shows the values of the general stability constants of complex compounds of silver (I) with 2-ethylimidazole, calculated according to the KEV program in the temperature range of 273.1-318.1 K.

Table 3. Values of the Total Stability Constants of Silver (I) Complexes with 2-ethylimidazole at 273.1-318.1K. J I=0.1mol/l

T,K	lgβ ₁	lgβ ₂
273	3,22±0,01	7,56±0,03
288	3,10±0,08	7,28±0,02

298	3,01±0,05	6,73±0,03
308	2,55±0,01	6,21±0,01
318	2,49±0,01	5,78±0,01

The data in Table 3 show unusual relations of the step stability constants ($K_{i+1} > K_i$) complexes of silver with 2-ethylimidazole. As a rule, with the increase of coordinated ligand molecules in the internal coordination sphere, the stability of sequentially formed complexes decreases. Similar data were obtained in the study of gold(I) complexation with 2-methylimidazole [18].

It can be seen from the data in the table that the increase in temperature does not affect the stoichiometric composition of the complex particles formed in the Ag-EM-H₂O system. As the temperature increases, the stability constants of all complex shapes decrease. This experimental fact is connected with the exothermic nature of the process of complexation.

Comparison of the stability constant of the bis-substituted silver (I) complex, which contains imidazole as a ligand [20], with the 2-methylimidazole complex of silver (I) showed that the introduction of an ethyl radical into the imidazole molecule leads to a decrease in the stability of the complex. It can be assumed that this is due to an increase in the basicity of the 2-ethylimidazole molecule and competition between silver(I) ions and a proton for the pyridine nitrogen atom of the imidazole molecule.

Stability constants were used to calculate the concentration of the formed complex particles and to construct the distribution curves of all complex forms formed in the Ag⁺-EM-H₂O system. Figure 4 shows the distribution diagrams of 2-ethylimidazole silver(I) complexes as a function of the EI concentration at 298.1 K.

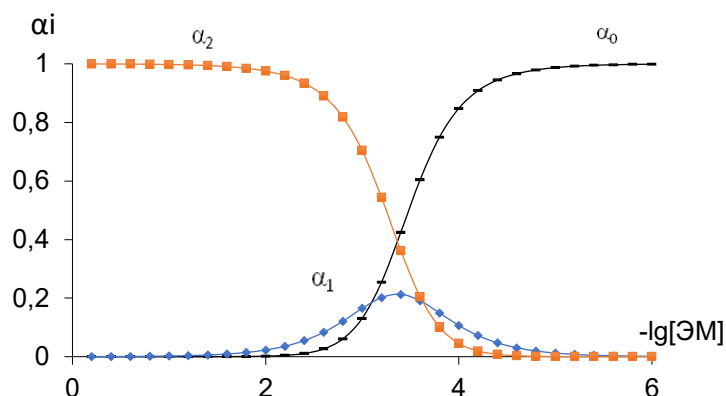


Fig.4. Distribution curves of 2-ethylimidazole silver(I) complexes at 298.1K: α_0 -AgNO₃; α_1 -[Ag(EM)]⁺; α_2 -[Ag(EM)₂]⁺.

As can be seen from Figure 4, the monosubstituted complex dominates in a narrow range of ligand concentration with a small yield. In the system Ag-EM-H₂O is mainly dominated by the bis-substituted complex, the yield of which at EM concentrations above $1 \cdot 10^{-2}$ mol/L is 100%.

Calculation of values ΔH and ΔS Complexation reactions were carried out by the method of temperature coefficient. The method of determining thermodynamic functions by this method is described in detail in [24]. Table 4 presents the values of the thermodynamic functions of the reactions of the formation of silver complexes (I) with EM.

Table 4. Values of thermodynamic functions of the process of formation of silver(I) complexes with 2-ethylimidazole

Reaction Equation	ΔG kJ/mol	ΔH kJ/mol	ΔS J/(mol·C)
Ag ⁺ + EM = [Ag(EM)] ⁺	-16,22	-29,38	-44,18
Ag ⁺ + 2EM = [Ag(EM) ₂] ⁺	-37,89	-68,22	-101,9

From the data in Table 4 it can be seen that the complexation reactions are exothermic. In the course of complexation reactions, the number of free particles in the system decreases at all stages, as evidenced by negative values of ΔS . It should be noted that the spontaneous course of complexation reactions in the Ag-EM-H₂O system is facilitated by a negative change in enthalpy and is not facilitated by the entropic contribution to the change in Gibbs energy.

CONCLUSIONS

As a result, conducted studies have found that the introduction of an ethyl radical into the imidazole molecule leads to an increase in its basic properties, which is associated with an increase in the electron density on the pyridine nitrogen atom of the heterocycle. Silver(I) with 2-ethylimidazole reacts in a stepwise manner to form two complex particles, the stability of which decreases with increasing temperature. It is shown that the formation of 2-ethylimidazole silver complexes is enthalpy stabilized.

The work was carried out at the Research Institute of the Tajik National University within the framework of the state assignment of the Republic of Tatarstan, project No. GR0119TJ00981. The discussion of the results was held jointly with the support of the Ministry of Science and Higher Education of the Russian Federation (project FZZW-2023-0008)

**REVIEWER: Davlatshoeva J.A.,
Candidate of Chemical Sciences**

REFERENCES

1. Mashkovskiy, M.D. Medicinal Means / M.D. Mashkovsky // – M., 2002. –T. 2. – № 14. – 608 p.
2. Mashkovskiy M.D. Medicinal Means / M.D. Mashkovsky // – M., 2005. –T. 2. –№ 15. – 1200 p.
3. Tran Than Tun Synthesis and Physicochemical Studies of Complex Copper(II) Bromide Compounds with Nitrogen-Containing Heterocyclic Bases: Autoref... Diss. Ph.D. –M., 2007. – 17 p.
4. Zaitseva S.V., Macroheterocycles / S.V. Zaitseva, S.A. Zdanovich, O.I. Koifman // – 2012. –T. 5. –№ 1. – 81 p.
5. Olivier-Bourbigou H., Ionic liquids and catalysis: Recent progress from knowledge to applications / H. Olivier-Bourbigou, L.Magna, D. Morvan // Journal homepage: www.elsevier.com/locate/apcata Applied Catalysis A: General. –2010. General 373. – Pp. 1-56.
6. Jarosik A., Conductivity of ionic liquids in mixtures / A. Jarosik, S.R. Krajewski, A. Lewandowski, P. Radzimski // Journ. of Molec. Liquids. – 2006. – Pp. 43-50.
7. Assouli B., Effect of 2-Mercaptobenzimidazole and Its Polymeric Film on the Corrosion Inhibition of Brass (60/40) in ammonia solution / B. Assouli, A. Srhiri. // Corrosion Science. – 2004. – V. 60. – P.399.
8. Hartley, F., Equilibrium in solutions / F. Hartley, K. Berges, R. Alcock // - M., 1983. – 365 p.
9. Albert, A., Konstanty ionizatsii acidov i obaseniy [Ionization constants of acids and bases]/ A. Albert., E. Sergent // Izdatelstvo «KHIMIYA». – M., 1964. – 180 p.
10. Surayo, S.B., Stability of silver complexes with 2-mercaptoimidazole. / S.B. Surayo, A.S. Sodatdinova, S.M. Safarmamadzoda // National Academy of Sciences of the Republic of Tatarstan. Dushanbe, 2022. –T.46. –№ 11-12. –Pp. 687-693.
11. Sodatdinova, A.S., Acid-basic properties of 1-methyl-2-mercaptoimidazole. / A.S. Sodatdinova, S.M. Safarmamadzoda // Vestnik TNU. – 2021. –№1. – Pp.145-157.
12. Safarmamadzoda, S.M. Influence of temperature on the stability of 2-ethylimidazole complexes Au (III) / S.M. Safarmamadzoda, D.S. Kurbonbekov, D.A. Kurbonbekov // From chemistry to technology step by step. – 2022. – T. 3. –Vol. 3. –Pp.58-64.
13. Mirzokhonov, D.Ch. Complexation of cadmium (II) with 1-methyl-2-mercaptoimidazole in the interval 283-323K / D.Ch. Mirzokhonov, K.S. Mabatkadamzoda, S.M. Safarmamadzoda // Bulletin of the Tajik National University. –2016, – No 1-3 (200). –Pp.138-143.
14. Aminjanov, A.O. Complexation of copper(II) with 1-methyl-2-mercaptoimidazole in a medium of 7 mol/l HCl / A.O. Amindzhanov, K.A. Manonov, Gamal Abdelaziz Husain Abdelrahman // Journal of Physical Chemistry. – 2016. –T. 61. – №1. –Pp.86-91.
15. Skorik, N.A., Compounds of cobalt (II), zinc and copper (II) with malic acid and imidazole / N.A. Skorik, E.I. Buholtseva, M.M. Flipova // Vestnik Tomskogo gosudarstvennogo Universiteta. Chemistry. –2015. – №2. – Pp.87-100.
16. Sodatdinova, A.S. Thermodynamics of Ag (I) complexation with 1-methyl-2-mercaptoimidazole / A.S. Sodatdinova // Vestnik Tadzhikskogo natsional'nogo universiteta. Natural Sciences Series. –2020. – №4. –Pp. 301-310.
17. Sodatdinova, A.S., complexation of silver (I) with 1-methyl-2-mercaptoimidazole in the water-ethanol solvent / A.S. Sodatdinova, T.R.Usacheva, S.M.Safarmamadzoda // Izv. Higher Educational Institutions. Chemistry and Chemistry. Technology. 2022. – T. 65. Vol. 8. –Pp.22-31. DOI: 10.6060/ivkkt.20226508.6645.

18. Bakhromi, D. Complexoformation of gold (I) with 2-methylimidazole / D. Bakhrom, S.M. Safarmadzoda, D.A. Muborakkadamov // *Izv. Higher Educational Institutions. Chemistry and Chemistry. technology.* 2023. T. 66. Vol. 4. –Pp. 27-34. DOI: 10.6060/ivkkt.20236603.6713.
19. Budu G.V., Complexoformation of silver with some heterocyclic amines in water-ethanol solutions / G.V. Budu, A.P. Thoryak // *Journal of Inorganic Chemistry.* – 1980. –T.25. –Issue 4. –Pp.1006-1008.
20. Bobosaidzoda, S. Thermodynamics of Ag(I) Complex Formations with 2-Mercaptoimidazole in Water–Dimethyl Sulfoxide Solvents / S. Bobosaidzoda, Kh. Akimbekova, E. Molchanov, T.R. Usacheva, S.M. Safarmamadzoda. // *Inorganics.* –2023. –11 (199) <https://doi.org/10.3390/inorganics11050199>
21. Surayo, S.B. Influence of solvent composition on acid-basic and complex-forming properties of 2-mercaptoimidazole/S.B. Surayo, A.S. Sodatdinova, S.M. Safarmamadzoda // *Bulletin of the Tajik National University. Series of natural sciences,* 2022. – №3. –Pp.327-339.
22. Mehkov A.N., KEV: a free software for calculating the equilibrium composition and determining the equilibrium constant using UV-Vis and potentiometric data / A.N Mehkov, G.A. Gamov // *Talanta,* –2019. – V. 198. – 200 p.
23. Mirzokhonov D.Ch., Complexation of cadmium (II) with 2-methylimidazole in aqueous and hydroalcoholic solutions / D.Ch. Mirzokhonov, K.S. Mabatkadamzoda, S.M. Safarmamadzoda // *Izv. Higher Educational Institutions. Chemistry and Chemistry. Technology.* 2023. T. 63. №10. –Pp.36-45. DOI: [10.6060/ivkkt.20206310.6201](https://doi.org/10.6060/ivkkt.20206310.6201)
24. Mabatkadamzoda K.S., Complexation of silver (I) with thiopirin at 278-317K. / K.S. Mabatkadamzoda, Y.K. Kudratulloev, A.S. Sodatdinova // – 2018. – T.61. – No4. –Pp.382-384.

COMPLEXATION OF SILVER (I) C 2-ETHYLIMIDAZOLE

The acid-base properties of 2-ethylimidazole were studied by pH-metric titration (EM). Using the literature data and our own results, a number of changes in the acid-base properties (pKa) of imidazoles have been established: ethylimidazole (7,93)> imidazole (7,05)>2-phenylimidazole (6,48)>2-aminobenzimidazole (6,11)> benzimidazole (5,53)>2-phenylbenzimidazole (5,23)>2-mercaptoimidazole (2,97)>1-methyl-2-mercaptoimidazole (2,11). Method The process of complexation of silver(I) with 2-ethylimidazole in the temperature range of 273-318K was investigated using potentiometric titration using a silver electrode. It has been established that the increase in temperature does not affect the stoichiometric composition of complex particles formed in the Ag-EM-H₂O system. The results obtained show that as the temperature increases, the stability constants decrease. On the basis of diagrams, the distribution of complex particles depending on the ligand concentration is shown that in System Ag-EM-H₂O is mainly dominated by the bis-substituted complex, the yield of which at EM concentrations above 1·10⁻² mol/l is 100%. The thermodynamic functions of the formation of 2-ethylimidazole silver complexes have been calculated. It has been established that complexation reactions are exothermic. Spontaneous occurrence of complexation reactions in the system Ag-EM-H₂O contributes to a negative change in enthalpy.

Keywords: Silver(I), 2-ethylimidazole, protolytic equilibrium, complexation, stability constants, thermodynamic functions, distribution diagram .

Information about the authors: Sodatdinova Anjuman Sadridinovna – Tajik National University, Doctoral students of the department analytical chemistry **Address:** 734025, Dushanbe, Republic of Tajikistan, Rudaki Avenue, 17. **Phone:** (+992) 938-13-66-56. **E-mail:** anjuman87@mail.ru.

Akimbekova Khazon Azizamadovna - Khorog State University named after I.I. Nazarshoev. Faculty of Natural Sciences, Assistant of the Department of General Chemistry. **Address:** M41, Khorog city, Republic of Tajikistan, Shirinshah Shakhtemur Avenue, 28. **Phone:** (+992) 935-42-74-77. **E-mail:** hazon22@mail.ru.

Usacheva Tatyana Rudolfovna - , Ivanovo State University of Chemistry and Technology, Doctor of Chemical Sciences, Head of the Department of General Chemical Technology, Associate Professor. **Address:** 153000, Ivanovo, Russia, Sheremetevsky Avenue, 7. **Phone:** +7-910 -87 -11 -25- **E-mail:** oxt@isuct.ru.

Safarmamadzoda Safarmamad Muboraksho – Tajik National University, Vice-rector for science and innovation of doctor of chemical sciences, professor. **Address:** 734025, Dushanbe, Republic of Tajikistan, Rudaki Avenue, 17. **Phone:** (+992) 938-27-04-04. **E-mail:** sash65@mail.ru.

Article received 02.01.2024
Approved after review 26.02.2024
Accepted for publication 15.04.2024

MODIFICATION OF α , β , γ -AMINO BUTYRIC ACIDS WITH C₆₀ FULLERENES AND THEIR STUDY

Kodirov M.Z., Bobizoda G.M., Zafarov S.Z.

In nature, there are amino acids that are absent in protein hydrolysates or are contained in them only in very small quantities [1, p.373]. These amino acids include α , β , γ -aminobutyric acids. Aminobutyric acids are intermediate products of the metabolism of certain amino acids. Among aminobutyric acids, the following are of practical interest: α -aminobutyric acid (CH₃CH₂CHNH₂COOH); β -aminobutyric acid (CH₃CH₂NH₂CHCOOH); β -aminobutyric acid [NH₂CH₂CH(CH₃)-COOH]; γ -aminobutyric acid (NH₂CH₂CH₂CH₂COOH); β -hydroxy- α -aminobutyric acid or L-threonine (CH₃CHOHCHNH₂COOH).

α -Aminobutyric acid is a product of protein metabolism in a living organism. However, it was not found in natural peptides. In biochemistry it is considered homoalanine and is a non-proteinogenic alpha amino acid. Non-proteinogenic amino acids are amino acids that do not participate in protein biosynthesis, since many of them are toxins and enzyme inhibitors in various metabolic reactions [2, p.102]. In the human body, α -aminobutyric acid is involved, for example, in the biosynthesis of ophthalmic acid. Like other amino acids, it can exist in the form of two stereoisomers: *D*-butyrine and *L*-butyrine [3, p.84]. Free α -aminobutyric acid is found in human blood and urine; an increase in its content is observed with pathological aminoaciduria, for example, with the so-called Fanconi syndrome. α -Aminobutyric acid (*L*-isomer) is formed in the body of animals during the transamination reaction from α -ketobutyric acid, a breakdown product of L-methionine. In animal tissues and in cell suspensions of microbes, α -ketobutyric acid is, in turn, formed from DL- α -aminobutyric acid as a result of oxidative deamination and transamination reactions. The transition of methionine to α -aminobutyric acid is an irreversible process. Predictions about the partial replacement of methionine in animal nutrition with α -aminobutyric acid were not confirmed [4, p. 234].

β -Aminobutyric acid is an isomer of α -aminobutyric acid that is also found in plants, where it may play a role in transmitting impulse signals. It is capable of inducing plant resistance to disease, as well as increased resistance to abiotic stress when processing plants [5, p. 322]. β -Aminobutyric acid increases plant resistance to various diseases and has a direct effect on plant pathogens, activating the plant immune system, and helps to effectively resist viral infections. β -Aminobutyric acid causes protective reactions in plants by both physical and biochemical methods. The exact mechanism depends on the plant species and pathogens.

γ -Aminobutyric acid (GABA) is formed by decarboxylation of L-glutamic acid by decarboxylases of certain bacteria in plants and animal tissues. In animals, decarboxylation of glutamic acid occurs intensively in brain tissue, which normally contains about 50 mg% γ -aminobutyric acid. γ -Aminobutyric acid in the nervous system plays a critical role in the transmission of electrical charge during nervous excitation, according to which γ -aminobutyric acid and its derivatives, as well as glutamic acid, are used clinically to treat a number of nervous and mental diseases [6, p. 123]. One of the main components of the pool of free amino acids in the brain of various animals is γ -aminobutyric acid, a product of decarboxylation of glutamic acid. The γ -aminobutyric acid transformation cycle in the brain includes three coupled enzymatic reactions called the GABA shunt.

GABA is the most widespread inhibitory neurotransmitter in the nervous system. In mammals, it is localized in the nerve endings of inhibitory neurons in the central nervous system. GABA inhibits the bioelectrical activity of not only the brain of vertebrates, but also the nerve chains and ganglia of invertebrate animals. Accordingly, GABA and the enzymes of its metabolism are also localized in the nervous structures of invertebrates, coinciding with the location of inhibitory synapses. The physiological effect of GABA is due to interaction with

special receptors. Under normal conditions and with normal methods of administration, GABA practically does not penetrate the blood-brain barrier.

In order to maintain stability, suppress toxicity and increase the effect of aminobutyric acid isomers on living organisms and plants, we decided to add fullerene C₆₀ to the NH₂ group of aminobutyric acid and obtain N-fullerene C₆₀-aminobutyric acid by the mechanism of nucleophilic addition and study of some physicochemical properties and conformational features.

RESULTS

Fullero-C₆₀-α-aminobutanate, fullero-C₆₀-β-aminobutanate and fullero-C₆₀-γ-aminobutanate were synthesized in 52, 64 and 83% yield.

The main physical constants of the obtained compounds are given in Table 1.

Table 1. The main physical constants of the compounds obtained

№ п/п	Names of compounds	, %	T _{пл.} , °C	R _f [*] А	R _f Б	R _f В
1	Fullero-C ₆₀ -α-aminobutanate	52	322-325	0,93	0,56	0,59
2	Fullero-β-amino-butanate	64	>360	0,84	0,77	0,71
3	Fullero- γ -amino-butanate	83	>360	0,73	0,61	0,63

R_f^{*}) А- (C₂H₅)₃N : NH₄OH : CH₃OH : H₂O (10:10:200:400);

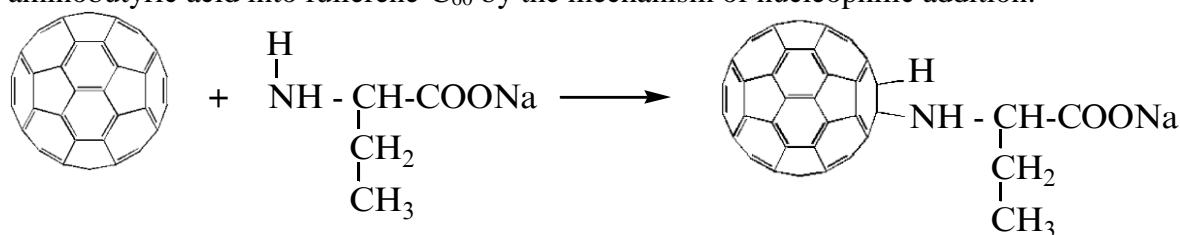
Б- ДМCO : CH₃OH : H₂O : NH₄OH (15:20:10:5);

В- CH₃OH : ДМФА : NH₄OH (1:2:2). Iodine vapor developer

Discussion

One of the approaches to the synthesis of amino acid derivatives of C₆₀ fullerene is the thermal method of binding amino acids to C₆₀ fullerene, which we first used in the laboratory [7, p. 51]. From the literature it is known that most amino compounds and amino acids [8, p. 211] in the reaction with fullerene C₆₀, according to the mechanism of nucleophilic addition, tends to join at position 1,2 of the hexogen ring of the benzene structure of fullerene-C₆₀ between carbon atoms having a double bond, since in the intermediate RC₆₀ the largest negative charge is localized at position 2 [9, p. 397]. Spatially bulky molecules can join at the 1,4 position of the benzene ring.

Taking into account the polyene properties of fullerene C₆₀ and its electroacceptor properties, the most important method for us [10, p. 142; 11, p. 182] was the introduction of α-aminobutyric acid into fullerene-C₆₀ by the mechanism of nucleophilic addition:



This synthesis method allows the synthesis of the main product N-fullero C₆₀-α-aminobutanate in good yield and ideal purity.

The initial stage of this synthesis (1) is to obtain an alkaline dimethylformamide solution of an amino acid by dissolving a crystalline amino acid in an alkaline dimethylformamide at pH 9-9.5. Then the corresponding amount of a solution of C₆₀ fullerene in bromobenzene was added to this solution [12, p. 13 author] and stirred the reaction medium on a magnetic stirrer for 9-10 hours at a temperature of 70-80°C. In this case, a change in the color of the reaction medium from violet to dark brown is observed [13, p. 103].

As the reaction proceeds, the color of the reaction mixture and the pH of the medium gradually change. Upon completion of the reaction, the reaction medium is neutralized by adding 6n. hydrochloric acid. The reaction mixture is evaporated on a rotary evaporator and a brown crystalline product is obtained [14, p. 76; 15, p. 105]. The resulting precipitate is washed first with toluene to get rid of unreacted fullerene, and then with alkaline methanol to clean the product from

unreacted amino acids, and then with methanol several times. Chromatographically pure fullerene- C_{60} - α -aminobutanate is obtained with a yield of 52%. The resulting product dissolves well in a mixture of water and dimethyl sulfoxide. The identity and purity of the resulting substance was verified by thin layer chromatography and IR spectroscopy. Chromatographic data and the melting point of the resulting substance confirm the formation of fullerene- C_{60} - α -aminobutanate.

A number of changes were observed in the IR spectra of fullerene- C_{60} , α -aminobutanate (Fig. 1) and the reaction product of fullerene- C_{60} - α -aminobutanate (Fig. 2). In the IR spectrum of fullerene- C_{60} , characteristic spectra appear in the regions of 3200-3600 cm^{-1} , 2800-3200 cm^{-1} , 1000-1200 cm^{-1} and 400-600 cm^{-1} , confirming the formation of the intended compounds. In the region of 3300-3450 cm^{-1} , bands characteristic of C_{60} -NH- are observed, in the region of 1725-1700 cm^{-1} , bands characteristic of COOH are observed. In the IR spectrum of α -aminobutanate itself, the spectra corresponding to 400-600 cm^{-1} and 2800-3000 cm^{-1} corresponding to NH^+ disappear. The spectra of stretching vibrations in the region of 2800-3000 cm^{-1} have minimal intensity and turn into spectra with low amplitude.

Fig.1. IR- spectrum of α -aminobutanate

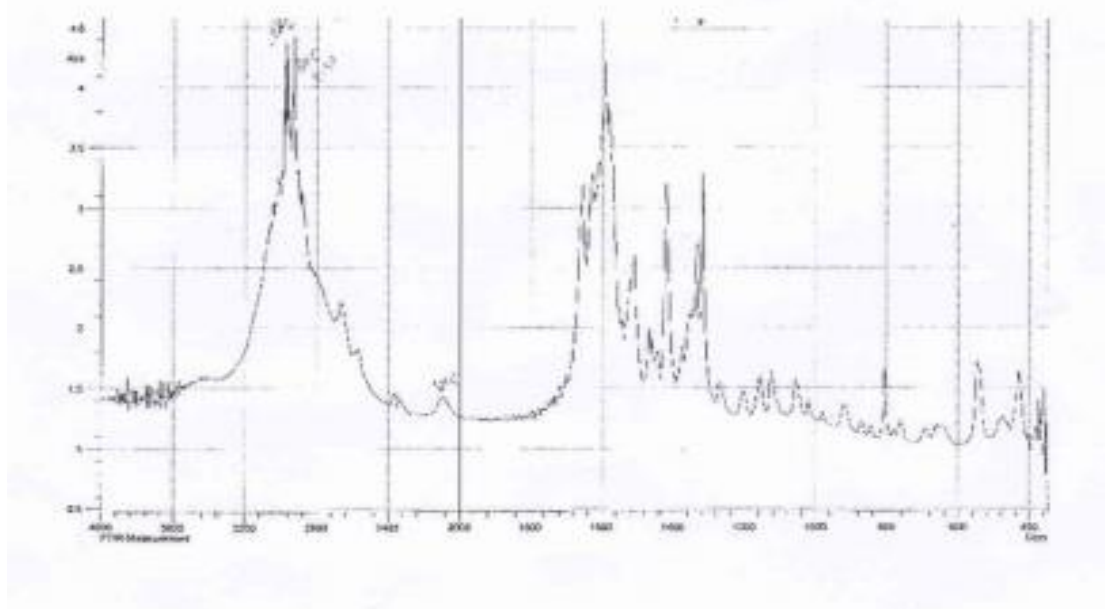
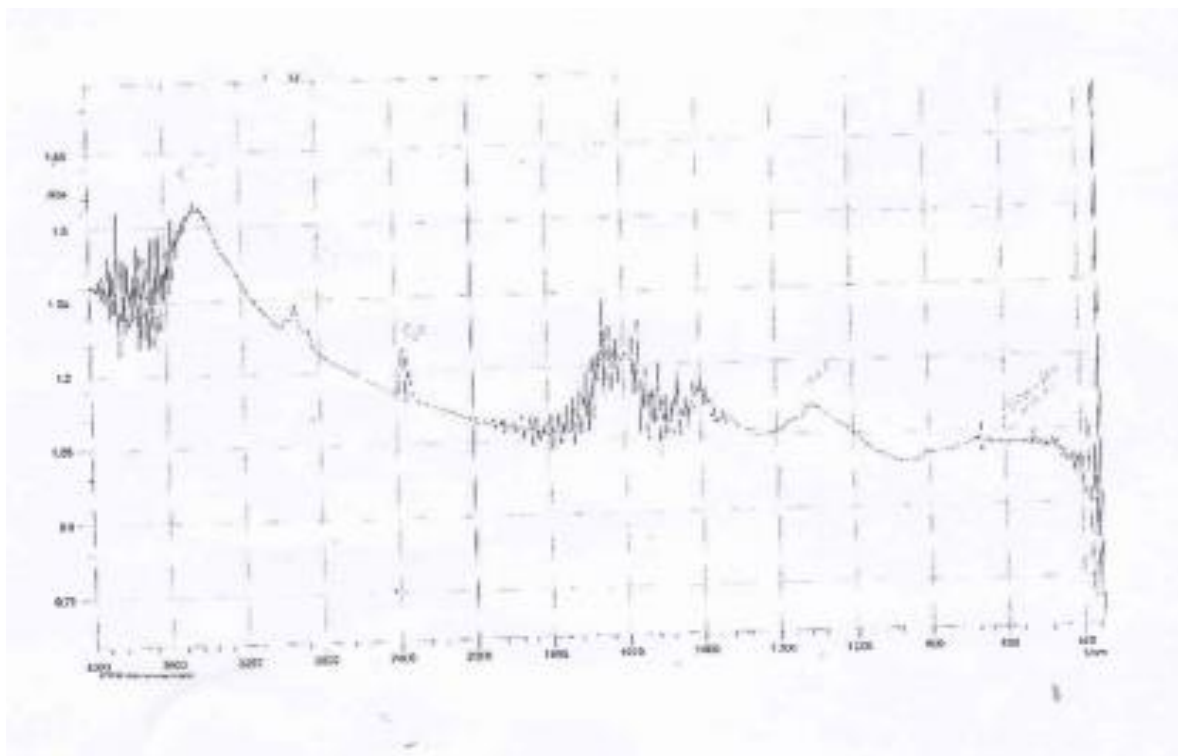
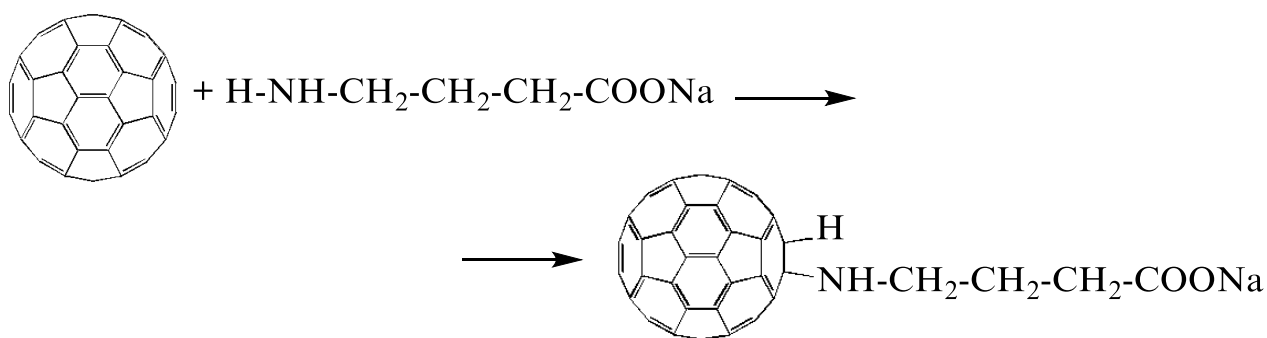


Fig.2. IR- spectrum of Fullerene- C_{60} - α -aminobutanate



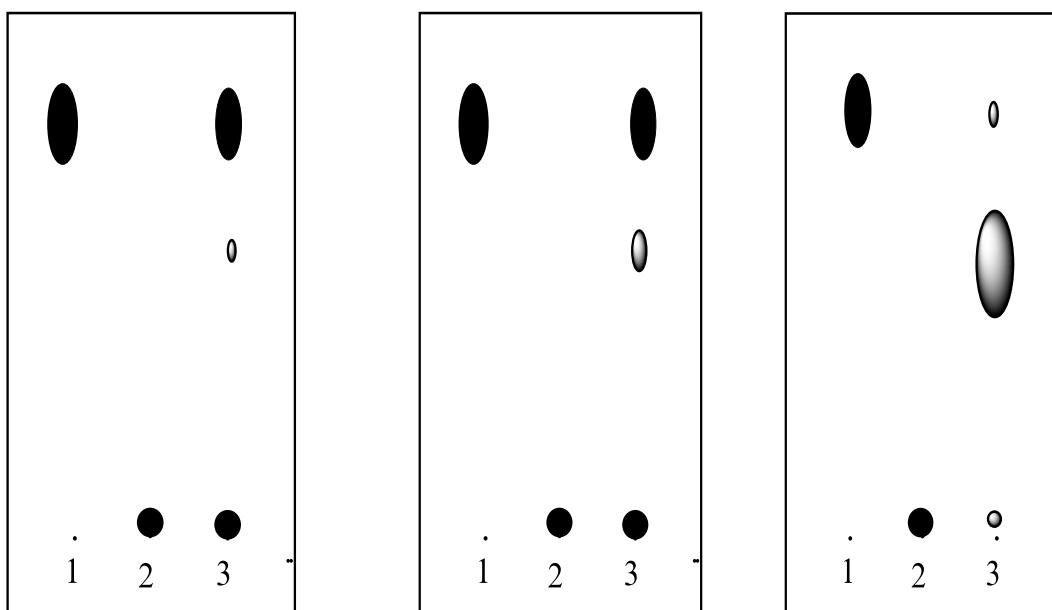
From Fig. 1 it follows that in terms of yield, the three (1,2,3) isomers differ from each other, the main reason and factor of which may be the location of the NH₂ group along the chain of molecules from the -COOH group of the amino acid, which changes the degree of nucleophilicity of the amino group with its electron-withdrawing property, affecting directly on the course of the reaction.

For the synthesis of fullerene C₆₀-β-aminobutanate and fullerene C₆₀-γ-aminobutanate, synthesis scheme (1) was also used with some change in the sequence of adding the monomer solution during synthesis, which is as follows:



Sodium salts of β-aminobutanate and γ-aminobutanate are added to a solution of fullerene-C₆₀ in bromobenzene separately. The reaction is carried out at a temperature of 80°C. The progress of the reaction is monitored using thin layer chromatography. Chromatographic data confirm that the reaction was successful (Fig. 3).

Fig.3. In the chromatogram: 1- aminoacids, 2-Fulleren-C₆₀, 3-stufige reakction. In the chromatographic system: (C₂H₅)₃N: NH₄OH: CH₃OH: H₂O (10 + 10 + 200 + 400; developer of a pair of iodine)



Upon completion of the reaction, the reaction medium is neutralized with 6N. HCl.

Processing and purification of the obtained substances is carried out as in the case of obtaining fullerene- C_{60} - α -aminobutanate. After purification and drying, the yield of fullerene- C_{60} - β -aminobutanate was 64% and fullerene- C_{60} - γ -aminobutanate was 83%. The main physical constants of the obtained compounds are given in Table 1.

MATERIALS AND METHODS

IR spectra were taken on a SHIMADRUFTIR Measurement instrument.

The melting points of the synthesized substances were determined on a heating table "Boetius" (Germany) with a heating rate of 4°C/min.

The purity, individuality of the synthesized compounds and the progress of the reaction were monitored by thin layer chromatography on Silufol UV-254 plates (Chemapol, Czech Republic) in the following solvent systems:

A- $(C_2H_5)_3N : NH_4OH : CH_3OH : H_2O$ (10:10:200:400);

Б- ДМCO : $CH_3OH : H_2O : NH_4OH$ (15:20:10:5);

В- $CH_3OH : ДМΦА : NH_4OH$ (1:2:2).

Synthesis of fullerene- C_{60} - α -aminobutanate (1). 0.080 g (0.11 mmol) of fullerene is dissolved in 2 ml of bromobenzene and heated to 60°C until completely dissolved. At the same time, a dimethylformamide solution of the sodium salt of α -aminobutyric acid is prepared starting from 0.014 g (0.11 mmol), which is added to the previously prepared solution of fullerene in bromobenzene. Then the reaction mixture is stirred on a magnetic stirrer at a temperature of 80°C for 9-10 hours using a reflux condenser. The reaction medium turns from purple to brown. In this case, a small amount of precipitate begins to form the solution, which is separated by filtration at the end of the reaction. The solution is neutralized with 6 N. HCl to pH 4.5-5 and evaporated on a rotary evaporator. The resulting precipitate is washed with toluene to separate unreacted C_{60} fullerene, with alkaline methanol to get rid of the remaining α -aminobutanoate, and then with methanol. The resulting crystalline product (1) is dried in air. The yield of the main product is 0,048 г (52%). $T_{m.} = 322-325^\circ C$.

$R_f = 0,93$ (A); $R_f = 0,56$ (Б); $R_f = 0,59$ (B); iodine vapor developer

Elemental analysis: (M_r : $C_{64}H_9O_2N$), calculated % C-93,31; H-1,09; N-1,70;

found % C-94,57; H-1,15; N-1,55

Synthesis of fullerene- C_{60} - β -aminobutanate (2). 0.250 g (0.35 mmol) of fullerene is dissolved in 20 ml of bromobenzene. To completely dissolve the fullerene, the solution is heated for 20 minutes at a temperature of 60-70°C. The solution turns purple. A previously prepared

solution of 0.045 g (0.35 mmol) of sodium salt of β -aminobutyric acid in dimethylformamide is added to the resulting solution of fullerene. The reaction mixture is stirred on a magnetic stirrer at a temperature of 80°C for 20 hours using a reflux condenser. In this case, the reaction medium turns from purple to brown. The pH of the reaction medium does not change. The progress of the reaction is monitored by thin layer chromatography. The reaction mixture is neutralized with 6 N. HCl to pH 4.5-5 and evaporated on a rotary evaporator. The crystalline residue is washed first several times with toluene and then with alkaline methanol. The remaining mass is air dried. The yield of the main product is 0,18 gr (64%). $T_{\text{mpt.}} = >360^\circ\text{C}$.

$R_f = 0,84$ (A); $R_f = 0,77$ (B); $R_f = 0,71$ (B); iodine vapor developer

Elemental analysis: (M_r : $\text{C}_{64}\text{H}_9\text{O}_2\text{N}$) calculated % C-93,31; H-1,09; N-1,70;

found % C-94,12; H-1,27; N-1,30.

CONCLUSION

Based on experimental facts and studying the course of the reaction of nucleophilic addition of α , β , γ -aminobutyric acids to the fullerene- C_{60} molecule, it was established that the addition of the NH_2 -group of amino acids to the fullerene- C_{60} molecule depends on the nucleophilicity of the NH_2 -group, and not on the degree of acidity and spatial shielding of NH_2 -group electrons by clouds.

**REVIEWER: Rajabov S.,
Doctor of Chemical Sciences,
Professor**

REFERENCES

1. Karrer P. Course in organic chemistry/ P.Karrer// Translation from German. Second edition. - L.: Chemical literature, 1962. - 1216 p.
2. Shugaley I.V. Protein chemistry. Textbook St. Petersburg / I.V. Shugaley, A.V. Garabadzhiu // - M.: Prospekt Nauki, 2010. - 200 p.
3. Yakovishin L.A. Selected chapters of bioorganic chemistry / L.A. Yakovishin // - Sevastopol: Strizhak-press, 2006. - 196 p.
4. Braunstein A. E. Biochemistry of amino acid metabolism / A. E. Braunstein // - M., 1949. - 426 p.
5. Great medical encyclopedia. Volume 1 / Editor-in-Chief Academician B.V. Petrovsky // - M.: "Soviet Encyclopedia", 1974. - 576 p.
6. Sytinsky I.A. Gamma-aminobutyric acid in the activity of the nervous system / I.A. Sytinsky // - L.1972. - 200 p.
7. Khalikov Sh. Connections to fullerene of C_{60} of alkyldiamino-, amino- and iminoacids with different molecular structures and the nucleophilicity / Sh. Khalikov, D. A. Sharipova, M. Umarchon, S.Z. Zafarov, M.Z. Kodirov // International Journal of Modern Chemistry. USA. - 2016. - 8 (1). - Pp.50-60.
8. Bianco, A. Fullerene-based amino acids and peptides / A. Bianco, T. Da Ros, M. Prato, S. Toniolo // J. Pept. Sci. - 2011. - Vol. 7. - Pp.208-219.
9. Fullerenes: textbook. aid for students universities / L. N. Sidorov, M. A. Yurovskaya, A. Ya. Borshchevsky and others // - M.: Exam, 2005. - 688 p.
10. Sharipova D.A. Synthesis and study of fullerene C_{60} amino acids. / YES. Sharipova, Z. Sorbon, S.V. Alieva, M.Z. Kodirov, Sh.Kh. Khalikov // Materials of the republican conference "Prospects for research in the field of glycerol chemistry: Synthesis of new derivatives of biologically active substances based on amino acids. - Dushanbe, 2015. - Pp.141-143.
11. Kodirov M.Z. Synthesis and study of fullero C_{60} -cycloserine and fullero C_{60} -serine / M.Z. Kodirov, D.A. Sharipova, Sh.H. Khalikov // Bulletin of the Tajik National University. -Dushanbe, 2018. - No. 4. - Pp. 181-188.
12. Islamova N.I. Abstract "Thermodynamics of dissolution of fullerene C_{60} in individual and mixed (CCl_4 - $\text{C}_6\text{H}_5\text{CH}_3$ and CCl_4 -1,2- $\text{C}_6\text{H}_4\text{Cl}_2$) organic solvents". - Ivanovo, 2005.
13. Khalikov Sh.Kh. Synthesis and identification of fullero C_{60} α -amino acids with antiviral properties / Sh.Kh. Khalikov, D.A. Sharipova, S.Z. Zafarov, M. Umarchon, S.V. Aliyeva // Chemistry of natural compounds. 2017 No.1. - Pp.102-108.
14. Khalikov Sh.Kh. Synthesis and study of fullerene C_{60} amino acids / Sh.Kh. Khalikov, D.A. Sharipova, S.Z. Zafarov // Materials of the international conference. Mathematics. Physics. Chemistry. Technology. Prague. - 12/27/2013 - 01/05/2014. - R. 75-77. - 12/27/2013 - 01/05/2014. - Pp.75-77.
15. Khalikov Sh.Kh. Synthesis and identification of fullero C_{60} α -amino acids with antiviral properties / Sh.Kh. Khalikov, D.A.Sharipova, S.Z.Zafarov, M.Umarchon, S.V.Aliyeva//Chemistry of natural compounds. - Uzbekistan. - 2017. - No. 1. - Pp.102-108.

MODIFICATION AND RESEARCH OF α , β , γ -AMINOIL ACIDS WITH FULLERENE C₆₀

In nature, there are amino acids that are not found in protein hydrolysates. These amino acids include α , β , γ -aminobutyric acids. α -Aminobutyric acid, which is formed in living organisms during the metabolism of proteins, is a non-proteinogenic alpha amino acid. In the human body, it is involved, for example, in the biosynthesis of ophthalmic acid. β -Aminobutyric acid is an isomer of aminobutyric acid, which is found in plants, where it can play a role in signaling. β -Aminobutyric acid is able to increase the resistance of plants to diseases and have a direct effect on pathogens of plant diseases, activates the immune system of plants. γ -Aminobutyric acid plays a crucial role in the transmission of nerve excitation. In order to maintain stability and increase the effect of aminobutyric acid isomers on living organisms and plants, we decided to attach C₆₀ fullerene to the NH₂ - aminobutyric acid group and obtain N-fullero C₆₀-aminobutyric acid for further study of biological properties. N-Fullero C₆₀-aminobutyric acid was synthesized using the thermal method of binding amino acids to C₆₀ fullerene. As is known, most amino compounds in the reaction with fullerene C₆₀ by the nucleophilic attachment mechanism can join at position 1.2 of the benzene ring of fullerene-C₆₀. Using this mechanism, 3 new compounds were synthesized: fullero C₆₀- α -aminobutanate, fullero C₆₀- β -aminobutanate, fullero C₆₀- γ -aminobutanate. The identity and purity of the obtained substances was checked by thin-layer chromatography and IR spectroscopy. Chromatographic data and melting points of the obtained substances confirm the formation of fullero-C₆₀- α -aminobutanate, fullero-C₆₀- β -aminobutanate and fullero-C₆₀- γ -aminobutanate.

Key words: fullerene-C₆₀, reaction, aminobutyric acid, thermal method, bromobenzene, dimethylformamide, spectrum, thin-layer chromatography.

Information about the authors: Kodirov Murod Zokirovich - Tajik National University, Candidate of Chemical Sciences, Associate Professor of Organic Chemistry Department. **Address:** 734025, Dushanbe, Republic of Tajikistan, Rudaki Avenue 17. **Phone:** 935983847. **E-mail:** kaf.org.chem@mail.ru.

Bobizoda Gulomkodir Mukkamal - Tajik National University, Doctor of Biological Sciences, Doctor of Pharmaceutical Sciences, Professor of Organic Chemistry Department. **Address:** 734025, Dushanbe, Republic of Tajikistan, Rudaki Ave., 17. **Phone:** +992-(918)-17-03-60. **E-mail:** bobievgm@mail.ru.

Zafarov Sorbon Zafarovich - Tajik National University, Candidate of Chemical Sciences, Senior Lecturer of Organic Chemistry Department. **Address:** 734025, Dushanbe, Republic of Tajikistan, Rudaki Ave., 17. **Phone:** +992-(937)-70-03-95. **E-mail:** Szafarov91@mail.ru.

Article received 20.11.2023

Approved after review 24.02.2024

Accepted for publication 10.04.2024

FORMATION OF HYDROXYL COMPLEXES OF Fe(II) IN AQUEOUS SOLUTIONS

Eshova G.B., Rahimova M., Davlatshoeva J.A.,

Miraminzoda F.

Introduction. The study of the processes of complexation of metals with various carboxylic acids and neutral organic ligands showed the formation of stable coordination compounds of various compositions, often mixed-ligand hydroxyl complexes that exhibit biological activity. When determining the stability of such complexes and carrying out thermodynamic calculations of chemical equilibria, it is necessary to know the composition and stability constants of hydroxyl complexes.

Hydroxyl complexation has been studied using various methods [1]. The hydrolysis process in the Fe^{3+} - Hg^{2+} - NO_3^- - H_2O and Fe^{3+} - Co^{2+} - NO_3^- - H_2O systems was studied using spectrophotometry, pH-metric titration, sorption and dialysis [2, 3]. The mutual influence of cations on hydrolytic and sorption behavior from the standpoint of heteronuclear complex formation was established and the distribution of various aqua- and hydroxy complexes of Fe(III) and Co(II) was calculated depending on the pH value of the solution in the region preceding the precipitation of hydroxide precipitation. It has been established that Fe(III) ions form homopolynuclear hydroxy complexes [3].

A method for experimentally determining the composition of polynuclear hydroxyl complexes, their degree of nuclearity and charge at various concentration conditions at which iron passes from an ionic to a nonionic state using the methods of dialysis, ion exchange and spectrophotometry is shown. In the case of Fe(III), it is concluded that under certain conditions dimers of the composition $\text{Fe}_2(\text{OH})_{24}^{4+}$ with the corresponding formation constants are formed in solution [4].

In [5], the processes of hydroxyl complexation of iron (III) in solutions of various compositions were studied using the oxidation potential method: $[\text{Fe}(\text{OH})(\text{H}_2\text{O})_5]^{2+}$; $[\text{Fe}_2(\text{OH})_2(\text{H}_2\text{O})_{10}]^{4+}$; $[\text{Fe}(\text{OH})_2(\text{H}_2\text{O})_4]^+$; $[\text{Fe}(\text{OH})_3(\text{H}_2\text{O})_3]^0$ and the formation constants of these coordination compounds were determined. This method was used to study the processes of complex formation of Fe(II) and Fe(III) with organic ligands [6, 7] at different ionic strengths of the solution.

This work was carried out to study the process of formation of hydroxyl complexes and mixed hydroxyl complexes in the Fe(0)-Fe(II)-glycine-water system at an ionic strength of 0.5 mol/l (NaClO_4) and a temperature of 298.15 K.

EXPERIMENTAL PART

The starting materials in the study of the iron complexation reaction were iron (II) perchlorate. Ferrous perchlorate salt was obtained according to the method described in [8]. The concentration of Fe(II) ions was determined by titration with a 0.1 N solution of fixonal $\text{K}_2\text{Cr}_2\text{O}_7$ in the presence of the indicator sodium diphenylamine sulfonate [9]. Aminoacidic acid grade "analytical grade" used without further purification. Sodium perchlorate (NaClO_4) was purified by filtration, and the concentration was determined by the gravimetric method [9]. The concentration of sodium hydroxide was determined by direct titration with a 0.1 M solution of hydrochloric acid in the presence of the indicator phenolphthalein. The titer of the NaOH solution was adjusted with succinic acid [10].

To fill the silver chloride electrode as a reference electrode, prepare an electrolytic key and a buffer vessel to maintain a constant diffusion potential, agar-agar and potassium chloride KCl were used.

The pH values of the system under study were controlled by a glass electrode, which was previously calibrated using standard buffer solutions. The EMF values were determined using a 150 MI pH meter. Stainless steel was used as a metal electrode, which is resistant to corrosion in

air, water, and some aggressive environments. The experiments were carried out in a special cell where the solution was mixed with purified nitrogen gas. The purification system consisted of three flasks, two of which contained ammonium vanadate dissolved in 25% sulfuric acid and amalgamated metallic zinc as a reducing agent, and the third flask for additional purification and washing of the purified gas contained distilled water.

The main research method was oxidation measurement, where the measured value was the electromotive force of galvanic cells composed of a combination of stainless steel - silver chloride for determining the oxidation potential and glass - silver chloride electrodes for determining the pH of solutions. Numerical values of the emf of the metal electrode system were used to determine the dependences of E on pCox, an indicator of the concentration of iron(II) ions and pH of the solution.

To obtain quantitative information about the processes occurring in the Fe(0)-Fe(II)-glycine-water system and to establish the exact composition of the most probable various forms of Fe(II) hydroxo complexes, to calculate the stability constant and to determine the areas of their dominance, we used the oxidation potential method Clark-Nikolsky [1, 11-14].

RESULTS AND DISCUSSIONS

In Fig. Figure 1 shows the experimental dependence of E-pH at $C_{Fe(II)}=1 \cdot 10^{-4}$; $C_{Gly}=3 \cdot 10^{-3}$ and ionic strength $I=0.5$ mol/l, where on the E-pH dependence curve, according to the theory of the oxidation method, the sequential formation of linear sections with slope angles equal to: 0, $-v/2$, $-v$, $-2v$ и $-v$, indicates stepwise complexation of Fe(II). These linear regions indicate the sequential addition of one or more numbers of hydroxyl groups to the iron ion.

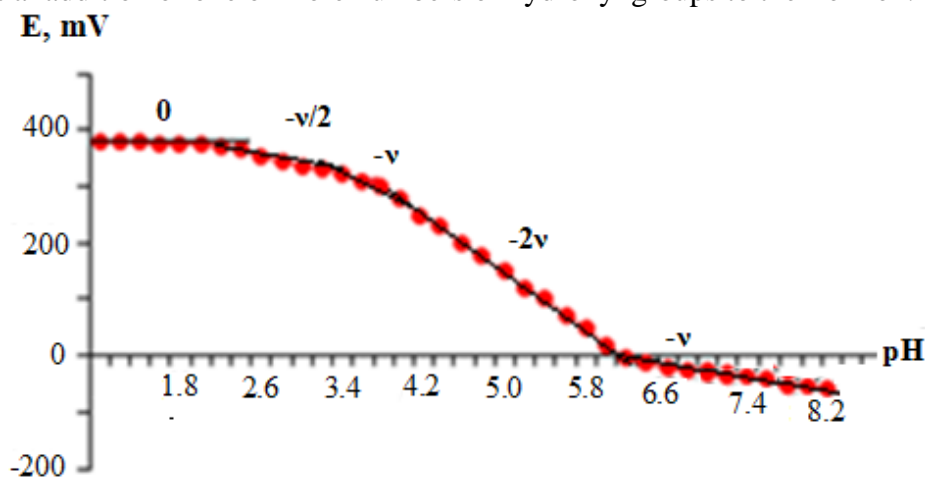


Fig.1. Dependence of ЭДС (E, mV) of the Fe(0)-Fe(II)-glycine-water system on pH at a temperature of 298.15 K; $I=0.5$; $C_{Fe(II)}=1 \cdot 10^{-4}$ и $C_{Gly}=3 \cdot 10^{-3}$ mol/l

To determine the number of nuclei of hydroxyl complexes, experimental dependences of E on $pC_{Fe^{2+}} = pC_{ox}$ were taken, which are presented in Fig. 2. The angular coefficient of these linear dependencies is equal to $-v/2$. According to the theory of average metering and the partial derivative equation:

$$\left(\frac{\partial E}{\partial pC_{ox}} \right)_{pC_{L,pH}} = -\frac{v}{2q} \quad (1)$$

$q=1$, therefore, we can conclude that mononuclear iron (II) complexes are formed at all pH values of the solutions under study.

The values of the angular coefficients and the expected composition of hydroxyl complexes are given in Table. 1, where $v=RT/F \cdot 2.303=59$ mV. Since two electrons are involved in the transfer reaction, the contribution of one ligand to the decrease in emf (E, mV) is equal to 30 mV.

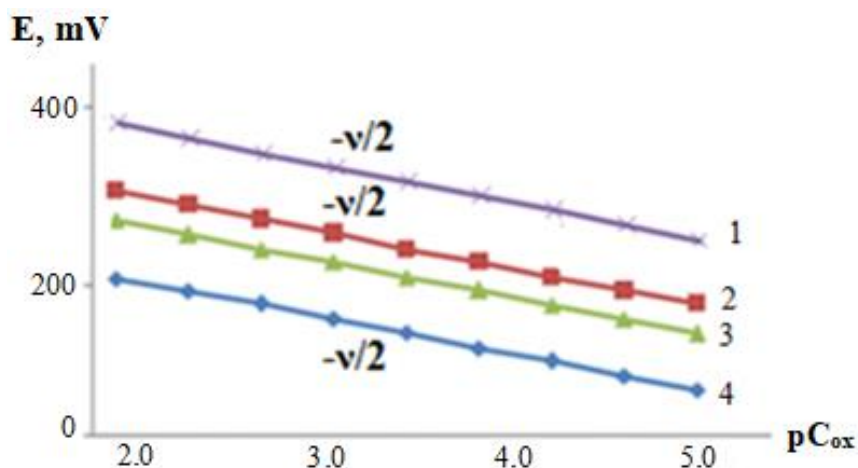


Fig.2. Dependence of the EMF of the Fe(0)-Fe(II)-glycine-water system on pCox at a temperature of 298.15 K; $I=0.5$; $C_{Fe(II)}=1 \cdot 10^{-4}$ и $C_{Gly}=3 \cdot 10^{-3}$ mol/l. The curves refer to pH: 1- 3.0; 2 - 4.0; 3- 5.0; 4 -6.0

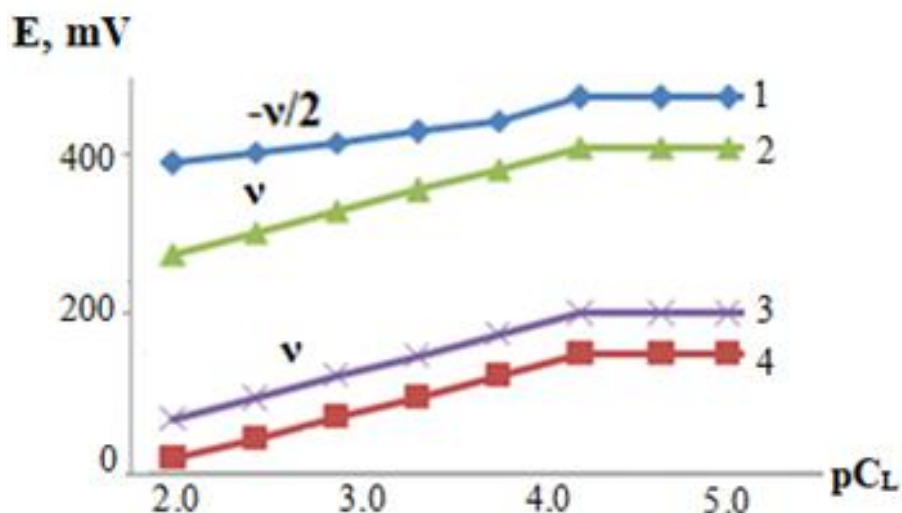


Fig. 3. Dependence of the EMF of the Fe(0)-Fe(II)-glycine-water system on pCL at a temperature of 298.15 K; $I=0.5$; $C_{Fe(II)}=1 \cdot 10^{-4}$ and $C_{Gly}=3 \cdot 10^{-3}$ mol/l. The curves refer to pH: 1- 3.0; 2- 4.0; 3 - 5.0; 4 - 6.0

Analysis of partial derivatives of the dependence of the EMF of a galvanic cell on the glycine concentration index pCL ($pCL = -\lg C_{Gly}$):

$$\left(\frac{\partial E}{\partial pC_L} \right)_{pC_{ox}, pH} = \frac{vsl}{2q} \quad (2)$$

allowed us to determine the number of protonated ligands (sl) included in the iron(II) complexes. In the range $pC_L=4.3 \div 5.0$ on the experimental curves of the E - pCL dependence, which are presented in Figure 3, a linear section with a slope of 0 is formed. This indicates the absence of complexation with glycine under these concentration conditions.

From Fig. 1 and table. 1 shows that in the Fe(0)-Fe(II)-glycine-water system at least four complex forms are formed: hydroxyl - $[Fe(OH)(H_2O)_5]^+$, $[Fe(OH)_2(H_2O)_4]^0$ и mixed hydroxo complexes- $[Fe(HL)(OH)(H_2O)_4]^+$, $[Fe_2(HL)_2(OH)_2(H_2O)_8]^{2+}$.

Table 1. Experimental values of the angular coefficients of the dependences of EMF on concentration variables of the Fe(0)-Fe(II)-glycine-water system at a temperature of 298.15 K; $I=0.5$; $C_{Fe(II)}=1 \cdot 10^{-4}$ and $C_{Gly}=3 \cdot 10^{-3}$ mol/l

№	Dependence of EMF on concentration parameters			Composition of the complexes
	pH	pC _{ox}	pC _L	
1	0	-	-	[Fe(H ₂ O) ₆] ²⁺
2	-v/2	-v/2	-	[Fe(OH)(H ₂ O) ₅] ⁺
3	-v/2	-v/2	v/2	[FeHL(H ₂ O) ₅] ²⁺
4	-v	-v/2	-	[Fe(OH) ₂ (H ₂ O) ₄] ⁰
5	-v	-v/2	v	[Fe(HL)(OH)(H ₂ O) ₄] ⁺
6	-2v	-v/2	v	[Fe ₂ (HL) ₂ (OH) ₂ (H ₂ O) ₈] ²⁺

Calculation of the equilibrium of hydroxyl complexation using the oxidative function involves taking into account all possible equilibria and compiling a stoichiometric matrix of the resulting forms. The general equation for the theoretical oxidative function is as follows:

$$f_T^0 = \frac{C_r}{C_o} \cdot 1 / \left\{ \sum_1^q \sum_0^s \sum_0^l \sum_0^k q \beta_{qslk}^{\frac{1}{q}} G_{qslk}^{\frac{q-1}{q}} [H_s L^{n-}]^{\frac{1}{q}} h^{\frac{-k}{q}} [M^{(z-e)+}]^{\frac{1}{q}} \right\} \quad (3)$$

To derive the general equation of the oxidative function of the studied system based on the resulting complex forms (Table 1), a stoichiometric matrix was compiled, which is given in Table 2.

Table 2. Chemical equilibrium model of the Fe(0)-Fe(II)-glycine-water system at a temperature of 298.15 K; I=0.5; C_{Fe(II)}=1·10⁻⁴ and C_{Gly}=3·10⁻³mol/l

Fe ²⁺ q	H ⁺ s	L ⁻ l	OH ⁻ k	Composition of the complexes	β _{qslk}	Fragments of the equation of the oxidative potential of the system
1	0	0	1	[Fe(OH)(H ₂ O) ₅] ⁺	β ₁₀₀₁	vlg(h ³ +β ₁₀₀₁ h ²)
1	1	1	0	[FeHL(H ₂ O) ₅] ²⁺	β ₁₁₁₀	vlg(h ³ +β ₁₁₁₀ K ₁ C _{a1} h ²)
1	1	1	1	[Fe(HL)(OH)(H ₂ O) ₄] ⁺	β ₁₁₁₁	vlg(h ³ +β ₁₁₁₁ K ₁ C _{a1} h)
2	2	2	2	[Fe ₂ (HL) ₂ (OH) ₂ (H ₂ O) ₈] ²⁺	β ₂₂₂₂	vlg(h ³ +2β ₂₂₂₂ ^{1/2} G ₂₂₂₂ ^{1/2} K ₁ C _{a1} h)
1	0	0	2	[Fe(OH) ₂ (H ₂ O) ₄] ⁰	β ₁₀₀₂	vlg(h ³ +β ₁₀₀₂ h)

Thus, substituting in equation (3) instead of q, s, l and k their numerical values from Table 2, we obtain the corresponding expression in the form of a general equation of the oxidation function, which is given below in the form of a calculated function using the Excel program:

$$=10000/(CUMMΠPOИЗB(D9+H$847*K$837*C9+SS$847*K$837*B9+2*КОРЕНЬ(Y847)*КОРЕНЬ(H879)*K$837*B9+$O$847*B9+$L$847*C9)/D9) \quad (4)$$

Equation (4) is the main expression for the theoretical calculation of formation constants and areas of dominance of hydrolytic forms. The true values of the constants are calculated by iteration by approximating the theoretical oxidation function to the experimental curve. The experimental oxidation function is calculated from the values of the oxidation potential measured on an oxidation meter according to the following expression:

$$f_3^0 = C_r / C_o \exp(E - E^0) n / v \quad (5)$$

In equation (5) the following notations are adopted: *f_{e0}* – experimental oxidative function; *E* is the experimentally measured value of the emf, *E₀* is the value of the standard emf, *n* is the number of electrons participating in the redox reaction, and *v*=2.303 RT/F. The remaining notations are the same as in equation (3).

The values of the experimental oxidative function, calculated according to equation (5), made it possible to construct graphs of the dependence of the oxidative function f_3^0 on pH, and according to expression (4), graphs of the dependence of the theoretical oxidative function on pH were constructed, which are shown in Fig. 4. Since the values of f_3^0 and f_T^0 have number with a decimal base, so these relationships are presented as a logarithmic relationship.

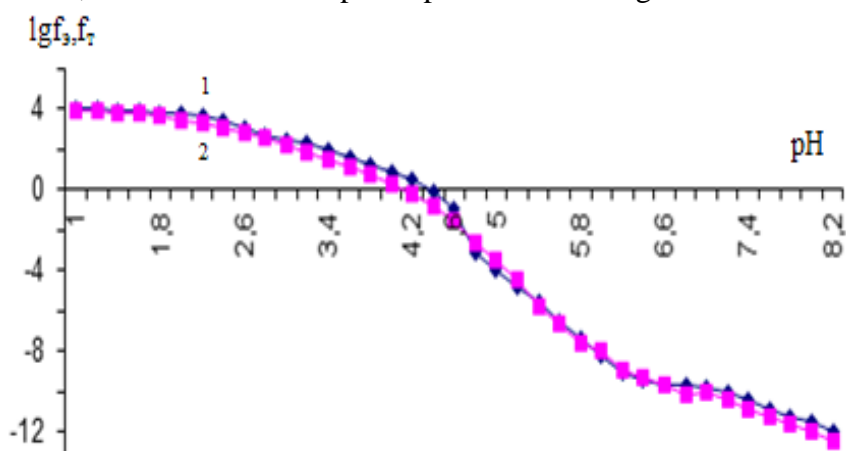


Figure 4. Dependences of the logarithmic values of the experimental - f_3^0 (1) and theoretical - f_T^0 (2) oxidation functions on pH in the Fe(0)-Fe(II)-glycine-water system at a temperature of 298.15 K; $I=0.5$; $C_{Fe(II)}=1 \cdot 10^{-4}$ and $C_{Gly}=3 \cdot 10^{-3}$ mol/l.

With the maximum approximation of the curves of the dependence of f_3^0 and f_T^0 on pH, the true values of the formation constants are found, which are presented in the tables of model parameters (Tables 3 and 4). All calculations and statistical data processing were carried out on a computer using Excel [15].

Table 3. Model parameters of coordination compounds of the Fe(0)-Fe(II)-glycine-water system as a function of pH at temperature: 298.15 K; $I=0.5$; $C_{Fe(II)}=1 \cdot 10^{-4}$ and $C_{Gly}=3 \cdot 10^{-3}$ mol/l

№ π/π	Area of existing comp. on the pH scale	Composition of the complexes	Maximum accumulation rate, α, %	pH	lg const. formation ($lg \beta_{qslk}$)
1	1.0-3.6	$[Fe(OH)(H_2O)_5]^+$	7.48	2.0	-2.46 ± 0.05
2	1.0-4.2	$[FeHL(H_2O)_5]^{2+}$	54.3	2.0	3.32 ± 0.04
3	1.2-4.6	$[Fe(HL)(OH)(H_2O)_4]^+$	85.1	3.6	0.78 ± 0.08
4	2.2-4.4	$[Fe(OH)_2(H_2O)_4]^0$	4.95	3.6	-5.37 ± 0.07
5	3.8-8.2	$[Fe_2(HL)_2(OH)_2(H_2O)_8]^{2+}$	100.0	5.6	10.99 ± 0.06

The calculations end with the determination of the final version of the mole fractions (degrees of accumulation) of complex forms and the construction of their distribution curve (Fig. 5).

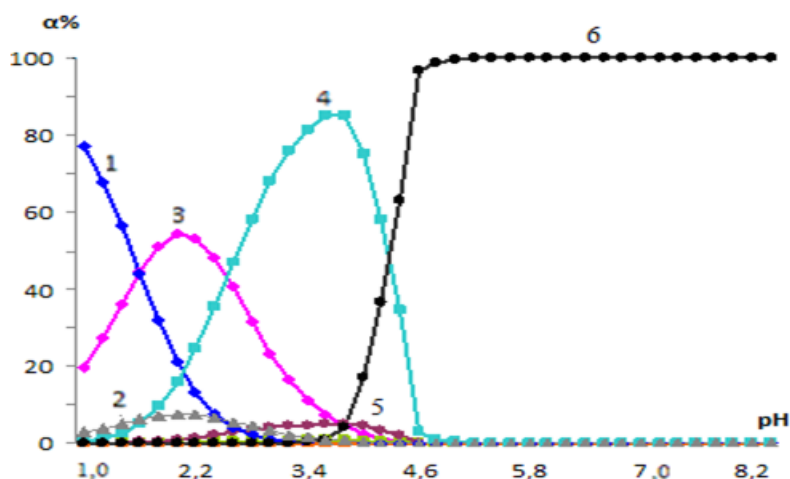


Fig.5. Mass fraction of free Fe(II) ions and its hydroxoforms in the Fe(0)-Fe(II)-glycine-water system at 298.15 K; I=0.5 mol/l. Curves refer to: 1 - $[\text{Fe}(\text{H}_2\text{O})_6]^{2+}$; 2 - $[\text{Fe}(\text{OH})(\text{H}_2\text{O})_5]^+$; 3 - $[\text{FeHL}(\text{H}_2\text{O})_5]^{2+}$; 4 - $[\text{Fe}(\text{HL})(\text{OH})(\text{H}_2\text{O})_4]^+$; 5 - $[\text{Fe}(\text{OH})_2(\text{H}_2\text{O})_4]^0$; 6 - $[\text{Fe}_2(\text{HL})_2(\text{OH})_2(\text{H}_2\text{O})_8]^{2+}$

The calculated equilibrium concentrations of free and bound iron(II) ions in hydroxo complexes are presented in Fig. 5 in the form of the dependence of α on pH. From the above diagram it can be seen that as the pH increases, iron ions gradually bind into compounds that are more complex in composition and stability.

The accuracy of the calculations can be seen from the practical coincidence of the dependences of the experimental and theoretical oxidative functions in the selected pH range (Fig. 4). The agreement between the theoretical and experimental oxidative functions is considered satisfactory if they are within the error of oxidation measurements, i.e. not exceeding $\pm 1-3$ mV. The satisfactory agreement between the experimental and theoretical curves indicates that the composition of hydroxo complexes in the studied system has been established quite accurately.

The greatest scientific interest is in studies of the behavior and mechanisms of formation of hydroxo complexes. In our work, we established the dependences of the content of various hydroxo complexes in a certain environment. Thus, it was determined that in the studied pH range the maximum content of hydroxo complexes is different.

CONCLUSIONS

The experimental results obtained show that in the studied system at the specified temperature, ionic strength of the solution and concentration parameters, coordination compounds of the following composition are formed on a perchlorate background: $[\text{Fe}(\text{OH})(\text{H}_2\text{O})_5]^+$; $[\text{FeHL}(\text{H}_2\text{O})_5]^{2+}$; $[\text{Fe}(\text{HL})(\text{OH})(\text{H}_2\text{O})_4]^+$; $[\text{Fe}(\text{OH})_2(\text{H}_2\text{O})_4]^0$ и $[\text{Fe}_2(\text{HL})_2(\text{OH})_2(\text{H}_2\text{O})_8]^{2+}$.

The first ferrous iron complex $[\text{Fe}(\text{OH})(\text{H}_2\text{O})_5]^+$ begins to form in the acidic region and exists in the pH range from 1.0 to 3.6.

The $[\text{Fe}(\text{OH})_2(\text{H}_2\text{O})_4]^0$ complex exists in the pH range from 2.2 to 4.4. Of all the resulting coordination compounds, its formation constant is minimal ($\log K_{1002} = -5.37 \pm 0.07$), and the maximum degree of accumulation is only 4.95%, therefore, when this complex is isolated from a solution in solid form, the yield of the product will be insignificant.

The complex composition is $[\text{Fe}(\text{HL})(\text{OH})(\text{H}_2\text{O})_4]^+$, one ligand is attached to the central complexing ion. The region of existence is from pH 1.2-4.6 (3.4 pH units), its formation constant is $\lg \beta_{1111} = 0.78 \pm 0.08$, its maximum degree of accumulation is 85.1% at pH 3.6. With such parameters, it is not effective to carry out the directed synthesis of such a complex, since the practical yield will also be insignificant.

The last complex has the composition $[\text{Fe}_2(\text{HL})_2(\text{OH})_2(\text{H}_2\text{O})_8]^{2+}$; two ligands are attached to the central complexing ion. It also has a very long range of existence from pH 3.8-8.2 (4.6 pH units), its formation constant is $\lg \beta_{2222} = 10.99 \pm 0.06$, it is relatively stronger than other complexes,

since when two ligands are added, the probability of the formation of strong coordination compounds of the chelate type increases. Its maximum degree of accumulation is insignificant and is 100% at pH 5.6. This compound can be isolated in the solid state.

Conflict of interest. The authors declare no conflict of interest.

REVIEWER: Suyariyon K.J.
Candidate of Chemical Sciences,
Associate Professor

REFERENCES

1. Rakhimova M. Processes of formation of iron hydroxo complexes in various media / M. Rakhimova, E.F. Faizulloev, M.U. Boboev, M.A. Ismailova // Monograph. – Germany: “LAPLAMBERT”, 2017. – 145 p.
2. Sokolovsky A.E. Hydroxo complex formation in the Fe^{3+} - Hg^{2+} - NO_3^- - H_2O system / A.E. Sokolovsky, E.V. Radion, N.V. Nazarenko // Journal of Applied Chemistry. 2002. - T. 75. No. 11. – Pp.1780-1783.
3. Sokolovsky A.E. Hydroxocomplexation in the Fe^{3+} - Co^{2+} - NO_3^- - H_2O system. Proceedings of BSTU. Ser. 2, Chemistry and technology of inorganic substances. 2021. No. 1 (241). – Pp.35-39 doi.org/10.52065/2520-2669-2021-241-1-35-39
4. Davydov Yu.P. Forms of presence of metal ions (radionuclides) in solution / Yu.P. Davydov, D. Yu. Davydov // Monograph. Minsk: Belaruskaya Nauka, 2011. – P.302.
5. Faizulloev E.F., Hydroxyl complexation of Fe (III) in solutions of various compositions. / E.F. Faizulloev, M.M. Rakhimova, M.A. Ismoilova, Kh.Ch. Kamilov // Bulletin of TNU. Series Natural Sciences. 1/4(153). – Dushanbe: Sino, 2014. – Pp.76 - 81.
6. Davlatshoeva J.A. /J.A. Davlatshoeva, G.B. Eshova, M. Rahimova, M.O. Guriev, L.V. Kvyatkovskaya // American Journal of Chemistry. 2017.7(2). – Pp.58- 65.
7. Rakhimova M. Formation of glycinate complexes of iron(II) in solutions of different ionic strengths / M. Rakhimova, G.B. Eshova, D.A. Davlatshoeva, L.V. Kvyatkovskaya, F. Miraminzoda // Russ. J. Phys. Chem. 2020, 94. – Pp. 1560-1564.
8. Koryakin Yu.V. Pure chemical reagents / Yu.V. Koryakin //M.: Chemistry, 1974. –406 p.
9. Suslennikova V.M., Kiseleva E.K. Guide to the preparation of titrated solutions / V.M. Suslennikova, E.K. Kiseleva // - L.: Chemistry, 1968. – 144 p.
10. Charlot G. Methods of analytical chemistry. Quantitative analysis of inorganic compounds / G. Charlot // - M.: Chemistry, 1965. – 930 p.
11. Yakubov Kh.M. Application of oxometry to the study of complex formation / Kh.M. Yakubov // - Dushanbe, 1966. – 121 p.
12. Pat. TJ 626 (Application No. 1300789 dated June 19, 2013). Bull. No. 97. 27.07. 2014.
13. Zakharyevsky M.S. / M.S. Zakharyevsky, L. Oxedometer measurements // - Chemistry, 1968. – 118 p.
14. Nikolsky B.P. / B.P. Nikolsky, L. Oxredmetry // Chemistry, 1975. – 304 p.
15. Walkenbach D. Formulas in Excel 2013 / D. Walkenbach // - M.: Dialectics, 2019. – 720 p.

FORMATION OF Fe(II) HYDROXYL COMPLEXES IN AQUEOUS SOLUTIONS

Formation of hydroxyl complexes in the Fe(0)-Fe(II)-glycine-water system from pH at $I=0.5$ mol/l, temperature 298.15 K, $C_{\text{Fe(II)}}=1 \cdot 10^{-4}$ and $C_{\text{Gly}}=3 \cdot 10^{-3}$ mol/l were studied by the Clark–Nikolsky oxidative potential method. Experimental curves of the dependence of the EMF of the system on the concentrations of hydrogen, iron(II) and glycine ions: pH, pC_{ox} , pC_{L} , respectively, are obtained. They allowed us to establish that the processes of complexation in the studied system proceed stepwise in a wide pH range from 1.0 to 8.2. The type and number of coordinated ligands and the total composition of the complex compounds formed were determined. Chemical models of complex formation reactions and model parameters of coordination compounds have been compiled. The values of the angular coefficients, the domain of dominance and the constants of the formation of complexes are determined. The formation of the following coordination compounds is shown: $[\text{Fe}(\text{OH})(\text{H}_2\text{O})_5]^+$; $[\text{FeHL}(\text{H}_2\text{O})_5]^{2+}$; $[\text{Fe}(\text{HL})(\text{OH})(\text{H}_2\text{O})_4]^+$; $[\text{Fe}(\text{OH})_2(\text{H}_2\text{O})_4]^0$ and $[\text{Fe}_2(\text{HL})_2(\text{OH})_2(\text{H}_2\text{O})_8]^{2+}$.

Keywords: EMF, complex, iron (II), glycine, model, ionic strength, oxidative function, iteration.

Information about the authors: Eshova Chaykhana Bobonazarovna - Tajik National University, Candidate of Chemical Sciences, senior researcher. Address: 734025, Dushanbe Republic of Tajikistan, Rudaki Avenue, 17. Phone: (+992) 918-23-01-82. E-mail: eshova81@mail.ru.

Davlatshoeva Jahonul Asankhonovna - Tajik National University, Candidate of Chemical Sciences, Associate Professor of the Department of Physical and Colloidal Psychology. Address: 734025, Dushanbe Republic of Tajikistan, Rudaki Avenue, 17. Phone: (+992) 938-98-96-62. E-mail: kfk@mail.ru

Rahimova Mubashirkhan -Tajik National University, Doctor of Chemical Sciences, Professor. Address: 734025, Dushanbe Republic of Tajikistan, Rudaki Avenue, 17. Phone: (+992) 918-76-90-70. E-mail: muboshira09@mail.ru

Miraminzoda Farida - Tajik National University, scientific Centurion. Address: 734025, Dushanbe

Republic of Tajikistan, Rudaki Avenue, 17. **Phone:** (+992) 987-27-18-93. **E-mail:** miraminzoda@mail.ru

Article received 11.10.2023
Approved after review 06.01.024
Accepted for publication 16.03.2024

USE OF BSC AFTER ACID SOLUTION TO DEVELOP THE EXPANSION PROPERTIES OF CEMENT

Rajabov Sh.Kh.

INTRIODOUCTION

Cement is not a natural material. Its production is a costly and energy-intensive process, but as a result, a popular construction material is obtained, which is used both separately and as a component of other construction materials (for example, plastering, concrete and reinforced concrete). [1, p. 102].

The production of cement includes two main stages: the first is the production of clinker, the second is the conversion of clinker to a powdery state and adding gypsum or other additives to it. For the production of cement clinker, it is necessary to make theoretical calculations of the composition of the material mixture. That is, the first level of production is considered to be the most expensive, and approximately 70% of the original cost of the product corresponds to it [2, p. 52].

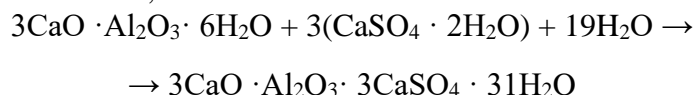
In modern times, the issue of cement production from man-made waste, by-products of the manufacturing industry or secondary mineral sources, which is the subject of research and study in this article, is considered topical [3, p. 28].

The purpose of our research is to reduce the original cost of ready-made cement clinker due to the reduction of the amount of valuable additives, as well as to increase the activity properties of clinker and to produce cement with expansion properties. [4, c. 101].

RESEARCH MATERIAL AND METHOD

During the application of the new technology of acid decomposition of solid wastes of aluminum production for the purpose of production of alumina and other fluorine salts, a large amount of solid calcium sulfate residue (calcium sulfate residue) remains as waste. The use of this type of waste in cement production is considered not only economically wise technology, but also a way to solve the environmental problem caused by the accumulation of aluminum production waste [5, p. 11].

Many adhesives develop a collapsing surface during curing. This situation can be solved by using expanding cements, which number approximately 48 types. In most cases, the expansion during the hardening of cement stone is explained by the formation of calcium hydrosulfoaluminate (CAH), the volume of which is much greater than the volume of the initial materials of the reaction product [6, p. 97]. The production of GSAK takes place in a system containing calcium aluminate (according to the general formula $n\text{CaO} \cdot m\text{Al}_2\text{O}_3$) and CaSO_4 in the presence of water. Such substances are especially found in Portland cement [7, p. 3]. During the hydration of portland cement, HSAC occurs with the transition of the following reaction:



The amount of GSAK in the composition of ordinary cement is insufficient for expansion. In order to produce it, it is necessary to add to the composition of cement an expanding additive containing insufficient amount of ingredients (calcium - CaO , aluminate - Al_2O_3 and sulfate - CaSO_4) in the required amount and in a certain ratio. Additives are made in different ways. As a component of calcium sulfate CaSO_4 , usually natural gypsum, some type of anhydrite or secondary products of some productions are taken [8, p. 845].

By cooking a mixture consisting of three materials (clay, limestone and gypsum), they obtain a product consisting of calcium sulfoaluminate ($3\text{CaO} \cdot 3\text{Al}_2\text{O}_3 \cdot \text{CaSO}_4$). Based on it, it is possible to make an expanding additive and an expanding cement. Often, an additive is used in the material mixture in order to produce expanded cement clinker. Depending on the degree of

expansion, cements are divided into non-shrinkable, expandable and hard (tensile) types. The last type has the highest expansion energy and can absorb the reinforcement and add additional tension to the concrete [9, c. 45].

RESULTS AND DISCUSSION

The purpose of the proposed research - the method of production of cement clinker using BSK - waste is to first calculate the raw ingredients, prepare the mixture by combining the raw ingredients in the mill, cooking in a rotating ball, cooling the clinker, dusting and adding activator plaster to amount is 3% [10, p. 203].

The assigned task will be achieved when the material mixture is calculated first, which is one of the most important conditions for the production of clinker with the given characteristics. The calculation of the material mixture is based on the determination of the ratio between the components, the chemical composition of the material and the given characteristics of the clinker [11, p. 47].

The composition and properties of Portland cement clinker are determined by the following indicators:

- chemical composition of clinker;
- indication of saturation coefficient and modules;

According to GOST, the saturation coefficient KS (saturation coefficient KH) is in the range of 0.8-0.95, silicate module $n = 1.7-3.5$, and clay module $p=1.0-3.0$.

During the preparation of portland cement (PS), according to the proposed research, a mixture of three components is made [12, p. 58]. Limestone, kaolin clay and BSK waste are used as the main materials, and plaster is added to regulate its hardening rate [13, p. 43].

The chemical composition of consumables is presented in Table 1.

Consumables	Chemical composition with %								Σ
	SiO ₂	Al ₂ O ₃	Fe ₂ O ₃	CaO	MgO	SO ₃	Изофа	Т.з.т	
Limestone	1,21	0,67	0,49	53,8	1,20	0,22	0,16	42,18	100
Clay	73,6	13,9	4,31	2,65	1,41	0,19	1,28	2,66	100
BSC waste	0,25	1,26	13,5	32,3	0,55	41,8	1,12	9,19	100

Table 1. Chemical composition of the components of the heated material and brought to 100%.

In order to perform the calculation of a three-component material mixture, we need to know the chemical composition of the material components and determine the magnitude of KS. We accept limestone, clay and BSC as waste materials [14, p. 101]. It is given: $KH = 0,92$.

$$\begin{aligned}
 a_1 &= C_1 - 2,8 \cdot S_1 \cdot KH - 1,65 \cdot A_1 - 0,35 F_1 \\
 b_1 &= C_2 - 2,8 \cdot S_2 \cdot KH - 1,65 \cdot A_2 - 0,35 F_2 \\
 c_1 &= 2,8 \cdot S_3 \cdot KH + 1,65 \cdot A_3 + 0,35 \cdot F_3 - C_3
 \end{aligned} \tag{1}$$

$$\begin{aligned}
 a_1 &= 53,8 - 2,8 \cdot 1,21 \cdot 0,92 - 1,65 \cdot 0,67 - 0,35 \cdot 0,49 = 49,42; \\
 b_1 &= 2,65 - 2,8 \cdot 73,6 \cdot 0,92 - 1,65 \cdot 13,9 - 0,35 \cdot 4,31 = -211,4; \\
 c_1 &= 2,8 \cdot 0,25 \cdot 0,92 + 1,65 \cdot 1,26 + 0,35 \cdot 13,5 - 32,3 = -24,83.
 \end{aligned}$$

$$\begin{aligned}
 a_2 &= n (A_1 + F_1) - S_1 \\
 b_2 &= n (A_2 + F_2) - S_2 \\
 c_2 &= S_3 - n (A_3 + F_3).
 \end{aligned} \tag{2}$$

$$\begin{aligned}
 a_2 &= 2,2(0,67+0,49) - 1,21 = 1,34; \\
 b_2 &= 2,2(13,9 + 4,31) - 73,6 = -33,5; \\
 c_2 &= 0,25 - 2,2 (1,26+13,5) = -32,2.
 \end{aligned}$$

We determine the ratio between the components:

$$x = \frac{c_1 b_2 - c_2 b_1}{a_1 b_2 - a_2 b_1} = \frac{(-24,8) \cdot (-33,5) - (-32,2) \cdot (-211,4)}{49,4 \cdot (-33,5) - 1,34 \cdot (-211,4)} = 4,36 \quad (3)$$

$$y = \frac{a_1 c_2 - a_2 c_1}{a_1 b_2 - a_2 b_1} = \frac{49,4 \cdot (-32,2) - 1,34 \cdot (-24,8)}{49,4 \cdot (-33,5) - 1,34 \cdot (-211,4)} = 1,14$$

Therefore, 4.36 parts of limestone and 1.14 parts of kaolin clay correspond to 1 part of remaining calcium sulfate in the material mixture. It is a percentage:

$$\text{Известняк} = \frac{x \cdot 100}{x + y + 1} = \frac{4,36 \cdot 100}{4,36 + 1,14 + 1} = 67,1\%$$

$$\text{Глина} = \frac{y \cdot 100}{x + y + 1} = \frac{1,14 \cdot 100}{4,36 + 1,14 + 1} = 17,5\%$$

$$\text{Отходы СКО} = \frac{1 \cdot 100}{x + y + 1} = \frac{1 \cdot 100}{4,36 + 1,14 + 1} = 15,4\% \quad (4)$$

With the same sample, the chemical composition of clinker is calculated, and during the calculation of the material mixture, it is preliminarily brought to the heated state of the substance [15, p. 126]. The result of the theoretical calculation of the chemical composition of the mixture of materials and clinker is presented in Table 2.

Table 2. The result of the theoretical calculation of the chemical composition of the mixture of materials and clinker

Consumables	Chemical composition, %								
	SiO ₂	Al ₂ O ₃	Fe ₂ O ₃	CaO	MgO	SO ₃	Изофа	Т.з.т	Чамъ
Limestone	0,81	0,45	0,33	36,1	0,81	0,15	0,11	28,3	67,1
Clay	12,9	2,43	0,75	0,46	0,25	0,03	0,22	0,47	17,5
BSC waste	0,04	0,19	2,08	4,97	0,08	6,44	0,17	1,41	15,4
Material mixture	13,8	3,07	3,16	41,5	1,14	6,62	0,5	30,18	100
Clinker $K = \frac{100}{100 - 30,2} = 1,43$	19,7	4,39	4,52	59,3	1,63	9,47	0,72	-	100

The calculation of the chemical composition of clinker is carried out when the chemical composition of the mixture of substances is known, without taking into account the loss during heating, TFT, and for this the following quantity is determined:

$$K = \frac{100}{100 - \text{ППП}} = \frac{100}{100 - 30,2} = 1,43, \quad (5)$$

Then we multiply it by the share of each oxide in the mixture of substances. So the amount of these oxides in the clinker composition is as follows:

$$\text{CaO} = 1,43 \cdot 41,5 = 59,3\%;$$

$$\text{SiO}_2 = 1,43 \cdot 13,8 = 19,7\%;$$

$$\text{Al}_2\text{O}_3 = 1,43 \cdot 3,07 = 4,39\%;$$

Similarly, we calculate the chemical composition of the rest and find the chemical composition of clinker with (%):

SiO ₂	Al ₂ O ₃	Fe ₂ O ₃	CaO	MgO	SO ₃	Изофахо
19,7	4,39	4,52	59,3	1,63	9,47	0,72

We determine the modules of the clinker composition:

$$KH = \frac{CaO - (1,65Al_2O_3 + 0,35Fe_2O_3)}{2,8SiO_2}$$

$$KH = \frac{59,1 \cdot (1,65 \cdot 4,39 + 0,35 \cdot 4,52)}{2,8 \cdot 19,7} = 0,92 \quad (6)$$

$$n = \frac{SiO_2}{Al_2O_3 + Fe_2O_3}$$

$$n = \frac{19,7}{4,39 + 4,52} = 2,2 \quad (7)$$

$$p = \frac{Al_2O_3}{Fe_2O_3}$$

$$p = \frac{4,39}{4,52} = 0,97 \quad (8)$$

Correspondence of the magnitude of KS (KN), silicate module n and clay module p with the given values confirms the correctness of the calculations [16, p. 155].

Based on the calculations, the percentage ratio of the material mixture was determined: limestone - 67.1%; clay - 17.7%, BSC - waste - 15.4%.

We put the prepared material mixture in the amount of 20-30 grams into a refractory corundum crucible. We covered the sample crucible with a cover made of refractory material, then placed it in a muffle test ball and kept it at a temperature of 1120-11800C for 60 minutes. We measured the temperature in the sphere using a platinum thermocouple. After isothermal storage, we remove the crucible with the sample from the sphere and cool it in laboratory conditions [17, p. 235].

After cooling, the clinker sample is crushed and pulverized, up to 3% of gypsum is added to the crushed product, it is well mixed, and expanding cement is produced. Sample cubes with dimensions of 50X50X50mm were made from the resulting expanding cement and tested for determination of strength during compression and 40X40X120mm for determination of strength during termination. We conducted a test analysis of the produced portland cement in a PSU-10 hydraulic press. When determining the strength gap during compression, the manometer reading at the sample failure point P is recorded and divided by the surface area of the piston S according to this formula:

$$R_{ок} = \frac{P}{S} \text{ кгс/см}^2; \quad (9)$$

We also implemented the strength gap during sample termination in the same way as the determination during compression. The strength gap during termination is calculated according to the following formula:

$$R_{u32} = \frac{Pl}{bh^2} \text{ кгс/см}^2; \quad (10)$$

where P is the weight of the breaker, kgs; l – distance between columns, cm; b – sample width, cm; h – sample thickness, cm [18, p. 11]. The obtained results confirm that the addition of up to 15.4% of BSC waste improves the crushing properties of clinker and the strength indicators of cement, while maintaining its expansion property at the required level. Table 3., [19, c. 263].

Table 3. The result of testing cement samples for strength during compression and termination in a hydraulic clamp of the PSU brand-10.

List of indicators	1 м/р	3 м/р	7 м/р	25 м/р	30 м/р
Strength during compression, MPa	27,3	30,1	31,7	47,1	47,4
Strength during termination, MPa	4,5	5,2	6,3	7,5	7,6

Based on the results of the research, the principle and technological plan for the use of residual waste containing calcium sulfate as a raw material in the production of cement is shown in Figure 7.

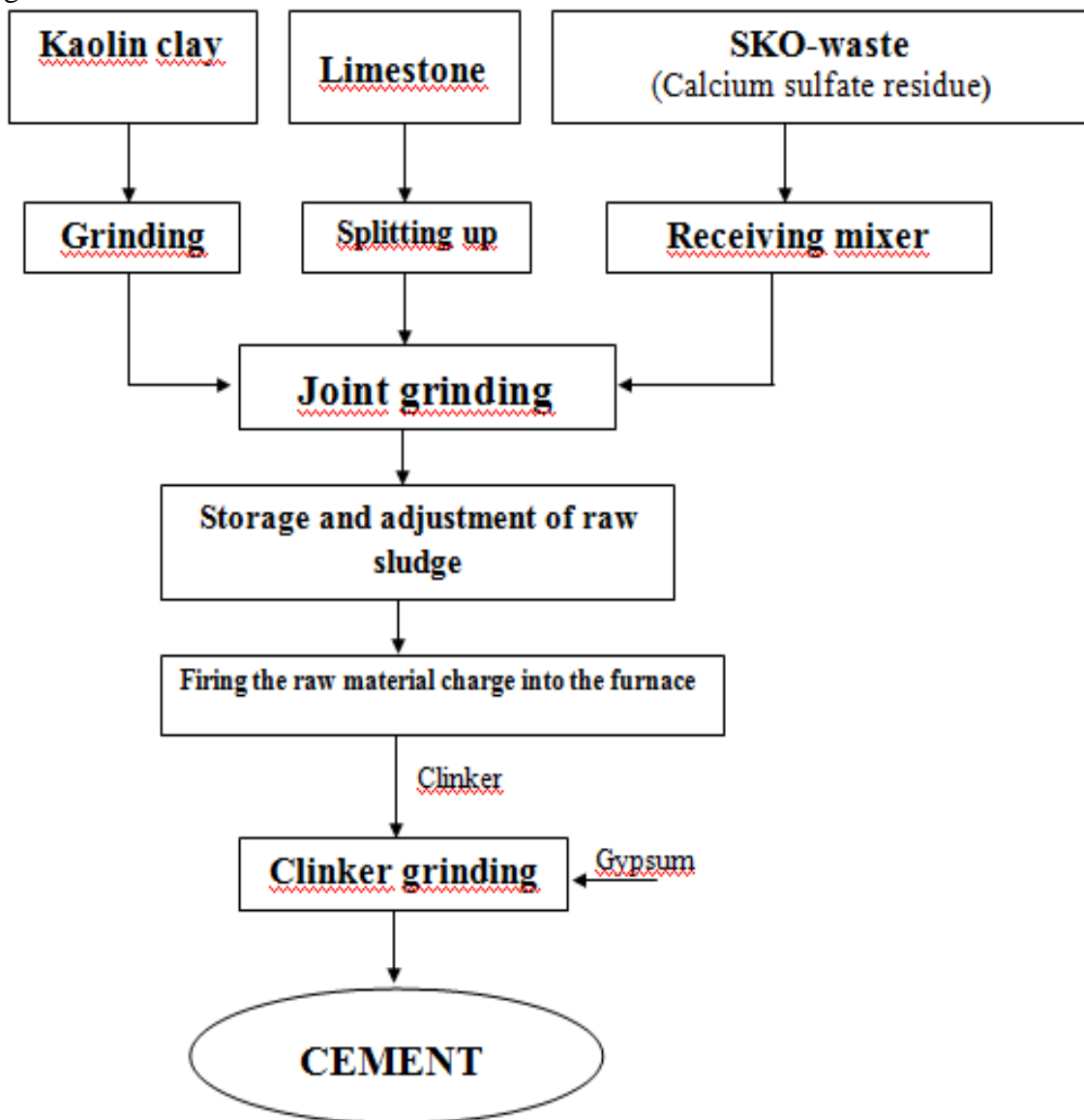


Fig. 1. The principle and technological scheme of the use of residual waste containing calcium sulfate as a raw material in the production of cement

Conclusion. When cooking a mixture consisting of 3 materials (clay, limestone and BSC - waste) an expanding cement product is produced. The use of BSK-waste in the production of cement is not only economically a smart technology, but also one of the ways to solve environmental problems during the storage of waste in aluminum production. [20, p. 406]. For this purpose, first of all, the raw ingredients are calculated, the mixture is prepared by grinding in a mill, cooked in a rotating ball, then flour is made, and gypsum is added as an activating additive in the amount of up to 3%.

**REVIEWER: Samihov Sh.R.,
Doctor of Natural Sciences,
Professor**

REFERENCES

1. But Yu. M. Chemical technology of binders. – M. / Yu.M. Booth, M.M. Sychev, V.V. Timashev // Higher school, 1980. – P. 472.
2. Volzhensky A.V. Mineral binders / A.V. Volzhensky // – M.: Stroyizdat, 1986. – P.463.
3. Lotov V.A. Composition, properties of cement raw materials, production and properties of Portland cement clinker / V.A. Lotov // Guidelines for laboratory workshops and independent work on the course “Cement Technology”. – Tomsk: Publishing house. TPU, 2006. – 32 p.
4. Palgunov P.P. Recycling of industrial waste / P.P. Palgunov, M.V. Sumarokov // – M.: Stroyizdat, 1990. – P. 346.
5. Kikava O.Sh. Construction materials from industrial waste - “Ecology and Industry of Russia”. / Kikava O.Sh. // - 12 - 1997. – Pp.23-28.
6. Galevsky G.V. Ecology and waste disposal in aluminum production. / G.V. Galevsky, N.M. Kulagin, M.Ya. Mintsis // - M.: Nauka, 2005. – P. 272.
7. Kabirov Sh.O. A method for complex processing of solid fluorine-containing waste from aluminum production. Small patent for invention No. 515 / Sh.O. Kabirov, Kh.S. Safiev, N.M. Sirochov, B.S. Azizov, Kh.A. Mirpochaev, D.R. Ruziev, N.P. Mukhamediev, Kh.E. Boboev, Sh.Kh. Radjabov // – Dushanbe, 2012.
8. Safiev Kh. Technology for producing cryolite and aluminum fluoride from alumina- and fluorine-containing waste from aluminum production / Sh.O. Kabirov, Kh.S. Safiev, N.M. Sirochov, B.S. Azizov, Kh.A. Mirpochaev, D.R. Ruziev, N.P. Mukhamediev, Kh.E. Boboev, Sh.Kh. Radzhabov // DAN of the Republic of Tajikistan. – Dushanbe, 2011. - T.54. - No. 10. – Pp.845-850.
9. Istomin, S.P. New directions in the technology of processing highly dispersed fluorine-containing waste from aluminum production. / S.P. Istomin, B.P. Kurikov, S.G. Myasnikova // Non-ferrous metals. - 1999.- No. 3. – Pp.45-47.
10. Sulimenko, L.M. Technology of mineral binding materials and products based on them: textbook. for universities. – 4th ed., revised. and additional / L.M. Sulimenko // – M.: Higher. school 2005. – P. 334.
11. Yakovets Yu.S., Recycling of aluminum waste / Yu.S. Yakovets, A.V. Nifantieva // Young scientist, 2020. - No. 11 (41). – Pp.46-49.
12. Istomin S.P. Study of the flotation method for producing cryolite. / S.P. Istomin, S.G. Myasnikova // Non-ferrous metals. - 1999. - No 3. – Pp.56-58.
13. Rakov E.G. Chemistry and technology of inorganic fluorides / Rakov E.G. // -M.: Publishing house MHTI im. DI. Mendeleeva, 1990. – P. 162.
14. Sulimenko L.M. Technologies of mineral binders and products based on them / L.M. Sulimenko // Textbook. for universities. – 3rd ed., revised. and additional. – M.: Higher. School, 2000. – P. 302.
15. Kulikov B.P. Recycling of aluminum production waste. / B.P. Kulikov // Istomin 2nd ed. – Krasnoyarsk, 2004. – P. 480.
16. Azizov B.S., Technology for processing the solid residue formed during the sulfuric acid decomposition of alumina- and fluorine-containing waste from aluminum production. / B.S. Azizov, Sh.O. Kabirov, D. R. Ruziev, A. Kh. Safiev, Sh. Kh. Radzhabov // DAN of the Republic of Tajikistan. – Dushanbe, - 2015, vol. 58, No. 2. – Pp.153-160.
17. Rajabov Sh.Kh., Application of secondary solid waste after acid decomposition as an active mineral additive. / Sh.H. Rajabov, A.S. Faizulloev. // Materials of the II International Scientific and Practical Conference of TNU. Modern problems of chemistry, application and their prospects: Dushanbe - May 14-15, 2021. – Pp.234-242.
18. Rajabov Sh.Kh. Application of secondary solid waste after acid decomposition as an active mineral additive. / Sh.H. Rajabov // Bulletin of Dangara State University. Series No. 4 (18) 2022. – Pp.6-14
19. Rajabov Sh.Kh. Studying the process of joint acid decomposition of fluorite concentrate and fluorine-containing waste from aluminum production. // Materials of the international scientific and practical conference “The use of modern teaching methods in educational institutions: Problems and prospects”, dedicated to the “2020-2040 years of the twentieth anniversary of the study of natural, exact and mathematical sciences in the field of science and education”, “65th anniversary of the Faculty of Chemistry of TNU ” and “55th anniversary of the Department of

Methods of Teaching Chemistry of the Faculty of Chemistry of TNU." / Sh.H. Rajabov // Dushanbe October 19-20, 2023. – Pp.262-269.

20. Rajabov Sh.Kh. The use of calcium sulfate containing aluminum production waste as an active mineral additive to Portland cement. // Materials of the international scientific and practical conference on the topic "Development of natural, exact and mathematical sciences in the present time: problems and prospects. / Sh.H. Rajabov // Dangara State University April 28 – 29, 2023: - "Mulkvar". – Pp. 405-410.

USE OF BSC AFTER ACID SOLUTION TO DEVELOP THE EXPANSION PROPERTIES OF CEMENT

Currently, the issue of obtaining cement from technogenic, by-products of industrial production or secondary mineral resources has become relevant. When introducing a new technology for sulfuric acid decomposition of solid waste from aluminum production in order to obtain secondary alumina and fluorine salts, a large amount of calcium sulfate-containing residue as tailings is formed. The use of these residues in cement production is not only an economically viable technology, but also a method for solving environmental problems that arise when storing aluminum production waste. The main goal of the study is to reduce the cost of producing cement clinker by reducing the amount of expensive additives and the use of SKO, as well as increasing the activity of clinker and obtaining expansive cement. The proposed composition of clinker and the method of producing cement based on it differ from the known one in that the raw material mixture is made up of 3 components and CKO waste is used as an active mineralizer. It has been established that during physical and mechanical testing, the resulting Portland cement is characterized by fairly high strength characteristics both in compression and in bending after 30 days.

Key words: cement, clinker, research, production, production, waste, SKO - waste, raw material mixture, expanding cement, compression, bending.

Information about the author: **Rajabov Shukhrat Kholmurodovich** – Tajik National University, candidate of technical sciences, associate professor of the department of chemical production technology. **Address:** 734025, Dushanbe, Republic of Tajikistan, Rudaki Avenue, 17. **Phone:** (+992) 555-22-11-85. **E-mail:** R.Shuhrat.Kh@mail.ru.

Article received 26.11.2023
Approved after review 30.01.2024
Accepted for publication 08.04.2024

COMPLEXATION OF IRON(III) WITH TSC AND FTSC IN H₂SO₄ SOLUTIONS OF VARIABLE COMPOSITION

Bobokalonov T.B., Hakimov F.Kh., Safarmamadzoda S.M.,

Mamadgaminova Z.R.

INTRODUCTION

Among the bioelements important for life, iron plays a dominant role as an activator of many catalytic processes in the body and is involved in the transport of gases in the blood. The hemoglobin molecule consists of the protein part of globin and heme, which is a Fe(II) complex with one of the porphyrins, the so-called protoporphyrin-IX. In this compound, the iron atom forms two covalent and two coordination bonds with the nitrogen atoms. The potential of complexation with iron(III) ions as a way to expand the spectrum of action of known drugs has been noted in many works, including thiosemicarbazones, which exhibit high biological activity and are widely used in medical practice. Thiosemicarbazide, in particular, is widely used in pharmacological practice as a convulsant.

In [1], the influence of diantipyrylmethane (DPM) and its homologues diantipyrylpropylmethane (DAPM) and diantipyrylphenylmethane (DAPPM) on the complexation of iron(III) with bis-(2,3,4-trihydroxyphenylazo)benzidine is discussed, and the optimal conditions for the formation of mixed-ligand complexes are found. The molar absorption coefficients and stability constants of iron(III) complexes were determined, and the influence of foreign ions and masking substances on complex formation was studied. In [2], the complexation of iron(III) with 3,4-dihydroxybenzoic acid (3,4-DHB, H₃L) in a wide range of pH and reagent concentrations was studied by electron spectroscopy and nuclear magnetic relaxation. The stability constant of the monoligand complex [FeL], in which rapid oxidation of the ligand by the central atom occurs, has been calculated. It was shown that, as in the case of other bidentate aromatic ligands, [FeL₂] and [FeL₃] complexes are also formed. According to the data obtained, iron(III) does not form polynuclear complexes with 3,4-DHB in aqueous solution. The existence of three complex compounds of iron(III) with 3,4-DHB of the metal composition: ligand – 1:1, 1:2, and 1:3 is shown, for which the spectral parameters (λ_{\max} , ϵ_{λ}), relaxation efficiency coefficients, and constants are determined sustainability. In [3], studies were carried out on the complexing ability of flotation reagents in relation to iron(II). The stability constants and thermodynamic parameters of complexes of sodium dialkyl diphosphates with iron(II) ions were determined, as well as temperature-dependent and temperature-independent characteristics of complexation reactions. The authors of [4] studied the complexation of iron (III) with salicylic acid (SA) and diphenylguanidine (DPG) in aqueous-organic solutions. It has been established that in this system there is an interaction between the individual components: Fe (III) – SA and Fe (III) – DPG. The optimal conditions for complex formation between iron (III), SA, and DPG in aqueous-acetone and aqueous-ethanol solutions were determined. It has been shown that the stability of complexes in water-ethanol solutions is higher than in water-acetone solutions. Iron trimethylacetate complexes with various ligands were studied by X-ray photoelectron spectroscopy (XPS) in [5]. The photoelectron spectra of Fe2p, Fe3p, O1s, and N1s were analyzed with the sequential replacement of Fe → O coordination bonds by Fe → N. In the X-ray photoelectron spectra of trimethyl acetate iron complexes, a satellite component was determined, indicating the high-spin state of the Fe(II) and Fe(III) atoms. The XPS results made it possible to determine the measure of covalency of the metal-ligand bond and identify two nonequivalent states for iron atoms. The authors of [6] managed to obtain an iron(III) complex with an asymmetric tridentate azomethine ligand 4,4-dodecyloxybenzoyloxybenzoyl – 4 – salicylidene - N' - ethyl - N – ethylenediamine, containing the counterion PF₆⁻. It has been established that the complexation reaction of an iron(III) salt with an asymmetric tridentate ligand leads to the formation of a 1:1 compound in an

octahedral complex. The EPR method has shown that iron(III) ions in the complex are in both low-spin (LS) and high-spin (HS) states. The NS and BC centers of iron(III) form a dimeric structure in which a water molecule and the PF₆⁻ counterion act as connecting bridges. It was found that for NS complexes located in the low-temperature phase (4.2 – 300 K), the state (dxz, dyz)₄(dxy)₁ is the ground state. It has been established that the transfer of a sample into a high-temperature, liquid-crystalline (387 – 405 K) phase is accompanied by a switching of NS electronic configurations (dxz, dyz)₄(dxy)₁ ↔ (dxy)₂(dxz, dyz)₃, reversible in temperature.

The study [7] presents results on the synthesis and investigation of new iron(III) complexes formed by the interaction of FeCl₃ with N-hydroxysuccinimide at varying ratios of the initial reagents (1:1, 1:2, and 1:3). Various physicochemical methods, including mass spectrometry, derivatography, IR spectroscopy, Mössbauer spectroscopy, and X-ray diffraction, were used to study, identify, and characterize the composition and structure of the synthesized complexes. The compounds obtained were tested in leather processing technology. By reacting an ethanol solution of semicarbazide hydrochloride, benzaldehyde, and morpholine, N-(1-morpholinobenzyl) semicarbazide Schiff base was synthesized [8]. Manganese (II) and iron (II) complexes were synthesized in ethanol solutions of Schiff base with metal (II) chloride, respectively. Gravimetry, spectrophotometry, potentiometry, molar conductivity, and IR spectroscopic analysis characterized the resulting complexes. It was found that the Schiff base and complex compounds are insoluble in water, soluble in most known organic solvents, but readily soluble in methanol and ethanol. The molar conductivity of manganese (II) and iron (II) complexes was determined as 3.78 and 6.90 Ohm⁻¹ cm²mol⁻¹, respectively, indicating their non-electrolytic nature. Potentiometric studies showed pK_a=5.40 for the Schiff base. The standard Gibbs free energies of Mn(II) and Fe(II) were determined as -65.79 kJ/mol⁻¹ and -60.35 kJ/mol⁻¹, respectively. The ratio of the starting reagents for complex compounds, determined potentiometrically and spectrophotometrically, was found to be 1:2. Examination of the IR spectrum of a Schiff base revealed band changes, indicating coordination of the Schiff base with metal ions.

The structure and composition of iron(III) salicylate complexes in ethanol were determined in [9]. UV spectroscopy, NMR measurements, the is molar series method, and thermal analysis were used to establish the compositions of the complexes in ethanol and in the solid state. The interaction of salicylic acid with iron(III) chloride in an ethanol solution led to the formation of a complex with the composition [FeC₆H₄OCOO]⁺. The salicylic ligand coordinated as a bidentate ligand. Thermal decomposition of the complex resulted in the formation of a compound of composition α-Fe₂O₃.

The work [10] presents data on the complexation of urea (U) with manganese (II), cobalt(II), iron(III), and copper(II) ions at different temperatures. Elemental analysis, magnetic sensitivity, conductivity measurements, infrared and thermal analysis (TG/DTG), scanning electron microscope (SEM), energy dispersive X-ray spectroscopy (EDX), and powder X-ray diffraction (XRD) were used to study the composition and structure of coordination compounds. The resulting complexes showed high molar conductivity, indicating their electrolytic nature. Antimicrobial activity against bacteria (*Escherichia Coli*, *Staphylococcus Aureus*, *Bacillus subtilis*, and *Pseudomonas aeruginosa*) and fungi (*Aspergillus Flavus* and *Candida Albicans*) was studied, demonstrating high efficiency. In [11], the authors synthesized a new picolinate-iron(III) compound, Fe(C₆H₄NO₂)₂(OH), from an aqueous solution of the picolinate-iron(II) complex. The compound was obtained by heat treatment of picolinate iron complexes from an aqueous solution at pH=3-7. In [12], complex compounds of Cu(II), Ni(II), Zn(II), Co(II), Mn(II), Fe(III), and Cr(III) with N4-(7'-chloroquinoline-4'-ylamino)-N1-(2-hydroxybenzylidene) thiosemicarbazone (HL) were obtained. IR spectroscopic and biological studies of the resulting complexes were carried out. The structures of the complexes were determined based on elemental analysis, spectroscopic data (IR, electron, ¹H and ¹³C NMR, and mass spectra), measurements of magnetic susceptibility, molar conductivity, and thermogravimetric analysis. The study of the electrical conductivity of solutions of the complexes showed the non-electrolytic nature of the complexes. The resulting complexes were shown to be mononuclear, with one ligand involved in

coordination with each metal atom. The connection was carried out through the sulfur atom of the thionic group, and azomethine nitrogen and phenolic oxygen also participated in the formation of mononuclear complexes, where thiosemicarbazone behaved as a monobasic tridentate ligand.

Coordination compounds of copper(II), nickel(II), cobalt(III), zinc(II), and iron(III) salicylates with thiosemicarbazide were studied in [13]. Elemental analysis, infrared spectroscopy, diffuse reflectance spectroscopy, and thermogravimetry characterized the resulting compounds. In [14], iron(III) complexes with a Schiff base were obtained with compositions $[\text{Fe}(\text{tsc-py})_2](\text{NO}_3)$ (1), $[\text{Fe}(\text{tsc-acpy})_2](\text{NO}_3)$ (2), and $[\text{Fe}(\text{tsc-VB}_6)_2](\text{NO}_3)$ (3), where tsc-py, tsc-acpy, and tsc-VB₆ are the corresponding Schiff bases derived from thiosemicarbazide (tsc) and pyridine-2-aldehyde (tsc-py), 2-acetylpyridine (tsc-acpy), and vitamin B6 (pyridoxal, tsc-VB6). The complexes were structurally characterized, and their photocytotoxicity was studied on HeLa cancer cells. X-ray structures of single crystals of complexes 1 and 2 showed a distorted octahedral geometry formed by the FeN₄S₂ core. Complexes 1 and 2 without the VB₆ fragment were not cytotoxic under light or dark conditions. Complex 3, however, exhibited significantly more photocytotoxicity in visible light (400-700 nm), likely resulting from its superior photosensitizing properties combined with increased uptake into cancer cells via VB₆ diffusive transport.

According to the literature, considering the hydrolysis of the iron(III) compound, complexation is recommended to be carried out in an acidic medium at an H₂SO₄ concentration of 0.1 mol/l or higher. At pH>7, iron(III) undergoes hydrolysis and is reduced to iron(II). Changes in the concentration of H₂SO₄ affect both the nature of complex formation and the stability of the resulting complexes. In [15], the authors studied the process of complexation of molybdenum(V) with 1,2,4-triazolethiol in a medium of 6 mol/l HCl at a temperature of 298 K. Using the Bjerrum method, the values of stepwise

Stability constants were determined, and the areas of dominance and the maximum yield of complexes and the resulting compounds were assessed in the system (NH₄)₂[MoOCl₅] - 1,2,4-triazolethiol. The studies established that the interaction of (NH₄)₂[MoOCl₅] with 1,2,4-triazole in a solution of 6 mol/l HCl produces complex particles containing from one to five coordinated molecules of 1,2,4-triazolethiol. In works [16-17], complex formation of iron(III) with thiosemicarbazide and 1-formyl-3-thiosemicarbazide in a 0.1 mol/l H₂SO₄ solution was studied. It was established that iron(III) forms three complex particles with thiosemicarbazide and two with 1-formyl-3-thiosemicarbazide. Stability constants and thermodynamic characteristics of the resulting complexes were calculated.

This work presents the results of a study on the complexation of iron(III) with thiosemicarbazide and 1-formyl-3-thiosemicarbazide in H₂SO₄ solutions with concentrations of 0.5, 1.0, and 2.0 mol/l and discusses the influence of the solution composition on the thermodynamic characteristics of the complexation reaction.

EXPERIMENTAL PART

The starting compounds, Fe₂(SO₄)₃·9H₂O and FeSO₄·7H₂O, obtained as per the methods described in [18], were utilized in this study. TSC-grade "T" underwent recrystallization from an aqueous solution, while FTSC was obtained following the procedure outlined in [19]. H₂SO₄ solutions of different concentrations were prepared from fixanals. A galvanic cell without transfer was employed for potentiometric titration, with the Fe(III)/Fe(II) redox system serving as the indicator electrode and a silver chloride reference electrode. Titrants comprised acidic solutions of corresponding ligands. System potential during potentiometric titration was monitored using a digital pH meter pH-150MP (E=±0.1). Each temperature-specific potentiometric titration was performed four times, with the equilibrium potential value on the indicator electrode stabilizing within 5-7 minutes. The cell's temperature was maintained constant by a water thermostat (± 0.5°C).

The equilibrium concentration of iron(III) ion was determined using the equation [20]:

$$\lg [\text{Fe}^{3+}] = \lg C_{\text{Fe}^{3+}} - \frac{\Delta E}{1,985 \cdot 10^{-4} \cdot T}$$

where: $[Fe^{3+}]$ – equilibrium concentration of iron ions at each titration point, mol/l; $\Delta E = E1 - E2$; $E1$ – initial potential of the system, mV; $E2$ – system potential at each titration point, mV; $C_{Fe^{3+}}$ is the concentration of iron (III) at each titration point taking into account dilution, mol/l; T -temperature, K. The equilibrium concentration of organic ligands $[L]$ was calculated using the equation, Leden: where: CL is the ligand concentration at each titration point taking into account dilution, mol/l; n is the amount of organic ligand attached to the metal; All calculations to determine and clarify the stability constants, as well as the mole fractions of complex particles formed in the solution, were carried out on a Pentium-4 computer using the Exce program.

RESULTS

The amount of particles formed during the interaction of iron(III) with TSC and FTSC was determined according to the method described in [21]. Figures 1 and 2 show the dependences of ΔE on $-\log[L]$ for thiosemicarbazide and 1-formyl-3-thiosemicarbazide complexes of iron(III) in H_2SO_4 solutions of various concentrations (0.5, 1.0 and 2.0 mol/l).

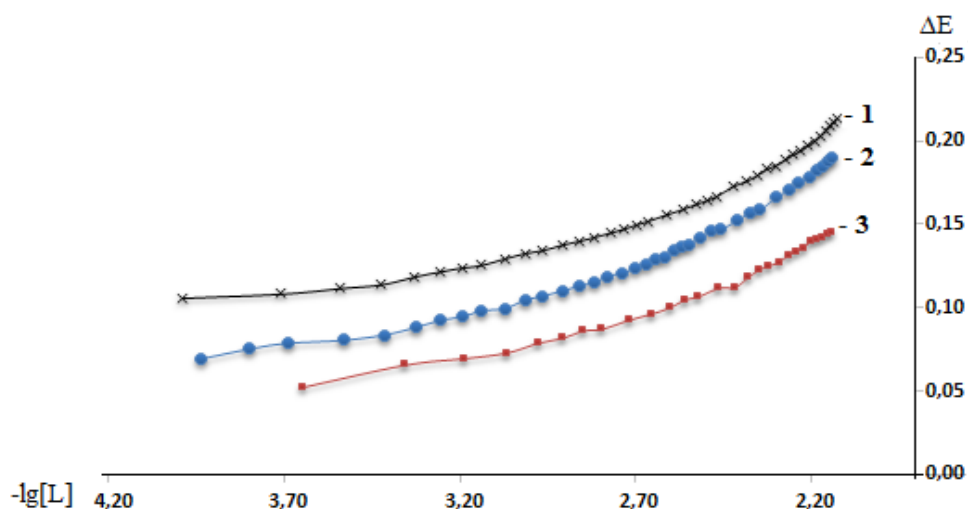


Fig. 1. Dependence of ΔE on $-\log[L]$ for iron(III) thiosemicarbazide complexes: 1) in a solution of 0.5 mol/l H_2SO_4 ; 2) in a solution of 1.0 mol/l H_2SO_4 ; 3) in a solution of 2.0 mol/l H_2SO_4 .

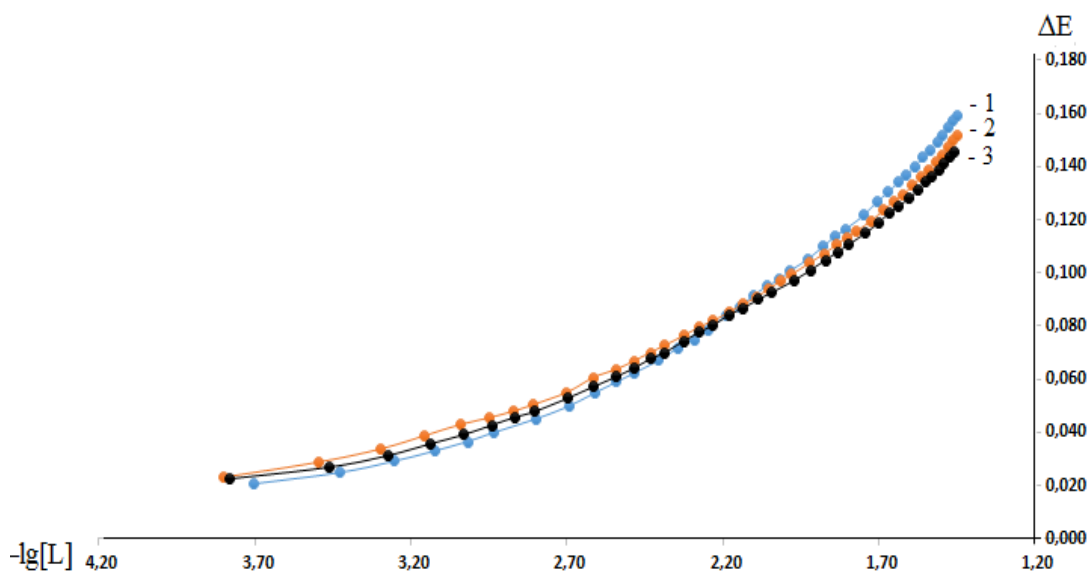


Fig. 2. Dependence of ΔE on $-\log[L]$ for 1-formyl-3-thiosemicarbazide complexes of iron(III): 1) in a solution of 0.5 mol/l H_2SO_4 ; 2) in a solution of 1.0 mol/l H_2SO_4 ; 3) in a solution of 2.0 mol/l H_2SO_4 .

Tables 1 and 2 show the values of the stability constants of complex compounds of iron(III) with thiosemicarbazide and 1-formyl-3-thiosemicarbazide in solutions of sulfuric acid of various concentrations calculated by the Leden method [21].

Table 1. Values of general stability constants of iron(III) thiosemicarbazide complexes in solutions of sulfuric acid of various concentrations, at 298K

Sulfuric acid concentration, mol/l	Stability constants		
	$\lg\beta_1$ $[\text{FeTSC}]^{3+}$	$\lg\beta_2$ $[\text{Fe}(\text{TSC})_2]^{3+}$	$\lg\beta_3$ $[\text{Fe}(\text{TSC})_3]^{3+}$
0,1	4,74±0,13	6,47±0,09	7,99±0,14
0,5	4,21±0,12	5,94±0,13	7,44±0,15
1,0	4,13±0,11	5,79±0,08	7,29±0,09
2,0	4,01±0,10	5,66±0,11	7,14±0,13

Table 2. Values of stability constants of 1-formyl-3-thiosemicarbazide complexes of iron(III) in solutions of sulfuric acid of various concentrations, at 298K

Sulfuric acid concentration, mol/l	Stability constants	
	$\lg\beta_1$ $[\text{FeFTSC}]^{3+}$	$\lg\beta_2$ $[\text{Fe}(\text{FTSC})_2]^{3+}$
0,1	4,33±0,11	6,12±0,13
0,5	3,57±0,10	5,45±0,10
1,0	3,43±0,07	5,36±0,12
2,0	3,35±0,09	5,29±0,14

In the picture No. 3 distribution diagrams of different forms of thiosemicarbazide depending on the pH of the medium are presented.

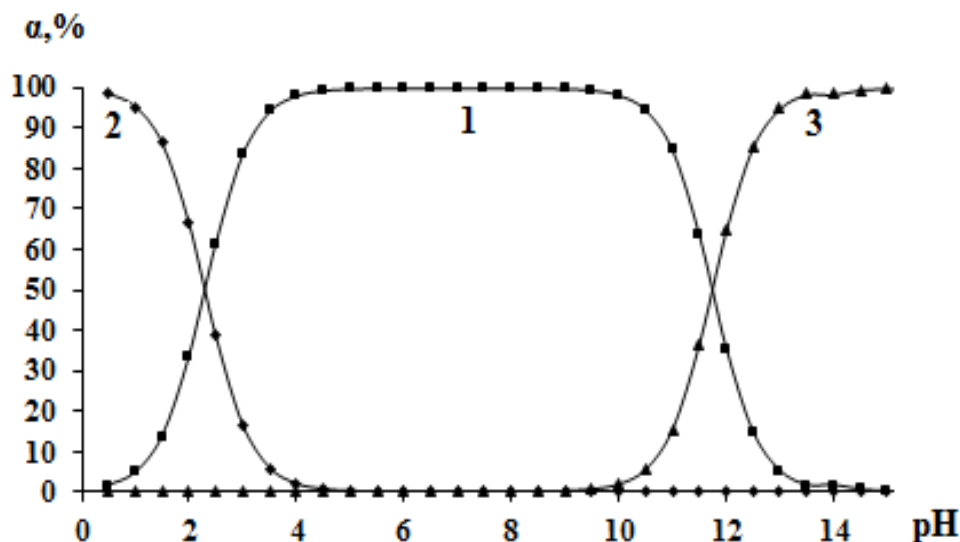


Fig. 3. Distribution diagrams of various forms of thiosemicarbazide depending on the pH of the solution: 1) TSC; 2) HTSC⁺; 3) TSC⁻

Table 3 shows the ΔG values of iron(III) complex compounds with thiosemicarbazide and 1-formyl-3-thiosemicarbazide in sulfuric acid solutions of various concentrations, calculated using the equation $\Delta G = -2,3RT \lg\beta_i$.

Table 3. $\Delta_r G$ values for the formation of thiosemicarbazide and 1-formyl-3-thiosemicarbazide complexes of iron(III) in sulfuric acid solutions of different concentrations, at 298K

Composition of complex particles	$\Delta_r G$, kJ/mol			
	Sulfuric acid concentration, mol/l			
	0,1	0,5	1,0	2,0
$[\text{FeTSC}]^{3+}$	-27,0105	-23,9903	-23,5345	-22,8506
$[\text{Fe}(\text{TSC})_2]^{3+}$	-36,8687	-33,8486	-32,9938	-32,2530
$[\text{Fe}(\text{TSC})_3]^{3+}$	-45,5303	-42,3962	-41,5414	-40,6867
$[\text{FeFTSC}]^{3+}$	-24,6741	-20,3433	-19,5456	-19,0897
$[\text{Fe}(\text{FTSC})_2]^{3+}$	-34,8743	-31,0564	-30,5435	-30,1446

Fig.4 shows the dependence of the change in the Gibbs energy of transfer $\Delta_r G_p$ ($\Delta_r G_p = \Delta_r G_{\text{H}_2\text{SO}_4(0,5)} - \Delta_r G_{\text{H}_2\text{SO}_4(0,1)}$) of the reaction of formation of iron complexes

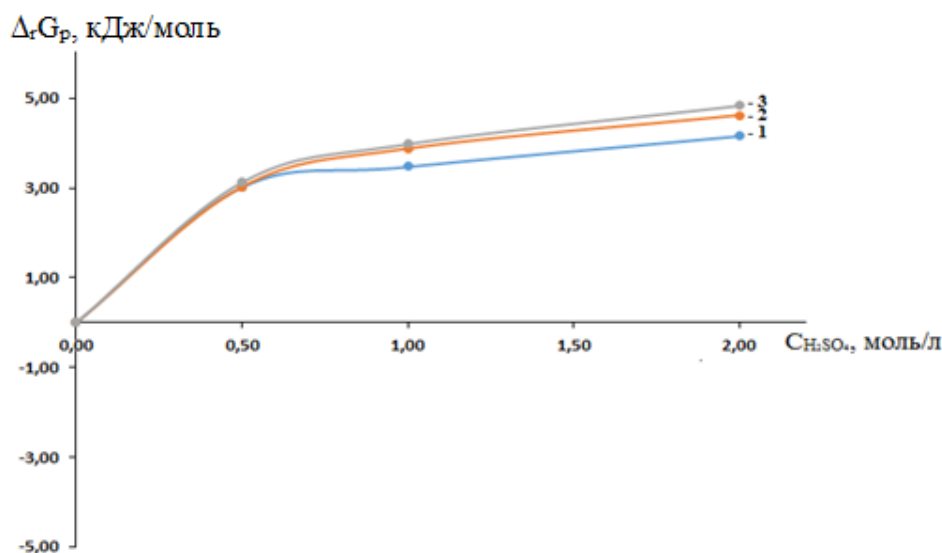


Fig.4. Change in the Gibbs energy of transfer of the reaction of formation of iron(III) complexes with TSC: 1) $[\text{FeTSC}]^{3+}$; 2) $[\text{Fe}(\text{TSC})_2]^{3+}$; 3) $[\text{Fe}(\text{TSC})_3]^{3+}$

DISCUSSIONS

The conducted studies revealed that the nature of complex formation between iron(III) and thiosemicarbazide (Fig. 1) remains largely unchanged with an increasing concentration of sulfuric acid. The complex formation continues in a stepwise manner, and at all concentrations of H_2SO_4 (0.1 - 2.0 mol/l), three distinct complex particles are observed. A similar trend is noted in the examination of complex formation between iron(III) and 1-formyl-3-thiosemicarbazide (Fig. 2). Notably, it was found that as the concentration of sulfuric acid in the solution increases, the stability constants of iron(III) complex compounds with both thiosemicarbazide and 1-formyl-3-thiosemicarbazide decrease (Tables 1 and 2).

To interpret the obtained experimental data, we investigated the acid-base properties of thiosemicarbazide and its acyl derivative. Through pH-metric titration, we determined that the acid ionization constant of the protonated form of TSC is $\text{pK}_a = 1.82 \pm 0.07$, while for FTSC, the pK_a value is 4.4. Consequently, both ligands, TSC and FTSC, exhibit characteristics of very weak bases in aqueous solutions. Analyzing the diagram data (Fig. 3), it becomes apparent that thiosemicarbazide begins to undergo protonation at $\text{pH} = 3.5$. Considering the acid-base properties of TSC and FTSC, it can be postulated that the decrease in the stability of iron(III) with these

organic compounds (Tables 1, 2) as the concentration of hydrogen ions increases in the solution is linked to the competition between the proton and the metal ion for the organic ligand.

Furthermore, the conducted studies indicate that the ΔG value for all complex forms formed in the Fe(III)-TSC(FTSC)-H₂SO₄ system becomes more positive with an increasing concentration of H₂SO₄ in the solution (Table 3, Fig. 4).

CONCLUSIONS

1. Regardless of the experimental temperature and H₂SO₄ concentration, a slight decrease in the stability constants of iron(III) complexes is observed when transitioning from TSC to FTSC. The proximity of the numerical values of the stability constants of iron(III) complexes with TSC and FTSC results from the identical coordination of organic ligand molecules to iron(III).

2. It has been demonstrated that the Gibbs energy for the formation of all complex forms is negative, and its numerical values become more positive with an increase in the number of organic ligand molecules in the inner sphere of the complex. As the concentration of H₂SO₄ in the solution rises, the stability of the complexes decreases, attributed to the protonation of organic ligands in the solution.

**REVIEWER: Suyariyon K.J.,
Candidate of Chemical Sciences,
Associate Professor**

REFERENCES

1. Alieva, R.A. Complexation of iron (III) with bis-(2,3,4-trihydroxyphenylazo) benzidine in the presence of diantipyrylmethane and its homologues / R.A. Alieva, M.F. Mamedova, F.M. Chiragov // Baku State University. - 2007. -No. 3. – Pp. 29-33.
2. Amirov, R.R. Complexation of iron (III) with 3,4-dihydroxybenzoic acid in aqueous solutions / R.R. Amirov, A.B. Ziyatdinova, A.N. Solodov, A.V. Vanyukova, Yu.I. Zayavkina // Scientific notes of Kazan University. -Natural Sciences. -2010. -T. 152. Book 4. – Pp.238-247.
3. Amerkhanova, Sh.Kh. Assessment of thermodynamic parameters of the processes of complexation of sodium dibutyl dithiophosphate and diisopropyl dithiophosphate with iron (II) ions. Sorption and chromatographic processes / Sh.Kh. Amerkhanova, R.M. Shlyapov, A.S. Wali, F.J. Bekkulina // -2012. -T. 12. - Issue. 2. – Pp.304-310.
4. A Alikina, E.N. Study of complex formation in the iron(III) system salicylic acid-diphenylguanidine in water-acetone and water-ethanol solutions using the spectrophotometric method / E.N. Alikina, O.Yu. Alexandrova, P.M. Staroverova, E.S. Zaplatina // Bulletin of Perm University. -2016. -Issue 1 (21). – Pp.60-67.
5. Ivanova, T.M. X-ray electron spectra and structure of polynuclear iron complexes / T.M. Ivanova, A.V. Naumkin, A.V. Shchukarev, A.A. Sidorov, M.A. Kiskin, V.M. Novotortsev, I.L. Eremenko // News of the Russian Academy of Sciences. -Physical series. -2008. -T. 72. -No. 4. – Pp.551-557.
6. Gruzdev, M.S. Conversion of low-spin states in a monochelate Fe(III) complex with an asymmetric azomethine tridentate ligand / M.S. Gruzdev, N.E. Domracheva, A.I. Alexandrov, V.P. Osipova, U.V. Chervonova, A.M. Kolker, T.V. Pashkova, D.V. Barakhtenko // Journal of structural chemistry, -2012. -T. 53. -No. 6. – Pp.1090-1101.
7. Marian Crudu. New Coordination Compounds of Fe(III) with Ligand from Nhydroxysuccinimide, with Applications in Ecologic Leather Tanning Technologies / Marian Crudu, Doina Sibiecu, Dana Gurau, Rodica Rohana Constantinescu, Ana Maria Vailescu // REV. CHIM. (Bucharest). -66. -№7. -2015. – Pp. 958-962.
8. Aliyu, H.N. Synthesis and characterization of N-(1-morpholinobenzyl) semicarbazide manganese(II) and iron(II) complexes / H. N. Aliyu, H. Adamu // Bajopas Volume 2 Number 2 December. -2009. – Pp.143-148.
9. Olga Khalipova. The Composition and Structure of Iron(III) Complex Compounds With Salicylic Acid in Ethanol Solution and in The Solid Thin Film State / Olga Khalipova, Svetlana Kuznetsova, Vladimir Kozik // Prospects of Fundamental Sciences Development (PFSD-2016). – Pp.20007-1–020007-6.
10. Omar B. Ibrahim. Complexes of urea with Mn(II), Fe(III), Co(II), and Cu(II) metal ions / Omar B. Ibrahim // dvances in Applied Science Research. -2012. 3. – Pp.3522-3539.
11. Junki SATO. Synthesis of picolinate-iron(III) compounds through an aqueous solution process / Junki SATO, Makoto KOBAYASHI, Hideki KATO, Eunsang KWON, Masato KAKIHANA // Journal of the Ceramic Society of Japan, 2015. 123 [9]. – Pp. 751-755.
12. Khlood, S. In-vitro antibacterial, antifungal activity of some transition metal complexes of thiosemicarbazone Schiff base (HL) derived from N4-(70-chloroquinolin-40-ylamino) thiosemicarbazide / S. Khlood, Abou Melha // Journal of Enzyme Inhibition and Medicinal Chemistry. –August. -2008. -23 (4). – Pp. 493–503.
13. Koksharova, T.V. Coordination Compounds of 3d-Metals Salicylates with Thiosemicarbazide / T.V. Koksharova, S.V. Kurando, I. V. Stoyanova // ISSN 1070-3632. Russian Journal of General Chemistry. -2012. -Vol. 82, No. 9. – Pp. 1481–1484.

14. Tukki Sarkar. Significant photocytotoxic effect of an iron(III) complex of a Schiff base ligand derived from vitamin B6 and thiosemicarbazide in visible light / Tukki Sarkar, Samya Banerjee and Akhtar Hussain // Cite this: RSC Adv. -2015. 5. – Pp. 29276–29284.
15. Azizkulova O.A. Study of the process of complexation of molybdenum (V) with 1,2,4-triazololthiol in a medium of 6 mol/l HCl 298 K / O.A. Azizkulova, F.R. Khamidova, A.Sh. Egamberdiev, M.I. Abdulkhaeva, U.M. Jurabekov // News of OshTU, 2020 No. 2. – Pp.105.
16. Bobokalonov, T.B. Study of complex formation of iron (III) with thiosemicarbazide / T.B. Bobokalonov, S.M. Safarmamadov // ISSN 2413 – 452X Vestnik TNU 1/3(200). -Dushanbe "Sino", 2016. – Pp. 156-161.
17. Bobokalonov, T.B. Complexation of iron (III) with 1-formyl-3-thiosemicarbazide / T.B. Bobokalonov, S.M. Safarmamadov // - News of ANRT. -No. 3 (172). -2018. – Pp. 59-65.
18. Karyakin, Yu.V. Pure chemicals / Yu.V. Karyakin, I.I. Angelov // - M., -1974. – P. 209.
19. Carl-Friedrich Kroger, Wolf Sattler, Und Haus Beyer Die Umsetzung methyl substituierter Thiosemicarbazide mitaliphatischen Carbon-Sauren Liebigs. Ann. Chem. 196Bd. 643.P.128-135.
20. Hartley, F. Equilibria in solutions / F. Hartley, K. Burges, R. Alcock // - M.: Mir, 1983. – Pp. 365.
21. Novakovsky, M.S. Laboratory work on the chemistry of complex compounds / M.S. Novakovsky // Kharkov University. -1972. –217 p.

COMPLEXATION OF IRON (III) WITH TSC AND FTSC IN H₂SO₄ SOLUTIONS OF VARIABLE COMPOSITION

The process of complex formation of iron (III) with thiosemicarbazide and 1-formyl-3-thiosemicarbazide in H₂SO₄ solutions of various concentrations was studied using the potentiometric method. The stability constants of the resulting complexes were calculated, and the ionization constants of the ligands were estimated under the same conditions. It was shown that the stepwise nature of complex formation does not depend on the concentration of hydrogen ions. However, the stability of the complexes decreases with increasing pH. A study of the complex formation of iron(III) with thiosemicarbazide and its acyl derivative showed that there are both similarities and differences in the nature of complex formation. Both ligands react with iron(III) in a stepwise manner, forming stable complexes. With increasing temperature, the stability of the complexes increases. Changing the ionic strength of the solution and the concentration of H₂SO₄ equally affect the stability of the complexes. At the same time, moving from thiosemicarbazide to 1-formyl-3-thiosemicarbazide, the number of particles formed in the solution decreases, and the stability of the complexes decreases.

Keywords: complexation, iron(III), TSC-thiosemicarbazide, FTSC-1-formyl-3-thiosemicarbazide, stability constants, thermodynamic functions.

Information about the authors: **Bobokalonov Tojiddin Barotmakhmadovich** - Tajik National University, Candidate of Chemical Sciences, Senior Lecturer of the Department of Analytical Chemistry. **Address:** 734025, Dushanbe city, Republic of Tajikistan, Rudaki Avenue, 17. **Phone:** (+992) 918157026. **E-mail:** tojiddin_8989@mail.ru

Hakimov Firuz Kholikovich - Samarkand State University named after Sharof Rashidov, Candidate of Chemical Sciences, Associate Professor of the Department of Physical and Colloid Chemistry. **Address:** 140104, Samarkand, Republic of Uzbekistan, University Boulevard, 15. **Phone:** (+998) 915444450. **E-mail:** Xakimov-firuz@mail.ru

Safarmamadzoda Safarmamad Muboraksho - Tajik National University, Doctor of Chemical Sciences, Professor of the Department of Inorganic Chemistry. **Address:** 734025, Dushanbe city, Republic of Tajikistan, Rudaki Avenue, 17. **Phone:** (+992) 938270404. **E-mail:** sash65@mail.ru

Mamadgaminova Zebo Rahmatshoevna – Tajik National University, second-year master's student of the Department of Inorganic Chemistry. **Address:** 734025, Dushanbe city, Republic of Tajikistan, Rudaki Avenue, 17. **Phone:** (+992) 900550898. **E-mail:** mamadgaminovazebo@gmail.com.

Article received 02.01.2024

Approved after review 22.02.2024

Accepted for publication 12.04.2024

SYNTHESIS OF 6,8-DINITRO-11H-INDENO[1,2-b]QUINOXALIN-11-ONE AND 1,3-DINITRO-6H-INDOLO[2,3-b]QUINOXALINE BASED ON 4,6-DINITRO-o-PHENYLENEDIAMINE

Mukhtorov L.G., Karimov M.B., Shakhkeldyan I.V.,

Atroshchenko4 Yu.M.

One of the interesting and promising classes of heterocyclic compounds is indeno[1,2-b]quinoxaline, derivatives of which are used in medicine and are the basis for the development of new anti-inflammatory, antibacterial, antifungal drugs, and they also have antitumor activity. These derivatives are also used as dyes, anti-corrosion components, organic semiconductors, etc. [8-11]. Indolo[2,3-b]quinoxalines were first obtained in 1925. These substances contain indole and quinoxaline fragments in their molecules, and their chemistry is constantly being studied. Buu-Hoi N.P. and Saint-Ruf G. studied in detail their preparation by condensation of isatin and aromatic diamines [12]. They also proposed a new name for the studied class of compounds - indophenazines, since they, like phenazine with sulfuric acid, give a red color.

These compounds have various types of biological activity and, thus, take part in the creation of new drugs [13]. A study of literary sources showed that the main method for forming the structure of 11H-indeno[1,2-b]quinoxalin-11-one and 6H-indolo[2,3-b]quinoxaline is the reaction of o-phenylenediamine with ninhydrin in an acetic acid medium [14]. The possibility of expanding the range of derivatives of this class of compounds has generated great interest. For this purpose, a method was developed for the preparation of 6,8-dinitro-11H-indeno[1,2-b]quinoxalin-11-one, as well as a method for the synthesis of 1,3-dinitro-6H-indolo[2,3-b]quinoxaline, starting from 4,6-dinitro-ortho-phenylenediamine (2-amino-4,6-dinitroaniline). Since both of these starting substrates are inaccessible compounds, in the course of our research, schemes for their preparation were developed based on the use of accessible and relatively cheap phenol.

EXPERIMENTAL PART

Made using domestic and foreign-made devices. IR spectra were recorded on an FSM 2202 Fourier spectrometer in KBr tablets (1:200) with a resolution of 4 cm⁻¹. ¹H NMR spectra were recorded on a Bruker DRX-400 spectrometer (400 MHz, DMSO-d₆), internal standard HMDS. ¹³C NMR spectra were recorded on a Bruker DRX-400 spectrometer (151 MHz, DMSO-d₆), internal standard HMDS.

Optimization of the geometric parameters of the structures under study and calculation of the total energy were carried out in the Firefly 8.2.0 software package [15] within the framework of the density functional theory approximation using the hybrid three-parameter Becke exchange functional [16] with the Lee-Yang-Parr correlation functional [17] (B3LYP) [18] and the Dunning basis set aug-cc-pVDZ [19]. Full geometry optimization was carried out without restrictions on the type of symmetry. All structures calculated in this work are stationary points on the PES, which was confirmed by analysis of the theoretical vibrational spectrum calculated from the Hessian, while for minima on the PES the diagonalized Hess matrix contains only positive terms.

2-amino-4,6-dinitroaniline. The synthesis was carried out according to a known procedure [20].

6,8-dinitro-11H-indeno[1,2-b]quinoxalin-11-one (2). 5 g (0.0252 mol) of 2-amino-4,6-dinitroaniline, 4.48 g (0.0252 mol) of ninhydrin and 150 ml of ice-cold CH₃COOH were placed in a round-bottom flask equipped with a reflux condenser and a magnetic stirrer. The mixture was heated in a boiling water bath for 6 hours. After the reaction was completed, the solution was left overnight to allow the precipitate to mature. The next day, the precipitate was filtered on a Schott filter and washed with cold isopropanol. Recrystallization was carried out from ethanol, and then the isolated precipitate was dried at room temperature and at 60°C. The resulting product is brown-green crystals. The yield was 75% (8.15 g), T_m = 281-283°C. IR spectrum (KBr): 1733 cm⁻¹

(C=O); 1581 cm⁻¹, 1541 cm⁻¹ (-NO₂). ¹H NMR spectrum (400 MHz, DMSO-d₆): δ 9.25 (d, J = 2.4 Hz, 1H), 9.21 (d, J = 2.4 Hz, 1H), 8.15 (d, J = 7.5 Hz, 1H), 8.01 (d, J = 7.4 Hz, 1H), 7.96 (t, J = 7.3 Hz, 1H), 7.86 (t, J = 7.4 Hz, 1H). ¹³C NMR (151 MHz, DMSO-d₆): δ 187.94, 160.64, 154.15, 148.05, 146.53, 141.75, 140.13, 137.10.

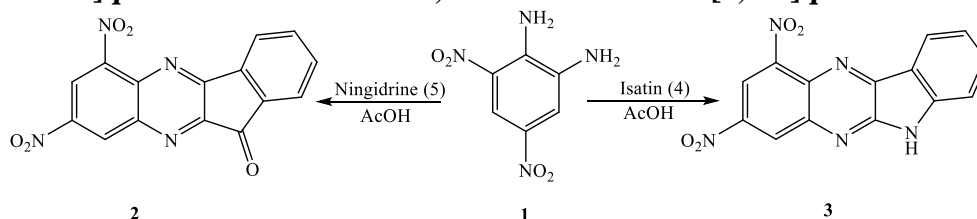
1,3-dinitro-6H-indolo[2,3-b]quinoxaline (3). In a round-bottom flask equipped with a reflux condenser and a magnetic stirrer, we placed 3 g (0.015 mol) of 2-amino-4,6-dinitroaniline, 2.27 g (0.015 mol) of isatin and 30 ml of glacial acetic acid. The mixture was heated in a boiling water bath for 9 hours. After the reaction was completed, the solution was left overnight to allow the precipitate to mature. The next day, the precipitate was filtered on a Schott filter and washed with cold isopropanol. Recrystallization was carried out from ethanol, and then the isolated precipitate was dried at room temperature and at 60°C. The resulting product is dark sand-colored crystals. The yield was 92% (2.76 g). R_f = 0.39. ¹H NMR spectrum (600 MHz, DMSO-d₆): δ 7.59 (ddd, J = 7.6; 1.4; 0.8 Hz, 1H), 7.50 (dd, J = 7.7; 1.3 Hz, 1H), 7.07 (td, J = 7.5, 0.9 Hz, 1H), ¹³C NMR (151 MHz, DMSO-d₆): δ 184.83, 159.80, 151.17, 144.01, 134.71, 133.10 and 118.26 m.d. Calculated, %: C, 54.39; H, 2.50; N, 22.70; O 20.71. Found, %: C 14H₇N₅O₄: C, 54.38; H, 2.28; N, 22.65; O, 20.69.

THE DISCUSSION OF THE RESULTS

In general, the general methods used in this work for the preparation of 6,8-dinitro-11H-indeno[1,2-b]quinoxalin-11-one and 1,3-dinitro-6H-indolo[2,3-b]quinoxaline are complex multi-stage processes presented in Scheme 1.

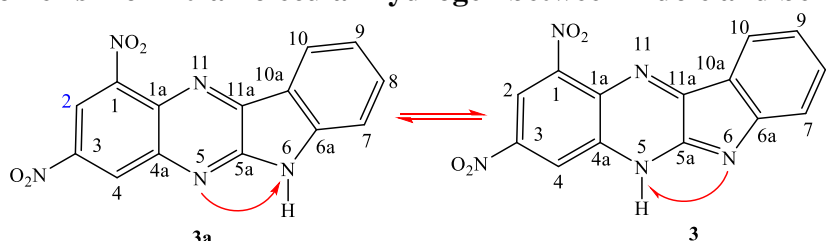
The synthesis of 6,8-dinitro-11H-indeno[1,2-b]quinoxalin-11-one and 1,3-dinitro-6H-indolo[2,3-b]quinoxaline was carried out by acylation between the imide (NH₂) and carbonyl (C=O) groups. From the starting compound 2-amino-4,6-dinitroaniline (1), the compound 6,8-dinitro-11H-indeno[1,2-b]quinoxalin-11-one (2). Next, the compound 1,3-dinitro-6H-indolo[2,3-b]quinoxaline (3) was obtained by intermolecular cyclization in the presence of commercially purchased indole-2,3-dione (isatin) in acetic acid solution. The formation of these compounds was proven using IR, ¹H and ¹³C NMR spectroscopy and elemental analysis.

Diagram 1. General plan for the synthesis of 6,8-dinitro-11H-indeno[1,2-b]quinoxalin-11-one and 1,3-dinitro-6H-indolo[2,3-b]quinoxaline



Data from literature sources [21] on indolequinoxaline derivatives showed that tautomerism of the intramolecular hydrogen of the imide group between the indole and benzene rings is possible (Scheme 2)

Diagram 2. Tautomerism of intramolecular hydrogen between indole and benzene rings



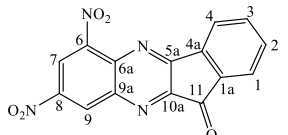
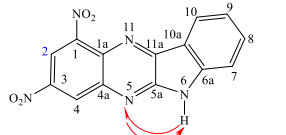
Geometric optimization and calculation of the total energy of compounds 3 and 3a were carried out using the DFT/B3LYP/aug-cc-pVDZ method in the gas phase. As the calculation data showed, structure 3a is more stable by 51.4 kJ/mol.

In the ¹H NMR spectrum of 6,8-dinitro-11H-indeno[1,2-b]quinoxalin-11-one, two groups of signals are observed. In a weaker field, the signals of the hydrogen atoms H7 and H9 of the dinitro-substituted ring of quinoxaline are presented in the form of two doublet signals at δ

9.25 and 9.21 ppm. with a spin-spin interaction constant of $4J_{2.5}$ Hz. The four-spin system of the benzannelated indene ring in a higher field is expressed by two doublets at δ 8.15 and 8.01 ppm. and two triplets at δ 7.95 and 7.86 ppm. ($3J = 7.4 - 7.5$ Hz). It should be noted that these signals are broadened. In the spectrum of the JAMR using the impulse sequence of DEPT-135, the amplitude of the quarterly carbon atoms of the carbon is positive ($\Delta C = 187.94, 106.64, 145.15, 148.05, 146.53, 141.75, 140.13, 138.44, 137.10$ M.D.), and the S. groups are negative (negative groups ($\delta_c = 137.86, 135.20, 129.53, 125.07, 124.04, 120.25$ ppm). In the weakest field at $\delta_c = 187.94$ ppm. a signal from the carbonyl carbon atom C=O is observed. Thus, the data obtained can serve to identify 6,8-dinitro-11H-indeno[1,2-b]quinoxalin-11-one by 1H NMR spectroscopy. The structure of the synthesized compound is confirmed by NMR spectroscopy data. In the weakest field at δ 11.02 ppm. a broadened singlet of the NH proton of the indole fragment is detected. It is interesting to note that at δ 8.98 ppm. a broadened singlet is also observed, which can be attributed to the NH proton of the quinoxaline fragment, if we assume the possibility of 5H – 6H tautomerism (Scheme 1). The signals of the H2 and H4 protons of the dinitroaromatic fragment combine into a common singlet at δ 9.05 ppm. In the δ region 6.91-8.98 ppm. signals of the 4-spin proton system of the fused benzene ring of indole are observed. At the same time, the peaks of aromatic protons are well resolved and appear in the form of a doublet of triplets of the H8 proton at δ 6.11 ppm. ($J = 7.9; 0.8$ Hz), a doublet of doublets of doublets of the H7 proton at δ 7.59 ppm. ($J = 7.6; 1.4; 0.8$ Hz), a triplet of doublets of the H9 proton at δ 7.07 ppm. ($J = 7.5; 0.9$ Hz) and a doublet of doublets of the H10 proton at δ 7.50 ppm. ($J = 7.7; 1.3$ Hz). In the spectrum of the homonuclear H-H correlation COZY there are peaks corresponding to the SCV through 3 bonds (Jortho).

The molecular structure of 1,3-dinitro-6H-indolo[2,3-b]quinoxaline is also confirmed by ^{13}C NMR spectroscopy data. In the spectrum of the analyzed compound, signals from 14 nonequivalent carbon atoms should be observed, 8 of which are quaternary, and 6 are tertiary. In the NMR spectrum using the DEPT-135 pulse sequence, the signal amplitudes of the quaternary carbon atoms are positive ($\delta C = 184.83, 159.80, 151.17, 144.01, 134.71, 133.10$ and 118.26 ppm), and the amplitudes of the CH groups are negative ($\delta C = 138.83, 128.49, 125.13, 123.22$ and 112.66 ppm). In this case, the signals of carbon atoms C1 and C3, as well as C2 and C4, appear in the spectrum in the form of general signals at δC 133.10 and 128.49 ppm, respectively. This fact is probably also associated with the possibility of NH tautomerism.

Two-dimensional heteronuclear CH correlation spectra HSQC and HMBC. In the HSQC spectrum, correlation peaks of the coupling constant are observed through 2 $^1J_{C-H}$ bonds, which helps to assign signals to tertiary carbon atoms: $\delta C = 133.10$ (C1, C3), 128.49 (C2, C4), 112.66 (C7), 138.83 (C8), 123.22 (C9) and 125.13 (C10) ppm. This assignment is confirmed by the presence of correlation peaks in the HMBC spectrum, corresponding to the VSWR through 2 and 3 bonds. For the NH proton of the indole fragment, a weak correlation peak NH/C5a is detected in the HMBC spectrum, which makes it possible to isolate the signal of this carbon atom at δC 184.83 (C5a). The signals of carbon atoms C1a (δC 144.01 ppm) and C4a (δC 134.71 ppm) can be detected by coupling constants with the protons H2 and H4 of the quinoxaline fragment, and carbon atoms C6a (δC 151.17 ppm) and C10a (δC 118.26 ppm) – according to the coupling constant with the protons H7 – H10 of the indole fragment. A signal that does not have correlation peaks in the NMBC spectrum at δC 159.80 ppm. can be assigned to the quaternary carbon atom C11a. The structures of 6,8-dinitro-11H-indeno[1,2-b]quinoxalin-11-one (3-3a) and 1,3-dinitro-6H-indolo[2,3-b]quinoxaline (7) were determined methods of spectral analysis (Fig. 1-9). The results are shown in Table 1.

								
№ атома	δH, м.д.	δC, м.д.	HSQ C (1H/13C)	HMB C (1H/13C)	δH, м.д.	δC, м.д.	HSQ C (1H/13C)	HMBC (1H/13C)
1	8.01 (д)	125.07	H ¹ /C ¹	H ¹ /C ³ , H ¹ /C ² , H ¹ /C ^{4a} , H ¹ /C ¹¹	-	133.10	-	-
1a	-	138.44	-	-	-	144.01	-	H ² /C ¹ ; H ² /C ^{1a}
2	7.86 (т)	135.20	H ² /C ²	H ² /C ¹ , H ² /C ⁴ , H ² /C ^{1a}	9.05 c	128.49	H ² /C ²	-
3	7.96 (т)	137.86	H ³ /C ³	H ³ /C ¹ , H ³ /C ⁴ , H ³ /C ² , H ³ /C ^{4a}	-	133.10	-	-
4	8.15 (д)	124.04	H ⁴ /C ⁴	H ⁴ /C ² , H ⁴ /C ^{1a} , H ⁴ /C ^{5a}	9.05 c	128.49	H ⁴ /C ⁴	H ⁴ /C ³ ; H ⁴ /C ^{1a} , H ⁴ /C ^{4a}
4a	-	140.13	-	-	-	134.71	-	-
5a	-	160.64	-	-	-	184.83	-	-
6	-	148.05	-	-	-	-	-	-
6a	-	137.10	-	-	-	151.17	-	-
7	9.25 (д)	120.25	H ⁷ /C ⁷	H ⁷ /C ⁹ , H ⁷ /C ^{6a} , H ⁷ /C ⁸ , H ⁷ /C ⁶	6.11 дт. (7.9:0.8)	112.66	H ⁷ /C ⁷	H ⁷ /C ^{10a}
8	-	146.53	-	-	7.59 ддд. (7.6; 1.4; 0.8)	138.83	H ⁸ /C ⁸	H ⁸ /C ¹⁰ ; H ⁸ /C ^{6a}
9	9.21 (д)	129.53	H ⁹ /C ⁹	H ⁹ /C ⁷ , H ⁹ /C ^{6a} , H ⁹ /C ^{9a}	7.07 тд. (7.5; 0.9)	123.22	H ⁹ /C ⁹	H ⁹ /C ⁷ ; H ⁹ /C ^{10a}

				$H^9/C^8,$ H^9/C^6				
9a	-	141. 75	-	-	-	-	-	-
10	-	129. 53	-	-	7.50 ТД. (7.7;1. 3)	125. 13	H^{10}/C^1 0	$H^{10}/C^{6a};H^{10}/$ C^8
10a	-	154. 15	-	-		118. 26	-	-
11	-	187. 95	-	-	-	-	-	-
NH	-	-	-	-	8.98 с. 11.02 с.	-	-	NH/C^{5a}

Table 1. Data from $^1H,^{13}C$ spectra and heteronuclear correlation (HSQC, HMBC)

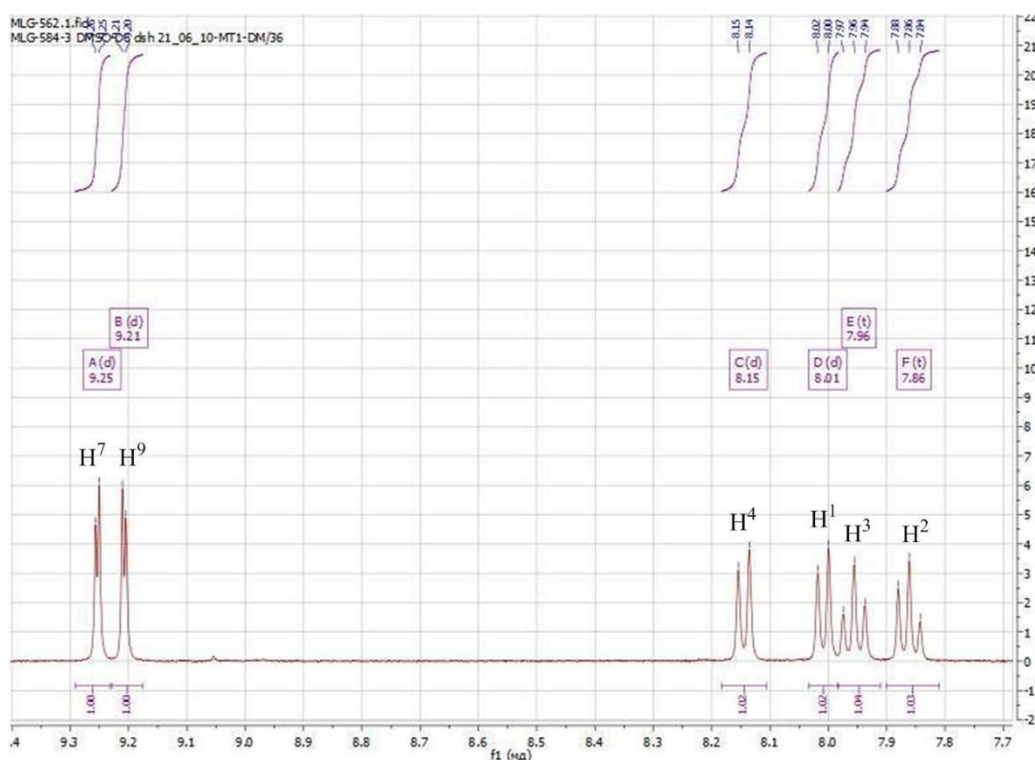
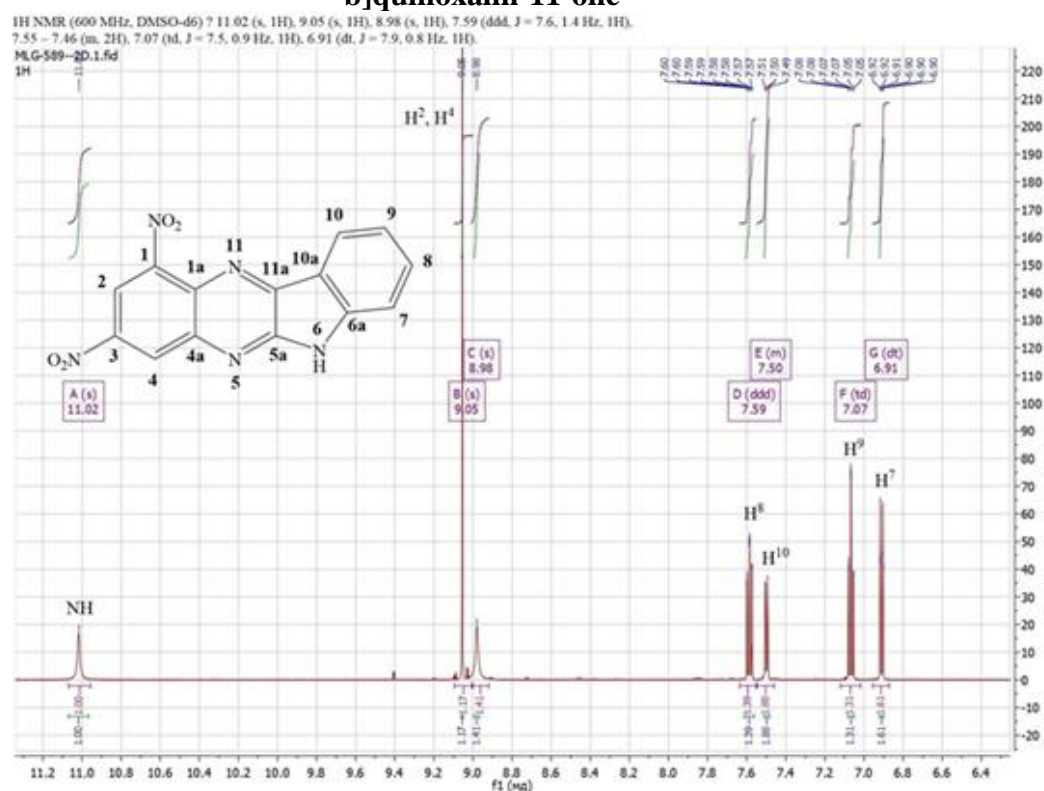
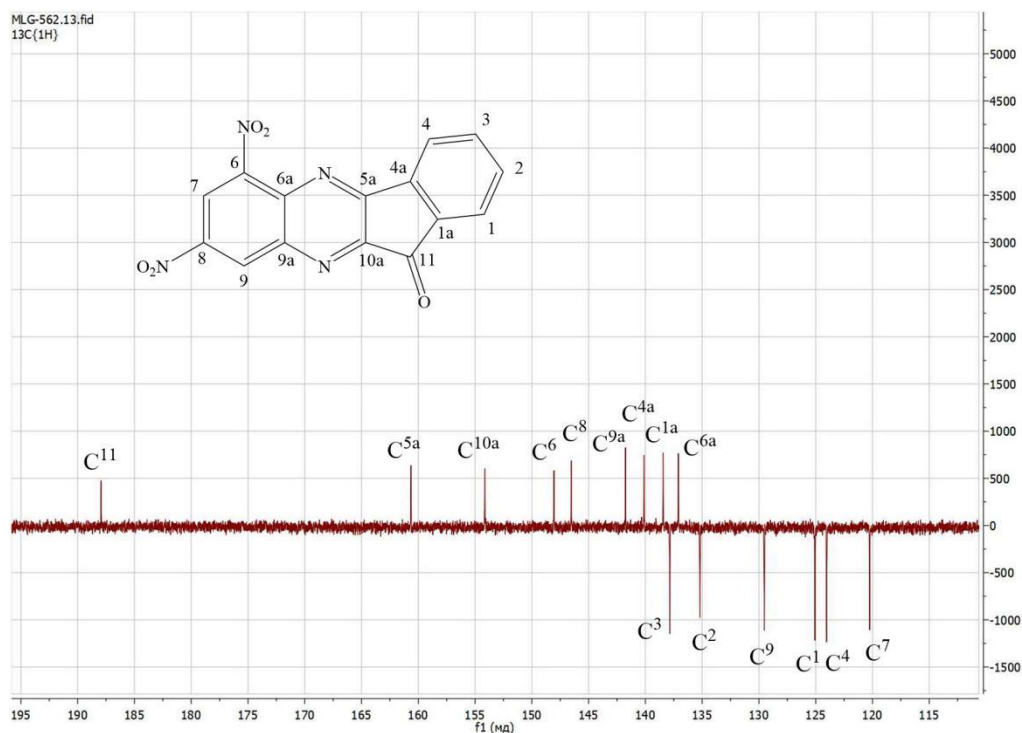


Fig. 1. 1H NMR spectrum (400 MHz, DMSO-D6) of 6,8-dinitro-11H-indeno[1,2-b]quinoxalin-11-



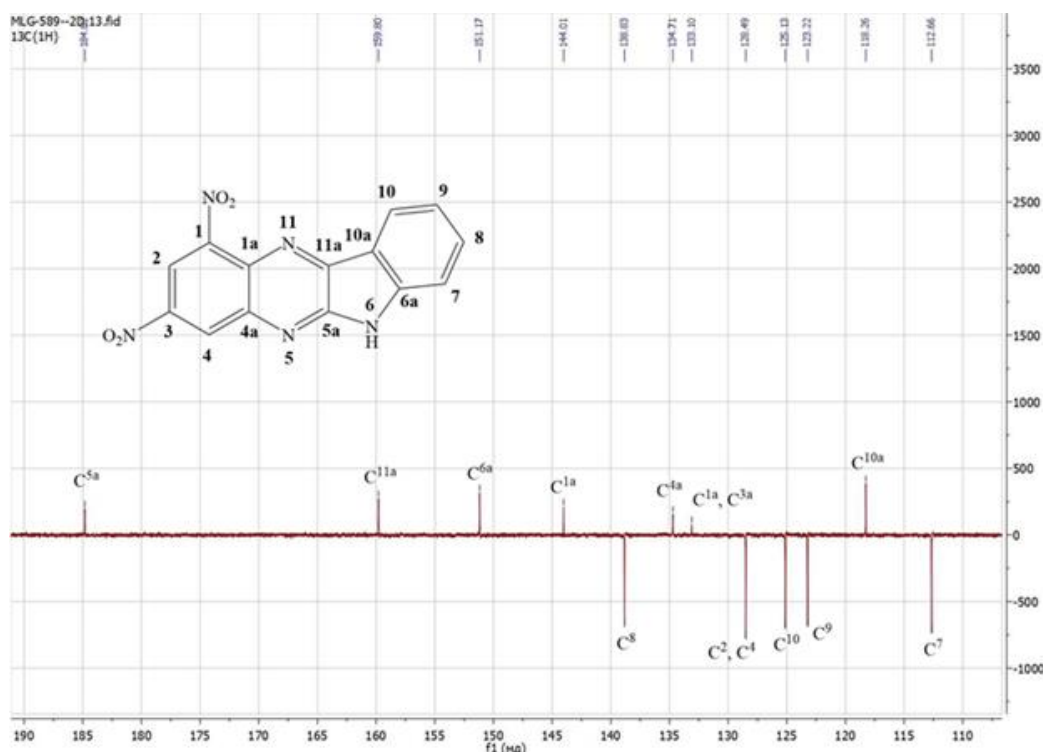


Fig. 4. ^{13}C NMR spectrum (151 MHz, DMSO- D_6) of 1,3-dinitro-6H-indolo[2,3-b]quinoxaline

CONCLUSIONS

As part of the expansion of the group of quinoxaline derivatives, multi-stage syntheses of compounds not previously described in the literature were developed and carried out - 6,8-dinitro-11H-indeno[1,2-b]quinoxalin-1-one and 1,3-dinitro-6H-indolo [2,3-b]quinoxaline, carried out by a new method of intermolecular cyclization in the presence of commercially purchased triketohydrin dehydrate (ninhydrin) and indole-2,3-dione (isatin) in acetic acid solution. The list of reagents used, as well as the conditions for carrying out the reactions, were determined experimentally. These compounds, like quinoxaline derivatives, have various types of biological activity and, thus, can be used in the creation of new drugs. A study of the literature on indolequinoxaline derivatives established the possibility of tautomerism of the intramolecular hydrogen of the imide group between the indole and benzene rings. Using IR, ^1H , ^{13}C NMR, HMBC and HSQC spectroscopy, the structure of the obtained compounds was proven, and their physicochemical characteristics were determined. The developed synthesis methods are distinguished by relative ease of execution, mild conditions, availability of reagents and make it possible to obtain the target products with a yield of 75% (for 6,8-dinitro-11H-indeno[1,2-b]quinoxalin-1-one) and 92% (for 1,3-dinitro-6H-indolo[2,3-b]quinoxaline).

**REVIEWER: Manonov K. A.,
Candidate of Chemical Sciences,
Associate Professor**

REFERENCES

1. Cabal M.P., 1,2,1, 3, and 1,4-Diazines and Related Systems. Modern Heterocyclic Chemistry / M.P. Cabal, J. Alvarez-Builla, J.J. Vaquero, J. Barluengo, Six-Membered Heterocycles // Weinheim. Wiley-VCH Verlag & Co. 2011. – Pp.1683 – 1776.
2. Shibinskaya M.O., Synthesis and biological activity of 7H-benzo[4,5]indolo[2,3-b]-quinoxaline derivatives / M.O. Shibinskaya, S.A. Lyakhov, A.V. Mazepa, S.A. Andronati, A.V. Turov, N.M. Zholobak, N.Ya. Spivak // European Journal of Medicinal Chemistry. 2011. – Pp.1237-1243. doi:10.1016/j.ejmech.2010.11.040
3. Luo X., Cinnamil- and Quinoxaline-Derivative Indicator Dyes for Detecting Volatile Amines in Fish Spoilage / X. Luo, L.-T. Lim // Department of Food Science, University of Guelph. Guelph. 2019. – 13 p. doi:10.3390/molecules24203673

4. Achelle S., Luminescent materials incorporating pyrazine or quinoxaline moieties / S. Achelle, C. Baudequin, N. Plé // *Dyes and Pigments*. Elsevier. 2013. V 98. N. 3. – Pp.575-600. doi:10.1016/j.dyepig.2013.03.030
5. Kim H., Synthesis and Characterization of Quinoxaline Derivative as Organic Semiconductors for Organic Thin-Film Transistors / H. Kim, M. R. Reddy, S.-S. Hong, C. Kim, S.Y. Seo // *Journal of Nanoscience and Nanotechnology*. 2017. V 17. N. 8. – Pp.5530-5538.
6. Jonathan L., Quinoxaline-oligopyrroles: Improved pyrrole-based anion receptors / L. Jonathan, M. Hiromitsu, M. Toshihisa, M.L.Vincent, F. Hiroyuki // *Chem. Commun.* 2002. N. 8. – Pp.862 – 863.
7. Gu Z., cytotoxic evaluation and DNA binding study of 9-fluoro-6H-indolo[2,3-b]quinoxaline derivatives / Z. Gu, Y. Li, S. Ma, S. Li, G. Zhou, S. Ding, Zhang J., Wang S., Zhou C. *Synthesis*, // *RSC Advances*. 2017. V 7. N. 66. – P.41869-41879. doi:10.1039/c7ra08138c
8. Kovrizhina A., 11H-Indeno[1,2-b]quinoxalin-11-one 2-(4-ethylbenzylidene)hydrazine / A. Kovrizhina, E. Samorodova, A. Khlebnikov // *Molbank*. 2021. N. 4. – 7 p.
9. Tseng C.-H., Discovery of indeno[1,2-b]quinoxaline derivatives as potential anticancer agents / C.-H. Tseng, Y.-R. Chen, C.-C. Tzeng, W. Liu, C.-K. Chou, C.-C. Chiu, Y.-L. Chen // *European Journal of Medicinal Chemistry*. 2016. V. 108. – Pp.258-273. doi:10.1016/j.ejmech.2015.11.031
10. Singh R., Recent advancement in the synthesis of diverse spiro-indeno[1,2-b]quinoxalines: a review / R. Singh, D. Bhardwaj, M. R. Saini // *RSC Advances*. 2021. V. 11. N. 8. – Pp.4760–4804. doi:10.1039/d0ra09130h
11. Obota I.B., Obi-Egbedi N.O. Indeno-1-one [2,3-b]quinoxaline as an effective inhibitor for the corrosion of mild steel in 0.5M H₂SO₄ solution / I.B. Obota, N.O. Obi-Egbedi // *Materials Chemistry and Physics*. 2010. V. 122. – Pp. 325-328.
12. Buu-Hoi N.P, Soc / Buu-Hoi N.P, Saint-Ruf G. Bull. // *Chim. Fr.* 1960, 1920.
13. Pereira J.A., Quinoxaline, its derivatives and applications / J.A. Pereira, A.M. Pessoa, M.N.D. Cordeiro, R. Fernandes, C. Prudêncio, J.P. Noronha, M. Vieira // *A State of the Art review*. *Eur. J. Med. Chem.* 2015. V. 97. – Pp.664–672. doi:10.1016/j.ejmech.2014.06.058
14. Ruhemann S. Cyclic di- and tri-ketones. *J. Chem. Soc / S. Ruhemann // Trans.* 1910. V 97.
15. Granovsky A. A. Firefly version 8.0. – 2016. – URL: [http / A. A. Granovsky // classic.chem.msu.su/gran/firefly/index.html](http://A.A.Granovsky/classic.chem.msu.su/gran/firefly/index.html).
16. Becke A. D. Density-functional thermochemistry. III. / A. D. Becke // *The role of exact exchange*. *J. Chem. Phys.* 1993. T 98. N. 7. – Pp.5648-5652.
17. Lee C. Development of the Colle-Salvetti correlation-energy formula into a functional of the electron density / C. Lee, W. Yang, R. G. Parr // *Physical review B*. 1988. T 37. N. 2. – P. 785. doi:10.1103/physrevb.37.785
18. Stephens P. J., Ab initio calculation of vibrational absorption and circular dichroism spectra using density functional force fields / P. J. Stephens, F. J. Devlin, C. F. Chabalowski, M. J. Frisch // *The Journal of Physical Chemistry*. 1994. T 98. N 45. – Pp. 11623-11627. doi:10.1021/j100096a001
19. Dunning Jr T. H. Gaussian basis sets for use in correlated molecular calculations. I. The atoms boron through neon and hydrogen / T. H. Dunning Jr // *The Journal of chemical physics*. 1989. V. 90. N. 2. – P. 1007-1023.
20. Corona P., Synthesis of N-(5,7-diamino-3-phenyl-quinoxalin-2-yl)-3,4,5-substituted anilines and N-[4[(5,7-diamino-3-phenylquinoxalin-2-yl)amino]benzoyl]-L-glutamic acid diethyl ester: Evaluation of in vitro anti-cancer and anti-folate activities / P. Corona, M. Loriga, M. P. Costi, S. Ferrari, G. Paglietti // *European Journal of Medicinal Chemistry*. 2008. N 43. – Pp.189-203. doi:10.1016/j.ejmech.2007.03.035
21. Grachev V. T., Tautomerism, electronic structures, and electronic spectra of indolo[2,3-b]quinoxaline and its derivatives / V. T. Grachev, A. V. Ivashchenko, S. P. Ivashchenko, B. G. Gerasimov, V. N. Lisyutenko, B. E. Zaitsev // *Chemistry of Heterocyclic Compounds*. 1982. V. 18. – Pp. 974–978. doi:10.1007/bf00513446

SYNTHESIS OF 6,8-DIHYDRO-11H-INDENO[1,2-b]QUINOXALINE-11-ONE AND 1,3-DIHYDRO-6H-INDOLO[2,3-b]QUINOXALINE BASED ON 4,6-DINITRO-O-PHENYLENEDIAMINE

The primary tasks of organic chemistry include the production of new nitrogen-containing heterocyclic systems. Quinoxalin derivatives are fragments of many biologically active and pharmacologically important compounds [1]: agonists and antagonists of various receptors, drugs with high antibacterial or antiviral activity [2]. In addition, they are known to be used as dyes [3], effective electroluminescent materials [4], organic semiconductors [5], "building blocks" in the synthesis of anionic receptors [6] and DNA-binding agents [7]. As part of the study, syntheses of compounds not previously described in the literature - 6,8-dinitro-11H-indeno[1,2-b]quinoxaline-1-one and 1,3-dinitro-6H-indolo[2,3-b]quinoxaline-1-one and 1,3-dinitro-6H-indolo[2,3-b]quinoxaline- were carried out. 6,8-dinitro-11H-indeno[1,2-b]quinoxalin-1-oh was obtained by the reaction of 2-amino-4,6-dinitroaniline, ninhydrin and glacial acetic acid when the mixture was heated in a boiling water bath for 6 hours and the sediment matured overnight. After filtration of the precipitate on the Schott filter, it was washed with cold isopropanol, recrystallized from ethanol, the isolated precipitate was dried at room temperature and at 60°C. 1,3-dinitro-6H-indolo[2,3-b]quinoxalin was synthesized during the reaction of 2-amino-4,6-dinitroaniline, isatin and glacial acetic acid. The mixture was heated in a boiling water bath for 9 hours. After the end of the reaction, the solution was left overnight to mature the precipitate. The next day, the sediment was filtered on a Schott filter, washed with cold isopropanol.

Recrystallization was carried out from ethanol, and then the isolated precipitate was dried at room temperature and at 60°C. The structure of the obtained compounds was established using ¹H, ¹³C NMR data and heteronuclear (HMBC, HSQC) correlation NMR spectroscopy, as well as data from elemental analysis, mass and IR spectroscopy. The developed synthesis methods are characterized by relative simplicity of execution, mild conditions, availability of reagents and allow obtaining target products with a yield of 75% (for 6,8-dinitro-11H-indeno[1,2-b]quinoxaline-11-one) and 92% (for 1,3-dinitro-6H-indolo[2,3-b]quinoxaline).

Keywords: condensation, isatin, ninhydrin, aromatic 4,6-dinitro-o-phenylenediamine, 6,8-dihydro-11H-indeno[1,2-b]quinoxaline-11-one, 1,3-dinitro-6H-indolo[2,3-b]quinoxaline.

Information about the authors: Mukhtorov Loik Gurgovich – Tula State Pedagogical University named after N. Tolstoy, Center for Advanced Technological, Chemical and Biotechnological Excellence, Researcher **Address:** 300026, Tula, Lenin Ave., 125. LLC "Lvinka". **Phone:** +7 (953) 188-46-16. **E-mail:** mukhtorov.loik@mail.

Karimov Makhmadkul Boboevich – Branch of the National Research Technological University "MISIS", Doctor of Chemical Sciences, Professor. **Address:** Republic of Tajikistan, Dushanbe, Nazarshoeva street, 7. **Phone:** +992 (919) 410241. **E-mail:** karimovm.b@mail.ru

Shakhkeldyan I.V. Department of Chemistry. Tula State Pedagogical University named after L.N. Tolstoy. Lenin Avenue, 125, Tula, 300026. Russia. Tel: 8 (4872) 357808; **E-mail:** reaktiv@tspu.ru.

Atroshenko Y.M. Center of Technological Excellence "Advanced Chemical and Biotechnologies" FGBOU VO "Tula State Pedagogical University named after L.N. Tolstoy". Lenin Avenue, 125, Tula, 300026. Russia. Tel: +7 (919) 0870595; **E-mail:** reaktiv@tspu.ru.

Article received 25.12.2023

Approved after review 17.02.2024

Accepted for publication 08.04.2024

CONTENTS MATHEMATICS

Odinaev R.N., Afzalshokhi S. Use of linear programming methods for solving the problems of optimizing the advertising budget of a bank.....	3
Murodov P. S., Prutzkow A. V. Mathematical model of fuzzy recognizing of the topics of scientific articles using syntactically related words.....	12
Talbakov F. M. On the approximation of uniform almost-periodic functions by some sums and integrals.....	19
Pejman J. Poverty line, poverty threshold, poverty forecasting, methods	28

PHYSICS

Radzhabov T. M., Causal physics: cross-sectional area instead of mass.....	37
Solikhova M. I., Kurzina I. A., Khojazoda T. A., Khojaev A. T., Daibova E. B. Effect of barrier discharge on germination energy and germination of "navruz" wheat seeds in the open field.....	47
Makhsudov B.I., Egamov M.Kh., Rahimova U.J. The effect of surfactant concentration on changes in the plane of polarization of light passing through the lcd medium.....	56
Juraev K. Sh., Juraeva G. Kh. Investigation of the stationary phenomenon of heat transfer in a cylindrical condensed medium.....	62
Imom M. Sh., Romodanov V. L., Farhod R., Odinaev S. F. Investigation of the scintillation response of neutrons and gamma-quants by the method of removing superimposed pulses.....	75
Sultonov N., Akobirova A. T., Naimov U. R., Rakhmatov B. A., Khamrokulov R. B. Structural changes in cdte single crystals upon irradiation with heavy ions of inderent gases.....	89

CHEMISTRY

Shokarimov S. M., Naimov N. A., Ruziev J. R., Rafiev R. S., Aslonov A.A., Safiev H. Study of the technology for obtaining a mixture of silicofluoride and sodium fluoride from a by-product of hydrofluoric acid production.....	98
Sodatdinova A.S., Akimbekova Kh.A., Usacheva T.R., Safarmamadzoda S.M. Complexation of silver(I) c 2- ethylimidazole.....	109
Kodirov M. Z., Bobizoda G. M., Zafarov S. Z. Modification and research of α , β , γ - aminoil acids with fullerene c_{60}	117
Eshova C. B., Davlatshoeva J. A., Rakhimova M., Miraminzoda F. Formation of fe(II) hydroxyl complexes in aqueous solutions.....	124
Radjabov Sh. Kh. Use of bsc after acid solution to develop the expansion properties of cement.....	132
Bobokalonov T. B., Khakimov F. Kh., Safarmamadzoda S.M., Mamadgaminova Z. R. Complexation of iron(III) with TSC and FTSC in H_2SO_4 solutions of variable composition.....	139
Mukhtorov L. G., Karimov M. B., Shakhkeldyan I.V. Atroshenko Y.M. Synthesis of 6,8-dihydro-11H-indeno[1,2-b]quinoxaline-11-one and 1,3-dihydro-6H-indolo[2,3-b]quinoxaline based on 4,6-dinitro-o-phenylenediamine.....	147

**BULLETIN OF THE TAJIK NATIONAL UNIVERSITY.
SERIES OF NATURAL SCIENCES**

Scientific edition "The Bulletin of the Tajik National University. Series of natural sciences" is a scientific publication, which publishes the basic scientific results of dissertations for the degree of Candidate of Sciences, for the degree of Doctor of Science. The magazine contains scientific articles faculty, graduate students, doctoral candidates of the Tajik National University and other higher educational institutions of foreign republic and abroad.

The journal accepts scientific articles in the following fields of science: mathematics, physics and chemical sciences.

The journal is included in the Russian Science Citation Index (RSCI) database and regularly provides information in the form of metadata to the RSCI.

The full-text version of the magazine is available on the publication's website (www.vestnik-tnu.com).

**BULLETIN OF THE TAJIK NATIONAL UNIVERSITY.
SERIES OF NATURAL SCIENCES**

2024. No. 2.

Worked on the number:

Executive editor: S.M.Mukhidinova

English language editor: S. Hakimova

Publishing center

Tajik National University

by publishing a scientific journal

“Bulletin of the Tajik National University.

Series of natural sciences:

734025, Republic of Tajikistan, Dushanbe, Rudaki Avenue, 17.

Magazine website: www.vestnik-tnu.com

E-mail: vestnik-tnu@mail.ru

Tel.: (+992 37) 227-74-41

Signed for publication on May 17, 2024